Contribution to the Ultra-Fast Charging of Electric Vehicles – The Configurable Modular Multilevel Converter (CMMC)

THÈSE N^{O} 6934 (2016)

PRÉSENTÉE LE 4 MARS 2016

À LA FACULTÉ DES SCIENCES ET TECHNIQUES DE L'INGÉNIEUR
LABORATOIRE D'ÉLECTRONIQUE INDUSTRIELLE
PROGRAMME DOCTORAL EN ENERGIE

ÉCOLE POLYTECHNIQUE FÉDÉRALE DE LAUSANNE

POUR L'OBTENTION DU GRADE DE DOCTEUR ÈS SCIENCES

PAR

Rosa Martel Danoary TSIRINOMENY

acceptée sur proposition du jury:

Prof. D. Dujic, président du jury
Prof. A. Rufer, directeur de thèse
Dr A. Gascher, rapporteur
Dr S. Colombi, rapporteur
Prof. M. Paolone, rapporteur

ÉCOLE POLYTECHNIQUE
FÉDÉRALE DE LAUSANNE
Suisse
2016

Préface

Aujourd'hui, une voiture électrique (VE) représente une acquisition chère et impliquant de nouvelles habitudes d'utilisation, voire même de conduite. Pourtant, le pétrole devient rare au vu de la déplétion pétrolière, et la consommation cumulée commence à être plus importante que les ressources disponibles. Cette situation a entraîné des bouleversements dans les pays grands producteurs de pétrole comme la Libye, la Syrie, le Nigéria, etc. Afin d'amortir cette déplétion pétrolière, plusieurs négociations ont été initiées par les membres permanents du conseil de sécurité de l'ONU (Organisation des Nations Unies) et l'Allemagne. Par exemple, le 2 avril 2015, sur le campus de l'EPF-Lausanne, un compromis a été trouvé sur le programme nucléaire iranien. Cet accord permettra de débloquer une grande quantité de pétrole sur le marché international. Quoi qu'il en soit, les enjeux politiques et économiques dans l'approvisionnement pétrolier deviennent extrêmement décisifs. Ainsi, même si la sortie du pétrole s'avère être un processus lent, l'électrification des voitures conventionnelles qui fonctionnent au détriment du pétrole devient nécessaire. En effet, les voitures électriques telles qu'elles existent aujourd'hui ont besoin de plus de temps pour se recharger que pour rouler, à cause de la pauvreté en puissance de recharge de leur batterie embarquée. Le déploiement massif des infrastructures de recharge rapide depuis les années 2000 apparaissait comme une meilleure alternative pour augmenter la pénétration des voitures électriques sur le marché de l'automobile. Ce qui semble bien loin d'être le cas, car une grande diversification de standards de recharge s'est instaurée dans les pays industrialisés; que ce soit au niveau des bornes de recharge, ou au niveau de la technologie des batteries embarquées. Cette dernière a fait tomber le taux d'attraction de rouler en électrique. Néanmoins, dix ans plus tard, la multiplication des fabricants de voitures électriques à grande échelle donne une nouvelle lueur d'espoir. Ces voitures restent encore chères, mais leur autonomie commence déjà à être passablement acceptable pour un conducteur qui roule moins de 150 km par jour et qui dispose d'un parc privé de recharge. Telles sont les problématiques autour des voitures électriques. Cette situation nous a poussé à établir un projet de recherche doctorale dont les enjeux majeurs consistent à investiguer la possibilité de concevoir un système de recharge avec une grande flexibilité, du point de vue de la compatibilité avec les infrastructures d'alimentation; que ce soit avec les prises de distribution électrique à basse tension, ou avec n'importe quelle borne de recharge rapide ou lente. La voiture électrique devrait aussi être conçue de manière à offrir une recharge bidirectionnelle pour une gestion plus intelligente de puissance et d'énergie électrique. Autrement dit, les véhicules ne devraient plus être de simples charges pour le réseau électrique mais plutôt des acteurs effectuant des échanges bidirectionnels afin de promouvoir des gains financiers partagés entre les acteurs tout en rechargeant efficacement les véhicules participants. Tout en sachant que les voitures de-

vraient avoir une densité de puissance et un rendement très élevé aussi bien qu'une grande robustesse et fiabilité. Ce qui nous amène à cette présente thèse de doctorat intitulée «Contribution to the Ultra-Fast Charging of Electric Vehicles – The Configurable Modular Multilevel Converter (CMMC)». Un concept configurable et intégré nous paraît très adéquat pour répondre à l'exigence technique imposée par les voitures électriques. Cette méthode implique par contre une grande intégration de semiconducteurs de puissance dans tout le système, mais cela n'est pas effrayant car l'évolution électronique se fait avec l'intégration des transistors d'après la loi de Gordon Moore.

Martel Tsirinomeny

Remerciements

Ce travail de thèse a été réalisé au sein du Laboratoire d'Électronique Industrielle (LEI) de l'Ecole Polytechnique Fédérale de Lausanne dans le cadre d'un projet suisse sur la recharge ultra-rapide de voitures électriques. Ce projet interinstitutionnel, qui a été financé par la CCEM[1] et « Swiss Electric Research », est aussi connu sous l'acronyme anglais UFCEV (Ultra-Fast Charging of Electric Vehicles). Dans ce cadre, j'ai eu la chance de participer à un projet de grande envergure qui a réuni des institutions académiques et industrielles avec des expertises multidisciplinaires. C'est pourquoi j'aimerais remercier la CCEM et « Swiss Electric Research » pour leur soutien financier dans ce projet.

Je tiens à remercier sincèrement et particulièrement le *Professeur Alfred RUFER*, mon directeur de thèse, pour sa bienveillance à mon égard et pour m'avoir accepté comme assistant-doctorant au sein de son équipe. Je tiens aussi à le remercier pour l'encadrement de mes travaux de recherche ainsi que pour la confiance qu'il m'a octroyée. Cela m'a permis d'évoluer rapidement dans mes travaux de recherche. Ce fut un honneur pour moi d'être son assistant, et je souhaite qu'il puisse trouver dans cette thèse la reconnaissance que je lui adresse.

Je tiens aussi à remercier le *Professeur Charles Bernard ANDRIANIRINA* pour ses encouragements, sa qualité d'écoute, il a toujours été à mes côtés même de loin depuis le début de ma thèse.

Je voudrais offrir mes respectueux remerciements également aux membres du jury qui ont porté leur jugement sur ce travail. Mes remerciements s'adressent particulièrement à Dr. Silvio Colombi de General Electric (GE) Switzerland, qui a pris le temps de lire cette thèse et m'a donné un retour très constructif. Mes remerciements s'adressent aussi à Dr. Alain Gascher de Renault-Paris, qui a donné beaucoup d'avis critiques et constructifs sur ma thèse et particulièrement sur le démonstrateur, cela m'a permis de mettre en valeur les aspects plus intéressants de la thèse.

Je voudrais aussi remercier les partenaires du projet UFCEV pour leur contribution dans le cadre de ce projet : *Hardi HOIMOJA, Michail VASILADIOTIS*, *Hans Björn PÜTTGEN*, *Massimiliano CAPEZZALI, Mélanie GUITTET, Donat ADAMS, Olivier PAJOT, Andrea VEZZINI, Gzegorz DRIECHCIARUK, Jürgen BIELA, Daniel CHRISTEN*.

Je tiens aussi à remercier particulièrement *Madame Gina STEINKE,* ma collègue de bureau qui a passé des heures à relire mes papiers et ma thèse, et avec qui j'ai partagé des discussions intéres-

[1] CCEM: Competence Center Energy and Mobility

santes. Je tiens aussi à remercier particulièrement mes collègues de laboratoire qui ont travaillé dans l'ombre pour l'aboutissement de mes travaux de recherches : *Uriel FRED, Roberto ZOIA* et *Roland WETTER.*

Je tiens aussi à remercier les anciens membres du staff du LEI: *Maria ANUTIA, Mahbod HEIDARI*, *Sébastien WASTERLAIN, Philippe BARRADE, Nicolas CHERIX, Stephan KENZELMANN, Antoine BEGUIN, Christian ROD, Simon DELALAY, Sylvain LEMOFOUET* et ainsi que les autres que je ne peux pas tous énumérer.

Mes remerciements s'adressent aussi à l'équipe du nouveau laboratoire d'électronique de puissance (PEL) voisin dirigé par le *Professeur Drazen DUJIC* pour les innombrables choses qu'on a partagé ensemble. Je voudrais aussi remercier le *Professeur Elison MATIOLI* pour ses encouragements, cela m'a beaucoup remonté le moral. J'aimerais aussi remercier particulièrement Cécile Pache et sa famille pour le soutien moral qu'ils m'ont apporté.

Je partage humblement ma joie à toute ma famille à Madagascar. Et enfin une pensée à mon défunt père.

Martel Tsirinomeny

Summary

Configurable Modular Multilevel Converter (CMMC)

It is generally agreed that one of the drawbacks of a conventional vehicle is the inability to always reach the best operating point of the engine and the inability to regenerate the kinetic energy. Meaning, even with the help of the gearbox or automatic transmission, there is no way to reach more efficient operating points without increasing the power and then there is nowhere to store the excess of the energy converted. Electric vehicles (EVs) offer an opportunity for intelligent motion by working at the best operating point during driving mode, as well as a smart energy management during charging mode. However, it is well-known that the EV has been criticised due to its range anxiety, its limited compatibility with various charging points, its high cost, as well as its limited capability to ride-through a thermal runaway, etc.

Today, the range anxiety seems to be resolved by the fact that a significate development is foreseen in the field of the battery cells market for portable equipment such as cell phones, pads, laptops, etc; the same battery technology can be deployed for EVs. Actually, battery packs in EVs tend to have high energy and power densities which will exert a strong thermal stress upon them. This means that individual battery cells are more prone to decline away and eventually fail early because of an excessive loss of capacity and an increase of the internal resistance caused by accelerated aging. Moreover, for electromechanical reasons, each cell is totally unbalanced in operating mode. Therefore, a suitable battery management system should be installed and the capability of the EV to ride-through thermal runaways must be guaranteed. Furthermore, in order to overcome the difference between AC and DC charging station standards, the EV on-board charger has to be flexible for various levels of charging modes (from AC household basic supply to AC or DC ultrafast charging). In order to meet the EV requirements, an advanced power converter which driven efficiency, power density is required. Therefore, the configurable modular multilevel converter (CMMC) has been introduced. It is part of a family of modular multilevel converters, also known as MMC, M2C or DSCC. Hence, its heritage allows bringing the whole advantages to EV applications. In addition it carries the surname of configurable because the converter plays a double role: in fact, it merge the traction converter and the bidirectional charger as well as the battery balancer converter, which not only increases the modularity and the scalability of the power modules but it reduces the cost, condenses the volume. In detail, the concept is linked to the idea of replacing the branch inductance of the standard MMC by the tapped stator windings of the traction motor itself. This allows operating the stator windings as current filter during charging mode. In addition, the famous EV battery pack is split into the MMC submodule. This will increase the fault ride-through capabilities of the Flex-EV battery against thermal runaways, by increasing the capability of the system to work under fault condition. In addition, states of charge (SoC) balancing are implemented at the level of modulation in order to balance that submodule battery state of charge. This is based on a selecting and sorting algorithm, which connect and disconnect the batteries

submodules actively according to the sign of the generated AC current wave form and the SoC of the submodules batteries. For instance, positive AC current charge the batteries submodules whereas negative current discharge the batteries submodules. In terms of the design requirements, the voltage and current rating of the CMMC is defined by the charging configuration. For instance, for charging with a 400 V three-phase network, the defined branches voltage should correspond to this voltage level in order to allow the modulation. However, the applied voltage can be double by improving the isolation of the electrical machine; henceforward the speed can be doubled. This would be a solution for an EV racing car. Regarding to the configurability of the system, the configuration mode is controlled by a shifted angle between the upper-branches and lower-branches currents. This new concept allows interfacing the Flex-EV to the worldwide charging infrastructure. It should be noted that the plug should be configurable with various charging points.

Today, there is a long-term trend towards bi-directional and flexible charger functions not only for drawing current from the grid but also for feeding available energy back into it; the charging power can be controlled in such way to inject/absorb active and reactive power. Therefore the Flex-EV is not only design to draw current from the grid but also as power source, which can be used in standalone application, in micro-grid, in extended local grids or interconnected grids of large territory. In the frame work of the CMMC semiconductors, the key requirements are given by the high power density, high efficiency, high ruggedness and reliability. The device which would mainly dominate this application is the MOSFET, since it trends to have the best mix characteristics; it is voltage controlled and therefore easy to drive. The MOSFET is also modulated so that the low voltage, high current have relatively low state voltage drop. Its structure doesn't include an integrated body-drain diode, so the circuit designer is free to choose an antiparallel diode in a way that suits the best the application: For minimum switching losses and low electromagnetic interference, a diode with a small reverse charge and soft recovery characteristic is optimal. In addition, the CMMC device are operated at a low blocking voltage and low switching frequency; this permits to decrease the switching losses and the therefore the volume and the weight of the heat sink.

Martel Tsirinomeny

Keywords

ULTRA-FAST, LITHIUM-TITANATE, UFCEV, CMMC, FLEX-EV

Zusammenfassung

Der Konfigurierbare modulare mehrstufige Umrichter (CMMC)

Es ist allgemein bekannt, dass es zu den Nachteilen eines konventionellen Fahrzeuges gehört, dass es nicht immer im optimalen Betriebsbereich des Motors arbeitet und es Beschränkungen bei der Rückgewinnung der kinetischen Energie gibt. Das heißt, dass es selbst beim Einsatz von Getrieben keinen Weg gibt, den optimalen Betriebsbereich zu erreichen ohne die eingesetzte Kraft gleichzeitig anzuheben. Hierbei ist es nicht möglich die überschüssige Energie zu speichern. Elektrische Fahrzeuge (EVs) bieten die Möglichkeit intelligenter Mobilität, indem sie beim Fahren immer in einem optimalen Wirkungsbereich arbeiten, sowie ein smartes Energiemanagement im Lademodus ermöglichen. Allerdings wurden EVs in der Vergangenheit in verschiedener Hinsicht kritisiert – sei es wegen der beschränkten Reichweite, der beschränkten Kompatibilität der verschiedenen Ladesysteme oder der limitierten Fähigkeit thermischen Belastungen stand zu halten, um nur einige zu nennen.

Heutzutage scheint das Reichweitenproblem weitgehend gelöst zu sein, da signifikante Entwicklungen im Bereich der Batterien für portable Geräte, wie Handys, Tablets oder Laptops erwartet werden und dieselbe Technologie auch für EVs genutzt werden kann. Batteriepacks für EV besitzen i.d.R. eine hohe Energiedichte, die mit starken thermalen Belastungen für die Batterien einhergeht. Individuelle Batteriezellen sind daher mit dem Risiko behaftet, nachzulassen und nach gewisser Zeit auszufallen, da die Zellen exzessive Kapazitätsverluste und einen Anstieg der inneren Wiederstände durch beschleunigte Alterungsprozesse erfahren. Des Weiteren sind aufgrund elektromagnetischer Grundvoraussetzungen alle Zellen während der Nutzung durchweg instabil. Deshalb sollte ein geeignetes Batterie-Management-System installiert werden und die Fähigkeit eines EV bei einem thermischen Durchgehen weiterzufahren muss gegeben sein.

Um die Unterschiede zwischen AC- und DC-Ladestationen bewältigen zu können, erfordert ein On-Board-Ladesystem in einem EV eine hohe Anschlussflexibilität für eine Reihe von Lademethoden (von einfacher Haushalts AC-Versorgung bis hin zum superschnellen AC- oder DC-Laden).

Um die verschiedenen Anforderungen eines EV zu befriedigen, ist ein hoch entwickelter Leistungsumrichter erforderlich, welcher die Anforderung an Effizienz und Leistungsdichte erfüllt. Deswegen wurde der konfigurierbare modulare mehrstufige Umrichter entwickelt. Er ist Teil einer modularen, mehrstufigen Umrichter-Produktreihe, auch bezeichnet mit MMC, M2C oder DSCC. Indem er diese Produktreihe fortführt, baut der CMMC auf die bisherigen Vorteile für alle EV-Einsätze auf. Zusätzlich trägt der Umrichter „konfigurierbar“ im Namen, da der Umrichter zwei Funktionen wahrnimmt: Zum einen funktioniert er als Ladestation, zum anderen als Traktionsstromrichter, wodurch die Leistungsdichte bei gleichzeitiger Kostenreduzierung erhöht wird, da nun der Umrichter für Traktion und Laden kombiniert werden kann. Genauer gesagt basiert das Konzept auf der Idee, die Zweig-Induktoren eines normalen MMC durch die Ständerwicklungen eines offenen Motors mit mittigen Anschlüssen zu ersetzen. Dadurch können die Ständerwicklun-

gen als Spannungsfilter beim Laden genutzt werden. Außerdem können die standardmäßigen Teilmodul-Kondensatoren durch adäquate Batterien (definiert durch die Spannungs- und Stromkapazität des CMMC) ersetzt werden.

Ein normales Batteriepack wird dadurch in ein mehrstufiges Modul unterteilt, das die Fähigkeit der EV-Batterie erhöht, trotz eines thermischen Durchgehens weiter zu operieren. Der Ausgleich des Ladezustands (SoC) wird durch Selektions- und Sortierungsalgorithmen auf Modulebene eingeführt, die die Verbindung zum Teilmodulumrichter steuern. Die Nennspannung und der Nennstrom des Umrichters sind hierbei durch die Ladeanordnung definiert. Um z.B. mit einem 400 V, dreiphasigen Netz zu laden, sollte die definierte Zweigspannung Üb für die gleiche Belastung ausgelegt sein, um die Aussteuerung zu ermöglichen. Wenn der elektrische Motor durch ein doppelsterniges, kaskadierendes Teilmodul (SM) versorgt wird, wäre ein normaler 400-V-Motor ausreichend. Die angeschlossene Spannung kann jedoch auch verdoppelt werden, wenn die Isolierung des Motors entsprechend verbessert wird, wodurch eine Verdopplung der Geschwindigkeit erreicht werden kann. Das wäre eine typische Anwendung für elektrische Rennautos.

Diese neue Anordnung erlaubt den Anschluss von EVs an eine weltweite Ladeinfrastruktur. Es muss allerdings darauf hingewiesen werden, dass dies voraussetzt, dass der Stecker flexibel an verschiedene Ladestationen angeschlossen werden kann.

Die Hauptanforderungen an einen CMMC-Halbleiter sind daher eine hohe Leistungsdichte, eine hohe Effizienz, große Robustheit und Zuverlässigkeit. Angepasst an den CMMC kann der Halbleiter die entsprechenden Spannungen und Stromstärken schalten, sowie seine Betriebsfrequenz wechseln. Der MOSFET mit Diode bietet die beste Kombination zwischen Leistungsdichte, Temperatur, Ladezyklus und Preis an.

Martel Tsirinomeny

Contents

List of Figures

List of Tables

2 UFCEV: Flex-EV

List of Abbreviations

ACRONYM	**Abbreviation Coded Rendition Of Name Yielding Meaning**
CAES	Compressed Air energy Storage
CAN	Controller Area Network bus
CC	Constant Current
CMMC	Configurable Modular Multilevel Converter
COP	Conference of the Parties
CP	Constant Power
CV	Constant Voltage
DoD	Depth of Discharge
ESD	Energy Storage Device
Flex-EV	Flexible Electric Vehicle
FPGA	Field Programmable Gate Array
GPO	General Purpose Outputs
GUI	Graphical User Interface
HVDC	High Voltage Direct Current
ICE	Internal Combustion Engine
ISS	Integrated Storage System
LFP	Lithium Iron Phosphate
LMO	Lithium-Manganese Oxide
M2C, M2LC	Modular Multilevel Converter
MMC	Modular Multilevel Converter
MMI	Man Machine Interaction
NCA	Nickel Cobalt Aluminium
NEDC	New European Driving Cycle
PFC	Power Factor Corrector
PWM	Pulse Width Modulation
RFB	Redox Flow Batteries
SFOS	Swiss federal Office of Statistics
SIS	Split Integrated Storage
SMES	Superconducting Magnet Energy Storage
SoH	State of Health
SoS	State of Charge
SPI	Serial Peripheral Interface bus
TDI	Turbocharged Direct Injection
TGV	Train à Grande Vitesse
TOSA	Trolley bus Optimisation System Alimentation
TTW	Tank To wheel
UFCEV	Ultra-Fast Charging of Electric Vehicle
UFCS	Ultra-Fast Charging Station
VCO	Voltage Oriented Control
VW AG	Volkswagen group

4 UFCEV: Flex-EV

Chapter 1 Introduction

"I think there are more politicians in favour of electric cars than against. There are still some that are against, and I think the reasoning for that varies depending on the person, but in some cases, they just don't believe in climate change - they think oil will last forever"

Elon Musk, CEO and product architect of Tesla Motors, as well as the chairman of SolarCity

6 UFCEV: Flex-EV

1.1 Generality

First of all, it is generally agreed that many people believe that there is no urgent interest to use electric vehicles because they feel satisfied with the conventional cars with affordable oil. Since electric vehicles are limited in range and take more time for refuelling in comparison to conventional cars, hybrid vehicles (HEV) seem a fascinating alternative for reducing the fuel consumption. The HEV are generally much more expensive than conventional combustion engine cars, because they include two electrical machines (motor and generator) and an internal combustion engine as well as an expensive battery with a complex distributed energy management unit. Moreover, these hybrid vehicles will never be zero-emission vehicles, since they have internal combustion engines. Today, the internal combustion engine efficiency reaches its apogee, where the increasing of efficiency becomes utterly difficult; Volkswagen (VW) cheated on the US emissions test over five years, by embedding in car software which allows reducing the emission significantly [1] during the test. This is really a frightening, when a such big car manufacturer like VW were to go that route for reducing the CO_2 emissions. In spite of the CO_2 emissions, conventional cars are still preferred by our society. It appears that our society is not aware of the vagaries of the weather which is due to the global warming and the climate change. It is well-known that thermal cars offer the possibility to drive with sufficient range to reach every destination, whereas the electric vehicle driver has the fear that the vehicle has an insufficient range to reach the desired destination or the compatible charging point. However, the massive use of thermal cars leads to the growing dependency on fossil which has a huge impact on environment; this is mainly caused by the spilled oil and the greenhouses gases.

First, an oil spill is the release of liquid petroleum hydrocarbon into the environment especially in marine areas, due to human activity. During the last decade, spilled oil has posed serious threats to fresh water and marine environments. It affects surface resources and a wide range of subsurface organisms that are linked in a complex food chain that includes human food resources. Spilled oil can harm the environment in several ways, including the physical damages that directly impact wildlife and their habitats (such as coting birds or mammals with a layer of oil), and the toxicity of the oil itself, which can poison exposed organisms. Some organisms may be seriously injured or killed very soon after contact with the oil in a spill (i.e.: In Niger Delta, multi-national oil corporation do not respect the environment by excessive oil drilling). The international tanker owners pollution federation has tracked 9’351 accidental spills that have occurred since 1974 [2]. Also, clean-up and recovery from an oil spill is difficult and depends upon many factors, including the type of oil spilled, the temperature of the water (affecting evaporation and biodegradation), and the types of beaches involved. Therefore, it is utterly important to protect the wildlife by reducing the quantity of imported oil.

Second, since the 1880, the average global temperature has been risen by approximately 0.88°C according to NOAA (National Oceanic and Atmospheric Administration) of the United States of America (USA); the June 2015 was the warmest June on record for the globe. Many scientists believe that more and more extreme weather conditions have been caused by the climate change in

recent years. For example, in summer 2003, 15'000 people in France died as a result of a heat wave. In fact, heat from sun is normally held in the earth's atmosphere by natural greenhouse gases. These keep the planet warm and without them the average temperature would be about -18°C instead of 14°C. However, more and more heat is being kept in the atmosphere because of man-made greenhouse gases, particularly carbon dioxide (CO_2), which is produced by burning oil and gas. This global warming is already causing changes in the weather all over the world. Experts believe that more and more places are going to be affected by the climate change in the future. And when the ice caps at the North and South poles melt and sea levels rise further, many towns and villages near the coast will be flooded. This is a frightening thought because more than half of the world's population lives near the coast. The COP 21, also known as the 2015 Paris climate conference, is expected to bring new breath of solution for the environment degradation. In fact, a lot has been written about what governments and businesses should do to slow down global warming. However, there is also a lot we can do to save oil consumption by using electric cars. Global issues such as climate change, clean water, sustainability, waste management, emission reduction, and minimizing raw material and energy use have caused many engineers to re-think existing approaches to engineering design in critical areas. As people become increasingly aware of those environmental impacts, in 2010, the energy centre of EPF-Lausanne along with partners decided to start the Ultra-Fast Charging of Electric Vehicles (UFCEV) research project in order to propose a workable alternative solution to the question of the too long charging time of EV's, a factor that is today a clear limitation for their penetration. This puts together experts coming from several Swiss institutions as well as market leading firms in related fields (EPF-Lausanne, ETH-Zürich; EMPA-Dübendorf, BFH-Bienne, Léclanché SA, ESORO, PSA Peugeot-Citroën, etc.). Starting from the specification of the electric vehicles main challenges, several academicals solutions have been proposed where some of the exciting methods are developed in this doctoral thesis. Moreover, this doctoral thesis, intituled "Contribution to the Ultra-Fast Charging of Electric vehicles – the Configurable Modular Multilevel Converter" aims to deal with the re-think of the EV architecture design. A new approach based upon the three-phase modular multilevel converter (MMC) structure with integrated storage system (ISS) is proposed. This technology brings the synergic integration of electrical, electromechanical, electronical and computer systems of the electric vehicles. This new power conversion is not only designed for achieving the ultimate power management between the embarked battery and the mechanical EV driveline, but it is also able to control the circulation of the energy between the EV battery and various charging infrastructures (from standard household plug to DC or AC high power charging stations). By construction, the power electronics is easily scalable and configurable. Inherently, the converter itself dynamically balances the state of charge of the battery modules. In short, this concept is attended to give the best compromise between charging and driving time ratios, between charging flexibility and the EV design complexity. To do so, this chapter 1 is dedicated to the introduction where the ultrafast charging of electric vehicle is emphasised, then the possible methods for optimizing the charging-driving times ratio under a limited grid connection is described. The chapter 2 addresses a particular attention on Optimizing Electric Vehicle driving-recharging time ratio a under limited grid connection. After, chapter 3 is dedicated to the proposed Flex-EV: general concept. The chapter 4 is devoted to the CMMC modelling and control. Next, chapter 5 is devoted to the experimental validation. Finally, a conclusion and future work are given where the flexible electric vehicle perspectives are emphasised.

1.2 Main challenges for electric vehicles

It is generally agreed that the New European Driving Cycle (NEDC) which reflects both urban and extra-urban driving conditions, is set as standard to characterise the energy consumption of small vehicles. It should be noted that, being hard to succeed, this driving cycle has strongly been criticized. This is generally important to assess the ability to supply sufficient power during driving. However, the key problem of electric vehicles is the range flow rate[2]; meaning, on one side, how the electric vehicle charging can be comparable to tanking a gasoline car, and on the other side, how the EV autonomy can be competitive to the range of a conventional cars.

1.2.1 The uncompetitiveness of the electric cars

The following Table 1.1 shows a comparison between the VW Golf 7, a Renault Zoé and a Nissan Leaf. The diesel car corresponds to the Golf 7, 2.0 TDI with 150 horse power (110 kW) and 6 speeds, and which is the car of the year 2013 according to Geneva motor show. Its consumption is 5.7/4.1/4.7 litres per 100 km [3]. Between the two compared electric vehicles, the Renault Zoé has a lower storage size than the Nissan Leaf nevertheless it has the higher autonomy. This is the reason why the range flow rate[2] is the key parameter for assessing the performance of an electric vehicle; it takes into account both the charging and the driving route. In fact, the Zoé uses the so-called Chameleon charger, which is a combined on-board AC fast-charger for up to 43 kW [4] whereas the Leaf uses the CHAdeMO standard charger for up to 50 kW. However, it is shown that the electric vehicles are incomparable with the diesel car in term of range flow rate; therefore the diesel car is still attractive. This is mainly due to the limited capability of the electric vehicle battery in regards to the ultra-fast charging.

Parameters	**Golf VII**	**Renault Zoé**	**Nissan Leaf I**
Consumption	5.7/4.1/4.7 l/100km	11 kW·h/100 km	15 kW·h/ 100 km
Fuel tank/ storage size[3]	45 l	22 kW·h	24 kW·h
Autonomy[4]	1000 km	210 km	199 km
Refilling	35 l/min[5] (22 MW)	587 W·h/min[6] (43 kW)	640 W·h/min (50 kW)
Range flow rate	777 km/min	5.3 km/min	4.3 km/min
Record : km/ 24-hour	N/A	1618	1154
Comparable price	22’700 -CHF	22’900-CHF	26’230-CHF

Table 1.1: comparison between diesel car and electric cars

Then, the next paragraph is dedicated to give a general overview of electric vehicle batteries.

[2] Range flow rate: driving range resulting with a minute charging/fuelling time [13]
[3] Available stored energy in lithium-ion battery
[4] NEDC results, average speed
[5] Standard fuel station fuel flow
[6] CHAdeMO charger in 30 minutes 80% of battery capacity

1.2.2 The limited capability of electric vehicle batteries

An evident penalty for electric vehicle (EV) owners is the limited average range while driving long distances on highways, which is defined by the battery performance. In order to lengthen the total travelling time, a substantial progress is expected in the area of on-board energy storage technologies. As for today, the commercially available solutions allow recharging of an EV within 20 min as minimum [5], [6]. High energy density lithium batteries, based mostly on the lithium-manganese spinel (LMO) or lithium-iron phosphate (LFP) electro chemistries are widely used by manufactures in order to reach the highest autonomy possible while having the disadvantage of long charging times in the scale of 6…8 h for charging power between 3…4 kW. Whereas high power density batteries require less time to recharge, their energy density and autonomy show poorer figures.

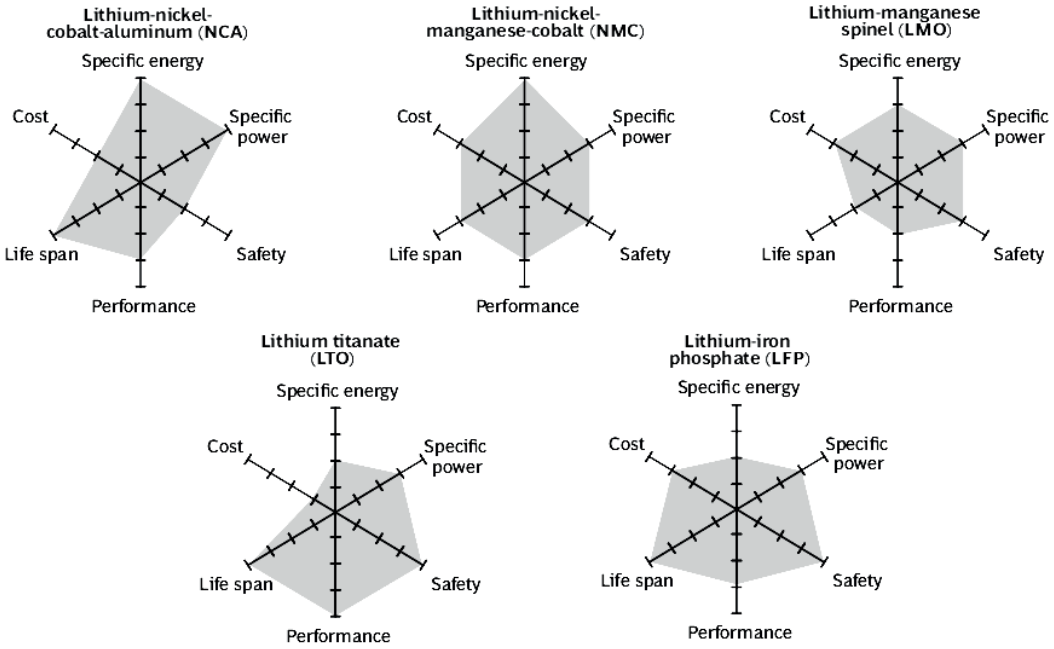

Figure 1.1: A comparison between main lithium ion battery chemistries [7].

A qualitative comparison between available EV battery chemistries is shown in Figure 1.1. It should be pointed out, however, that the manufacturers often specify the specific power as absolute maximum during a 10 s pulse, therefore the datasheet values should be interpreted with reservation unless there are more detailed figures available. Attention also needs to be paid to the different specific power for charging and especially for discharging. This means that the internal losses are not taking into account in the specification of the charging power. Figure 1.1 together with additional market research permits concluding that the optimal EV battery electrochemistry in terms of recharge-discharge symmetry, life span, specific power and energy is the lithium titanate (LTO, or chemically expressed $Li_4Ti_5O_{12}$) [8]. Even though, a strong progress is seen in battery technology; however the distribution grid is limited in power. The next paragraph is devoted to give an overview of the limited capability of the existing charging infrastructure.

1.2.3 The limited capability of the distribution grid

The distribution grid is limited in power (for the single-phase systems in Europe up to 3.6 kW and for three-phase connections 11 kW, respectively). For example, charging a 16 kWh battery from a standard 230 V, 16 A outlet takes approximately 6 h, after which the car is able to cover up to 150 km, as stated by the sellers. As the average daily distance for a car is estimated to be only 38 km [9] this charging method would satisfy the needs of the largest part of the drivers; however, for the driver segment often using long-stretch highways, a faster charging option to overcome the "range anxiety" must be guaranteed. For instance, a fuel tanking with the flow rate of 35 l/min (0.83 kg/dm^3) would require an equivalent power of 22 MW which is utterly absurd in comparison to charging of electric vehicles. Even when speaking of lower charging rates between five to ten minutes, a strong grid connection is essential if the battery's ability to admit high charging power is neglected. The situation becomes even worse if several EVs are being charged concurrently; in this case the charging station must have a buffer energy storage system. In order to illustrate this power demand, the load curve for the Ultra-Fast Charging Station (UFCS) must be studied. This is possible by investigating the distribution of the daily traffic in a given charging point. Therefore, the Swiss Federal Office of Statistics (SFOS) [10] traffic data has been taken. Then it has been processed to get presumable load diagrams to the Ultra-Fast Charging Station.

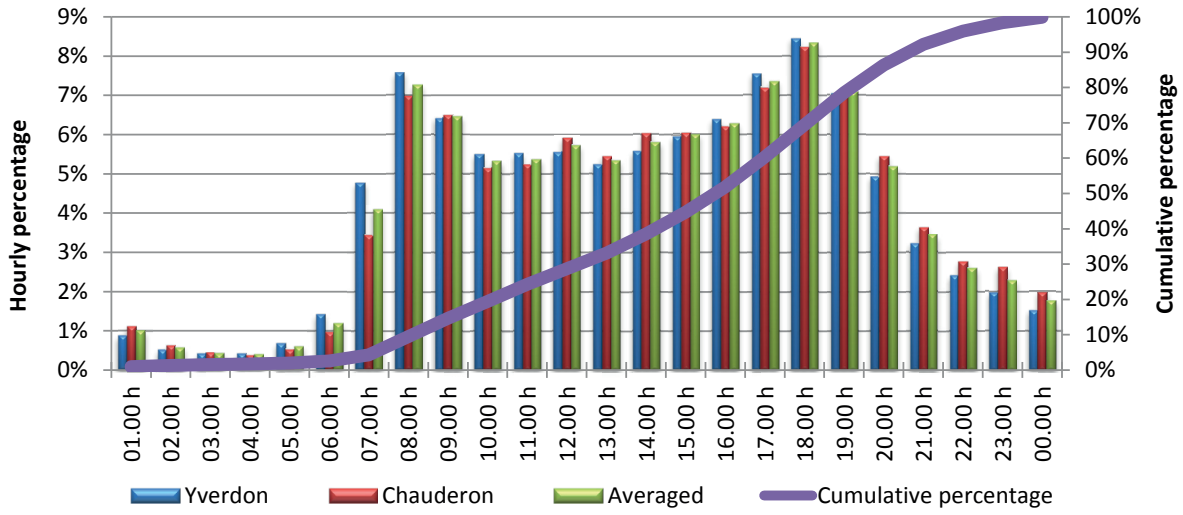

Figure 1.2: Typical daily traffic density distributions.

Figure 1.2 gives the distribution of the EVs numbers per day in percentage. In fact, it shows the typical traffic density distribution values for highway (tunnel Pomy near Yverdon) and urban conditions (Chauderon in Lausanne) in percentages. Therefore it is possible to extract a load generation procedure based on stochastic approach as proposed by [11] and [12]. The authors in [13] have carried out a simulation for 20, 50, 100 and 200 vehicles charged per day and in all their simulations, the charging time $t_{ch} = 5\ min$ was kept constant, independent of the state of charge (SoC) and the useful energy values, meaning variable charging power. For every objective number of charged vehicles per day, 10'000 Monte Carlo iterations were made. In case of overlaps (multiple

EVs charging simultaneously) the charging power sums up. Figure 1.2 shows that the peak power is relatively reached to evening rush hour; it corresponds approximatively to 8.4 % of the numbers of the EV per day. As a result, Table 1.2 shows the load values, requested from the grid according to the traffic between the defined regions. Thus, the scale of the power at the EV input and the transferred energy needed are absolutely significant regarding the grid utility power. It is trivial that a high power charging requires a deployment of extra buffering system in order to mitigate the impacts on the distribution grid.

	Power at EV input [kW]		**Transferred energy [kWh]**		
EV/day	Per EV	Station max	Mean	Median	Max
20	Mean: 230 Median: 214 Max: 697	1193	362	361	496
50		1421	908	907	1113
100		1733	1850	1850	2220
200		2218	3652	3651	4061

Table 1.2: Values for charging time $t_{ch} = 5$ min

However, since a fast charging station is not always operational with full power, the energy storage unit benefits from drawing from grid. Over the last decade, the most wide spreading charging station is based on the CHAdeMO standard, where the maximal charging current is limited mainly by the connector's maximum current of 120 A, could be as much as 50 kW. IEC 61851-23 has however drafted a 400 A/330 V DC-charging mode which could bring that power up to 132 kW in the future. It requires data communication in order to exchange control parameters between the on-board battery and the off-board fast-charger. This is a real issue because it leads to the incompatibility of some on-board EV batteries.

1.2.4 The diversification of the existing charging standards

Generally, electricity energy is distributed with alternating current (AC), whereas, batteries are a direct current (DC) sources. Therefore, power electronics are required to convert the alternating current into direct current for charging batteries. In the framework of EVs applications, this could be off-board or on-board chargers. EVs require a high power as well as compact charger. High power chargers are often implemented off-board because of size, whereas low power chargers are regularly embarked into the cars.

Mode	**Max current per phase**	**Max charging power per phase**	**Charger location**
1	AC 16 A	3.6 kW	On-board
2	AC 32 A	7.3 kW	
3	AC 63 A	14.7 kW	
4	DC 400 A	DC 150 kW	Off-board

Table 1.3: Charging modes according to IEC 61851-1, 230 V / 400 V voltage system [14], [15].

A combination of off-board and on-board charger are often implemented in order to achieve the appropriated compatibility regarding the voltage and the current ratings between the AC grid and

the EVs batteries. In the framework of ultrafast charging of electric vehicles, a direct connection to the medium voltage grid facility would be an appropriate solution in order to alleviate the power demand [8]. However, this leads to a demand of a huge change in the existing public infrastructure such as installations of medium voltage transformer and change in distribution line cables, which will cost a lot for governments. A similar scenario is seen in the railway application where the railway lines facilities have to be changed in order to accept the high speed train the so-called TGV (Train à Grande Vitesse). In fact, The IEC 60851 standard, applicable for conductive charging systems [14], defines four charging modes, as given in Table 1.3.

Nevertheless, a discrepancy between the above mentioned standard and the market situation exists. Usually the EV manufacturers prefer to sell their products in set with a Mode 1 one-phase on-board charger; as standard household 16 A sockets are used, which are de-rated to 10 A … 12 A at constant load, the charging power is even more limited, to 2.3 kW … 2.8 kW. Thus a small-sized EV with a 16 kWh traction battery would need at least 6 hours to fully recharge. The Mode 4, using off-board chargers, has been implemented by the CHAdeMO consortium [16]. But for today, its charging current is limited up to 120 A by the used connector, which enables to recharge a commercial EV within 20 min … 30 min depending on the battery capacity. As for Mode 3, the manufacturers have not yet reached an agreement on the standard connector, but the increased charging rate is achieved by reversing the power flow in the traction inverter and using motor windings as smoothing reactors, thus the charging power can be nearly equal to the rated driveline power. It uses the motor winding as a current filter during charging, therefore, the charging current is limited at the motor nominal current. A comparison between commercially available charging methods is given in Table 1.4.

Charging type	**Mode**	**Minimun charging time**	**Autonomy flowrate**
Domestic one-phase charging	1	6 h … 8 h	0.3 km / min
Three-phase semi-quick charging	3	20 min … 30 min	4 km / min
CHAdeMO semi-quick charging	4		
Diesel tanking for a family car	N/A	1 min 30 s	600 km / min

Table 1.4: Commercially available EV charging methods [15]

It shows that the charging power is the main problem for electric vehicle in order to be competitive against diesel cars.

1.3 The possibility of ultrafast charging under limited grid connection

It has been presented in the paragraph 1.2, that the challenges by electric vehicles are extremely complex; however in the framework of the UFCEV project, substantial work has been completed in order to overcome those difficulties. In particular, this paragraph is dedicated to a potential method to reduce the electric vehicle charging time and to increase the autonomy under limited grid connection. In order to address the point's described; the following topics are addressed in details: first, the impact of an ultrafast charging station on local distribution system update of existing systems and green-field designs, with specific attention to high short duration power peaks. Second, the detailed assessment of various energy storage technologies, both stationary and embarked, is including their applicability and interface issues. Third, the specification of high efficiency power electronics converters with the aim of achieving outstanding high efficiency of the converter systems for the fast charging station. And finally, the design and implementation of the required control electronics, with specific attention to energy efficiency.

1.3.1 Mitigation of the impacts of a UFCS on local distribution system

To decrease the UFCS impact on utility grid, the load must be at least partially decoupled from the mains grid source. This can be done by implementing energy storage elements, which act as buffer between the EV and the grid [9], [13], [15], [17]–[20]. Each port is characterised by power level P_{gr}, P_{EV}, P_{st} and conversion efficiency η_{gr}, η_{EV}, η_{st} , as depicted in Figure 1.3 above. It is worth mentioning that the same buffer-based principle has recently been used in pneumatic energy transmission for compressed air propelled vehicles [21]. The concept is to keep the system's overall energy balance over a specified time, allowing estimating instantaneous, mean and maximum power values and storage capacity based on the instantaneous storage power integration capacity based on the instantaneous storage power integration. In the example below, the objective grid load while levelling is based on matching the grid input to the hourly moving average EV charging power [9], [15].

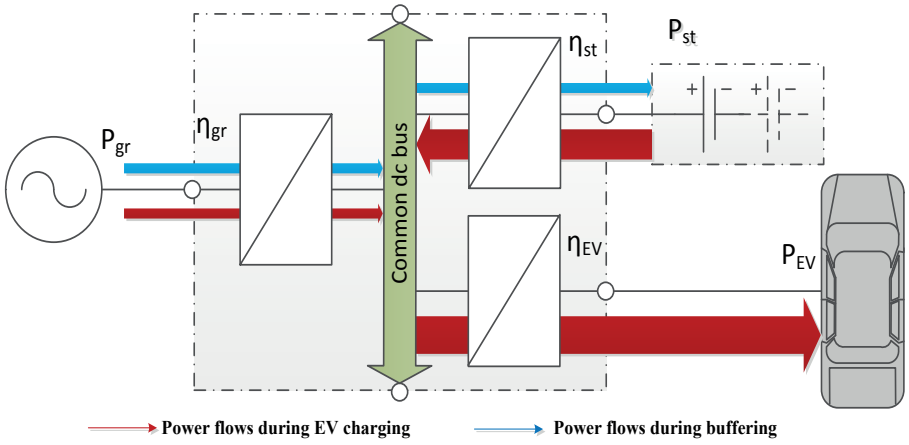

Figure 1.3: Buffered UFCS topology.

Any UFCS design must take into account the system's overall energy balance over a specified time:

$$\int_{t_1}^{t_2} \eta_{gr} \cdot P_{gr}(t) \cdot dt = \int_{t_1}^{t_2} \frac{1}{\eta_{EV}} \cdot P_{EV}(t) \cdot dt + \int_{t_1}^{t_2} \frac{1}{\eta_{st}} \cdot P_{st}(t) \cdot dt \tag{1.1}$$

The instantaneous storage power:

$$\begin{aligned} P_{st}(t) &= \frac{1}{\eta_{st}} \cdot \left[\eta_{gr} \cdot P_{gr,s}(t) - \frac{1}{\eta_{EV}} \cdot P_{EV}(t) \right] \rightarrow \text{EV charging} \\ P_{st}(t) &= \eta_{st} \cdot \eta_{gr} \cdot P_{gr,s}(t) \rightarrow \text{buffer charging} \end{aligned}, \tag{1.2}$$

Where $P_{gr,s}(t)$ is the desired instantaneous grid load set point. The storage energy balance:

$$E_{st}(t) = \Delta t \cdot \sum_{\tau=0}^{t} P_{st,\tau} \tag{1.3}$$

Necessary storage capacity:

$$E_{st} = \max\left[E_{st}(t)\right] - \min\left[E_{st}(t)\right] \tag{1.4}$$

Necessary storage charge and discharge power:

$$\begin{aligned} P_{st,ch} &= \max\left[P_{st}(t)\right] \\ P_{st,dch} &= \min\left[P_{st}(t)\right] \end{aligned} \tag{1.5}$$

It must be noted as positive storage power means charging (the buffer acting as sink) and negative discharging (buffer acting as a source). In fact, charging a vehicle during a few minutes cause a peaks in power distribution systems, especially during most loaded hours, since the impact of this ultra-fast charging on the power system can be alleviated by the application of intermediate energy storage system. Here exist two main buffering strategies: levelling and shifting. The buffering has more effect at lower utilisation rates in terms of station input power relationship to EV charging power. Load shifting, while being desirable from the overall grid management, needs more storage capacity than levelling. In addition, the load shifting is performed by allocating hourly grid set point values as mirror inverted to the vehicle hourly distribution, as illustrated in Figure 1.4.

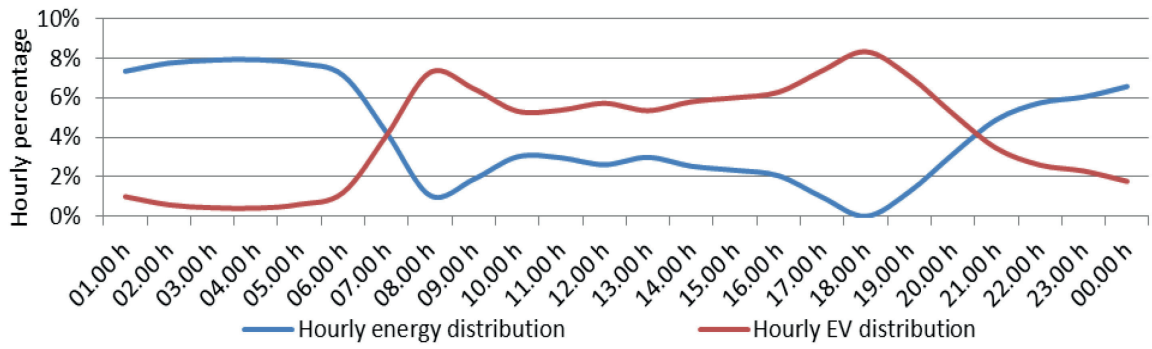

Figure 1.4 Load shifting explanation: hourly distributions for the vehicles and transferred energy from grid.

Load shifting helps to decrease the necessary grid tie, but requires more capacity and transfer power for the intermediate storage than levelling as depicted in the next Table 1.5.

It is shown in this Table 1.5 that, charging an EV during a few minutes causes peaks in power distribution systems, especially during the most loaded hours. In the worst case, the peaks cumulate when several vehicles are charged at the same time.

EV/day	**1 h levelling**			**Shifting**		
	$P_{gr}[kW]$	$E_{st}[kWh]$	$P_{st}[kW]$	$P_{gr}[kW]$	$E_{st}[kWh]$	$P_{st}[kW]$
20	64	76	427	33	248	456
50	112	144	730	84	639	761
100	196	218	733	157	1155	874
200	426	334	1381	322	2281	1637

Table 1.5: Grid and storage parameters for load levelling and shifting at $t_{ch} = 5$ min, without queuing

Therefore, it comes out that with buffering, the grid connection can even be made on the low-voltage side and in the proximity of a distribution substation. Thus, the input current for a buffered station charging 200 EV/day can be reduced to 630 A at a standard three-phase, 230 V/400 V connection. A sample curve 200 EV/day is shown in Figure 1.5. The load-side management would help to decrease the power levels even further thanks to the avoidance of overlaps. In practice, it means that the drivers must accept some waiting queues and longer charging times, as the station design is based on the average values.

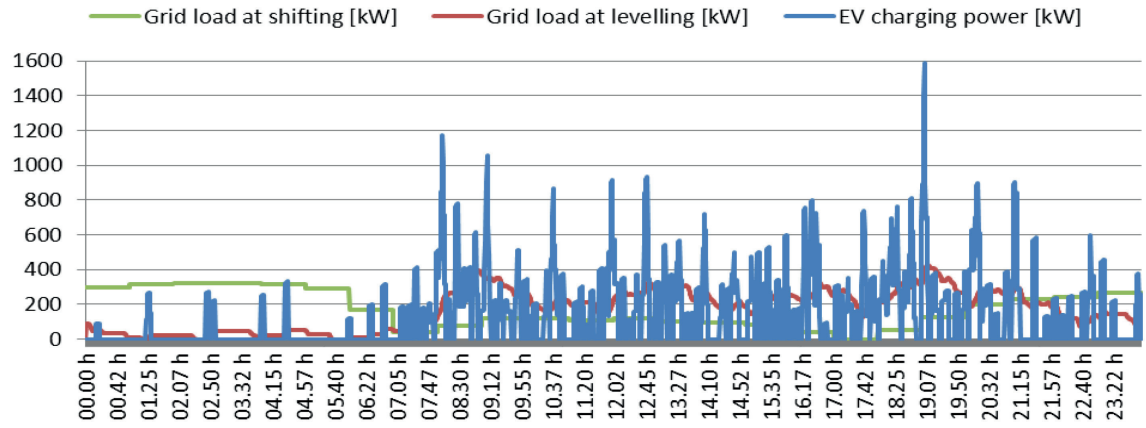

Figure 1.5 : load curves for 200 EV/day (without queuing).

The buffer instantaneous power is set by the number of simultaneously charged vehicles, i.e. the number of EV charging ports. It becomes evident, that the buffer charging power, limited by the objective grid load can be several times smaller than the discharging power into the EV battery. In this context, a detailed assessment of various energy storage technologies both stationary and embarked, including their applicability and interface issues is based on the basic methods of storing electricity in local scale.

1.3.2 Assessment of various stationary energy storage technologies

As stated before, the drivers have the habit to refuel with fossil gas (natural gas, essence, gasoil, etc.) in the time range between 2 … 5 minutes.

Technology	Energy density		Power density		For 200 EV/day		Lifetime
	[W·h/kg]	[W·h/l]	[W/kg]	[W/l]	mass [t]	V [m³]	[cycles]
Lead-acid	30	74	100	250	76	31	~ 1 000
Li-ion high-energy	200	630	220	650	11	4	~ 10 000
Li-ion high-power	80	140	750	1400	29	16	~ 10 000
Supercapacitor	6	7.6	5900	7400	380	300	~ 100 000
Flywheel	11	18	800	1300	207	127	~ 1 000 000
Compressed air (CAES)	23	24	23	24	99	95	~ 1 000 000
Redox flow batteries (RFB)	23	30	60	80	99	76	~ 10 000

Table 1.6 Comparisons of energetic characteristics of storage media [13]

Therefore the main challenge is to charge an EV battery within a time frame comparable to tanking petrol. In this context, one of the key factors is therefore to define the parameters for the design of future energy supply which enhances ultrafast charging of the vehicle batteries, while avoiding solicitations of the local distributions system. This avoids exceeding the distribution grid instantaneous power capabilities. In Table 1.6, the basic energetic data of different storage units is given together with a load shifting example for 200 EV/day (Figure 1.5). Including the financial considerations, a conclusion may be drawn that if the installation space and weight are not critical, as in stationary storage, compressed air would be a feasible solution. The indicative mass of 99 t and volume of 95 m³ is comparable to an eight-axis tank wagon, which can be placed underground.

Parameter	Unit	Explanation
Specific energy (energy density)	W·h/kg W·h/cm³	The relationship of usable energy to mass (gravimetric mE) or volume (volumetric VE).
Capacity	W·h	The amount of available energy stored in a storage unit.
Specific power (power density)	W/kg W/cm³	The relationship of usable power to mass (gravimetric mP) or volume (volumetric VP).
Calendar lifetime	Year	The expected lifetime
Power gradient	W/s W/min	The power variation rate in time
Power loss	W	The sum of recharge-discharge losses and auxiliary loads per time unit (self-discharge).
Transfer time	S min	The time between initiating energy exchange and discharging to 50 % of the initial capacity
Cyclic lifetime	Cycles	The maximum number of recharge-discharge cycles during calendar lifetime

Table 1.7 : Main technical characteristics of energy storage units

The Table 1.7 shows that each storage technology can be assessed by basic descriptive data, which allows comparing them in respect of the objective task. Besides the physical limitations on the storage medium, the overall characteristics are defined by the transmissibility of the power interface. However, the power interface must ensure bidirectional power exchange, i.e. the source and sink functionalities. Additional task of a power interface can be converting energy from one form to another, like in flywheel and compressed air systems. There, electricity is converted into mechanical energy and vice versa. In this case the conversion takes place in two stages: the first stage for electric and the second one for the electromechanical conversion. As a result, the input power is converted into mechanical power. The total power loss is the sum of the electric and electromechanical losses. This two-stage power interface can be described as an electric drive, where the converter constitutes the first and the machine the second level.
According to the Ragone theory (T. Christen and M. Claren), there are two main categories of storage devices:

1) *Potential storage*, where, the highest energy storage can be extracted from a storage device where its exchange occurs at the lowest power level. Examples:
   a) Electrochemical: batteries on lead-acid, lithium-ion, nickel metal-hydride etc.
   b) Electrical: supercapacitors.
2) *Kinetic storage*, where the highest energy storage can be extracted from a storage device where its exchange occurs at the highest power level. Examples:
   a) Mechanical: flywheels and compressed gas.
   b) Electrical: superconducting magnet (SMES).

It should be noted that the power density which is indicated by the manufacturers, is an admissible value in term of possible solicitation. Therefore, not the fully stored energy can be extracted for a given working condition [19]*. For instance, for a fast charging battery, the increase of the charging current induces an increase of the internal losses in the battery, which is not taken into account in the given power density.*

1.3.3 Assessment of various stationary energy storage cost

In the framework of the cost requirement, it is well-known that the basic economic data are based on:

1) The capital cost per unit energy
2) The capital cost per unit power
3) The capital cost per cycle.

These three parameters are the key factors for defining the investment cost. For illustration, Table 1.8 shows the indicative cost for storage. Hence, the best compromise between energy, power and lifecycle capital cost has to be found during the specification of the energy storage elements.

For instance, the Li-ion high energy is the most common used in stationary storage application, because it gives the best comprise between the energy and power densities, complexity, lifecycle

and investment cost. However, as the storage technologies will become more mature and the markets more saturated, the prices will gradually fall. Generally speaking, by the time, the energy storage elements become more and more accessible.

Technology	Investment costs		Per cycle cost
	[$/kW·h]	[$/kW]	[$/kW·h]
Lead-acid	300	500	0.5
Li-ion high-energy	800	3000	0.5
Li-ion high-power	2000	1600	0.5
Supercapacitor	7000	200	0.08
Flywheel	4000	300	0.08
CAES	50	700	0.02
RFB	500	1200	0.1

Table 1.8 : Indicative costs for storage [13]

Table 1.8 gives an indicative price of the potential energy storage system technologies for ultra-fast charging station. It should be noted that the chosen technology should have a very high power discharge, for charging the electric vehicle in very short time.

1.3.4 High efficiency power converters for UFCS

In fact, large load variations as seen from the local power system, at multiple levels, must be carefully assessed with special attention to feasible load changes at the coupling points. Consequently, ultra-fast charging of electric vehicles will require the deployment of storage technologies, such as high-capacity batteries and suitable mixtures of high-power and high-energy density subsystems, as depicted in following figure:

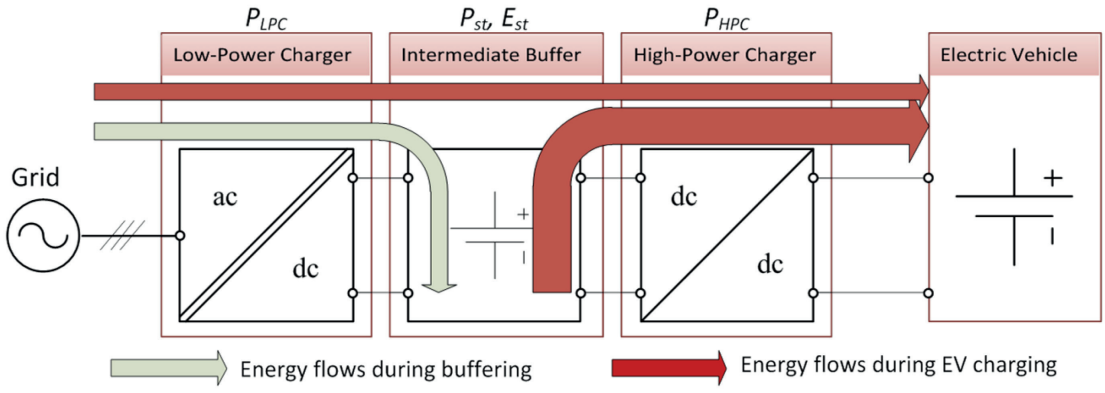

Figure 1.6: Decoupling an EV charging station from the grid by intermediate buffer [17]

This Figure 1.6 shows that, an additional appropriate power flow management will imply specific and dedicated power electronics conversion and control. Detailed system reliability analysis is es-

sential, as well as a better understanding of the limitations emanating from existing and future grid systems and apparatus; hence the impacts can be effectively mitigated by the load-side management and decoupling. The high power flow also requires examining the system topology of the power electronics converters and the optimisation of the power electronics systems for high efficiency and compact design with the focus on split battery based energy storage system.

For stationary application with direct connection into the grid, multistage power conversion is required as depicted in Figure 1.6. Starting from a low power (P_{LPC}) isolated ac/dc converter following by an intermediate buffer, then a paralleled high power charger (P_{HPC}) in order to increase the output current. This gives the best trade-off between cost and complexity of the system. However, the main challenge has to be found within the specification of parameters for the design of the future electric vehicle charging system, which include the ultrafast charger as well as a bidirectional power conversion for power quality. At the industrial electronics laboratory (LEI), different converters topologies have been investigated in terms of performances and costs; more details can be seen in [22] and [23].

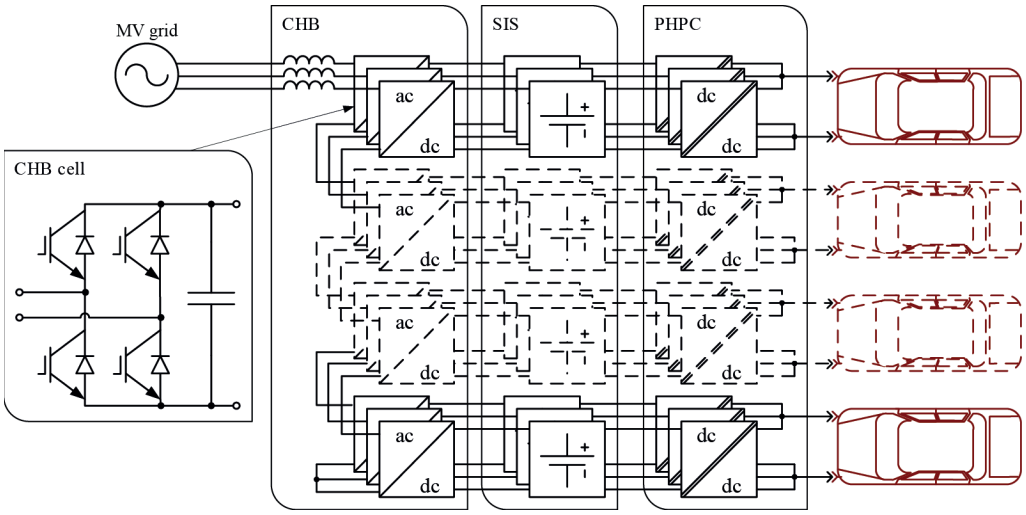

Figure 1.7: Architecture of an UFCS based on the cascaded H-Bridge and split integrated storage [17].

In fact, Figure 1.7 illustrates the typical architecture of an UFCS based on the cascaded H-Bridge and split integrated storage with medium voltage grid connection. This topology can be doubled and therefore performs the Double Star Cascade Cells (DSCC) [24] with split integrated storage (SIS) and parralled high power charge (PHPC).

Additionally, a high current multi-port charger is also a key requirement for interconnecting the charger with various grid sources (AC or DC), therefore the architecture in Figure 1.8 would be the preferred architecture for ultra-fast charging of electric vehicle [20]. In this figure, the low power charger is based on the so called Modular Multilevel Converter (MMC) [25]–[27], [28], [29], which is also used later in Chapter 3 for the architecture of the Flexible Electric Vehicle.

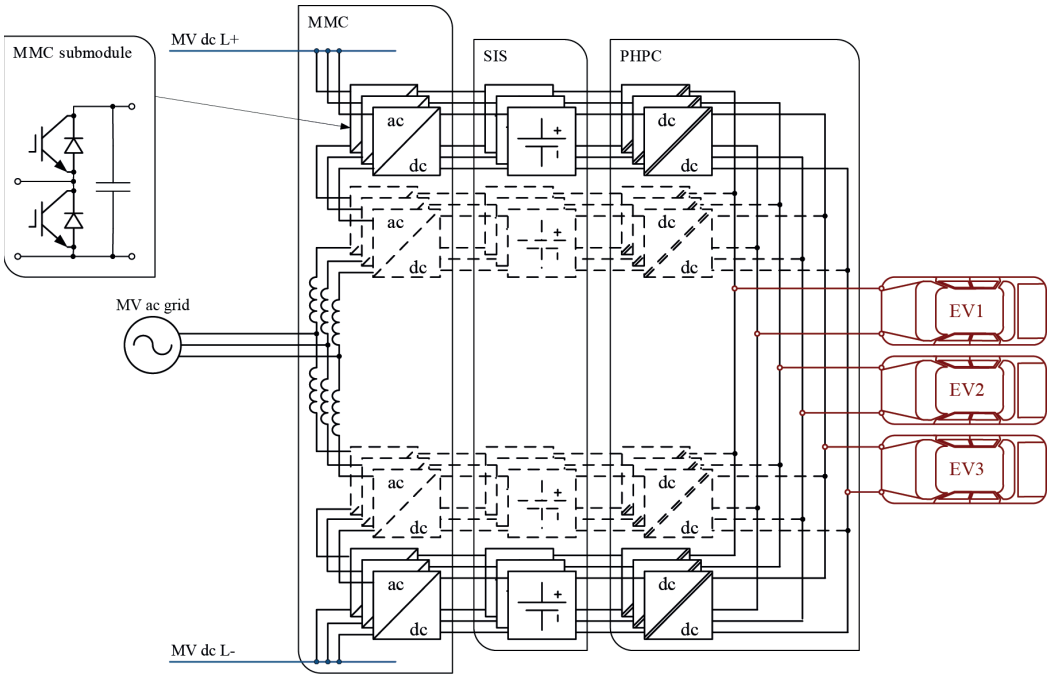

Figure 1.8: Architecture of an UFCS based on modular multilevel converter and split integrated storage

In some cases, the inductances of the conductors within a branch are already inductive enough, such as in drive application where the stator windings are already inductive enough in some cases. Therefore, it could be also based on tranformerless as depicted in the next Figure 1.9.

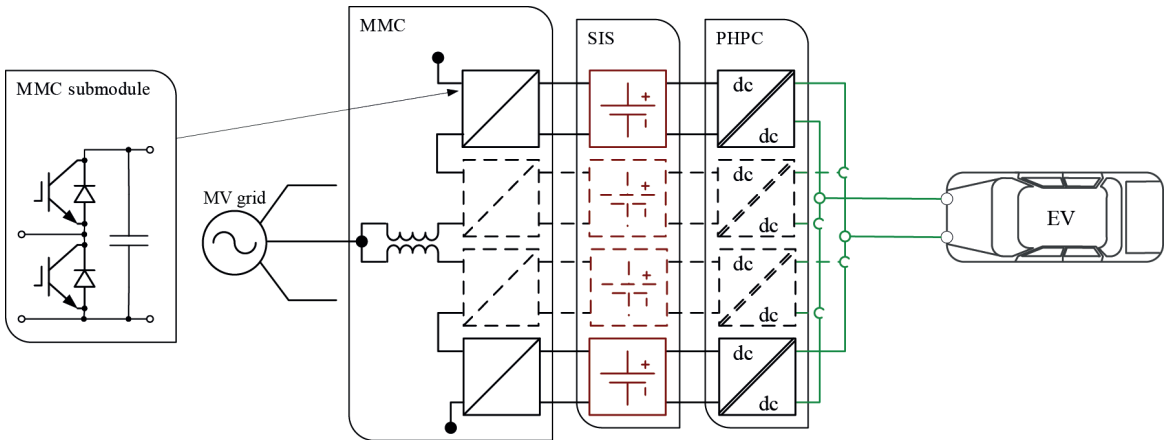

Figure 1.9: Detailed architecture of an UFCS based on MMC and split integrated storage

It should be noted that the cells or the submodules can be configured as half- or full-bridge converter. In fact the basic idea is the modularity and the possibility to scale the converter to any voltage and power level without major changes in layout or the component design. However, it is

difficult to find the best compromise between the DC bus-side control and the AC line currents control. In fact, it depends also on the topologies, however the increase of the line RMS current will increase the ripple of the submodules capacitors, and the reduction of the capacitors ripple will decrease the AC RMS current. This has a strong relationship to the optimal design of the sub-module capacitor and the AC filter inductance.

$$\begin{cases} \text{if} \quad \mathrm{RMS}(i_{AC})\uparrow \quad \Rightarrow \quad \text{therefore} \quad (C_{SM}\uparrow) \\ \text{if} \quad (C_{SM}\downarrow) \quad \Rightarrow \quad \text{therefore} \quad \mathrm{RMS}(i_{AC})\downarrow \end{cases}$$

1.3.5 The energy versus power densities of the EV's battery

The embarked EV battery combining both very high power density[7] and very high energy density is not yet available on the market. As for today, the commercially available solutions allow recharging of an EV within 20 minutes as minimum. High energy density lithium batteries, based mostly on the lithium-manganese spinel (LMO) or lithium-iron phosphate (LFP) electro chemistries are widely used by manufacturers in order to reach the highest autonomy possible with the disadvantage a low C ratio[8] in scale of 0.5 C from a conventional household socket. In details, the modern cathode materials for Li-ion battery are generally prepared in the lithiated (discharged) state, so that they can be paired with delithiated anode such as graphite. For ease of handling, it is desirable that the material be reasonably air-stable at room temperature. Furthermore, graphite anodes impose a penalty of approximately 0.1 V in average cell potential to Li metal. To compensate for this, and also to maximize energy density, cathode intended for use in Li-ion batteries have higher average potentials versus Li/Li^+ than earlier materials such as TiS_2 and vanadate developed for Li metal batteries.

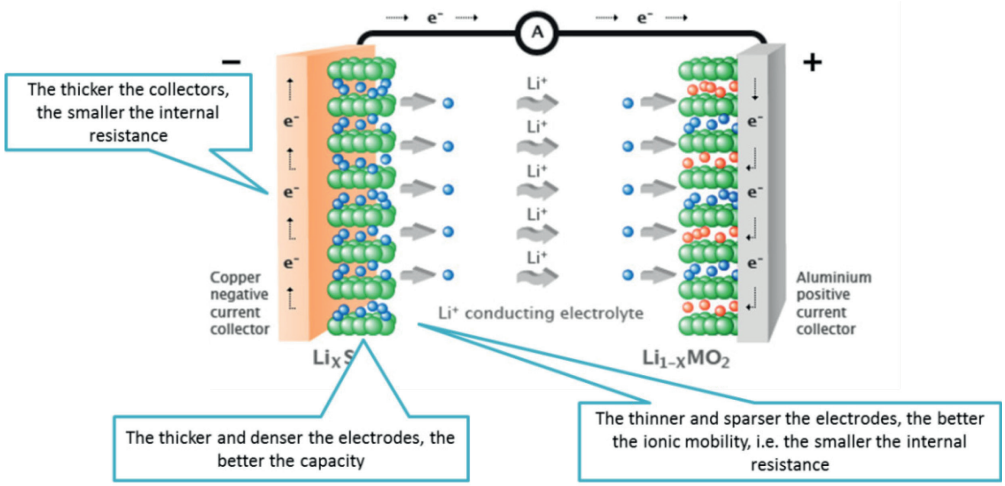

Figure 1.10: Typical structure of a Li-ion battery

In addition, the requirement for high specific capacity generally restricts choices to compounds containing first-row transition metals (usually $Mn, Fe, Co, and\ Ni$). Environmental and toxicity

[7] Power density and specific power is the power per unit volume or weight, respectively, often expressed as W/l or W/kg.
[8] C ratio: current over capacity ratio.

concerns have precluded the development of most V- or Cr-containing materials, although electroactive compounds containing the metals exist. The Figure 1.10 shows a typical structure of the Li-ion battery. It is a dual intercalation system, in which both the cathode and the anode have structures that allow reversible insertion and extraction of the lithium cations. In principle, the choice of the cathode greatly affects the performance and cost of Li-ion battery, because power density is defined by internal resistance. However, the thicker and dense the electrodes, the better the lower the internal resistance, this gives a better capacity. Although, the thinner and sparser the electrodes, the better the ionic mobility, means the higher the power density. For instance, the lithium titanate based battery (LTO) offers advantages in terms of power and chemical stability, for the reason that this technology lacks a solid electrolyte interface (SEI)[9], LTO-based batteries also have a lower cell voltage of around 2.5 V.

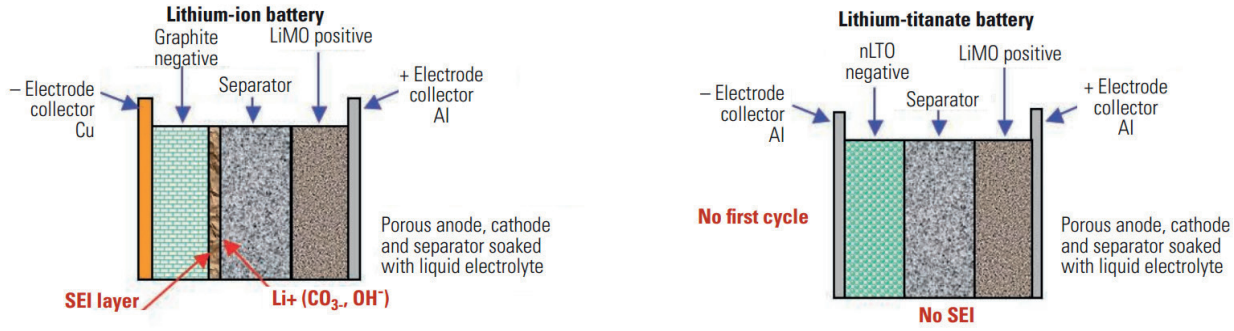

Figure 1.11: Comparison of a typical lithium-ion battery with a new lithium-titanate battery [8]

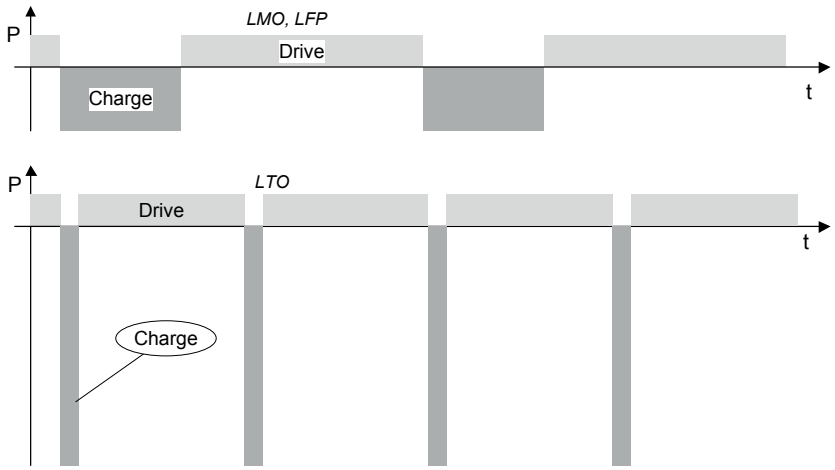

Figure 1.12: Charging-driving ratios for existing and proposed battery electro chemistries

[9] SEI: Solid Electrolyte Interface is a very thin (nanometer scale) layer formed on a lithium or lithiated graphite anode, which develops upon reaction with certain kinds of electrolytic solutions. The SEI is a specific kind of reaction layer that is ionically conductive but electronically insulating. It passivates the electrode, preventing further reaction with the electrolytic solution and allows reversible operation of the device.

Moreover, in the framework of on-board energy storage, one of the main problems is that the charge and discharge processes of a battery are asymmetrical in time, meaning that a sustainable recharge takes usually much more time than the discharge [15], as depicted in Figure 1.12.

In Figure 1.12, the LTO battery can be charged and discharged significantly more often than conventional lithium-ion batteries (LMO, LFP, etc.) because of the absence of particle fatigue, which plagues materials such as graphite. For instance, one of the well-known applications is the clean city smart bus in Geneva; it has been realized for Trolleybus Optimisation System Alimentation (TOSA) project [30]. In fact, it is the first full electric articulated bus that runs without overheat lines in Geneva, between Geneva Airport and Hôpitale.

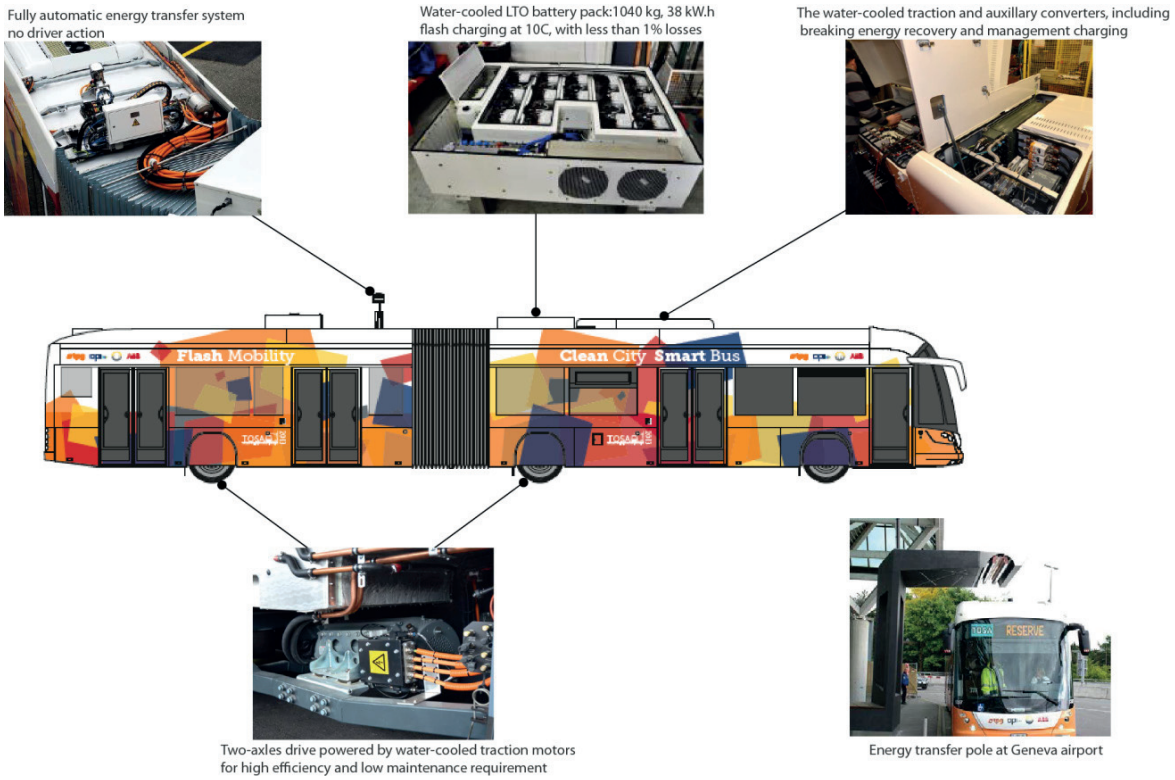

Figure 1.13: TOSA: Trolleybus Optimisation System Alimentation [30].

Figure 1.13 illustrates a description of the trolleybus. It is an impressive innovation which looks sustainable for the future mobility for public transportation. This innovative method reduces the need for overhead lines and minimises the infrastructure and operational cost of electric public transport.

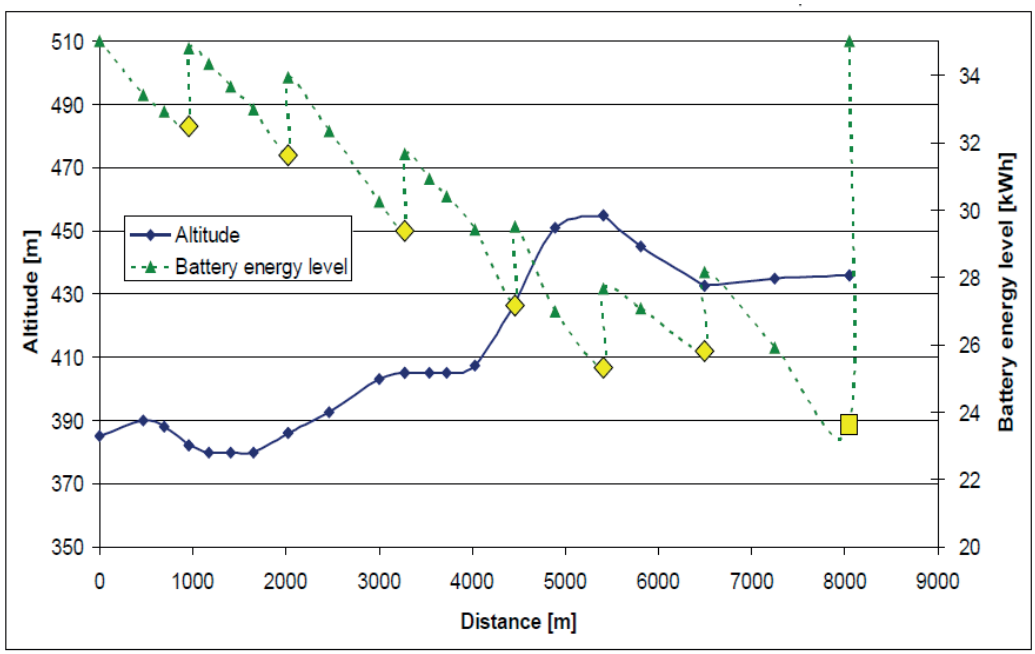

Figure 1.14: Battery energy level versus driving cycle profile, between Hospital and Geneva airport [30]

Figure 1.14 shows the load profile of the trolleybus during the working days. Depending on the direction, the energy consumption varies.

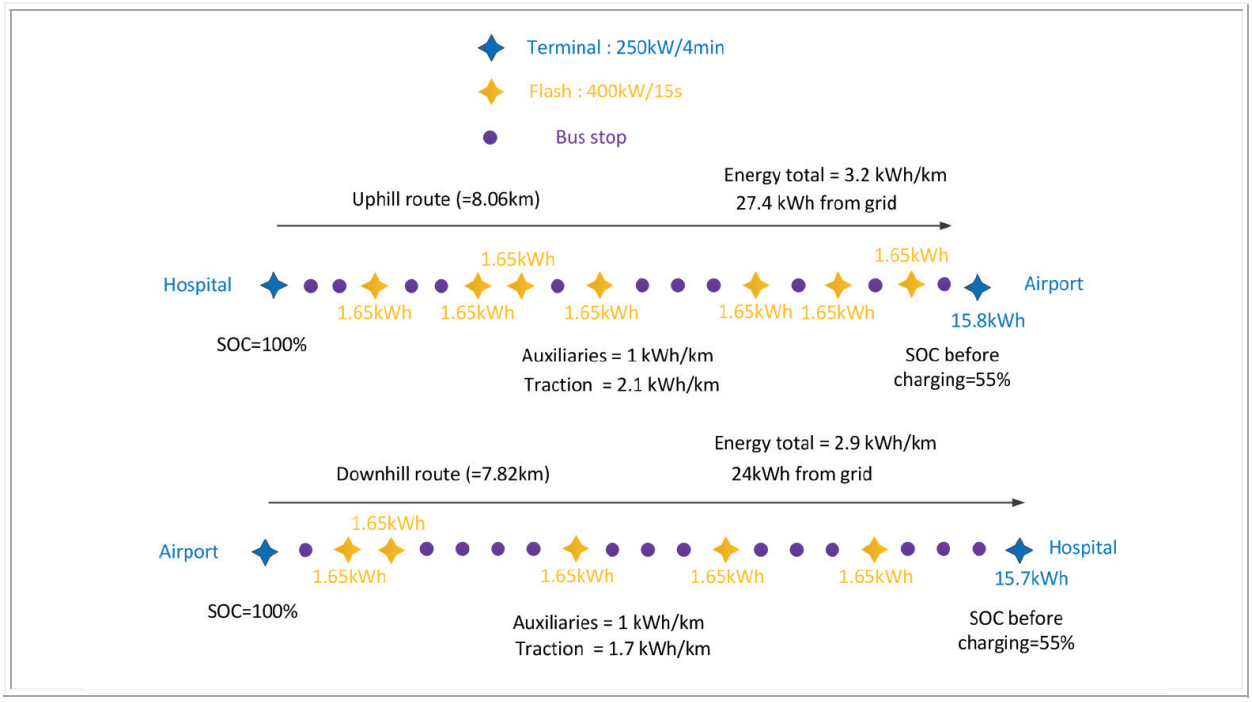

Figure 1.15: Energy consumption between Hospital and Geneva airport [30]

Figure 1.15 resumes the energy consumption of the trolleybus during the working days where it is seen that the energy consumption depends on the direct of the bus (Uphill route or downhill route). This approach is really smart because it demonstrates the performance of the trolley-bus in charging mode and in driving mode.

It should be noted that, according to the TOSA team, the great challenges that they were facing was the system integration; meaning, EVs require a very high compact design. The bus consists of:

- Fully automatic energy transfer system, meaning no driver action,
- Water-cooled lithium-titanate battery pack of 1040 kg , for 10 years lifetime,
- Water-cooled traction and auxiliary converters, which include respectively the energy recovery during the regenerative braking and the management charging.

Two co-axles drive powered by the water traction motors, for high efficiency and low maintenance requirement: power Max of 2*120 kVA, max speed up to 85 km/h.

Furthermore, TOSA stated that the lithium battery based on lithium titanate seems to give the best trade-off between power and energy densities, life cycles, cost and reliability. At the beginning of the project they were planning to implement supercapacitors, however the nLTO battery can handle the high power charge and has higher energy density in comparison to supercapacitors. In fact, it is a modified lithium-ion battery that uses lithium-titanates nanocrystals (nLTO) on the surface of its anode instead of carbon [31].

This gives the anode a surface area about 100 square meters per gram, compared to 3 square meters per gram for carbon, allowing electrons to enter and leave the anode quickly. This makes ultrafast recharging possible and provides high currents when needed. Conventional lithium-ion batteries can be typically charged about 1 000 times before they are no longer useful (about 3 years), whereas, cells using nLTO materials can achieve over 25 000 charge and discharge cycles (more than 20 years). In fact, the use of nano-size lithium titanate oxide (nLTO) to replace graphite makes a "zero strain" material. This means the material essentially does not change shape upon the entry and exit of a lithium ion into and from a particle. The reason is that nLTO material has a three-dimensional crystal structure which contains sites for lithium atom inclusion that are roughly the same size as the atom. Therefore there is virtually no stress or strain involved during the charge and discharge process.

1.3.6 The system integration challenge

In order to assess this high integration architecture, the e-drive and charger integration of the PEUGEOT B9E partner van version is shown in following Figure 1.16 where it is emphasized that the high integration is required in order to enhance a very high power density. In fact, this electric vehicle has been formerly used for the UFCEV project. In this figure, the dashed line represents the inverter and the charger which is designed to be very compact on the top of the power driveline.

Therefore, additional issues regarding the battery and the power conversion specifications are the fact that the trend goes to downsize the power conversion; this exerts a strong thermal stress upon the whole powertrain.

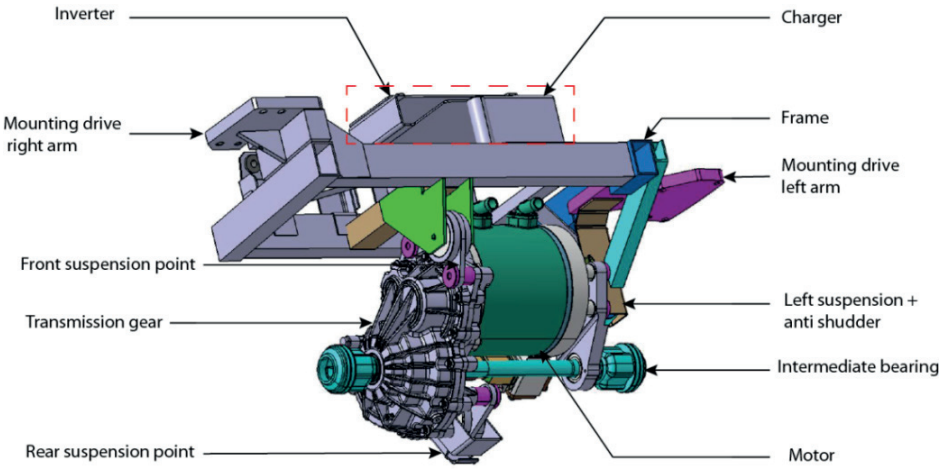

Figure 1.16: E-drive integration of PEUGEOT Partner van version (Courtesy UFCEV project)

	Technology challenges	semiconductors
Inverter	▪ High power density ▪ High voltage and high current ▪ Temperature capability and cooling ▪ Lifetime in harsh environment ▪ Weight and size	▪ IGBTS ▪ Diodes (Si, SiC) ▪ HybridPAcks ▪ Gate drivers
Battery management units	▪ Extension of battery life time ▪ Monitoring and control of battery ▪ Safe operation	▪ Discrete MOSFETs ▪ Battery management integrated circuit
Charger	▪ Efficient AC/DC or DC/DC conversion ▪ Handling of high currents ▪ High switching frequency (>40 kHz) ▪ Safety and communication	▪ Discrete MOSFETs ▪ Discrete IGBTs ▪ Discrete diode (Si, SiC) ▪ Easy PACKS
	Plug-in hybrid vehicle	Battery electric vehicle
Vehicle Specification requirements	▪ Size due to limited space in the existing vehicle designs ▪ Increased temperature capability to eliminate a separate cooling loop	▪ Drive train efficiency due to high battery cost ▪ Weight as part of overall efficiency

Table 1.9 The key requirements for innovative electric vehicle solutions [32].

The heat must be removed locally in order to avoid a heat propagation, for instance, fast switching devices such as SiC MOSFET should have a thermal management unit because they can lead to

premature failure of the whole power conversion and powertrain. The key requirements for innovative solutions can be summarised in Table 1.9, where it is shown that the key requirements for electric power conversion include a high power density, a high efficiency as well as high ruggedness and reliability, while EV battery chargers require a universal input; the flexibility of one phase / three phase supply and inherent safety concepts play a key role hereby [32], [33].

In addition, the battery packaging remains a last challenge for the battery designers. In fact, according to a specified threshold voltage, the battery management system (BMS) should be able to detect the overcharged and/or undercharged battery cell(s) as well as the overheated cell(s). Then the BMS automatically gives the appropriate reference to the controller and the state machine of the system.

Furthermore, it is generally agreed that the diversification in the charging standards, both seen from the existing fast charging stations as well as from the charge profile of the on-board battery breaks the integration of EV in the market. As a result the EV should be compatible with large range of voltage and current ratings.

This is the reason why this thesis is dedicated to a design of new architecture of electric vehicle which can answer those requirements. However, a critical requirement, especially with the off board charging system is the establishment of a common interface standard between the charger and the vehicle. Some company like ABB support CHAdeMO, DC fast charging, allowing every compatible vehicle to charge at a rate suitable to the individual vehicle's battery system characteristics. This standards is enclosed and supported by increasingly widespread group of organisations, including multiple leading vehicle original equipment manufacturers [34]. This leads to the monopolisation of the electric vehicle markets. On the other hand, a major part of SAE, previously known as the society of automotive engineers, are willing to integrate a bidirectional charging through the standard distributed generation (DG) with renewable energy. Even though, an optional external adaptor to charge from CHAdeMO has been proposed recently, the vehicles owners are faced with limited compatibility with the existing charging station infrastructures.

The electric vehicle concepts are facing a bottleneck. In short, the important problems facing electric vehicles are the possibility of short time charging as well as the compatibility with the available charging infrastructure (DC or AC sources), both seen from the battery itself as well as from the local supply system. Therefore, the research aims at providing viable solution for broad a universal and flexible integrated charging system. This concept is designed for a large range of charging infrastructures; from AC household basic supply to AC or DC ultrafast changing.

1.4 Conclusion

It is well-known, that ultra-fast charge stations (UFCS) as well as high autonomy cars are required to increase the penetration of the electric vehicles in the electro-mobility. However, the EVs suffer from generally too much time for charging and they are definitely limited in autonomy due to the limited power and energy densities of their embarked battery. The massive deployment of fast charging stations is believed to bring a prospective penetration of EV in the market. However the diversification in the charging standards, both seen from the existing fast charging stations as well as from the charge profile of the on-board battery, breaks this future perspective.

In fact, electrical energy is distributed with alternating current (AC), whereas, batteries are a direct current (DC) sources. Therefore, power electronics are required to convert the alternating current into direct current for charging batteries. In the framework of electric vehicle applications, this could be off-board or on-board chargers. EVs require a high power as well as a compact charger. High power chargers are often implemented off-board because of size, whereas low power chargers are regularly embarked into the cars. A combination of off-board and on-board chargers are often implemented in order to achieve the appropriate compatibility regarding the voltage and the current ratings between the AC grid and the EVs batteries.

In the framework of Ultrafast Charging of Electric Vehicles (UFCEV), a direct connection to the medium voltage grid facility would be an appropriate solution in order to alleviate the power demand [8]. However, this leads to a demand of a huge change in the existing public infrastructure such as installations of medium voltage transformers and change in distribution line cables, which will cost a lot for governments. A similar scenario is seen in the railway application where the railway lines facilities have to be changed in order to accept the high speed train the so-called TGV (Train à Grande Vitesse).

To decrease this Ultra-Fast Charging Station (UFCS) impacts on utility grid, the load must be at least partially decoupled from the mains grid source. This can be done by implementing energy storage elements, which act as buffer between the EV and the grid. However, The IEC 60851 standard, applicable for conductive charging systems, defines four charging modes, as given in Table 1.3 and Table 1.4.

Nevertheless, a discrepancy between the above mentioned standard and the market situation exists. Usually the EV manufacturers prefer to sell their products in set with a Mode 1 one-phase on-board charger; as standard household 16 A sockets are used, which are de-rated to 10 A … 12 A at constant load, the charging power is even more limited, to 2.3 kW … 3.6 kW. Thus a small-sized EV with a 16 kWh traction battery would need at least 6 hours to fully recharge. The Mode 4, using off-board chargers, has been implemented by the CHAdeMO consortium [16] and Tesla company. But for today, its charging current is limited up to 120 A by the used connector, which enables to recharge a commercial EV within 20 min … 30 min depending on the battery capacity.

As for Mode 3, the manufacturers have not yet reached an agreement on the standard connector, but the increased charging rate is achieved by reversing the power flow in the traction inverter and using motor windings as smoothing reactors, thus the charging power can be nearly equal to the rated driveline power. For instance, the chameleon charger which is used by the Renault Zoé is a combined charger for up to 43 kW. However, the charging current is limited at the motor nominal current.

Chapter 2 Optimizing electric vehicle driving-recharging time ratio a under limited grid connection

"Since the ecological movement appeared on the scene in the 1970s, an irreconcilable conflict has divided those who want to protect nature, and who call for reductions in mobility, comfort and growth, from those in business and industry who defend people's employment and purchasing power. Today, for the first time, this cleavage can be bridged, and the answer is clean technology. At last, technologies exist which can simultaneously protect the environment in a cost-effective manner and bring profits to companies."

Bertrand Piccard, solar impulse pilot

2.1 Introduction

Recently, Renault Zoe distance world record of 1‘618 km in 24 hours has been reached with 18 times fast recharging with 43 kW and about 9 hours of standing still during charging. This results in an average consumption of 20 kWh/ 100km and a charge/range ratio of 1:2.

Figure 2.1: Renault Zoé

This is an exceptional achievement, and it highlights the performance of both charging and driving of the Renault Zoé. It also showcases a great approach for testing electric vehicles because it includes the fast charging as well as the driving process. In the framework of the UFCEV project, for the demonstrator, the partners have planned to beat this record; therefore many investigations have been undertaken based on an ultra-fast charging car battery, which would allow charging the energy for driving another 100 km in 5 min. This is technically feasible based on today's existing cell chemistry if limitations for life cycle requirements are allowed. The weight of the total battery cells is limited to 380 kg, and the packaging factor is 1.4. The on-board battery is designed to handle the high power charging (210 kW). In addition, the minimum energy content of 80% DOD is used in order to operate the battery in the linear window. On the other hand, a transportable ultra-fast charging station has been realized (see appendix), with a buffer battery capacity of 29 kWh. The ultra-fast charging station with a charging power of 210 kW allows the charging of the car battery in 5 minutes. Unfortunately the word record has not been realized for some technical issues. However, the approach for designing the ultra-fast charge car battery is used in this thesis. In fact the method uses an increase of the range flow-rate, which is the driving distance augmentation per time unit of recharge, expressed in km/min or km/h. This depends on the EV’s battery power density and the overall efficiency of the EV’s powertrain.

In this chapter, we will start with the specification of the required handle EV power based on a typical model of electric vehicle; this gives us the needed energy for achieving the highest performance in terms of range flow rate in km/min during 24 hours. Then, the EV embarked battery can be specified. This requires a simulation based on a dynamic behaviour of the electric vehicle during the driving mode. Also it required a specification of the charging profile. Finally, the specification of the Flex-EV battery parameters can be deduced.

2.2 Specification of the required EV power and energy

2.2.1 Studied EV's model

The design of an EV ultrafast charging compatibility evaluation tool starts with creating a generic EV model, composed of the main battery and traction subsystems (Figure 2.2).

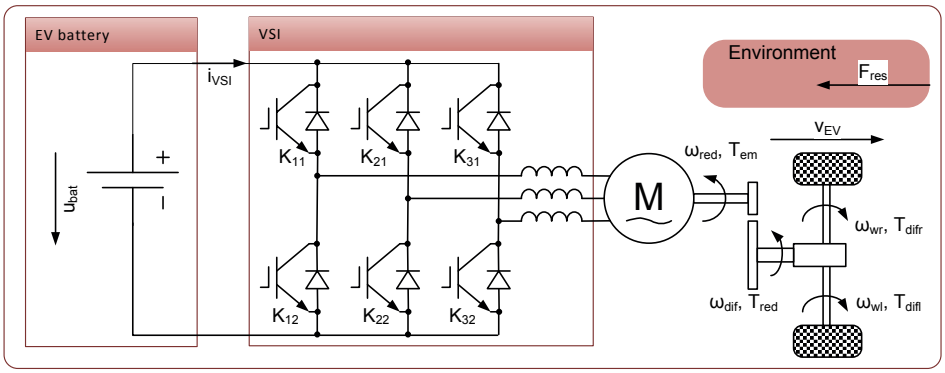

Figure 2.2: Studied EV model

In the battery subsystem, the cell modules supply the vehicle with electric energy. Braking energy is totally recovered during deceleration. The traction subsystem is composed of an electric machine and a full bridge voltage source inverter (VSI). Transmission gear is used to adapt the speed ratio between wheels and the motor shaft, followed by a mechanical differential changing the speed ratio between the two traction wheels.

The equivalent mass of the vehicle m_{eq} comprises, besides the actual mass m_{EV}, the inertia of rotating parts, expressed by additional inertia percentage γ = 2 %...5 % for road vehicles.

$$\begin{cases} m_{eq} \cdot \dfrac{d}{dt} v = F_{tot} - F_{res} \\ m_{eq} = m_{EV} \cdot (1+\gamma) \end{cases} \tag{2.1}$$

The resistive force F_{res} posed by the environment, is a sum of three basic components:

1) rolling resistance, determined by vehicle's mass and tyre friction;
2) aerodynamic resistance, determined by vehicle's geometry and velocity squared;
3) slope resistance, determined by the vehicle's mass and slope angle.

The difference between total force F_{tot} delivered by the drivetrain and three-component resistive force F_{res} builds up the so-called dynamic force, accelerating or decelerating the vehicle in dependence of the sign.

2.2.2 Baseline EV parameters

In order to define a baseline parameter for the Flex-EV, a 5 seats passenger car has been chosen because it is the most common one in mobility. This paragraph is therefore dedicated to specify the relevant parameters for computing the required power and energy with respect to the previous profile test. Of course, it is possible to study also the vehicle dynamic model; however this is almost similar to the Internal Combustion Engine (ICE) cars.

Parameters	**Electric car**
Estimated weight	1700 kg
Tire	254/40 R18 front and 295/35 R18 rear
Drag coefficient	0.29
Front area	2.47 m^2
Useful energy	8.4, 11.2, 16 [kWh]
Reference speed	80, 100, 120, 140, [km/h]
Efficiency	η1 = 0.93, η2 = 0.98

Table 2.1: The EV study parameters

Table 2.1 gives the parameters for an EV. Those parameters allow computing the required power/energy for driving at a given speed. In this table, the conversion efficiencies η1, η2 represent respectively the efficiency of the tires and the efficiency of the mechanical transmission (driveline). In short, Table 2.1 is used to compute the total drag force of the car for different speeds. However, the methods are explained in the following paragraph in order to have a better insight of the simulation results.

2.2.3 Charge profile

It is generally agreed that it really difficult to measure the stored charge in the battery, however it is possible to estimate it by measuring the voltage and the current. Therefore, the stored charge is predictable; therefore it becomes important to known the trajectory of the SoC according to the measured voltage and current.

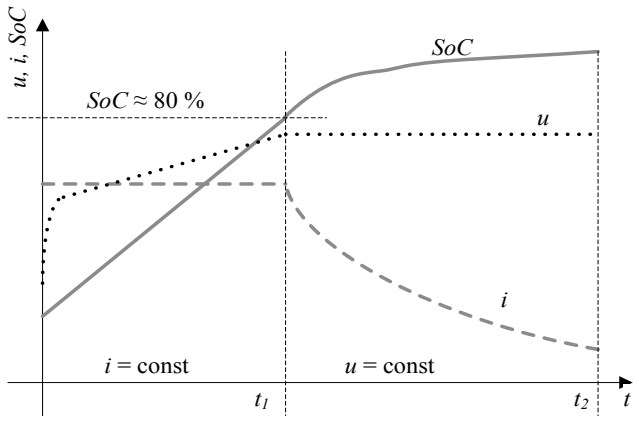

Figure 2.3: A typical battery charging

Figure 2.3 illustrates a typical battery charging profile. Basically, it consists of two stages:

- The first stage corresponds to the constant current (CC), while the voltage is increasing linearly with the state of charge (SoC)
- The second stage corresponds to the constant voltage (CV), while the current is decreasing until the battery is fully charged

The maximum state of charge value at high charging rates is obtained by utilizing only the constant current part of the battery charging curve (Figure 2.3), where the charging is interrupted at the terminal voltage cut-off level in order not to damage the battery. The remaining 20 % can be delivered at constant voltage; this process has, however, an asymptotic characteristics [35].

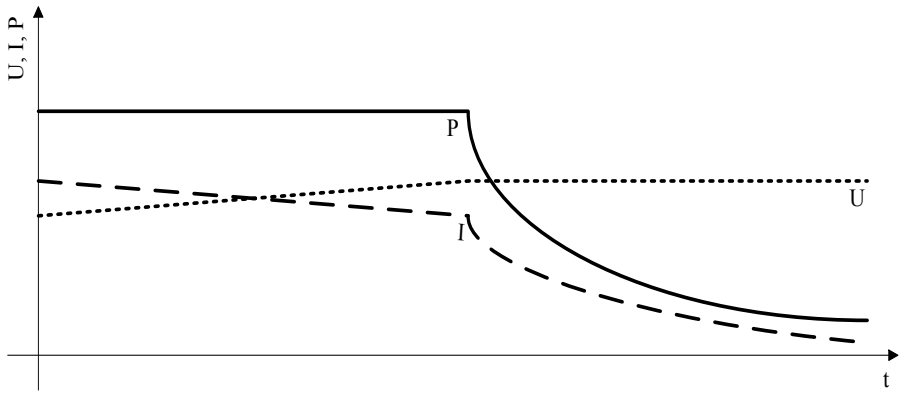

Figure 2.4: Example of a constant power – constant voltage charging curve

Figure 2.4 illustrates the typical example of the charging profile with constant power and constant voltage. To avoid excessive inrush currents, the charger output voltages is equalised with the battery voltages prior to charging. This is done in the precharge state. For instance, a three-pole or three single-pole contactors between the charging station and the EV are often served to that purpose additionally to mechanical isolation.

In this case, the EV charging current can be expressed as:

$$\begin{cases} I_{EV} = x_t \cdot I_f \cdot t & \text{if } 0 \le t \le t_s \quad \text{and start mode} \\ I_{EV} = I_f & \text{if } t_s < t \le t_s + t_{CC} \quad \text{and CC mode} \\ I_{EV} = f(P,U,t°) & \text{if } t_s < t \le t_s + t_{CP} \quad \text{and CP mode} \end{cases} \tag{2.2}$$

The variable x_t in Equation (2.2) represents the current rise rate, which can be defined in the upstream supervisory controller. For example, if the final charging current I_f = 600 A is to be reached within 3 s, x_t = 200 A/s. As by the Flex-EV, the presence of isolating contactors with grounding detection between the EV and the charger helps to equalise the splits battery.

It should be noted that the operating stage shall be set by a flag, sent by the supervisory controller, which determines the transitions between these two stages.

In the frame work of the MMC with split integrated energy storage the upper arms and the lower arms are performed by a double star cascaded submodules cells. However the common mode current is the only component which contributed to the charge or the discharge of the upper and the lower arms battery submodules. The common mode current can be divided into parts; I_{o_up} and I_{o_low} which represent respectively the average circulating currents in three phase upper and lower arms. The maximal value for I_{Bat_max} is defined by the available charging power P_{ch} and minimal voltage across the charging terminals

$$I_{bat,\max} = \frac{P_{ch}}{U_{bat,\min}} \tag{2.3}$$

In addition, the CMMC charging has two working modes:

1) current source mode with setpoints for I_{o_up} and I_{o_low} ;

2) voltage source mode with setpoints for U_{Bat_up} and U_{Bat_low} .

The charge balancing between the upper and the lower arms is done in the level of the common mode current injection control. More detail can be seen later in chapter 4.

2.2.4 Charging time versus driving time

To shorten the recharging time t_{ch} in comparison to the actual driving time t_{dr}, their values must be expressed first. The driving time $t_{dr,i}$ from charging spot $i-1$ to charging spot i depends on the rated battery capacity E_{EV} (expressed in kWh), the energy consumption at given speed E_{100} (expressed in $\mathrm{kWh}/100\ \mathrm{km}$), the vehicle's road speed v (expressed in $\mathrm{km/h}$), the initial state of charge after previous recharging $SoC_{start,i-1}$ and finally the state of charge before next charging $SoC_{stop,i}$. Therefore the driving time can be expressed as:

$$t_{dr,i}(v) = E_{EV} \cdot \frac{SoC_{start,i-1} - SoC_{stop,i}}{E_{100}(v) \cdot v} \tag{2.4}$$

The charging time $t_{ch,i}$ at the charging spot i depends on the EV energy E_{EV}, the $SoC_{stop,i}$, the obtained state of charge $SoC_{start,i-1}$ and the available charging power $P_{ch,i}$ (for simplification the charging power is constant):

$$t_{ch,i} = E_{EV} \cdot \frac{SoC_{start,i} - SoC_{stop,i}}{P_{ch,i}} \tag{2.5}$$

Equation (2.4) is rather a hint for economic driving, as the longest range is achieved by a proper selection of driving pattern, departing with the maximum available charge and continuing until the

full depletion of the battery. As self-evident and expressed by (2.5), the charging time depends on the available charging power and the battery capacity utilization.
The average speed v_{av} is defined by the road speed and the times t_{dr} and t_{ch}. It can be analytically expressed, that the same average speed can be kept while charging more often and utilizing only the partial capacity of the battery:

$$v_{av,i} = v \cdot \frac{t_{dr,i}}{t_{dr,i} + t_{ch,i}} \tag{2.6}$$

The cells configuration plays an important role in the calculation of the power losses. The power loss is given by the following equation:

$$P_{loss,EV} = \frac{n_{cell,s}}{n_{cell,p}} \cdot R_{cell} \cdot i_{ch}^2 \tag{2.7}$$

In (2.7) $n_{cell,s}$ is the number of serial cells in the battery whereas $n_{cell,p}$ is number of cells in parallel strings and i_{ch} is the charging current. In fact, i_{ch} depends on the EV battery coulomb capacity q_{EV} which is expressed in Ah, on the objective charging time t_{ch} which is expressed in minutes and on the available reachable SoC range ΔSoC_{EV}:

$$i_{ch} = \frac{q_{EV}}{t_{ch}} \cdot 60 \cdot \Delta SoC_{EV} \tag{2.8}$$

It should be noted that the manufacturers often prefer to demonstrate the relative charging and discharging currents, i.e. the current and coulomb capacity ratio instead of time:

$$i_{ch}^* = \frac{i_{ch}}{q_{EV}} \tag{2.9}$$

For the equation (2.9), the right dimension should be h^{-1}. Battery manufacturers, however, refer to this value as C-rate, giving e.g. the characteristics for 0.5 C, 1 C, 10 C etc. To avoid confusion with the unit for electric charge – the coulomb – this expression should not be promoted.

$$i_{ch} = \frac{i_{dch} \cdot t_{dch}}{t_{ch}} \tag{2.10}$$

The perspective on-board battery is composed of three strings of serial cells. Due to differences between the charging and discharging currents, the losses of those processes were separately calculated as follows:

$$\begin{cases} E_{ch\_losses} = R_{cell} \cdot {i_{ch}}^2 \cdot t_{ch} \\ E_{dch\_losses} = R_{cell} \cdot {i_{dch}}^2 \cdot t_{dch} \end{cases} \tag{2.11}$$

In order to calculate the efficiency, firstly the internal energy accumulated in the cell was estimated based on the nominal parameters and losses during discharge at the nominal current:

$$E_{cont} = (u_{rated} \cdot Q_{nom} + R_{cell} \cdot {i_{rated}}^2) \cdot \Delta SoC \tag{2.12}$$

2.3 Simulation

The well-known New European Driving Cycle (NEDC) is used by EV manufactures (Mitsubishi, Nissan, BMW, Renault, Peugeot, etc.) for attesting the performance of electric vehicles. However, it does not take into account the charging time. Therefore, the Nissan Leaf and the Renault Zoé initiate the new approach for EV performance evaluation. The idea consists of driving the longest distance in 24 hours.

2.3.1 The tentative of the 24 hours round trip with electric vehicle

The approach consists of an electric road trip during 24 hours. In fact, it aims to drive the longest distance as possible during 24 hours. Until today the record is owned by Renault Zoé. 18 times charging in 24 hours and a range of 1698 km. In this context, a simulation along a Nardò track has been carried out in order to assess the required energy.

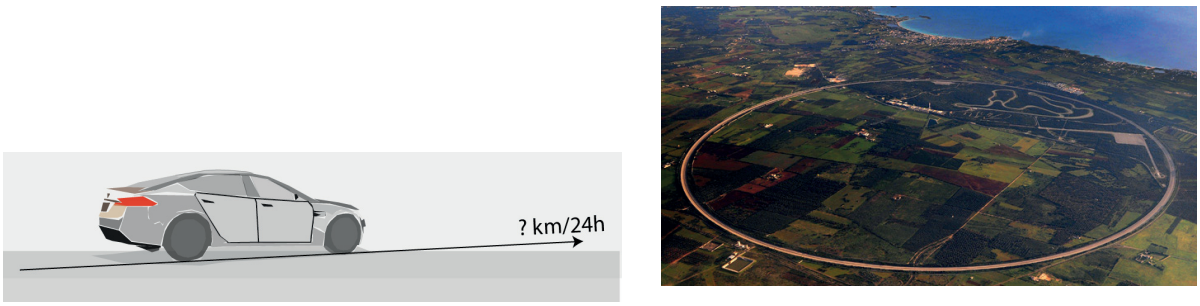

Figure 2.5: 24 hours road trip on the Nardò Track

Thereafter, we have implemented the profile of Nardò track in the Model-Based Design in order to compute the range. In fact, the geographical coordinate of the Nardò track has been gathered from Google Earth™. This allows deducing the track profile and for instance the slope which has a strong relationship to the resistance forces of the electric vehicle during testing.

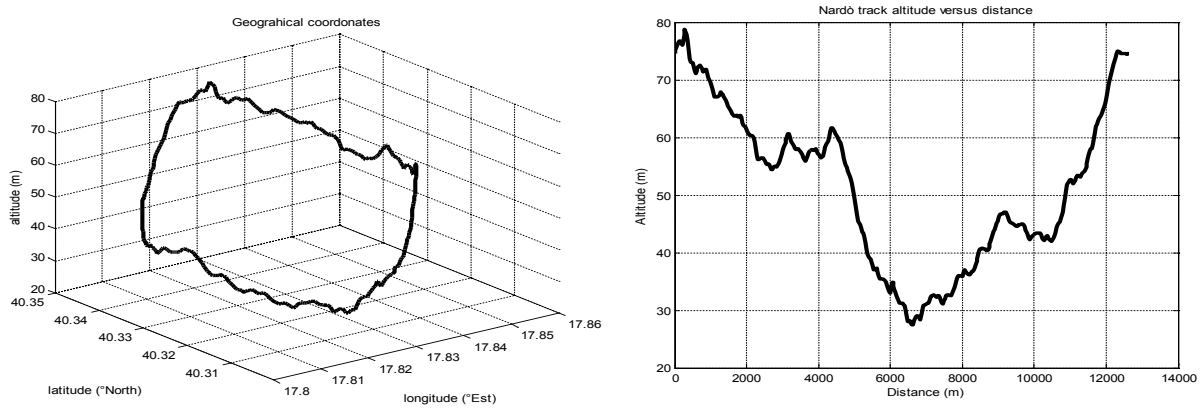

Figure 2.6: Nardò geographic coordinated and altitude

Figure 2.6 shows the Nardò geographical coordinated on left and its corresponding altitude on the right. Therefore, the slope is deduced. Regarding the power flow, the traction power is positive when the power flows from the battery to wheels, whereas the traction power is negative while the kinetic energy from wheels is regenerated into the battery.

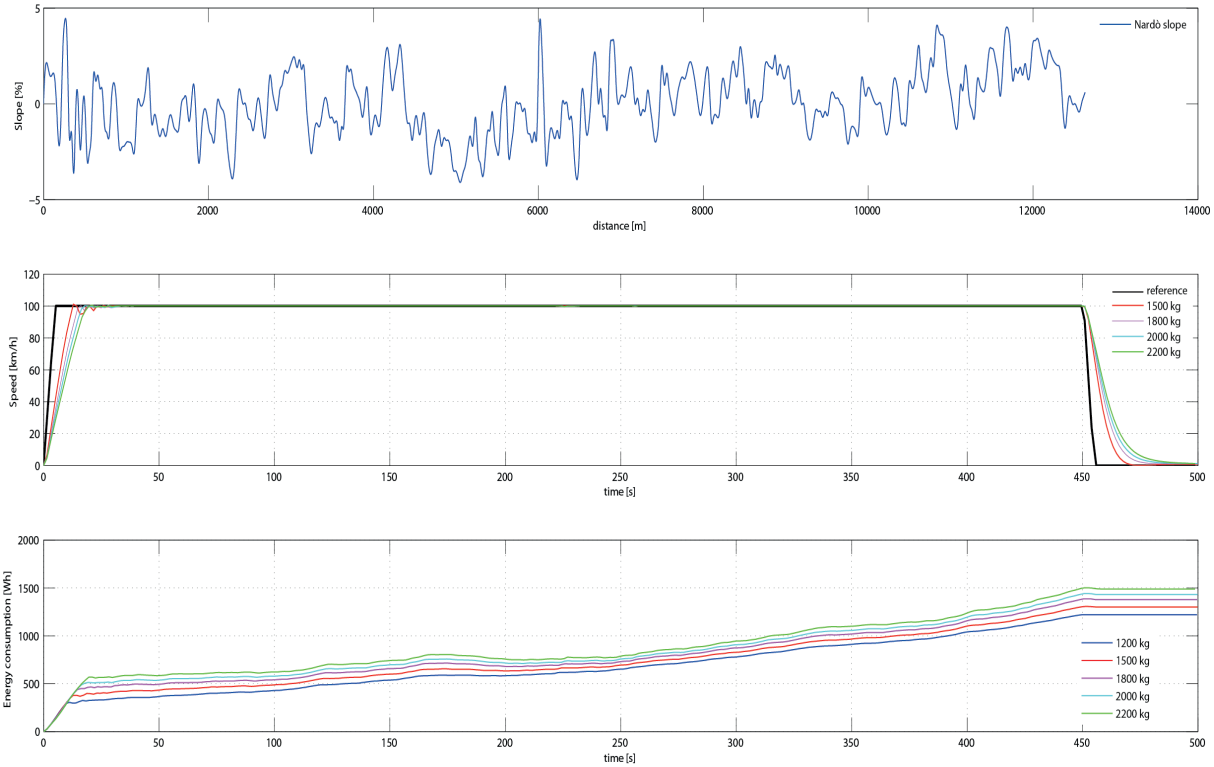

Figure 2.7: Energy consumption in function of the EV mass at cruise speed of 100 km/h for on cycle

Figure 2.7 shows a simulation of an electric vehicle driving along the Nardò track. It is shown that the energy consumption has a strong relationship with the mass of the car; the more weight the car has the more the energy consumption increases.

2.3.2 Description of the test

The teams of the UFCEV partners investigate the possibility for realising a 24-hours electric vehicle road trip in order to validate the performance of the UFCS in real life. The objective consists of driving the longest distance as possible during 24-hours. The UFCS will be placed close the track in order to charge the vehicle cyclically, a cycle is consisting of two times, the one for driving and the second for charging. Then, the cycle is repeated during 24 hours.

Therefore, the best compromise between charging time and driving time has to be found in order to achieve the longest distance. The travels will last during 24 hours. Figure 2.8 illustrates the 24 hours trips based on ultra-fast charging of 5 min and a driving time of 55 min. The travels will last

during 24 hours, the limited charging current of the embarked EV battery at 10 C is considered as well as the impact into the grid facilities.

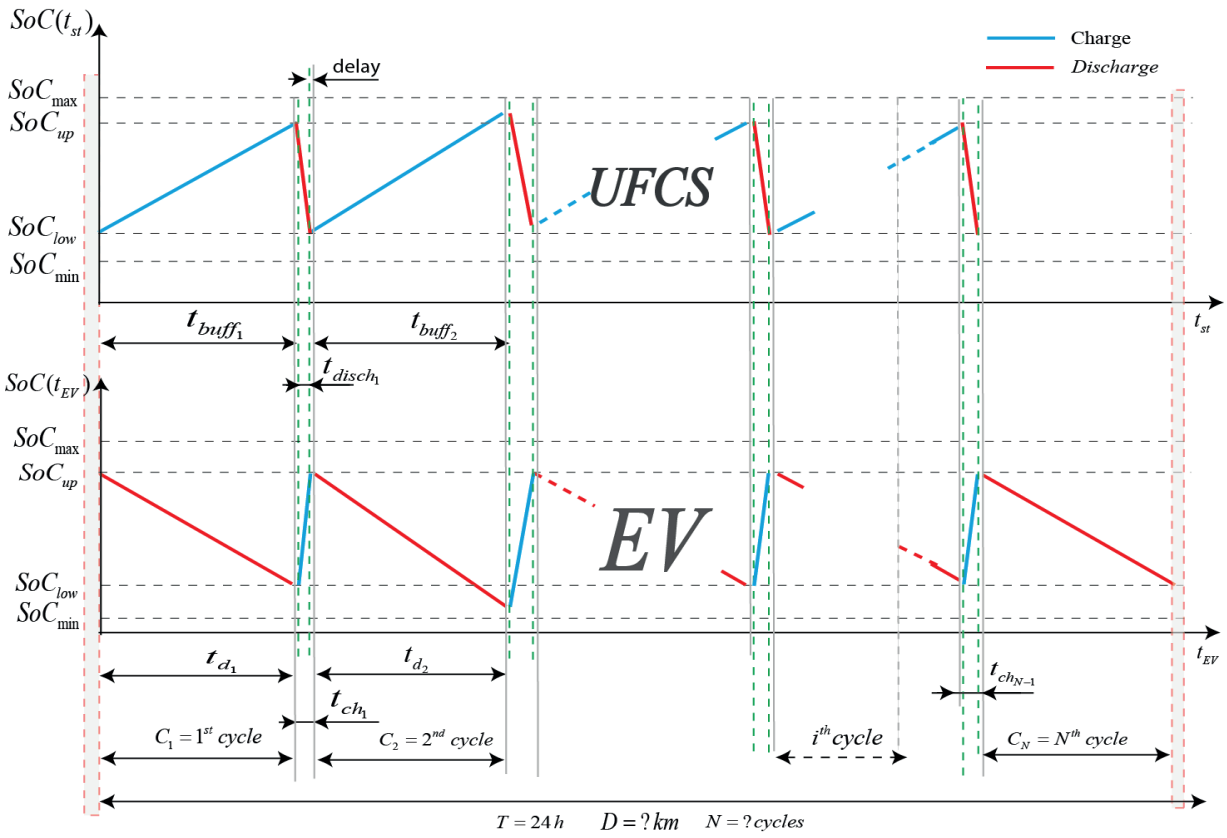

Figure 2.8: Range, cycles, and EV driving time [10]

However, it is assumed that, there are equal dead times of one minute during entering in the charging station, as well as one minute for the exit, that is the reason why of the plus 2 delay in Figure 2.8 for each cycle. The unbalance of the state of charge is neglected; meaning the amount of energy put into the car during charging time is always the same and the vehicle is running at constant power during the driving time.

10

N: the cycle number during 24 hours,
t_{ch}: charging time including the delay due to plug and unplug of the charge as well as the entering and the exit for each cycle.
t_d: driving time in minutes
E_{EV}: useful energy onboard in the car.
E_{st}: the output energy from the buffer terminals.

E_{gr}: the energy taken from the grid: $\begin{cases} E_{gr}^{16} = \sqrt{3} \cdot 16A \cdot 400V \cdot t_{ch} / 60 \quad [kWh] \\ E_{gr}^{32} = \sqrt{3} \cdot 32A \cdot 400V \cdot t_{ch} / 60 \quad [kWh] \end{cases}$

2.3.3 Simulation results

It is well-known that the most efficient cruising speed depends on: one hand, on the dynamics behaviour of the car, and on the other hand, on the power density of the embarked EV battery. Figure 2.9 shows the possible range of the car according to the speeds. It shows that it is possible to reach 3000 km in 24 hours using 16 kWh of energy with an average speed of 125 km/h.

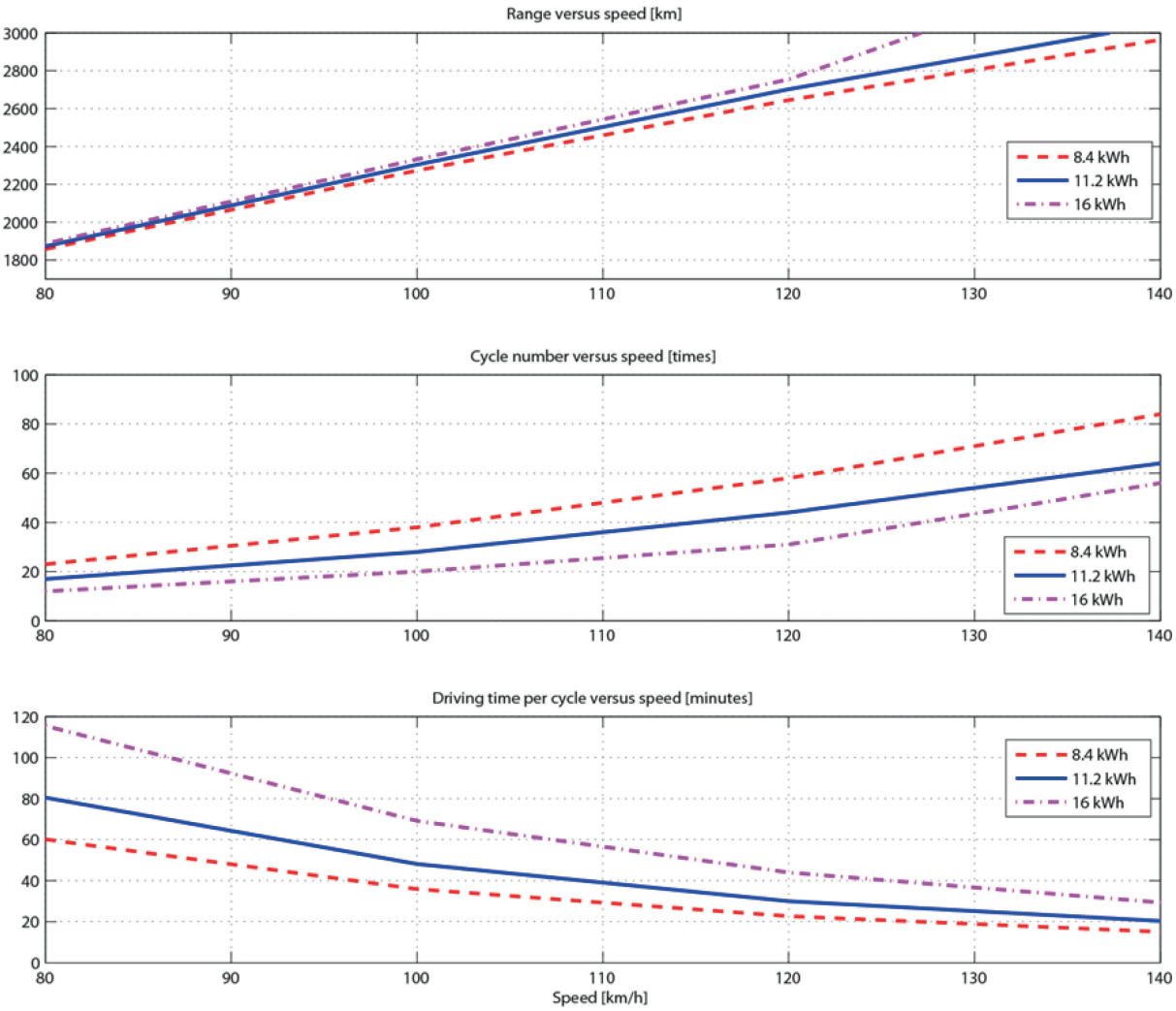

Figure 2.9:The possible range in km and driving time per cycle in min for different cruise speeds

However, the energy consumption is increasing drastically when the speed is increasing. This causes a reduction of the driving time. Therefore, it requires many cycle in comparison to the energy consumption at low speed around 85 km/h cycle numbers.

It should be noted that it is trivial to see a flexion of the speed-energy curve at some point because the energy versus speed has a U shape curve. In other word the energy is proportional to the square of the speed

Table 2.2 summaries the simulation results, where the charging power is 96 kW at input of the EV, including whole efficiency conversion during EV charging mode. This table emphasis the range and

the charging number during 24 hours. This result is utterly important for those who want to validate the performance of their electric cars, because it is based on real data. The approach seems to be the best method for optimising EV driving-recharge time ratio under limited grid connection.

Speed [km/h]	Range [km]	Consumption [km/ 100 km]	t_d [min]	km in 24-h	Recharge [times]
	For embarked energy equal to 8.4 kWh				
80	80.17	10.46	60.14	1855	22
100	59.77	14.03	35.87	2267	37
120	45.38	18.47	22.70	2636	57
140	35.14	23.84	15.08	2948	83
	For embarked energy equal to 11.2 kWh				
80	107.3	10.43	80.50	1871	16
100	80.21	13.95	48.13	2300	28
120	61.06	18.31	30.00	2695	43
140	47.45	23.56	20.35	3045	63
	For embarked energy equal to 16 kWh				
80	153.9	10.39	115.4	1886	11
100	115.2	13.87	69.15	2329	19
120	87.95	18.17	44.00	2749	30
140	68.54	23.31	29.40	3135	46

Table 2.2: Simulation results of the 24 hour EV road trip

It should be noted that, the recharge driving ratio is the recharge times over the driving time. For a useful embarked energy of 16 kWh, the recharge/driving ratio is approximately 1/7. However, this ratio is flexible according to the charging power, driving power, etc.

2.3.4 Conclusion

In general, during the driving mode the battery will be discharged with 1 C, however the regenerative braking and the abrupt acceleration require high C-rate currents. However, it is shown that the increase of the speed reduces the driving time. Therefore with the same useful energy of 16 kWh, the driving time is limited up to 120 min par cycle. In terms of energy saving, it seems that a small car of 8.4 kWh would give the best compromise for reaching the longest driving distance in 24 hours, with an average speed of 90 km/h. This reduces also the charging time up to 2…3 min, however the range would be limited up to 2200 km in 24 hours. It should be noted that a dead time of twofold 2.5 min has been taken into account during the charging time at every cycle. In fact the mechanical energy is not linearly proportionally with the energy consumption at the battery side because it depends on:

- The efficiency of the battery according to the charge and discharge conditions
- The efficiency of the group powertrains. In order to get a better insight of those constraints, it is optimal to start by the notion of Ragone plots and then continue by the evaluation of the internal losses in the battery. This allows assessing the extractable and deliverable energies of the Flex-EV

2.4 High power charging versus power losses for Flex-EV

2.4.1 Ragone plots

It is generally agreed that the Ragone plots [36] provide the available energy of Energy Storage Device (ESD) for constant active power request. Of course, it depends on the nature of the energy storage device which can be various: electromechanical, chemical, mechanical, etc. However, the specification of an ESD must be done with respect to the operating condition. The plots are used for limiting the extractable power on the ESD versus the useful power. So, depending on the voltage source $V(q)$, the stored charge q, an internal resistance R and an internal leakage inductance L , the electrical dynamic is governed by a second order differential equation for $q(t)$.

$$L\ddot{q} + R\dot{q} + V(q) = -\frac{P}{\dot{q}} \tag{2.13}$$

The dot indicates the differentiation with respect to the time. In particular, for batteries and capacitors, the leakage inductance can be neglected ($L = 0$), therefore the equation becomes:

$$R\dot{q} + V = -\frac{P}{\dot{q}} \;\Leftrightarrow\; R\ddot{q} + V\dot{q} + P = 0 \tag{2.14}$$

The solution of this second order equation is given by:

$$\dot{q} = I = \frac{U_0}{2R} \pm \sqrt{\frac{U_0^2}{4R^2} - \frac{P}{R}} \quad , \tag{2.15}$$

The operand $\pm$ depends on the sign of the current flow; it is basically positive during charging and negative during discharging. It should be noted that the open circuit voltage U_0 is linked to the initial energy E_0 and the initial charge q_0 by the following equation:

$$U_0 = \frac{E_0}{q_0} \tag{2.16}$$

Nevertheless, it should be noted that this charge q_0 is not directly measurable; a good estimation would satisfy the control of the state of charge (SoC).

2.4.2 Design of the battery storage device for the Flex-EV

This paragraph is dedicated to define the useful energy that has a strong relationship with:

- The extractable /deliverable power, which depends on the useful energy
- The balancing condition

- The configuration of the battery pack
- The energy management system

In order to illustrate the extractable and the deliverable power, it is optimal to model the battery according to the Ragone theory:

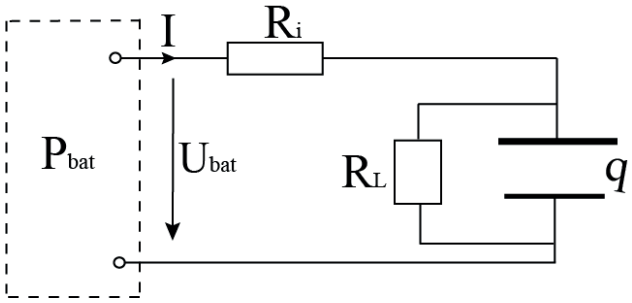

Figure 2.10: Equivalent model of a battery cell

Figure 2.10 represents a general model of a battery cell, where, R_i represents the internal resistance, R_L represents the self-discharge resistance. q is the stored charge at a given time, which is the state variable. For lithium battery, $R_L \gg R_i$, therefore the self-discharge can be neglected.

$$P_{bat} = U_{bat}.I = (\frac{E}{q} - R_i I)I \tag{2.17}$$

This formula (2.17) shows that the power loss depends on the internal resistance R_i and the battery current I. The internal energy E depends on the current.

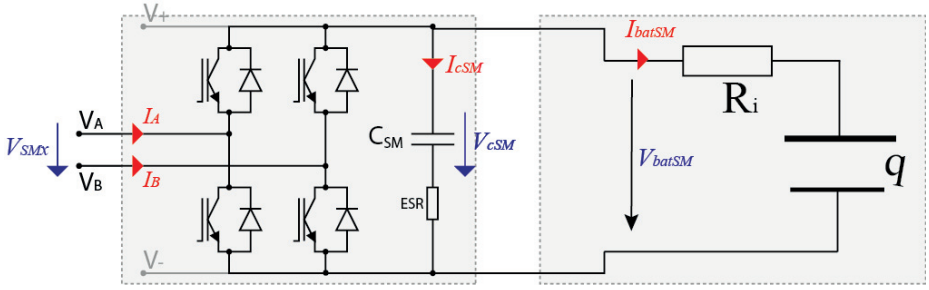

Figure 2.11: Representation of the CMMC submodule with battery model

Therefore the battery voltage is not linearly proportional with the battery current. The current I depends of the transferred power. The Figure 2.11 reminds the circuit model of the CMMC submodule, where the Energy Storage Device (ESD) consists of a capacitor in parallel with ultra-fast charge battery; it seems that the transferred power depends only on the duty cycle of the submodule converter. That is only true if and only if all submodules into the CMMC are connected. This is not possible for the modulation with balancing algorithm because some submodules must be disconnected in order to generate AC wave form. This stored charge in the submodule depends

on the median of the AC current and the firing angle of the submodule converter. However for the sizing of the battery cell, the worst case is considered, where the battery cells are expected to handle a high current up to 10 C- rate during charge and discharge. More details regarding the charge equation can be seen later in chapter 4.

2.4.3 Flex-EV battery requirements

According to the present state-of-the-art, the position of the electric vehicles in the electro-mobility demands an ultra-fast charge station (UFCS) as well as a high autonomy cars. However, the embarked EV battery combining both very high power density and very high energy density is not yet available on the market

	Cell maker	Chemistry	Capacity	Configuration	Voltage	Weight	Volume	Energy density	Specific Energy	Used in:	
		Anode/Cathode	Ah		V	Kg	Liter	Wh/liter	Wh/kg	Company	Model
1	AESC	G/LMO-NCA	33	Pouch	3.75	0.80	0.40	309	155	Nissan	Leaf
2	LG Chem	G/NMC-LMO	36	Pouch	3.75	0.86	0.49	275	157	Renault	Zoe
3	Li-Tec	G/NMC	52	Pouch	3.65	1.25	0.60	316	152	Daimler	Smart
4	Li Energy	G/LMO-NMC	50	Prismatic	3.7	1.70	0.85	218	109	Mitsubishi	i-MiEV
5	Samsung	G/NMC-LMO	64	Prismatic	3.7	1.80	0.97	243	132	Fiat	500
6	Lishen Tianjin	G-LFP	16	Prismatic	3.25	0.45	0.23	226	116	Coda	EV
7	Toshiba	LTO-NMC	20	Prismatic	2.3	0.52	0.23	200	89	Honda	Fit
8	Panasonic	G/NCA	3.1	Cylindrical	3.6	0.045	0.018	630	248	Tesla	S

Table 2.3: Current EV cells [31]

Table 2.3 gives a great picture of the actual EV cells, it is shown that most of the anode are based on graphite material except for Toshiba which has LTO anode. In addition, it has the lowest specific energy and voltage; this is the main drawback of the LTO based battery. However, it has a very high power density, which allows charging the car in a very short time.

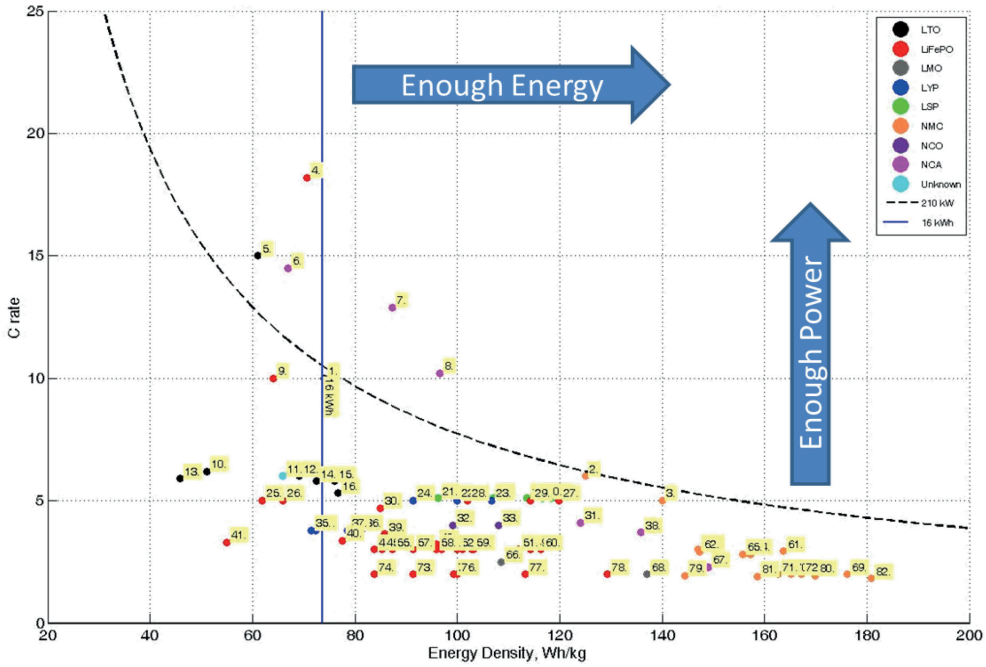

Figure 2.12: C-ratio versus energy density for system mass 380 kg and packaging factor 1.4

This Figure 2.12 shows the C ratio versus the energy density for different technology of batteries. In fact, lithium-titanate ($Li_4Ti_5O_{12}$, referred to as LTO in the battery industry) is a promising anode material for certain niche applications that require high rate capability and long cycle life. LTO offers advantages in terms of power and chemical stability, for the reason that this technology lacks a solid electrolyte interface (SEI), which allows the LTO battery to work efficiently in extreme temperatures and significantly reduces thermal runaway risk. In short, by removing the highly reactive graphite from the system design, and instead using nano-structured lithium-titanate materials as the negative electrode material, no significant interaction takes place with the electrolyte. Nevertheless, LTO-based batteries have a lower nominal voltage around 2.25 V. Nevertheless, substantial progress is expected in the field of on-board energy storage technologies in order to increase the penetration of electric vehicle in the mobility.

2.4.4 The test profile

It is well-known that the automotive design starts often with simple calculations with a Microsoft Excel file in order to define the basic dynamic performance of the vehicle. In particular, for the electric vehicles design, the battery design plays an important role on the level of the specification. Some basic calculations can be done easily with fixed values; however more advanced simulations are required to find the best compromise between performance, cost, life time and sustainability.

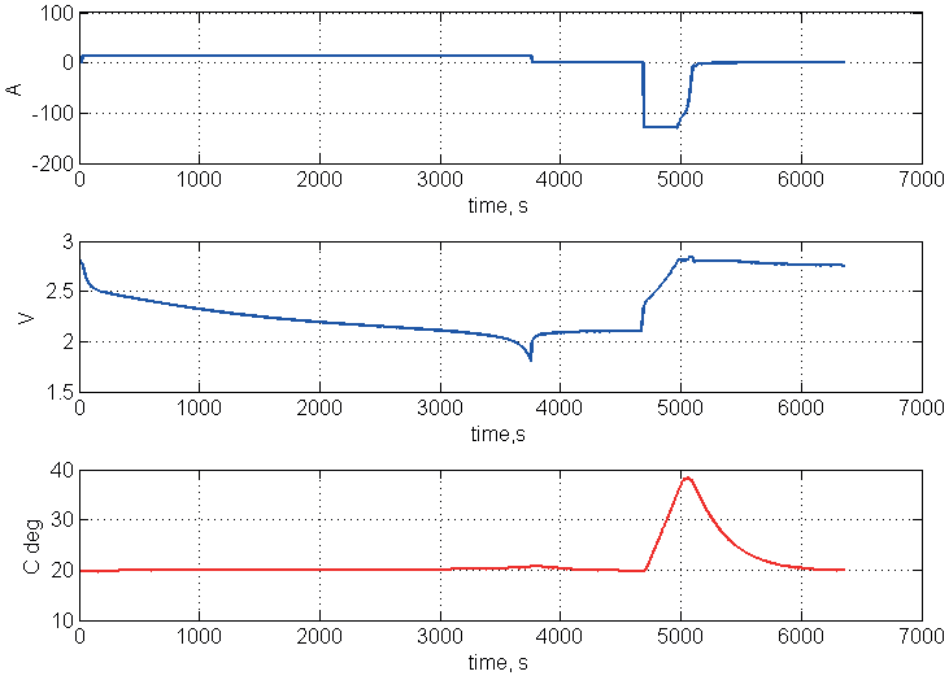

Figure 2.13: Special profile test of the on-board battery (*courtesy UFCEV project*)

This Figure 2.13 shows a special profile test of a lithium-titanate cell, based on a 13 Ah cell, from Altairnano technology. a discharge at 1 C during the first 3600 s (60 min) and an ultra-fast charging of 10 C during the next 10 min. The current and the voltage as well as the variation of temperature

are plotted. These experimental results have been acquired in the frame work of the UFCEV project. It is shown that the temperature increases drastically during the ultrafast charging, however it is far from the temperature limit of 55°Celsius, as stated by the manufacturer. Furthermore, at the end of the charging process (at 3600 s), the cell voltage (V) jumps due to the voltage drop across the internal resistance of the battery cell. This is very important in an ultra-fast charging battery; therefore particular attention is payed to the specification of the batteries extractable/deliverable power. It is also shown that 1000 seconds are required for cooling down the battery cell, at an ambient temperature of 20 degrees Celsius. This allows also computing the air/liquid mass flow for cooling down the battery cells, with respect to the first law of thermodynamic. In short, this test profile allows specifying the required power and the useful energy. Therefore simulations with different C-rates are required in order to assess the dissipated energy during the charging and discharging process.

2.4.5 The characteristic of the nLTO battery

It is generally agreed that there are many battery technologies which are able to fulfil the profile-test in the Figure 2.13 ; some of them are already on the market and some are still under development [35]. However, Altairnano technology has demonstrated their competence by proposing the nLTO battery which has convinced several industries and academic developers such as TOSA, UFCEV, etc.

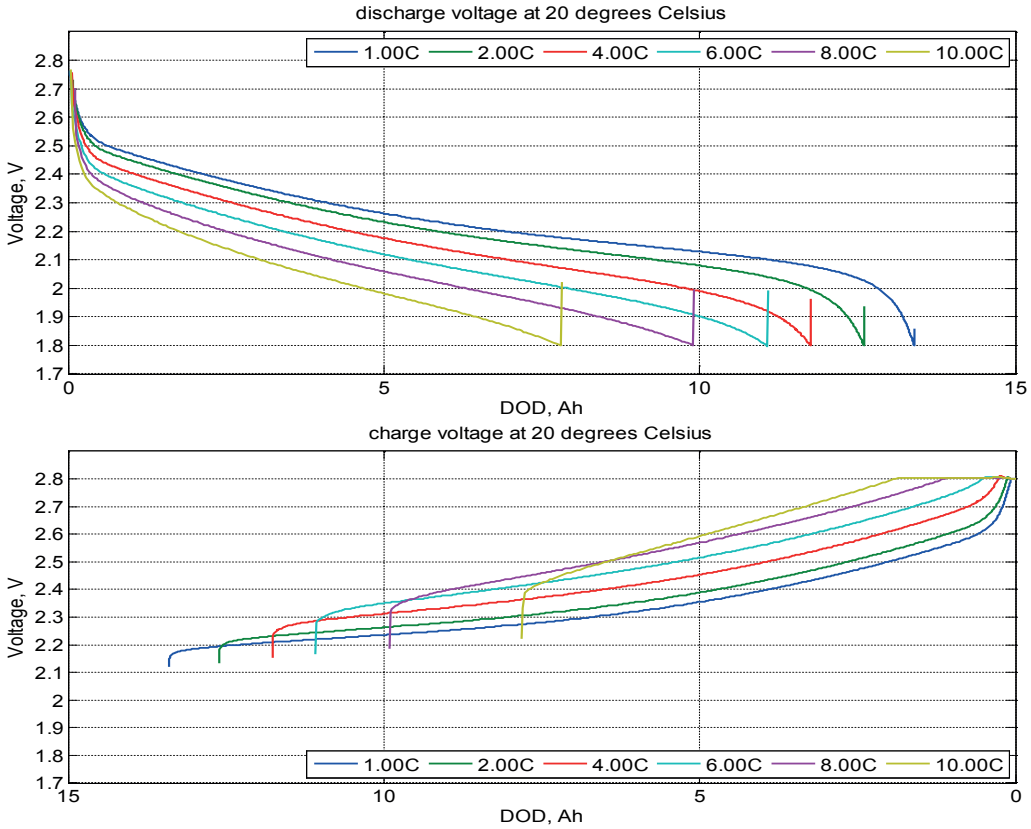

Figure 2.14: Discharge and charge voltage at 20 degree Celsius versus C-rate

Figure 2.14 shows the voltage versus the Depth of Discharge (DoD) according to different C-rates. It is shown that this nLTO based battery has a symmetrical behaviour for both charging and discharging mode according to the C-rate charging current. However, the voltage drop is increasing also as a function of the C-rate charging. This means that the internal losses are also increasing. This has a direct impact on the energy efficiency. In order to define the extractable and deliverable power it is essential to define the required power and energy during the profile test.

2.4.6 EV battery specification based on nLTO

As for today, the commercially available solutions allow recharging of an EV within 20 minutes as minimum. High energy density lithium batteries, based mostly on the lithium-manganese spinel (LMO) or lithium-iron phosphate (LFP) electro chemistries are widely used by manufacturers in order to reach the highest autonomy possible with a disadvantage low C ratio[11] in scale of 0.5 C from a conventional household socket. Although, high power density batteries require high C ratio in scale of 10 C, their energy density and autonomy show poorer figures. In fact the datasheet as well as the result in Figure 2.14 can be summarized in the following table:

Altairnano 13Ah	Value	Unit
Nominal Capacity	13	Ah
Maximal current	130	A
SOC in actual usage	0.6	from 20% to 80%
Available capacity	7.8	Ah
Required Current to discharge the available capacity at 5 min	93.6	A
Required current C-ratio for given SoC window to discharge at 5 min	7.2	C
Required current to charge cell at 55 min	8.5	A
Discharging C-ratio at 55 min (only for information)	0.92	C
Average charge voltage at 124.8 A	2.48	V
Nominal Voltage (at 1C ratio)	2.25	V
Total energy to be stored	14	kWh
Cell Weight	0.4	kg
Cell Volume	0.22	l
Maximal cell voltage	2.8	V
Minimal cell voltage	1.5	V

Table 2.4: Altairnano 13 Ah Car battery parameters

Table 2.4 gives the important data which has been extracted from the datasheet. It emphases the capability of this battery to handle the high C-rate current. However, the dissipated energy is not highlighted. Also, it gives the baseline calculation for the battery cell based on the 13 Ah nLTO form Altairnano. It is shown that the increase of the charging and discharging C-rate induces an increase of internal energy losses. Also, it decreases the round trip efficiency; for instance, here

[11] C ratio: current over capacity ratio.

the round trip efficiency is around 0.886. From the cell level, it is important to assess the parameters in pack level, here there are two baselines calculation where the first is based on 16 kWh and the second is based on 32 kWh.

Parameter	**Value (16 kWh)**	**Value (32 kWh)**	**Unit**
SoC range in use	78	78	%
Cell numbers:	660	1320	-
Weight of cells	264	528	kg
Volume of cells	145	290	ltr
Effective energy density	53	53	Wh/kg
Required Charging Power - 5 min	**205.5**	**411**	**kW**
Required Charging Energy- 5 min	**17.1**	**34.2**	**kWh**
Discharged energy	**14**	**28**	**kWh**
Round trip efficiency	**82.3**	**82.3**	**%**
Connection - cell in parallel/series	3p/220s	3p/440s	-
Voltage range	484 - 545	968 - 1091	V
Battery Charging Current	607	607	A
Approximate battery weight	370	740	kg
Approximative battery weight with CMMC	280	545	kg

Table 2.5: Battery packaging specification baseline for 16 kWh and 32 kWh

Table 2.5 gives a great summary of the important parameter for the battery packaging. Knowing the internal energy content of the cell, the total cell efficiency, which is in fact also the CMMC efficiency, is calculated as follows:

$$\eta_{bat} = \frac{P_{bat,tot}}{P_{dch\_cell}} \cdot \eta_{cell} \tag{2.18}$$

It should be noted that this efficiency is not included in the datasheet from the battery manufactures. Therefore, attention should be paid on the power density, which is indicated on the datasheet.

2.5 Conclusion

Throughout this chapter, ultrafast charging issues of battery were studied and a step-by-step design methodology for an on-board ultrafast EV charging was shown. It is designed to give a baseline for the Flex-EV designer with ultra-fast charge battery.

In order to specify a baseline approach for the design of the Flex-EV battery, a special profile test has been chosen, this is based on discharging for 55 min and charging for 5 min. This would avoid a queuing in the charging station according to the statistical study in the first chapter (study based on typical traffic in Switzerland). This would correspond roughly to the usable energy of 14 kWh. However, for a battery cell of 13 Ah, the useful energy of 14 kWh would not satisfy the required voltage of the CMMC for Flex-EV. Therefore, 28 kWh of usable energy is used as the baseline parameters for the Flex-EV. Then, simulations of the overall system were performed in order to demonstrate the performance of the approach. This chapter focuses on the performance evaluation of the electric vehicle in the long distance driving. The question is: today, are the EVs are competitive with combustion engine cars? In order to gain the upper hand in this challenge, the best trade-offs between charging and discharging time should be found out, meaning an EV must be recharged more frequently than by using existing battery though the average speed is improved. It should be pointed out that the EV driving time should be sufficient enough in order to let the UFCS to accumulate the amount of required energy for the next cycle, because the grid power is limited at 22 kW.

The main advantages of the approach can be explained by:

1. With ultrafast charging, the EV average speed in long distance driving is improved thanks to less time spent at charging stops.
2. The load, imposed to the grid by ultrafast charging, can be leveled by decoupling the vehicle from the mains by the application of energy buffers.
3. With buffering, the EV can be charged from a 400 V, 32 A low voltage outlets, allowing a charging interval of one EV in less than an hour.
4. The partial use of buffer capacity gives a possibility to exploit the battery more effectively at smaller charging and discharging rates, e.g. for grid support (buffer-to-grid applications). However in this variant, the converters and battery must be designed to operate in a wider voltage range.
5. With cost, mass and volume restrictions, the EV battery is optimally based on lithium iron titanate cells. Electrochemical storage, however, is related to additional losses thanks to poorer roundtrip efficiency than ultracapacitors for example.

During the ultra-fast charging, the transferred power can be kept constant while forcing the charging current to the value, where the product of high power charger input voltage and current corresponds the set-point under the voltage limits of the buffer and EV batteries as well as current limits of the current-carrying components. Additional limitations can be given by the temperature. All these adjustments can be carried out by the upstream supervisory controller, which changes the current set-point value incrementally to match the preset conditions.

Chapter 3 Flex-EV: general concept

"Everything is self-evident"

René Descartes

3.1 State of the art of the EV's

3.1.1 Introduction

Today, there is a long-term trend towards bi-directional and flexible charger functions, not only for drawing current from the grid but also for feeding excess energy back into it. For instance, the voltage can be controlled by injection of reactive power. This keeps frequency and voltage within narrow band. The well-known droop[12] control is used to control of grid parameters such as the frequency and the voltage, where the frequency decreases with increasing load (active power), and the grid voltage can be increased by injecting capacitive reactive power whereas this voltage can be decreased by delivering inductive reactive power.

It is well known that after the Fukushima disaster, there are radical shift into green energy sources in distributed grid generation. Since the green energy depends on the weather behaviour, this change will have strong impacts on the stability of the whole grid. The electric vehicle integration has to follow with a significant contribution in smart grid congestion management. However, the bidirectional charging function is not yet available for the commercial electric vehicles.

With the rapid increase of power electronic systems in electrical energy grid applications, multilevel topologies gain in importance. These converters allow overcoming the specific weak points of high-blocking voltage semiconductors with respect to their static and dynamic properties. Multilevel systems are therefore the key technology for efficient and cost-effective power electronic systems in high- and medium-power applications.

Nowadays, in the electrical energy grid, the well-known three-level NPC inverters are widely used for small and medium power traction and solar inverters, however the new family based on the Modular Multi-level Converter (MMC/M2C) principle has found its way into high-power and transmission systems (HVDC). Besides grid field tied systems, many other applications can be covered by multilevel converters. In the framework of the EV application, the Configurable Modular Multilevel Converter (CMMC) offers a large flexibility in order to handle the different voltage levels and current intensities in electric vehicle's battery charging and discharging. It is a smart method to achieve a high power density and a compact power conversion for electric vehicles. It allows interfacing EVs to worldwide charging infrastructures, meaning from the standard household single phase socket to direct-current (DC) ultra-fast charging stations. This concept is based on integration of the motor subsystem and the battery management subsystem as well as the universal and flexible charging subsystem. In fact, the power conversion is based on Modular Multilevel Converter (MMC) [37] with split integrated storage (SIS) based on battery modules [20]. The standard EV architecture is presented in the next paragraph 3.1.2 and the basic on-board charger is recalled. Then the combined charging system is introduced in paragraph 3.2.2. Thereafter section 3.3 is dedicated to the Battery packaging, and then section 3.3.6 is dedicated to the concept of the Flex-EV architecture where its design requirements are emphasized.

[12] Droop control is a control strategy commonly applied to generators for primary frequency control (and occasionally voltaqe control) to allow parallel generator operation (e.g. load sharing).

3.1.2 Standard EV architecture concept

An important goal for electric vehicles is overcoming the disparity between their cost of development, production and operation, with respect to those of equivalent Internal Combustion Engine (ICE) vehicles. Usually, the electric vehicle architecture consists of the main battery and traction subsystem as depicted in Figure 3.1. In the battery system, the cell modules supply the vehicle with electric energy through the DC bus. More often, a half-bridge DC/DC converter is used to adapt the variable voltage from the battery to the quasi-constant voltage of the DC bus. Braking energy is partially recovered during deceleration.

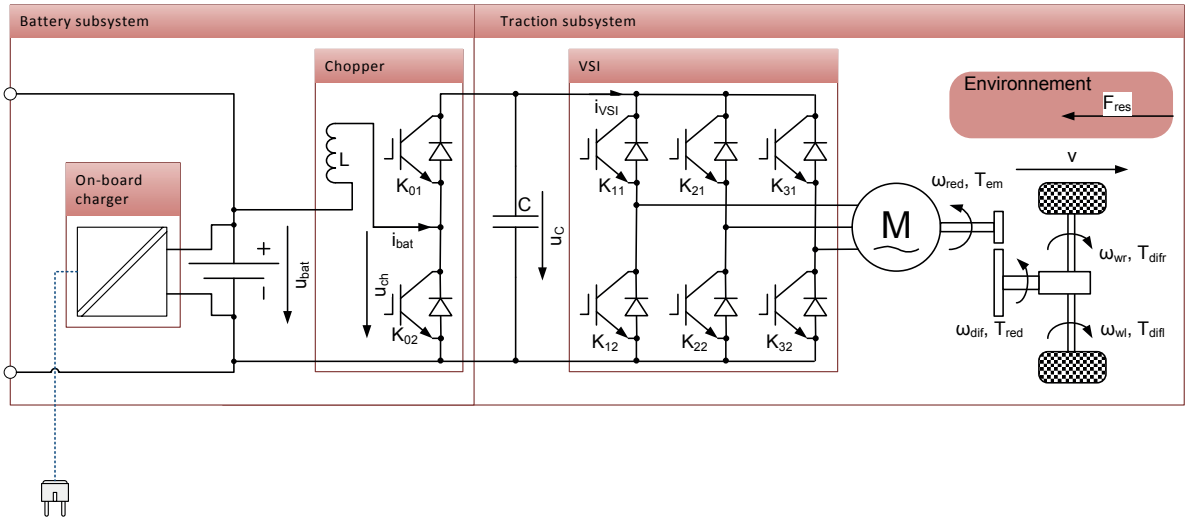

Figure 3.1: EV basic architecture

The traction subsystem is composed of an electric motor and a full-bridge Voltage Source Inverter (VSI). Transmission gear is used to adapt the speed ratio between wheels and the motors shaft, followed by a mechanical differential for changing the speed ratio between the two traction wheels.

3.1.3 Performance evaluation of the ultrafast charge battery in NEDC

This paragraph is dedicated to demonstrate the performance evaluation of the ultrafast charging battery such as LTO in comparison to the standard “quick” charge battery such as lithium ion which is based on LMO. A simulation using the New European Driving Cycle (NEDC) has been conducted, where the parameters are based on real data from car and batteries manufacturers. For instance the EV data corresponds to the Mitsubutsi iMiEV, whereas the battery data corresponds to the Lithium titanate from Altairnano. Firstly, a simulation with the original battery is conducted, and then secondly the EV parameters were kept however the LTO battery parameters have been implemented. Of course, this induces change in weight and power density for the iMiEV. Indeed, 16 kW·h LTO battery pack is used with estimated mass of 390 kg in comparison to original Mishibutsi iMiEV 250kg. The specific power of the PMSM is estimated 2.2 kg/ kW. Therefore, the total estimated mass of EV with 3 passengers is 1450 kg. More details can be seen in the article [38].

3.1.3.1 The model based design

A French research team from the L2EP (a Laboratory from University for Sciences and technologies of Lille) developed a methodology for analysis and representations of energy flows in a multi-disciplinary system such as electric vehicles; this approach is called Energetic Macroscopic Representation (EMR). It has been developed to propose a synthetic description of the multidisciplinary conversion system [39] and it is utterly a straight forward approach for students. Therefore, the simulation model has been realized based on this EMR tool, it gives a systematical approach for modelling the EV model as well as its control. In fact, the movement of an EV is simulated during the New European Driving Cycle (NEDC), which reflects both urban and extra-urban driving conditions and is set as standard to characterize the energy consumption of small vehicles. The simulation model helps to validate the battery's ability to supply sufficient power to follow the NEDC load curve.

3.1.3.2 The Energetic Macroscopic Representation

The performance of the upgraded EV is modelled using the Energetic Macroscopic Representation (EMR). It is a graphical description, which organizes the system into interconnected basic subsystems: accumulators, sources, conversion and distribution. All elements are connected according to the interaction principle. The product of the action (for example, the force) and reaction (for example, the velocity) always leads to the power exchanged by the connected elements. Moreover, all elements are described using the physical causality (i.e. integral causality). These properties enable a systematic deduction of the control scheme. For the EV battery, two tape of battery has been considered:

- Ultra-fast charge battery which has a very high power density but a quite low energy density.

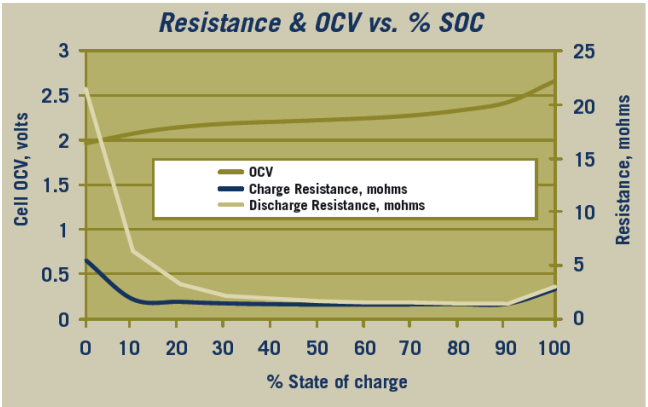

Figure 3.2: Extract data from the cell specification of the 13 Amp Hour cell nLTO battery (*Altairnano*)

Figure 3.2 shows the open circuit voltage and the internal resistance values for charge and discharge for the nLTO battery based on 13 Ah from Altairnano. It can be seen that the OCV is the same for both charge and discharge, however the internal resistance is different for charge and

discharge. Therefore, the EV battery can be modelled as a series circuit of nonlinear open-circuit voltage OCV and different resistances for charging and discharging (Figure 3.3).

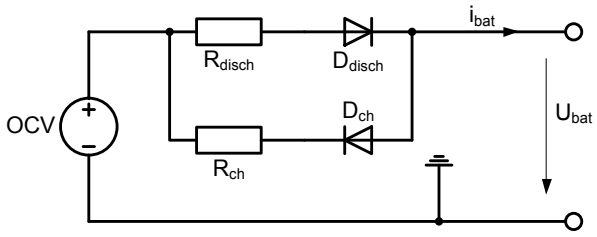

Figure 3.3: Battery model

- Fast charge battery which has high energy density but a quite low power density

Figure 3.4 shows the LFP battery, OCV and the main internal resistance, these are experimental results are from UFCEV project. It is shown that the OCV is not symmetrical between charge and discharge process.

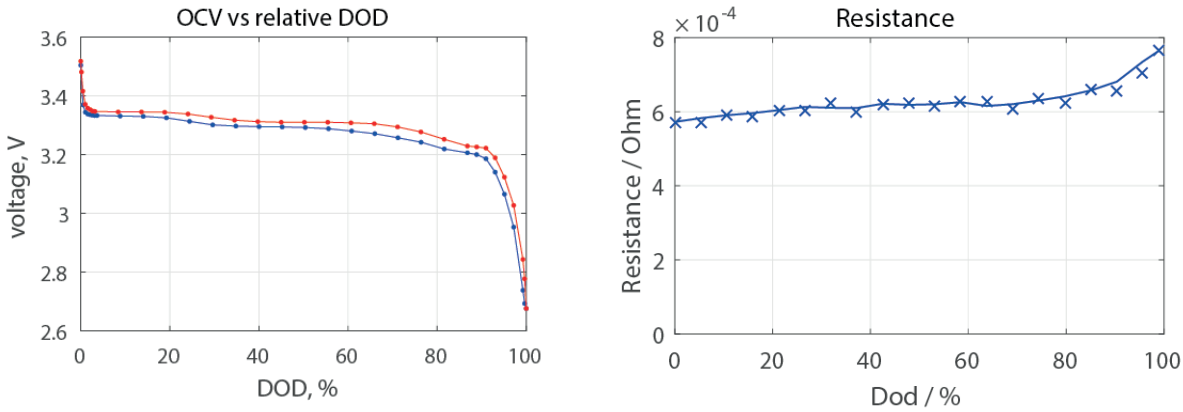

Figure 3.4: Lishen battery parameters(LFP 130 Ah battery cell [13])

On the left side, the red curve represents the OCV during charge whereas the blue curve represents the OCV during discharge. On the right side, the main internal resistance is the same for the both operation (charge or discharge). Thereafter, the OCV and internal resistance have been implemented in the simulation model for both LTO battery and LFP battery. By comparing the results in Figure 3.2 and in Figure 3.4, it can be seen that the LTO battery has a lower internal resistance that the LFP based battery. This is due to the lack of the Solid Electrolyte Interface (SEI) in the nLTO battery.

In addition, it is well-known that the battery state of charge (SoC) has a strong relation with coulomb (ampere-hour) capacity Q_{bat}, with the charge or discharge current as well as with the previous state of charge. This can be expressed as:

[13] Experimental results from UFCEV project

$$SoC(t+1) = SoC(t) + \int_0^{t+1} \frac{i_L}{Q_{Bat}} dt = SoC(t) + \frac{\Delta t}{Q_{Bat}} \sum_{i=t}^{t+1} i_{L,\Delta t} \tag{3.1}$$

Back to electric vehicle system representation, the chopper is represented as an electric conversion element. The dc bus is represented by a capacitor as energy accumulation element with voltage u_C as the state variable.

$$C \frac{d}{dt} u_C = i_{bat} - i_{VSI} \tag{3.2}$$

The chopper inductance L is represented by an accumulation element with the current i_{bat} as action variable. This current depends on the battery pack voltage u_{bat}, chopper voltage u_{ch} and internal resistance r_{bat}.

$$L \cdot \frac{d}{dt} i_{bat} + r_{bat} \cdot i_{bat} = u_{ch} - u_{bat} \tag{3.3}$$

For electromechanical the conversion, a permanent magnet synchronous machine (PMSM) is chosen thanks to enhanced power density and ample use in EV design.

$$i_{VSI} = \frac{T_{em}\omega_{red} - P_{loss}}{u_C} = \frac{T_{em}\omega_{red}}{u_C} - \eta_{em} i_{VSI} \tag{3.4}$$

In (3.4), T_{em} stands for electromechanical torque at the motor shaft, ω_{red} for the input angular speed on the reduction gear, P_{loss} for the power loss and η_{em} for the electromechanical conversion efficiency. The latter value is not constant, but depends on the actual motor operating point. In Figure 3.5, the motor efficiency map for Toyota Prius is shown, the values are scaled for further modelling to match actual drivetrain power.

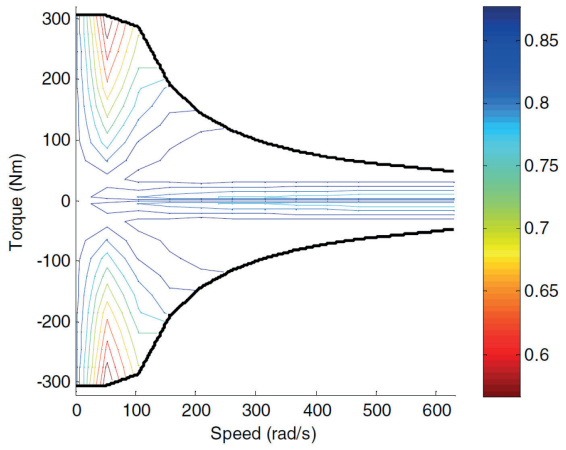

Figure 3.5: A 30 kW PMSM efficiency map for Toyota Prius[14]

[14] Observatoire du Véhicule d'Entreprise: http://www.observatoire-vehicule-enterprise.com/

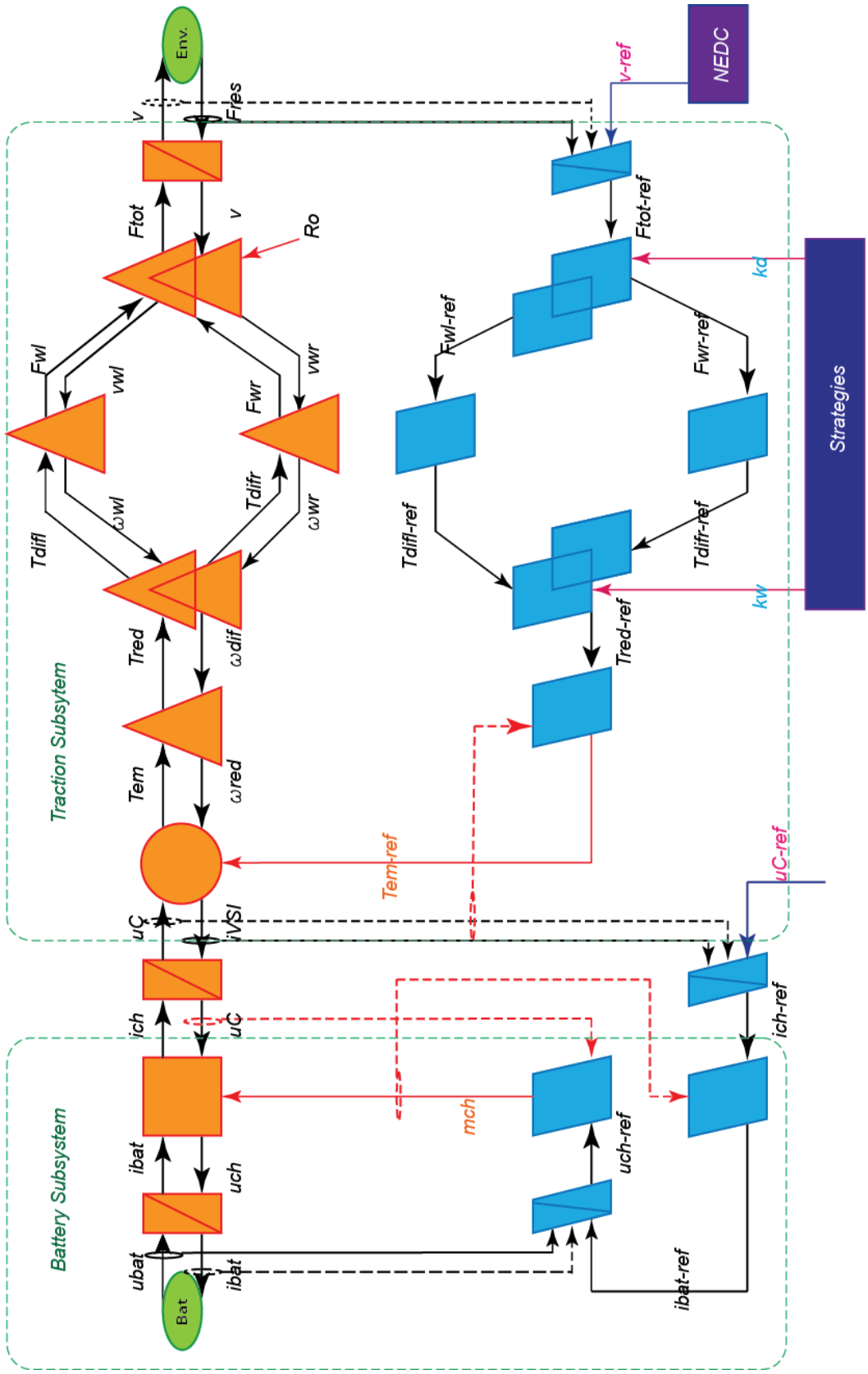

Figure 3.6: EV model, based on the energetic macroscopic representation

The reduction gear is represented by a mechanical conversion element with transmission ratio k_{red} and efficiency η_{red}.

$$\begin{cases} T_{red} = \eta_{red} \cdot k_{red} \cdot T_{em} \\ \omega_{red} = k_{red} \cdot \omega_{diff} \end{cases} \quad (3.5)$$

The differential is represented by a mechanical coupling element with transmission ratio k_{dif} and efficiency η_{dif}, enabling the left and right wheel to spin at different angular speeds ω_{wl} and ω_{wr}, respectively.

$$\begin{cases} T_{dif} = \eta_{dif} \cdot k_{dif} \cdot T_{red} \\ \omega_{dif} = k_{dif} \cdot (\omega_{wl} + \omega_{wr}) \end{cases} \quad (3.6)$$

The wheels are represented by a mechanical conversion element with radius R_w:

$$\begin{cases} F_{wl} = \dfrac{1}{R_w} T_{difl} \\ F_{wr} = \dfrac{1}{R_w} T_{difr} \end{cases} \quad (3.7)$$

$$\begin{cases} \omega_{wl} = \dfrac{1}{R_w} v_l \\ \omega_{wr} = \dfrac{1}{R_w} v_r \end{cases} \quad (3.8)$$

$$\begin{cases} F_{wl} + F_{wr} = F_{tot} \\ v_l + v_r = v \end{cases} \quad (3.9)$$

The chassis is represented by an accumulation element with the velocity of electric vehicle v as the objective state variable. Finally, inversion based control, which is depicted by the parallelograms with light blue color is depicted in the Figure 3.6. This is deduced from the inversion of the EMR and PI controllers are used to control the objective velocity and dc bus voltage.

3.1.3.3 The simulation results

Figure 3.7 shows the vehicle simulation results with state-of-the-art “quick” charging battery. Here, the charging current is numerically equal to twofold coulomb capacity. The initial SoC of the battery is taken equal to 80 %, which is a usual upper limit with constant current charging. During a 1200 s (20 min) cycle, approximately 0.75 kW·h is withdrawn from the main battery. The nega-

tive power values reflect regenerative braking, which is limited by the EV drivetrain and the battery itself. The poor tank-to-wheel (TTW) efficiency can be explained both by the battery performance and the losses inside the battery itself.

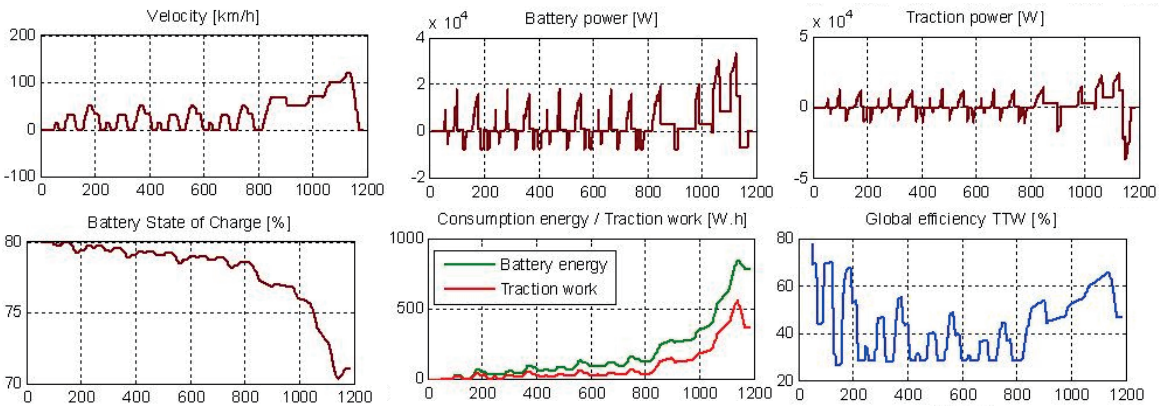

Figure 3.7: Simulation results with ”quick” charging battery

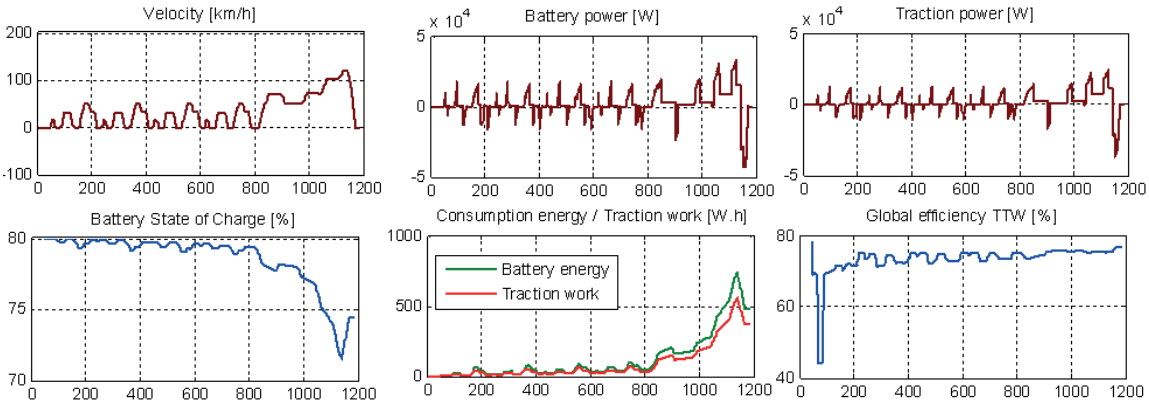

Figure 3.8: Simulation results with ultrafast charging battery

However, under ultrafast charging conditions, the charging current equals tenfold coulomb capacity. The nLTO battery can more effectively absorb regenerative braking energy, thus improving overall TTW efficiency and reducing energy consumption per distance travelled (0.5 kW·h), meaning a battery with same capacity can provide more autonomy.

3.1.3.4 Discussion

In conclusions, one of the advantages of an ultrafast charge compliant EV battery such as nLTO is that it can absorb more regenerative energy in comparison with other chemistries. Therefore, in urban conditions, the range of the electric vehicle increases at the same battery capacity. A nLTO battery pack weighing in the range of 390 kg can yield autonomy of 210 km in comparison to a default iMiEV battery with 250 kg mass and 150 km NEDC range. In contrast, the major drawback

of ultrafast charge compliant battery is its quite low energy density, minimizing the vehicle range during the extra-urban driving conditions at the same mass and volume.

Although in order to increase the penetration of EVs, the trends are to shorten the charging time and to lengthen the autonomy. The proposed ultrafast charge compatible battery on nano lithium titanate (nLTO) gives the best compromise between the charging time and the distance covered. However, the NEDC doesn't relate the normal driving cycle in Europe and it has been monstrously criticized. For instance, it doesn't take into account the charging process for the electric vehicle testing. Therefore, the next paragraphs are dedicated to the state of the EV's on-board charger architecture.

It should be noted that at the starting of the simulation, in particular on Figure 3.8, it is shown that the global efficiency is decreasing drastically, this is normal because the global efficiency is a rolling average, also known as a moving average, which is a calculation to analyze data points by creating series of averages of the different subsets of the full data set. For electronic engineers, it can be viewed as an example of a low-pass filter used in signal processing, which is simply viewed as smoothing the data.

3.2 State of the art of the EV's on-board charger architecture

Standard on-board chargers are various; launching from a three-phase diode-bridge rectifier to several topological extensions; for instance the three phase boost and buck power factor corrector (PFC) rectifier circuits are derived [40], [41]. The two-level Δ – switch rectifier topology and the three-level Vienna rectifier topology are also well-known because they can achieve a very high efficiency (more than 98 %), whereas the 6-switch buck-type rectifier system and the Swiss rectifier are promising candidates for implementing a buck-type PFC front-end of an EV charger [42]. However, the most common architecture of an on-board charger for electric vehicle still consists of a Mode 1.

3.2.1 Mode 1: single phase charging.

Mode 1 charging level is limited basically at 3.6 kW for single phase charging. It consists of two parts: the first part is composed of an H-bridge voltage source converter, which is a single phase AC/DC converter with four quadrant capability that can be operated in the same manner as the voltage source inverter, which is described in Figure 3.9.

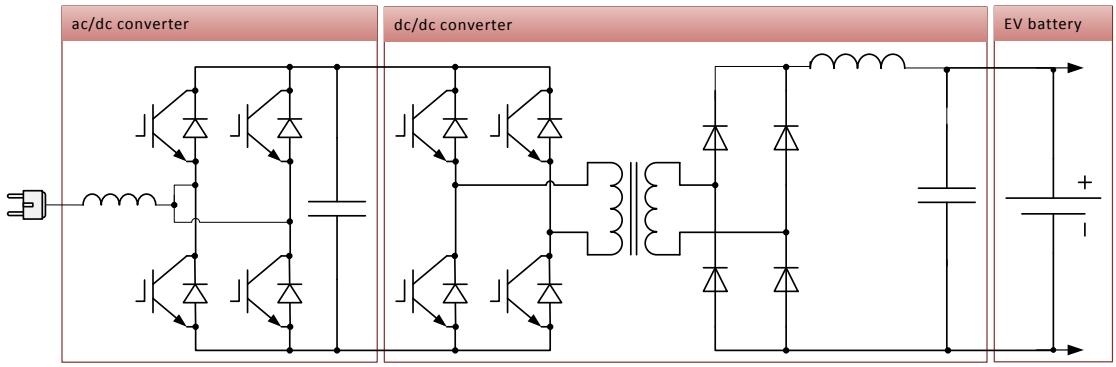

Figure 3.9: Typical example of the basic power charge architecture

In fact when operating as a DC power source with Pulse Width Modulation (PWM) control, a zero voltage condition can be obtained by turning on only one of the switches, with the current freewheeling through the switch and a diode. The second part is composed of a push pull converter, which is suitable for high power design. It drives the high frequency transformer with an alternating current and an isolated controllable voltage. It doesn't require extraordinary magnetic coupling; small core without airgap would be sufficient. However it has balancing problems which need to be controlled. This on-board charger is limited in power density because it includes bulky components and it is limited in charging power. Therefore, this limits utterly the range flow rate[15] of the EVs owners. Therefore, merging the charging converter with the motor inverter is a promising method because it is believed to bring an increase of the charging power density and it can contribute to the reduction of the power conversion effective costs [43].

[15] Range flow rate: driving range resulting of a minute charging/fuelling time [13]

3.2.2 Mode 2 and Mode 3: Combined on-board charger

The authors in the paper [44] give a great overview of various on-board integrated chargers in use today; it is stated that the on-board converters can be made inexpensive with only few additional components. Of course, this does not take into account the battery management power electronics and the flexibly with large range of charging infrastructures.
Here, the concept aims to use the existing traction converter as charging converter as well as the existing motor windings as current filter during charging in order to avoid a bulky inductance or a large transformer in the car. Actually, there are two methods for implementing this concept: the first is based on hard blocking of the rotor, by using an openable rotor circuit, this will avoid induced currents in the rotor circuit by opening the rotor circuit during charging mode; therefore the electromagnetic torque is cancelled. The second is based on soft blocking of the rotor by using the self-compensation of the stator fluxes. In order to get a better insight of these mechanisms, the next paragraphs are dedicated to the combined charger with and without load compensation.

3.2.3 Combined charger without load compensation

A three-phase motor with open end stator windings is required in order to be able to access both terminals of the stator windings. Therefore, the three-phase terminals of the stator are connected to the inverter/charger on one side and to the charging connector on the other side. It should be noted that this charging connector is mechanically short-circuited in order to couple the motor in star during driving mode. This method is usually implemented with open end synchronous motors where the inductor circuit supply can be opened during charging mode.

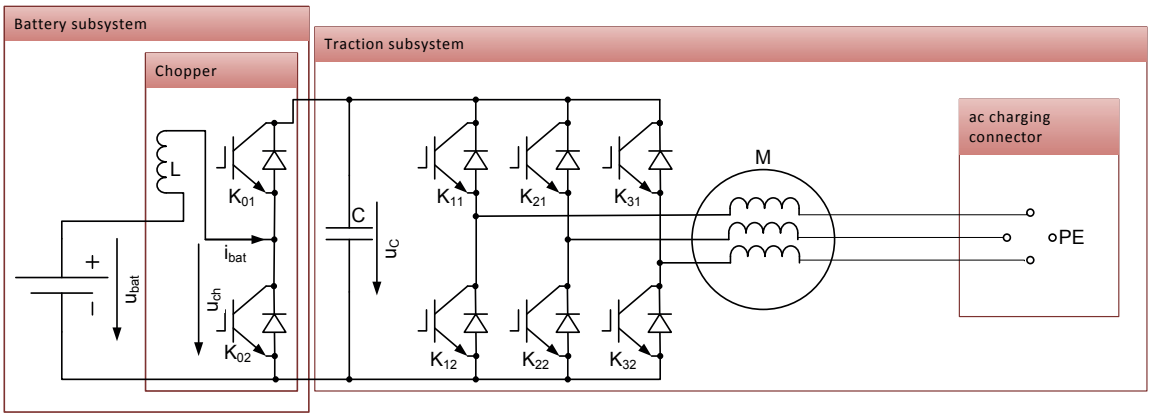

Figure 3.10: Typical example of a combined charging architecture without fluxes compensation

The main drawback of this approach is the fact that there is no possibility to avoid the transfer of energy to motor magnetic core. In addition, the implementation of this approach requires a mechanical openable rotor circuit. This leads to an increase of the cost of the motor. In particular, the chameleon charger from Renault is based on a combined charger without fluxes compensation

approach. The following Figure 3.11 illustrates the generated rotating magnetic fields in the magnetic core during the three phases charging.

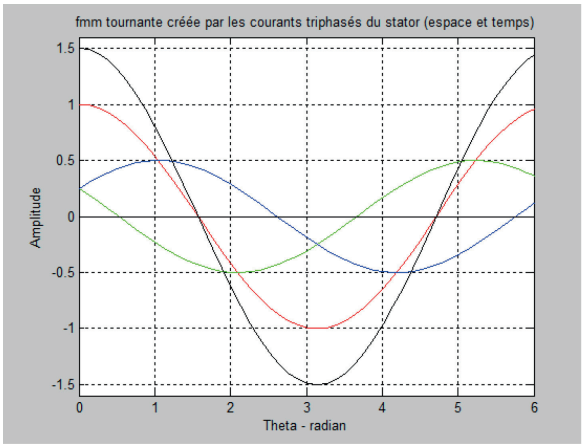

Figure 3.11: Simulation in space reference frame of the generated rotating magnetic field, produced by the three phases charging currents **without** flux compensation (per unit)

In fact, the three phase currents are represented by the green, blue and red curve whereas the produced rotating magnetic field is represented by the back curve. This means that a power flow is occurred from the stator to the rotor part of the motor during the charging. This the reason why the rotor circuit must be opened in order to avoid induced rotor fluxes. As a result, the efficiency of this charger is limited because the iron loss is not compensated. This is real problem when the power becomes high. Also, it required a special cooling system because the rotor which drives the cooling fan through a common shaft is not moving. This is reason why the next method based on soft-blocking of the rotor has been introduced in [45] [46].

3.2.4 Combined charger with load compensation

A motor with a tapped winding stator is used and it is supplied by a dual inverter [45], which is able to generate an opposite wave form current in the stator. This leads to the self-compensation of the electromagnetic torques during charging mode.

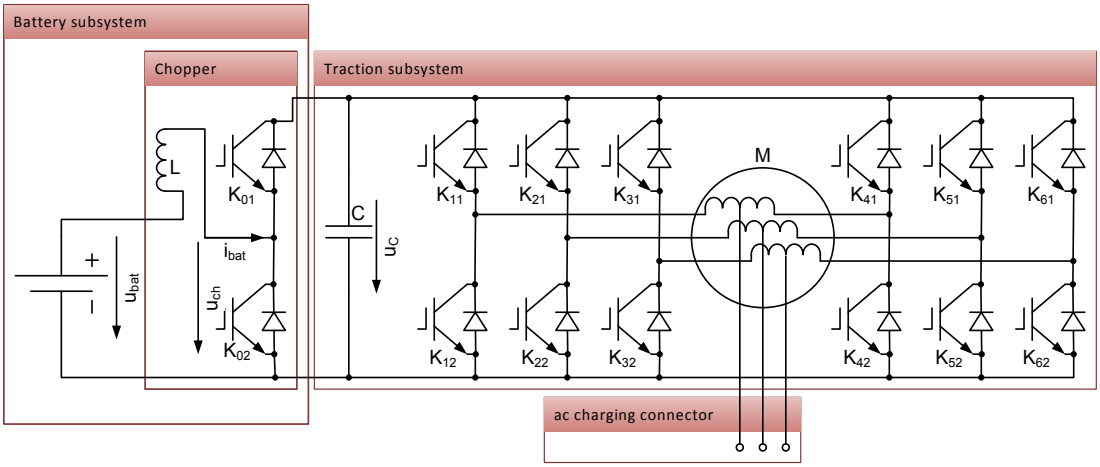

Figure 3.12: Typical example of a combined architecture with fluxes compensation

Figure 3.12 shows a typical example of a combined powertrain and power charger with soft blocking of the rotor during charging. This three phases AC charging mode corresponds to the charging mode level 2 and 3, as mentioned previously in Table 1.3 and Table 1.4.

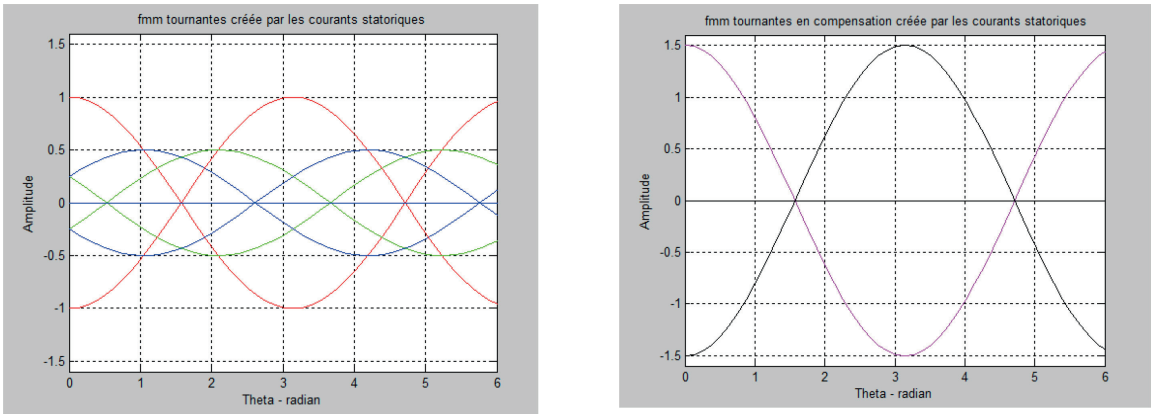

Figure 3.13: Simulation in space reference frame of the generated rotating magnetic field, produced by the three phases charging currents **with** flux compensation (per unit)

Figure 3.13 illustrates the compensation of the rotating magnetic field, produced by the six phase currents. On the left side, it is seen that each phase currents are canceling each other out. Therefore the generated rotating magnetic fields are cancelling each other out, as depicted on the right side of the Figure 3.13. This avoids the transferring of the power from the stator to the rotor part of the motor. There is a self-compensation of the magnetic current therefore the iron losses are cancelled. This approach has a better efficiency in comparison to the previous approach without flux compensation.

The charging mode level 1 could be performed by adding an extra mode 1 on-board charge such as in Figure 3.1. Unfortunately, the mode 4, which corresponds to the DC off-board fast charging is not included in this system, however it could be performed through high power chargers like in [17], [20].
Even though the combined on-board charger contributes massively to the high integration of EV power conversion, the fast DC on-board charger is still missing. Therefore, the extra chargers will add an extra cost for the customers. This is the reason why, the EVs remain expensive and bulky cars; the high power chargers are still heavy.

Moreover, it is generally agreed that the diversification on the charging standards, both seen from the existing fast charging stations as well as from the charge profile of the on-board battery breaks the integration of EV in the market. As result the EV should be compatible with a large range of voltage and current ratings. In addition, the battery packaging remains a challenge for the battery designers. Therefore, the main challenge is to be found within the specification of parameters for design of electric vehicle and its battery packaging, providing large flexibility for charging while avoiding incompatibility with the available charging infrastructure.

3.3 Battery packaging

3.3.1 Motivation

Similarly to the engine management system in gasoline cars, a gauge meter should be provided by the battery management in EVs. This indicates the state of the safety, usage, performance and longevity of the battery. Due to the volatility, flammability and entropy changes, a lithium-ion battery could ignite if an overcharge occurs. This is crucial, especially in electric vehicles applications, because an explosion could cause a fatal accident. Moreover, over-discharge causes reduced cell capacity due to irreversible chemical reactions. In fact, the battery packs tend to have high energy and power densities which will exert a strong thermal stress upon them. This means that individual battery cells are more prone to decline away and eventually fail early because of an excessive loss of capacity and an increase of the internal resistance caused by accelerated aging.

Moreover, for different reasons, each cell can be imbalanced in operating mode. Therefore, a suitable battery management subsystem (BMS) is utterly required. This can also warrantee the capability of the EV to ride-through thermal runaways. Therefore, a BMS needs to monitor and control the battery based on the safety circuitry incorporated within the battery packs. Whenever any abnormal conditions, such as over-voltage or overheating, are detected, the BMS should notify the user and execute the pre-set correction procedure. The BMS should include the following functions:

- Data acquisition
- Safety protection
- Ability to determine and predict the state of the battery
- Ability to control battery charging and discharging
- Cell balancing
- Thermal management
- Delivery of battery status and authentication to a user interface
- Communication with all battery components
- Prolonged battery life
- Integrated Charging system

3.3.2 Experiment

3.3.2.1 Description

The main purpose of this experiment is to study the imbalanced behaviour of the lithium iron phosphate (LFP) based battery behaviour. In fact, the module consists of twelve cells in series. For the testing on the module level, passive balancing is implemented, where twelve battery cells in series are balanced. In fact, each cell input has an associated MOSFET switch for discharging overcharged cells. This strategy is very simple and low cost as well as efficient because the lithium-ion battery voltage gradient is quite small in comparison to their nominal voltage. In the framework of the test design, a cylindrical frame has been implemented because this design allows cooling down

the battery cells properly since the air flows in 3D, which equalizes the air flow-rate for each battery cell. Furthermore, this strategy makes it possible to imperatively bypass the overheated module(s) and reconnect it again when its temperature is stabilized. It should be noted that NTC sensors are implemented in each cell, between the containers and the cells themselves to avoid a false measurement when the fan is running.

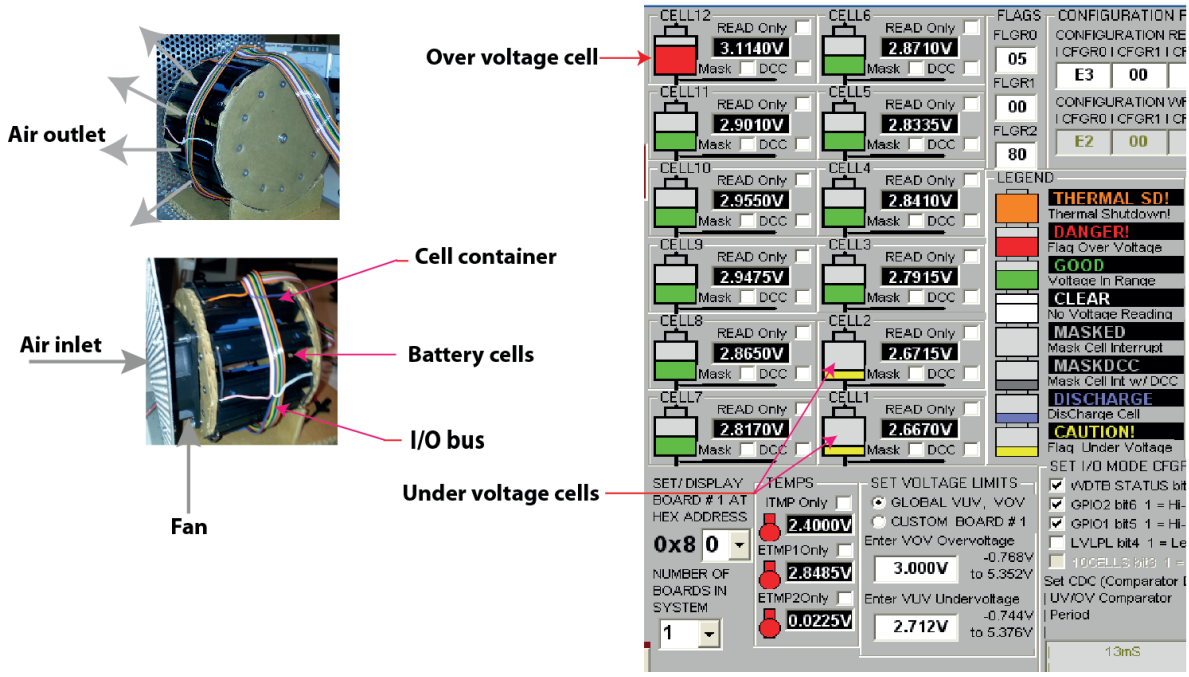

Figure 3.14: Battery module prototype on the left as well as its monitoring on the right. (Battery: LFP-18650 with a capacity of 1200 mAh and a nominal voltage of 3.25 V)

Figure 3.14 shows the module prototype and its graphical user interface (GUI) which monitors the voltage cells; the data is gathered continuously with a sample time of 13 ms. In fact, according to a specified threshold voltage, the battery management system (BMS) can detect the overcharged and/or undercharged battery cell(s) as well as the overheated cell(s). Then the BMS automatically gives the appropriate reference to the fan or and/or to the switches.

3.3.2.2 Conclusion

The passive balancing is simple to implement, however the waste of energy dissipate in the resistor for balancing is significant. In addition the auxiliary power supply energy consumption for the BMS is significant in comparison to the amount of energy which needs to be burn into resistances. Therefore this approach is not recommended for EV application where the energy saving is an important concern.

3.3.3 Cell balancing topologies

In paper [47], the authors give a great review of passive and active battery balancing (Figure 3.15). Many aspects which affect the choices of the hardware architecture, such as cost, size, control complexity, are evaluated.

3.3.3.1 Passive balancing

Passive balancing methods remove the excess charge from the fully charged cell(s) through passive, resistors element until the charge matches those of the lower charged cells in the pack or the charge reference. Here it is optimal to use switched shunting resistors because the method is based on removing the energy from the higher charged cell(s) not continuously but in a controlled way using switches/relays. This can be executed at the end of the charging process. The main drawback of this method is the fact that the excess energy from the higher charged cell(s) is dissipated as heat. But, it gives the best trade-off between complexity, cost and power density.

3.3.3.2 Active balancing

On other hand, the active cell-balancing methods remove charge from higher energy cell(s) and deliver it to lower energy cell(s) by comparing the voltage.

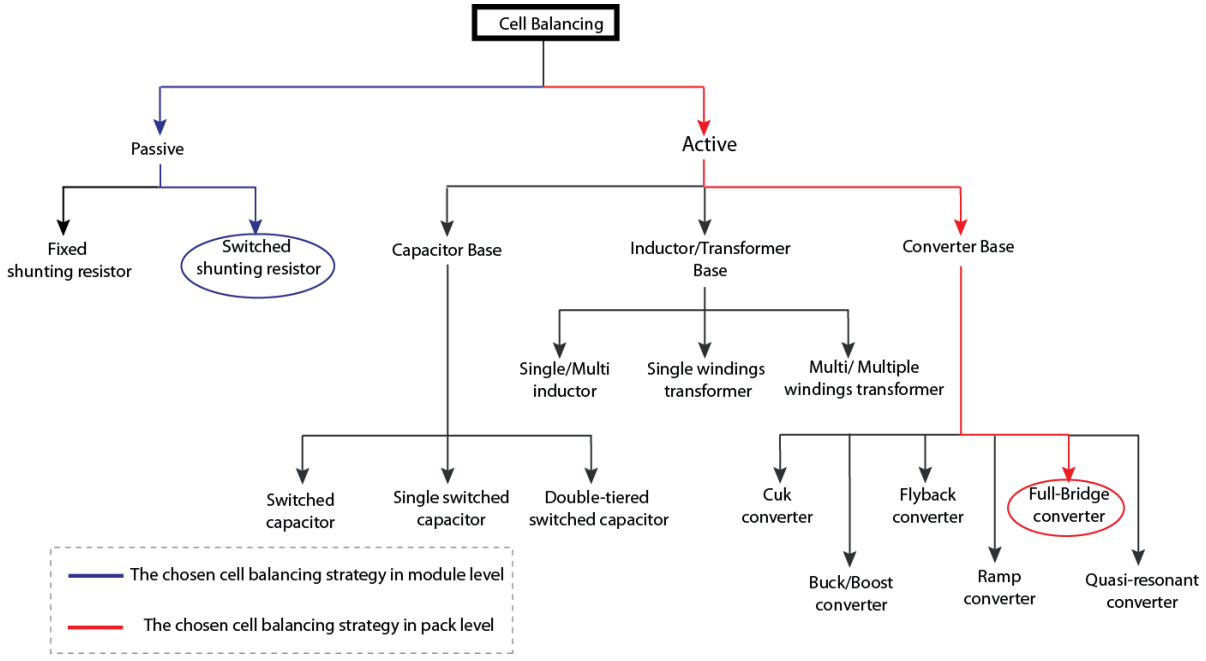

Figure 3.15: Cell balancing topologies

In this context, the full-bridge converter is chosen because it is very efficient and it can be combined with the driving and charging converter. The balancing topologies can be classified as passive and active balancing, as illustrated in Figure 3.15.

3.3.4 The BMS hardware architecture

Battery management system architecture is considered as either “centralized “or “distributed”:

3.3.4.1 Centralized BMS architecture

The centralized BMS consists of a single controller that handles all functions (monitoring, cell balancing, charge control, protection, cooling, etc.). This is less expensive than the distributed BMS, however, it adds a complex sense of lead harness which needs to be protected against short circuit and failure propagation.

3.3.4.2 Distributed BMS architecture

The distributed BMS contains a master controller in addition to multiple distributed boards that serve as voltage and temperature monitoring boards at a module level (submodule). This method allows limiting the damage propagation in case of failure, however it adds multiple electronics locations which are normally difficult to protect from conductive elements.

3.3.4.3 Hybrid BMS architecture

The hybrid BMS is a combination of centralized and distributed BMS by reducing the complexity of the whole BMS architecture and by increasing the flexibility in term of cost. For instance, the CMMC offers a centralized BMS on the pack level, which is based on a selecting and sorting algorithm, this is implemented in modulation level. A distributed BMS is required on the modules level for the individual battery balancing.

3.3.5 The BMS software architecture

The BMS contains a software package which is comprised of the following components:

- Application software: main controlling software, I/O processing, CAN communication, relay control, fault handling.
- Diagnostic: for the regulation of the operation and service.
- Algorithm suite:
  - State of Charge (SoC): determination of the remaining capacity of the battery.
  - State of Health (SoH): determination of the remaining life of the battery.
  - Power/current available: algorithm to communicate to the main controller the battery’s current state and the available charge/discharge power.

Next, particular attention is paid to the algorithm suite, since it represents over 90 % of the BMS software.

3.3.5.1 State of Charge (SoC)

The state of charge is the equivalent of a fuel gauge for the battery pack in electric vehicles. However, it is not measurable and therefore the estimation requires a strong level of battery cell characterisation and testing. This needs typically around 6 to 12 months of development for a baseline

algorithm starting from the first initiation. In fact the estimation of the state of charge is a complex computation, it is impossible to cover all the characterisation and testing of the given battery cell along its life cycle under an arbitrary operation mode. Therefore, this thesis concentrates exclusively on deterministic systems by measuring just the voltages across the battery modules. Mathematically different but closely related to the area of a robust control, which deals with the design of control laws that are guaranteed to perform even if the assumed model of the controlled system is incorrect, with the allowed deviations quantified in appropriate norms or under the possibility of imperfect controller design. It is believed that the most important and productive approach to know the state of the battery seems to be by measuring the voltage and plotting its corresponding PQt profile; this approach fits the design of the control system.

*3.3.5.2 Battery **PQt** profile*

The term PQt profile has been introduced, because it can give sufficient information about the state of the battery after measurements [48]. In the framework of smart grids, electric vehicles owners advertise to aggregators by giving their (P, Q) planes, which is a plot of its instantaneous active and reactive powers. In fact, the PQt profile advertised that the vehicles owners have to match the set point values (P_0, Q_0) that the aggregators are willing to reach for a defined time frame Δt_0, in order to buy/sell the ancillary services.

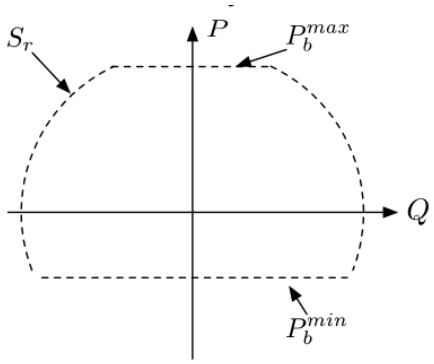

Figure 3.16: Typical PQt profile of a Lithium battery [48]

Figure 3.16 shows a typical PQt profile of a battery in defined time, the maximum P_b^{max} which is depicted in this figure, corresponds to the maximum active power that the battery can provide, whereas the P_b^{min} is the maximum active power that the battery can accept. However, this curve depends on the battery technology. It should be noted that, when an alternating current is applied to a battery module, the angle shift between voltage and current wave can be measured in order to get the PQt profile. This is the so called PMU which stand for Phasor Measurement Unit. The implementation methods can be seen in the paper [48]. However, the result can be also presented with Nyquist diagram of the complex impedance Z_{bat} :

$$Z_{bat}(f) = \frac{U_{bat}}{I_{bat}} \cdot e^{j2\pi f} \tag{3.10}$$

It should be noted that the *PQt* profile approach is limited on the engineering level; therefore the characterization and testing of the battery cells according to a given calendar should be done at manufacturing level.

3.3.5.3 State of health (SoH)

The state of heath allows distributing the battery life cycle of the battery module on the pack level. It has a strong relationship with the battery's degradation. It is not measurable therefore the estimation requires a strong level of battery cell characterisation. Also it requires a relevant testing, which needs typically around 5 to 10 months of development for a baseline algorithm starting from first initiation. However, this has a strong relationship with the degradation phenomena versus life cycle, In short, this estimation is complex. That is the reason why, the PQt profile can give a better estimation of the SoH, meaning that the battery impedance is directly proportional to the SoH. Nevertheless, the thermal testing and the characterisation aspects as well as the degradation of battery are not developed in this thesis, because the main focus is about the battery balancing.

3.3.6 EV's BMS design requirements

Over the last decades, the battery packaging has been an extreme challenge for increasing the EV's power density. In fact, there has been a great deal of interest recently in batteries which convert chemical energy to electrical energy for supplying the EVs electrical motor and providing ancillary services during charging operation. However, a number of problems have arisen in connection with the use of such electrical energy generating devices. For example, individual battery cell(s) typically furnish the electrical power of a few watts or less whereas many of the large applications require power in the kilowatt (kW) range. Also, the batteries provide a direct current output whereas most of the uses contemplated require alternating current and, particularly, quasi-sinusoidal voltage and current waveforms with small harmonic distortion. Moreover, most of such lithium batteries have very poor regulation, means that the voltage output differs markedly as a function of the current output.

It is apparent, therefore, that any power electronics using batteries must be able to combine many of the individual battery cells efficiently, and must be able to convert to direct current into alternating current. Further, the converter must yield a low impedance, quasi-sinusoidal output with small harmonic distortion. In fact the power conversion should include a programmed switching system for converting the direct current into alternating current or some other variable current, or for converting alternating current of one frequency into alternating current of another frequency. The system should therefore employ a number of stages connected in cascade. Each stage should include a battery cell string and static commutation cell means adapted to bypass the battery cell string, to interconnect the battery cell string with other electrical energy sources or storage units across a load in a programmed fashion and to reverse the direction of the current flow in the load to apply. In fact the power conversion should provide the following proprieties:

- a converter wherein a number of battery elements, each providing a quasi-constant voltage, are combined to furnish a time varying output voltage.
- an inverter furnishing a quasi-sinusoidal output whose harmonic content is controllable.

- an electric energy converter having a low impedance output.
- an arbitrary large voltage by combining a number of low voltage batteries modules.
- a power converter within great flexibility is permitted in the combination of individual devices and the manner in which these devices are combined to provide an output.
- a converter which include redundancy in order to increase the reliability of the electric car
- a converter within a great flexibility of multi-conversion DC/AC, AC/AC and AC/DC.

Back to literature; in 1975, Richard H. Baker invented a programmed switches system for converting direct current into alternating current, as depicted in Figure 3.17.

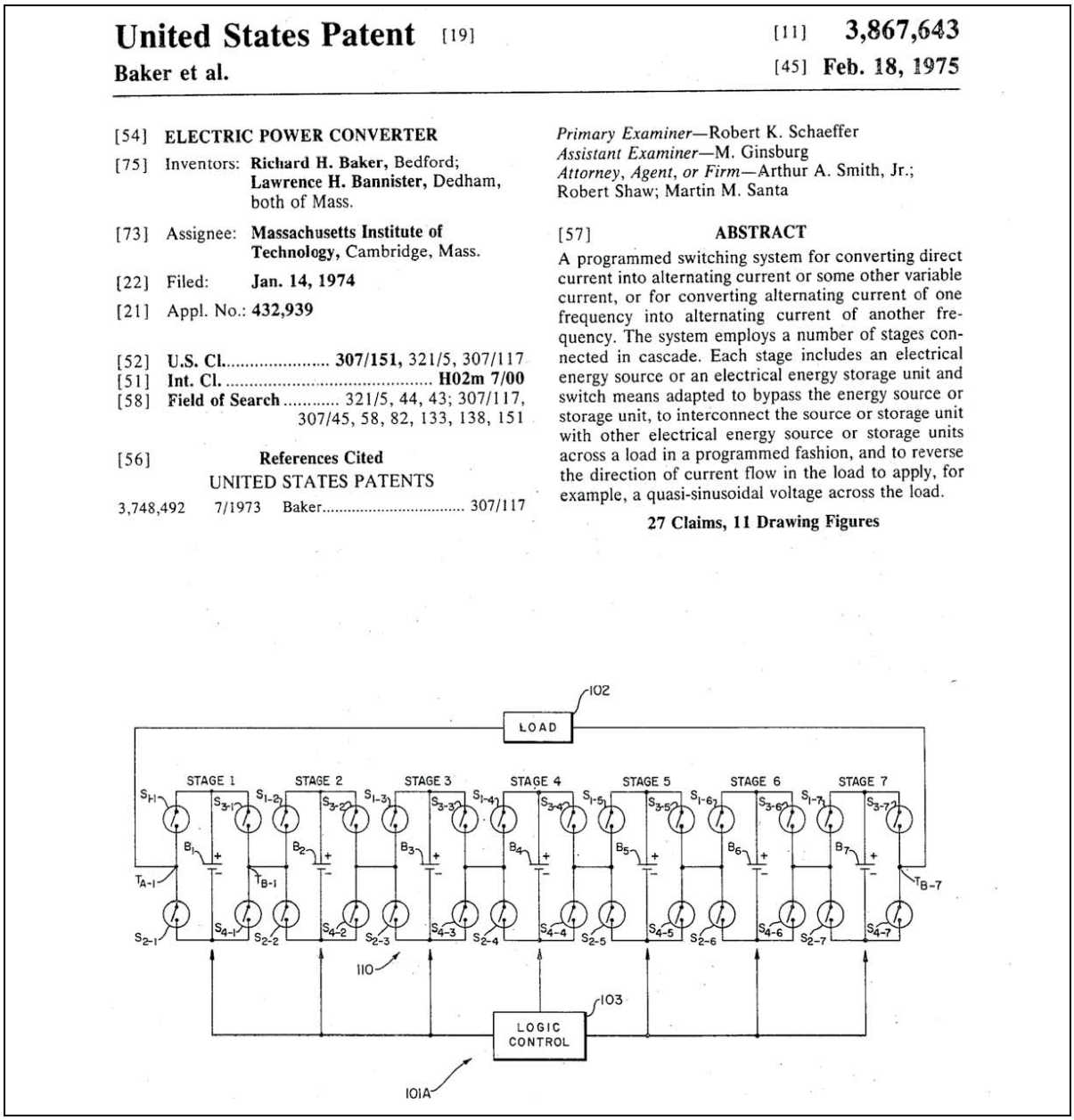

United States Patent [19]

Baker et al.

[11] **3,867,643**

[45] **Feb. 18, 1975**

[54] **ELECTRIC POWER CONVERTER**

[75] Inventors: **Richard H. Baker,** Bedford; **Lawrence H. Bannister,** Dedham, both of Mass.

[73] Assignee: **Massachusetts Institute of Technology,** Cambridge, Mass.

[22] Filed: **Jan. 14, 1974**

[21] Appl. No.: **432,939**

[52] **U.S. Cl.** **307/151,** 321/5, 307/117

[51] **Int. Cl.** **H02m 7/00**

[58] **Field of Search** 321/5, 44, 43; 307/117, 307/45, 58, 82, 133, 138, 151

[56] **References Cited**

UNITED STATES PATENTS

3,748,492 7/1973 Baker 307/117

Primary Examiner—Robert K. Schaeffer
Assistant Examiner—M. Ginsburg
Attorney, Agent, or Firm—Arthur A. Smith, Jr.; Robert Shaw; Martin M. Santa

[57] **ABSTRACT**

A programmed switching system for converting direct current into alternating current or some other variable current, or for converting alternating current of one frequency into alternating current of another frequency. The system employs a number of stages connected in cascade. Each stage includes an electrical energy source or an electrical energy storage unit and switch means adapted to bypass the energy source or storage unit, to interconnect the source or storage unit with other electrical energy source or storage units across a load in a programmed fashion, and to reverse the direction of current flow in the load to apply, for example, a quasi-sinusoidal voltage across the load.

27 Claims, 11 Drawing Figures

Figure 3.17: Extract of the Baker's patent in 1975 [49]

The system employs a number of stages connected in cascade where each stage includes an electrical energy storage unit and commutation cells, as depicted in Figure 3.17 above. The topology is based on a 4-quadrant converter It should be noted that, the battery in each stage consists of a series connection of battery cells and an H-bridge converter. However, this invention has been forgotten until the Modular Multilevel Converter has been introduced in 2002.

3.3.7 Modular Multilevel Converter (MMC) with integrated split energy storage

In 2002, the concept of Modular Multilevel Converter which is well-known with the acronym MMC, M2C and M2LC has been introduced by R. Marquart [50]. A Modular Multilevel Converter (MMC) is an attractive solution for power conversion without transformers. As MMC consists of cascade connections and floating DC capacitors, it requires continuous voltage monitoring. The MMC is one of the most promising multilevel converter topologies proposed in recent times. There are many advantages of this converter over conventional ones and the most significant features are the following: simple realization of redundancy, low device ratings, easy scalability and a possibility of common DC bus configuration for multi-drive applications.

Almost all of the existing investigations regarding this topology are based on the fundamental function of it, averaging and balancing control of the capacitor voltages. Capacitor voltage balancing or control can be obtained by a feedback control loop using voltage sensors.

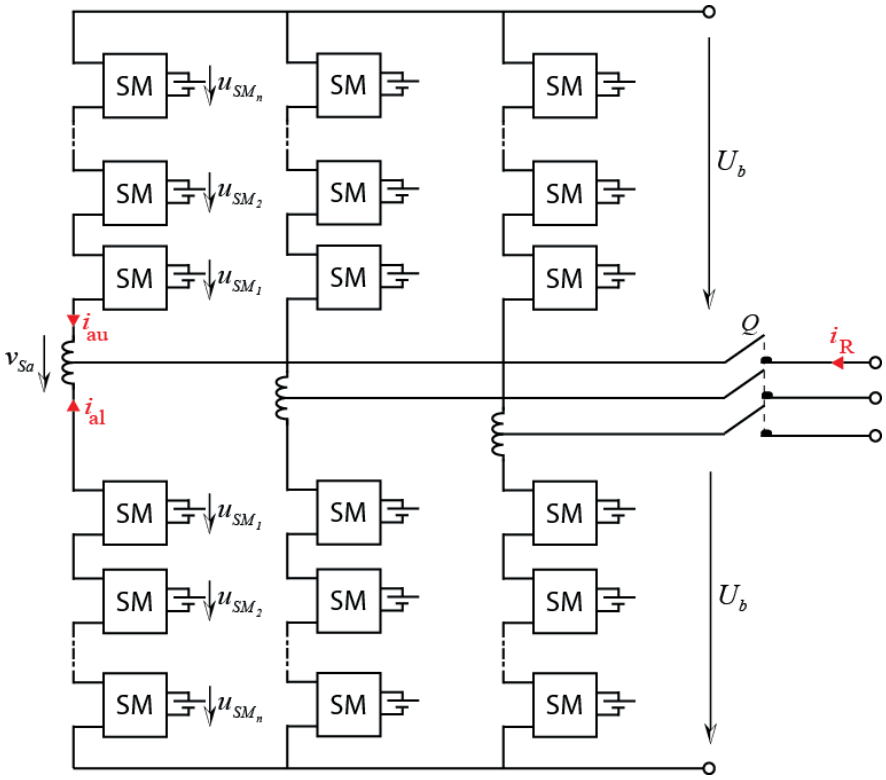

Figure 3.18: Typical scheme of modular multilevel converter with split integrated energy storage

On the one hand, using voltage sensors to measure the capacitor voltages is a relative straightforward approach. On the other hand, as the number of cascaded modules increases, it will be necessary to increase the number of voltage sensors which might result in an increased hardware complexity, which will influence negatively the system reliability. For reliable operation of inverters being part of the MMC, a decrease of the number of measurement sensors might be necessary. In the frame work of MMC application as compensator for asymmetrical grid or buffer for power leveling, etc. Figure 3.18 shows a base structure of modular multilevel converter (MMC) with split integrated storage (SIS). More often the submodule is based on two stages and 4-quadrant DC/DC submodule. This reduces the complexity of the internal voltage balancing. The next section is dedicated to the proposed architecture, so called Flex-EV which is based on the MMC.

3.4 Flex-EV architecture

3.4.1 Motivation

As seen from the vehicle side, the actual problem may be re-formulated by three distinctive EV-related terms of range, range flow-rate, charging compatibility:

1. *Range* is the average distance an EV is able to cover with the maximally recharged battery in given conditions (capacity, charging current, initial state of charge etc.). This depends also on the EV's aerodynamic shape, mass, as well as the EV's powertrain performance.

2. *Range flow-rate* is the driving distance augmentation per time unit of recharge, expressed in km/min or km/h. This depends on EV's battery power density and the overall efficiency of the EV's powertrain.

3. *The charging compatibly* is the flexibility of the EV to charge with a large range of charging infrastructures; from basic supply AC household to AC or DC ultra-fast charging station, meaning from level 1 to level 4 of charging infrastructure according to IEC 61.

Those three criteria determine the quantity duration and flexibility of intermediate recharges during a trip and as follows, the total travel time and average speed. Whereas the fuel tank capacity of an internal combustion engine powered car is independent of the tanking speed, the available capacity of an electrochemical battery is de-rated at high charging rates, and additional influence is posed by the ambient temperature. The tanking speed (resp. charging power) is directly related to range flow-rate; on the other side, the range of an EV decreases while increasing the charging power due to the electrochemical limitations of the traction battery. Thus a trade-off between range flow-rate and range itself is inevitable. However, bearing in mind that an average driver rarely drives hundreds of kilometers non-stop, the downgraded range could be acceptable if the ultrafast charging infrastructure coverage is sufficient. This is the reason why the concept of the Flex-EV has been introduced in this thesis.

3.4.2 Description

As seen before in paragraph 3.1.2, the EV hardware architecture consists of two main parts: first, the battery subsystem, which is composed of the battery pack with its system management units, and the on-board battery charger. Second, the traction subsystem, which is composed of the driveline (wheels, shaft, differential, gear, etc.), the electrical motor as well as the voltage source inverter (VSI). Paragraph 3.3 deals with the battery packaging where the battery management approach has been emphasized in order to deal with the battery balancing. Therefore a BMS architecture based on a cascaded H-bridge has been chosen on the pack level, whereas a switched shunt resistor BMS is kept on the module level. This choice gives the best tradeoff between power density, cost and complexity of the BMS. Since the final goal of the Flex-EV deals

with integration of a three-phase power electronics structure, this is able to control the circulation of energy between the embarked battery and a large charging infrastructure while providing a balancing strategy for the Split Integrated Storage (SIS) battery based. Then, a six phase cascaded H-bridge converter has been designed in order to form a three phase MMC based on H-bridge which supplies an open-ended three phases motor. This new power electronics structure is presented is called the “Configurable Modular Multilevel Converter”, with the given acronym CMMC.

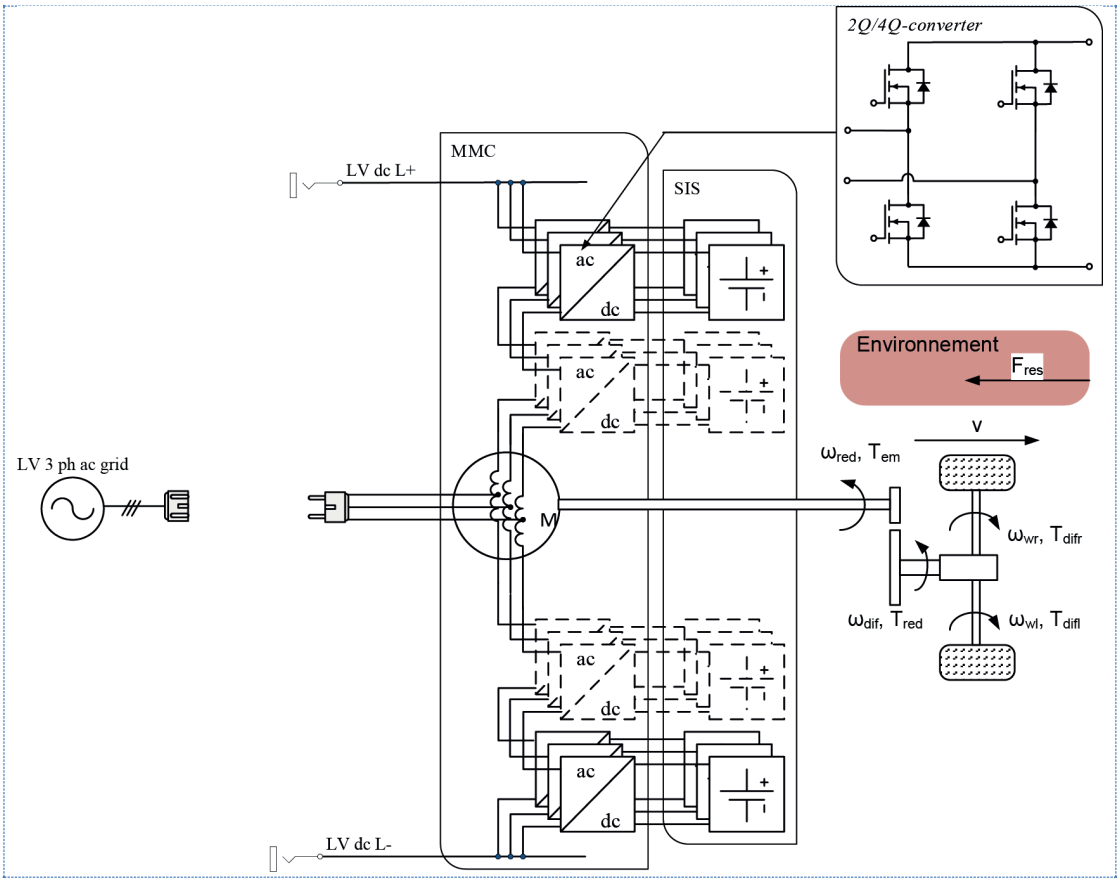

Figure 3.19: Flex-EV architecture

The configurable modular multilevel converter is considered as part of the family of modular multilevel converters. Hence, its heritage allows bringing the whole advantage to EV applications. In addition, it carries the surname of configurable because the converter plays a double role: in fact, it can work as traction converter as well as a charger, which increases the power density and reduce the cost by combining the traction and charger converters.

In detail, the concept is linked to the idea of replacing the branch inductances of the standard MMC by the tapped-windings of the stator. This allows operating the stator windings as current filters during charging mode. This strategy may reduce the use of raw materials like copper and iron because the overall EV converter size is reduced when compared to conventional distributed EV converters which include bulky components.

However, this brings the necessity to use semiconductors, electronics components as well as intelligence and controllability of power flow in a power conversion system. It should be noted that so far the BMS for EVs is composed by a large number of semiconductors and passive component for balancing the Depth of Discharge (DoD) of the battery cells and modules.

This is the reason why the battery packaging cost effectively becomes higher afterward in comparison to the battery cells cost. The CMMC offers an active balancing strategy of the battery modules DoDs by splitting the conventional battery into multi modules; this allows increasing the energy saving in comparison to the standard passive balancing. In fact, the BMS is centralized and this reduces the battery packaging cost in comparison to the standard distributed BMS.

In the framework of semiconductors, there is competition between several different devices to fill the position. The device which would mainly dominate powered MMC applications in the MOSFET, since it trends to have the best mix of characteristics. It is voltage controlled and therefore easy to drive. It is also modulated so that the low voltage, high current devices have a relatively low on-state voltage drop. Its structure doesn't include an integrated body-drain diode, so the circuit designer is free to choose an antiparallel diode in a way that suits the best the application. For minimum switching losses and low electromagnetic interference, a diode with a small reverse charge and soft recovery characteristic is optimal. In addition, the CMMC devices are operated at a low blocking voltage and low switching frequency; this permits to decrease the switching losses and therefore the volume and weight of the heat sink.

3.4.3 Flex-EV configurability

Regarding the configurability of the system, the configuration mode is controlled at the level of the modulation reference signals, by the shifted angle Ø between the upper and lower arm currents.

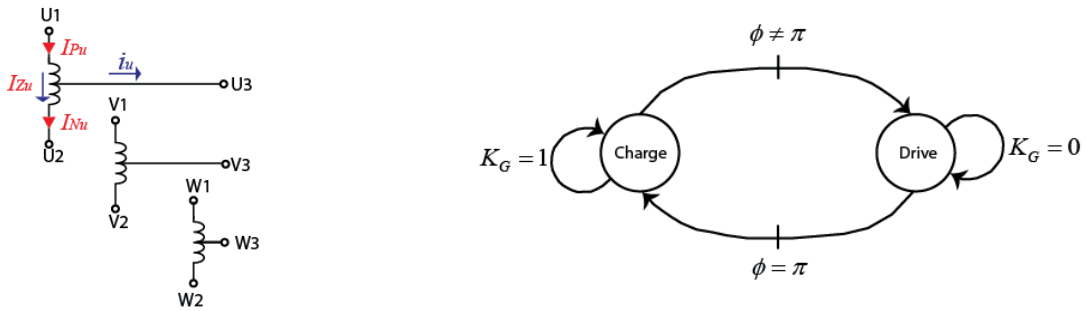

(a) The tapped stator windings

(b) State flow for the CMMC

Figure 3.20: Configurability principle of the CMMC

Therefore, attention is only paid to the U-phase, as depicted in Figure 3.20 (a), because the operating principle is identical among the three phase branches.

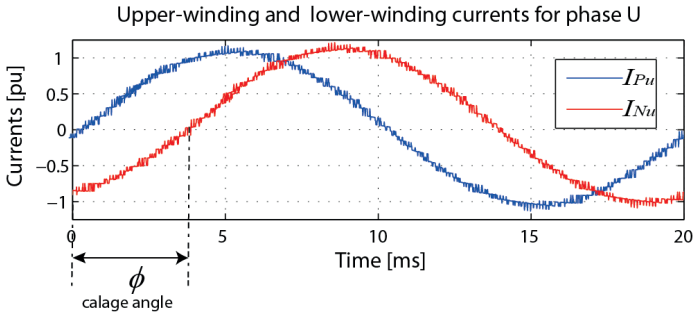

Figure 3.21: Illustration of the calage[16] angle

Figure 3.21 illustrates the shifted angle between the upper and lower arms.This is called “calage”.

$$i_{Pu} = \frac{i_u}{2} + i_{zu} \tag{3.11}$$

$$i_{Nu} = -\frac{i_u}{2} + i_{zu} \tag{3.12}$$

$$i_{Zu} = \frac{1}{2}(i_{Pu} + i_{Nu}) \tag{3.13}$$

According to the equations (3.11) and (3.12), the motor-current components contained in i_{P_u} and i_{N_u} are in opposite phase with respect to each other, meaning the shifted angle is $\emptyset = \pi$ during charging mode.

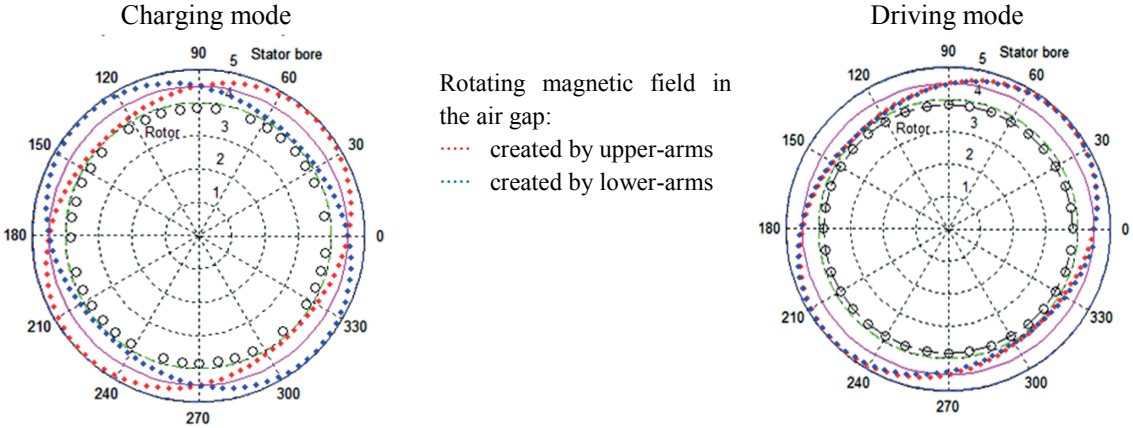

Figure 3.22: Simulation of rotor produced air gap traveling magneto motive force (mmf) wave for one magnetic pole-pair pitch of movement in 10 magnetic (electric) degree increments.

[16] Calage is the shifted angle between the upper and lower arm current of the stator windings

The Figure 3.22 illustrates the magnetic fluxes produced by the components, which are cancelled each other out. Therefore, the stator coupled inductor is only presented with the circulating current i_{Z_u} [51]. However, an electromagnetic torque is generated once $\emptyset \neq \pi$.

	Configuration				
Mode	Drive	Charge			Drive
Time (s)	]0.75….0.86 [	]0.86….1.00[	]1.00….1.10[	]1.10….1.21[	]1.22….1.25[
	Traction	**1~phase AC**	**3~phase AC**	**DC**	**Recuperating**

Table 3.1: simulation time versus configuration

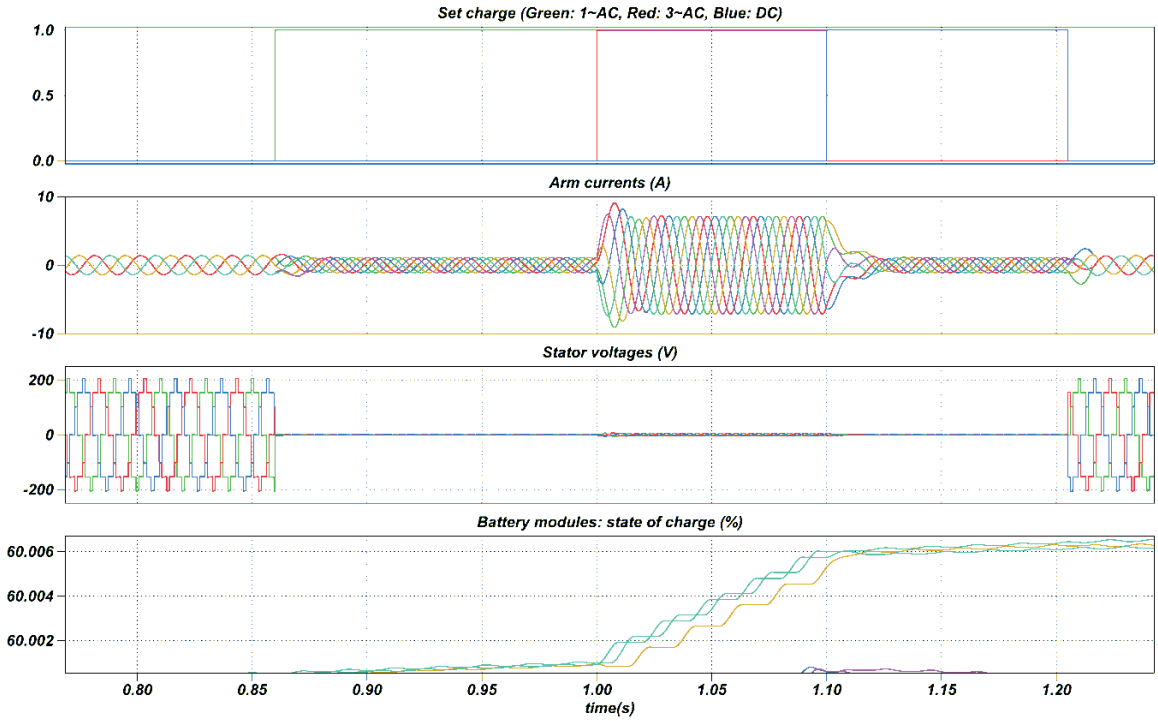

Figure 3.23: CMMC configurability illustration

Table 3.1 and Figure 3.23 illustrate the configurability of the topology by simulation. In fact during the driving and/or recuperating configuration, the stator voltages are different from zero in order to move the electric vehicle or regenerate the energy back in the battery. In contrary, during the charging configuration, the stator voltage is equal to zero because the arm voltage components cancel each other out. However, it should be noted that the rotor-angle is not controlled during charging mode. A specific mechanical anti-lock system is not required because the arm currents will not produce magnetic fluxes. This topology is flexible with large voltage levels according to the number of connected series modules versus modulation strategies. It is also modular because the battery pack is split into modules. So, the capability of the system on fault ride-through is increased by bypassing the faulted modules.

3.4.4 Flex-EV design specifications

It is generally agreed that the specification of an electric vehicle depends on the range flow rate, which has a strong relationship with the battery and the motor capabilities. However, the dimensioning of the CMMC also has important key parameters for optimising the design of the Flex-EV. In order to address these facts, only the fundamental value of the converter output voltage is taken into account. In fact, in terms of power transfer capability, the worst case occurs when the stator phase voltage (U_{s1}, U_{s2}, U_{s3}) needs to match the grid line-to-line voltage (U_{12}, U_{23}, U_{31}) during the AC charging operation mode, where ΔV is the possible variation of the grid voltage. To explain the dimensioning mechanism, a simplified scheme can be considered (Figure 3.24).

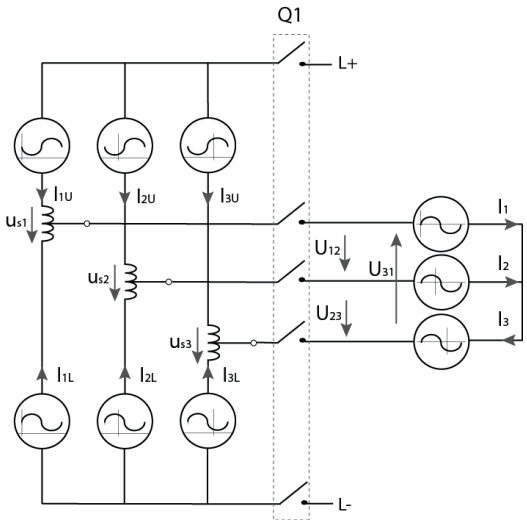

Figure 3.24: Representation of the CMMC in AC charging mode where Q1 can be closed

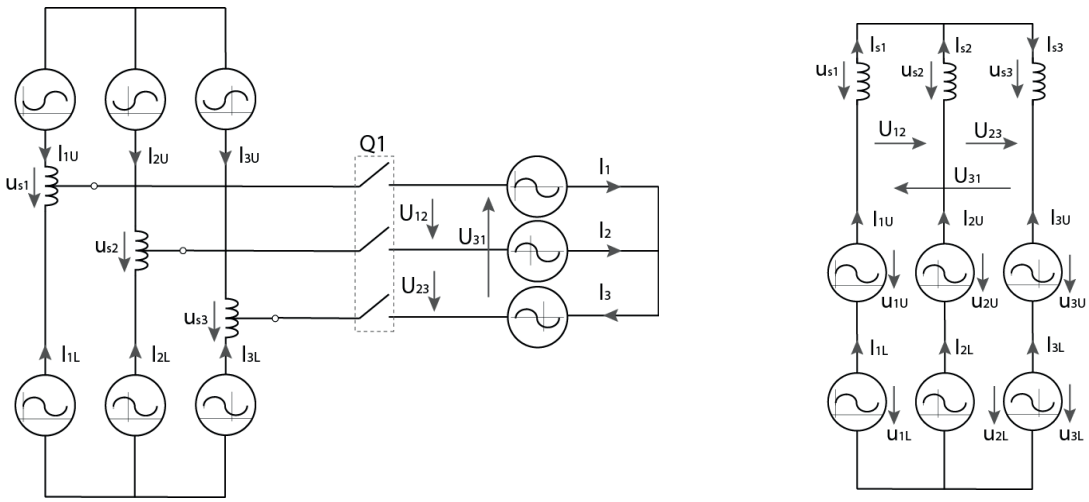

(a) CMMC model in charging mode no load (b) Equivalent CMMC model in driving mode

Figure 3.25: Simplified model of the CMMC

Since the phenomena are the same among the three phases, attention is only paid on the voltage law between phase 1 and phase 2, therefore, the voltage relation can be written as:

$$U_{s1,RMS} = \frac{U_{12,RMS} \cdot \Delta V}{\sqrt{3}} \tag{3.14}$$

Where, the voltage law is the necessary condition to specify the voltage and current ratings. The quantitative analysis that identifies when this limitation happens is presented as follows. S_{tot} is the total apparent power of the CMMC, (I_{1U}, I_{2U}, I_{3U}) are the upper-arm currents, (I_{1L}, I_{2L}, I_{3L}) are the lower-arm currents and (I_{s1}, I_{s2}, I_{s3}) are the stator currents, which can be deduced by:

$$I_{s1,RMS} = \frac{S_{tot}}{3 \cdot U_{s1,RMS}} \tag{3.15}$$

By considering the mesh between the phase 1 and the phase 2, with P the number of submodules in the upper- and N the number of submodules in the lower-arms, for proper operation, the minimum differential potential between L+ and L- is defined by:

$$m_i \cdot U_{dc} = \sum_{i=1}^{N+P} U_{1M_i} - \sum_{i=1}^{N+P} U_{2M_i} = U_{1U} + U_{1L} - U_{2U} - U_{2L} > U_{12,RMS} \cdot \sqrt{2} \tag{3.16}$$

where m_i is the modulation index, also called set value. This equation is the first boundary condition for setting a CMMC.

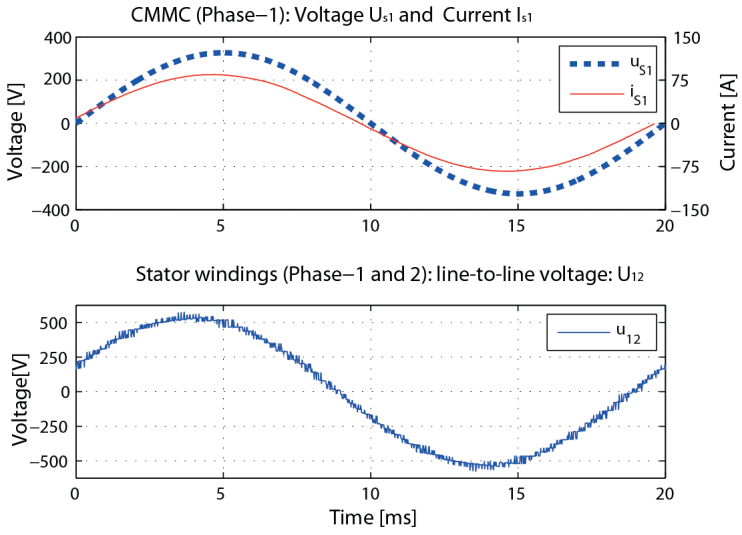

Figure 3.26: Typical example of the relation between the line-to-line voltage (grid voltage) and the stator phase voltage and current

The sum of the feeding voltage generated by the 4Q/2Q-converters in series should be strictly higher that the line-to-line peak voltage of the stator windings.

Figure 3.26 illustrates the relation between the line to line voltage and the stator phase voltage and current. The line-to-line stator voltage can be defined as:

$$U_{s1,RMS} - U_{s2,RMS} = U_{12,RMS} \tag{3.17}$$

It should be noted that by considering a two level modulation as the worst case for dimensioning the battery voltage, the branch voltages must be out of phase by half of the maximum of their magnitudes in order to generate the sinusoidal waveform of the line-to-line stator voltages.Then, the relation between the line-to-line voltage and the stator phase voltage can be written as:

$$U_{12,RMS} = \sqrt{3} \cdot U_{s1,RMS} = \sqrt{3} \cdot U_{s2,RMS} \tag{3.18}$$

Therefore, the individual modules output voltage can be defined by:

$$U_{1M_1} = \cdots = U_{1M_L} = U_{2M_1} = \cdots = U_{2M_L} = \frac{\sum_{i=1}^{L} U_{1M_i} + \sum_{i=1}^{L} U_{2M_i}}{N \cdot \sqrt{3}} > \frac{2 \cdot U_{12,RMS} \cdot \sqrt{2}}{N \cdot \sqrt{3}} \tag{3.19}$$

For instance: $U_{12,RMS} = 400$ V, $N + P = 10$, $U_{1M_i} = U_{2M_i} = U_{3M_i} = \frac{2*400*\sqrt{2}}{10*\sqrt{3}} \cong 65$ [V], for a maximum index modulation of 0.9 and an assumed variation of the grid voltage of $\Delta V = 5$ %, the battery module nominal voltage must be around 75 Volt to satisfy the sizing of the battery voltage. But, the minimum battery capacity depends on the motor current rating, which is defined during the charging mode where the stator phase currents are cancelling each other out.

$$I_{1U} = -I_{1L},\ I_{2U} = -I_{2L},\ I_{3U} = -I_{3L} \tag{3.20}$$

In this situation, the EV is connected to the grid for battery charging or for providing ancillary services, the fundamental voltage across the stator inductance must be large enough to allow circulating the needed current and to deliver the required power.

3.4.5 Illustration

In order to illustrate the previous baseline calculation, the following Figure 3.27 shows the stator currents, the generated line-to-line stator voltages, the arm voltages of the branch 1 and the branch 2 as well as the rotor mechanical speed. This simulation represents the direct starting of the CMMC in driving mode. The calculation is based on induction machine parameters with ratings of 3*380-420/440-480VY, 50/60Hz 118 kW, 2 pole pairs.

It is shown that the upper and the lower arms are in phase. Also they are positive. For instance, for the branch 1 and the branch 2, the superposition of these two adjacent branch voltages forms the line-to-line stator voltage U_{12}, which is represented by the waveform in blue color among those stator line-to-line voltages. This line-to-line voltage U_{12} is optimum when the branch voltage on

the phase 1 crosses the branch voltage on the phase 2. The same phenomenon is seen between the branch 2 and the branch 3 as well as between the branch 3 and 1. In fact, the generation of the internal voltage between the three phase branches is only defined by the internal voltage meshes. Thereafter, the stator voltages induce currents which in turn induce the electromagnetic torque. The starting speed is shown in Figure 3.27 where, three types of frequency are seen. The first correspond to a low frequency around 3 Hz which is due to the rotor inertia, the second is around 150 Hz due to the electric magnetization, and there is quite higher frequency due to the submodule cells commutation.

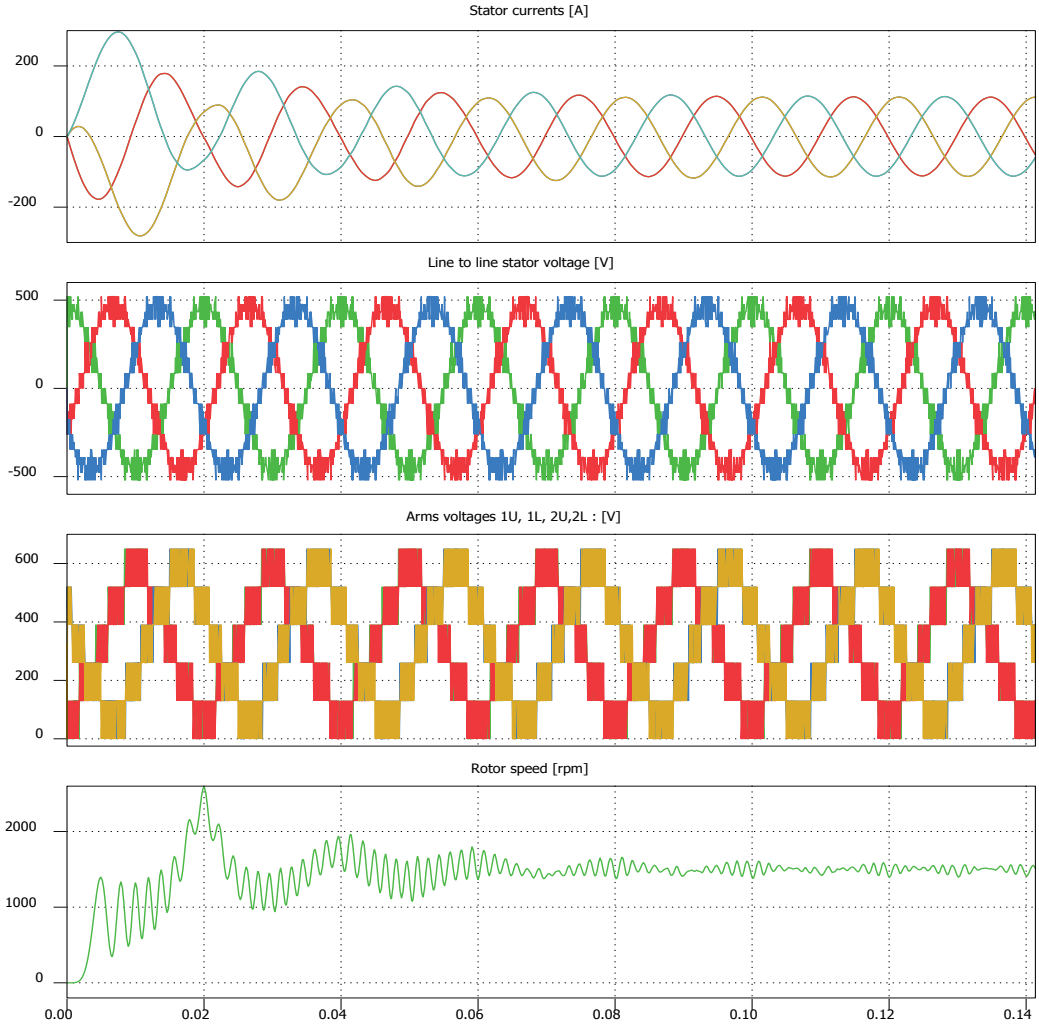

Figure 3.27: CMMC direct start operation (N=5)

This simulation illustrates the generation of an internal voltage between two adjacent-phases in CMMC three phase structures in open-loop operation.

3.5 Control circuit configuration

3.5.1 Generality

This paragraph is dedicated to provide a general overview of the CMMC control circuit. However, by its very nature, MMC control is a multidisciplinary subject; therefore it is reasonable to expect different approaches in MMC control theory. On the other hand, since the ultimate objective is to implement controllers in reals systems, some might take an ad hoc approach relying only on intuition and hands-on experience when designing the MMC control system. This MMC control can be classified in two main lines of work in MMC control theory, which sometimes have seemed to proceed in very different directions but which are in fact complementary:

1. One of these is based on the idea that a good MMC model should be available and that one wants to somehow optimize its behavior. For instance, physical principles and engineering specification can be and are used in order to compute the circulating current and the energy accumulated in each MMC arms. This allows firstly providing reliable and secure control of the reference powers, and secondly, to take into account the rational use of the energy flow in the MMC. This technique here is closely related to the classical calculus of variations and to other areas of optimization theory; the end result is typically a pre-programmed real-time active control.
2. The other main line of work is that based on the constraints imposed by uncertainty about the model or about the environment in which the MMC operates. The central tool is therefore, the use of feedback in order to correct for deviations from the desired behavior. For instance, various feedback control systems are used during actual droop control in order to compensate for errors from the precomputed generator speed. Mathematically, stability theory, dynamical systems, and especially the theory of functions of a complex variable, have had strong influence on this approach.

However, it is widely recognized actually that these two broad lines of work deal just with direct aspects of the same MMC problems and it does not make sense to make an artificial distinction between them.

Therefore it is optimal to propose a control circuit configuration and then the control designer is free to implement the suitable control approach, which relatively depends on the application, the depth of complexity and the cost of the implementation.

3.5.2 Configuration based on standard multivariable-PI controller

This first approach is based on the standard MMC control in literature [52], the method is based on multivariable-proportional-integral (PI) regulators and is claimed to provide fast dynamics and a zero steady states error.

3.5.2.1 Driving configuration

Here, the strategy used is called indirect imposition of the rotor flux through the component dq vector of the stator current (i_d^{ref} and i_q^{ref}) in rotor rotating frame (RRF). The principle looks like a very effective way of decoupling the complex multivariable structure of the induction machine. The main advantage is the direct access to the flux and torque, permitting a controlled field weakening and torque limit. In fact, the direct d-axis component of stator current represents the mag-

netizing vector, which represents the rotor flux of the machine. The magnetizing current should be maintained at maximum level which is limited below base speed by saturation of the iron-core and above base speed by the voltage of the CMMC, for instance, it is equal to nominal flux of the machine. However, in order to extend the speed range, the direct field weakening concept can be applied with constant power. This is depicted in the Figure 3.28.

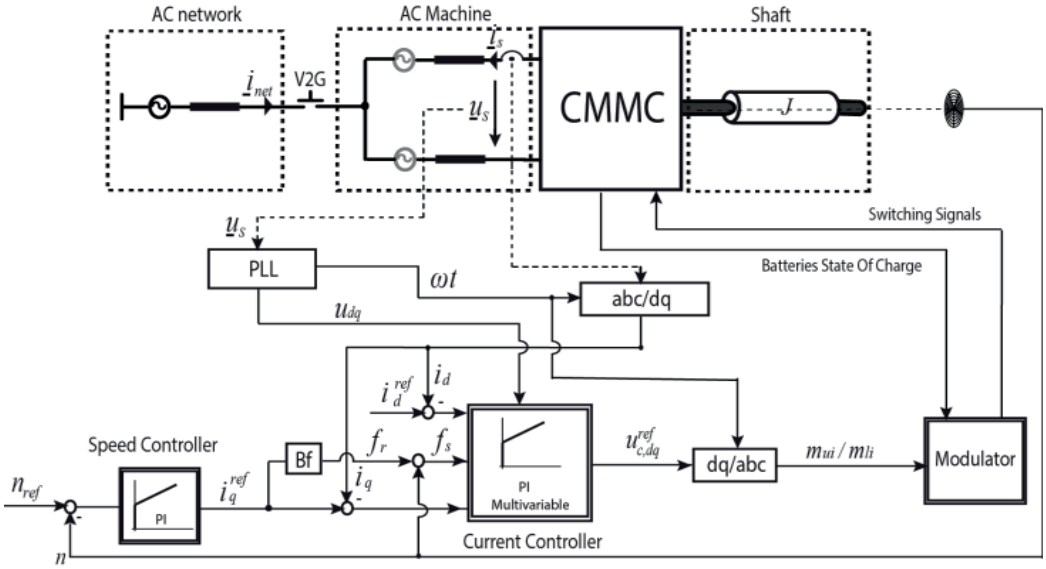

Figure 3.28: Structural diagram of the CMMC control with multivariable PI controller in driving mode

Moreover, in order to compensate the shaft inertia, the torque m_e or the speed n is controlled by a standard proportional integral (PI) controlled, and therefore it gives input to the q-axis component of the multivariable-PI controller which is depicted on the Figure 3.28.

$$m_e = \frac{x_h}{x_r} \cdot \psi_r \cdot i_{sq} \tag{3.21}$$

x_r represents the rotor leakage reactance and x_h represents the coupling stator and rotor magnetizing reactance. Then, the synchronous frequency f_s depends on the slip f_r which in turn depends on the rotor flux with the q-axis component of the multivariable-PI controller.

$$f_r = \frac{x_h}{\omega_r . T_r} \cdot \frac{i_{sq}^{ref}}{\psi_r} \tag{3.22}$$

ω_e is the nominal pulsation, n is the measured speed, T_r is the time constant, comparable to the field lag of the dc machine. ψ_r is the real part of the rotor flux. With one multivariable-PI current controller, the drive can be controlled by applying the well-known vector control. Furthermore, the torque can be positive or negative according to the sign of the i_{sq}^{ref} quadrature reference, that means the vehicle can be in forward mode or in regenerative braking mode according to the sign of the i_{sq}^{ref}. More details can be seen in the paper [46].

3.5.2.2 *Charging configuration*

During AC charging (V2G is switched on), the middle points of the stator windings are connected to the grid for charging the battery with an AC source or for providing ancillary services. In this context, the internally induced voltage $\underline{u}_i^S$ of the electrical machine disappears due to the self-compensation of rotating magnetic fields. Hence, the rotor current as well as the electromagnetic torque tends to zero. However, circulating current can induce a vibration of the shaft transmission. This is normal in MMC control because the circulating current is used to control the branch voltages as well as the vertical and horizontal balancing. Therefore an interlock is required in this case for safety reason. This can be illustrated on the simulation results (Figure 3.31) during the transient operation.

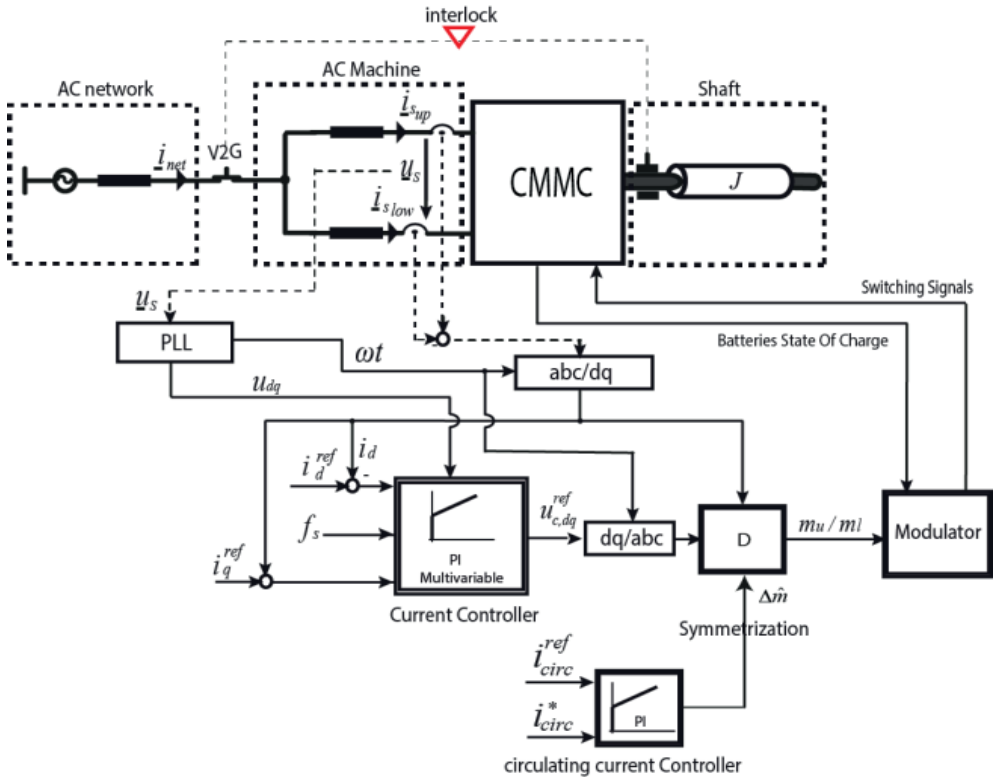

Figure 3.29: Structural diagram of the CMMC control with multivariable PI controller in charging mode

Figure 3.29 represents the structural diagram of the control during the charging mode operation. The purpose of this approach is to impose the required active and reactive power flows at the point of common coupling through the dq component of stator current. The principle looks like a very effective way of decoupling the complex multivariable control structure of the induction machine and grid. However, the active current should be maintained at the range of the battery in order to avoid overcurrent, limited below base charging current of the battery and above base current by the discharging current of the battery.

3.5.2.3 Structure diagram of the PI multivariable controller:

Since the control takes place in the rotating reference frame, the space vectors will be expressed in the same coordinate system. In the current case, it is reasonable to refer to the complex transfer functions describing the inverter and the asynchronous motor. Then, the control circuit block diagram adapted to a pseudo-continuous control will be presented. The structure of the multivariable PI controller will then be determined in a manner that the d- and q-axes become decoupled with the deduction of the controller time constants. Finally, the dynamic behaviour during the small setpoint variations can be demonstrated.

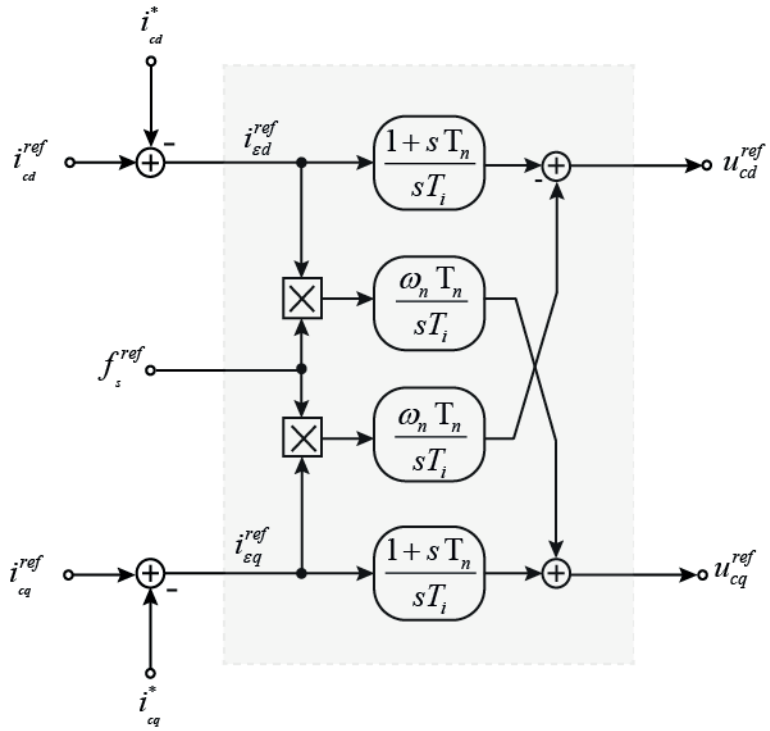

Figure 3.30: Structural diagram of the multivariable PI controller

Figure 3.30 illustrates the structure of a multivariable PI controller. As there are two inputs and two outputs, the more precise term would be a bivariable PI controller. As one sees, there is a conventional PI controller in two direct branches with the integral component $1/s \cdot T_i$. Nevertheless, in the crossing branches there is a I controller with the integral component $\omega_n \cdot T_n / s \cdot T_i$, thus generally more important than that of the direct branches. This integral component must be proportionally adapted to the stator frequency f_s, unless for the very low frequencies, the imposition of the crossing branches becomes predominant.

3.5.3 Dynamic performance evaluation of the control

In order to carry out the test, the configurability of the CMMC has been highlighted in this simulation, the simulation has been carried out during 3'000 ms, where the first 1'500 ms are dedicated to driving mode whereas the next 1'500 ms are dedicated to the charging mode.

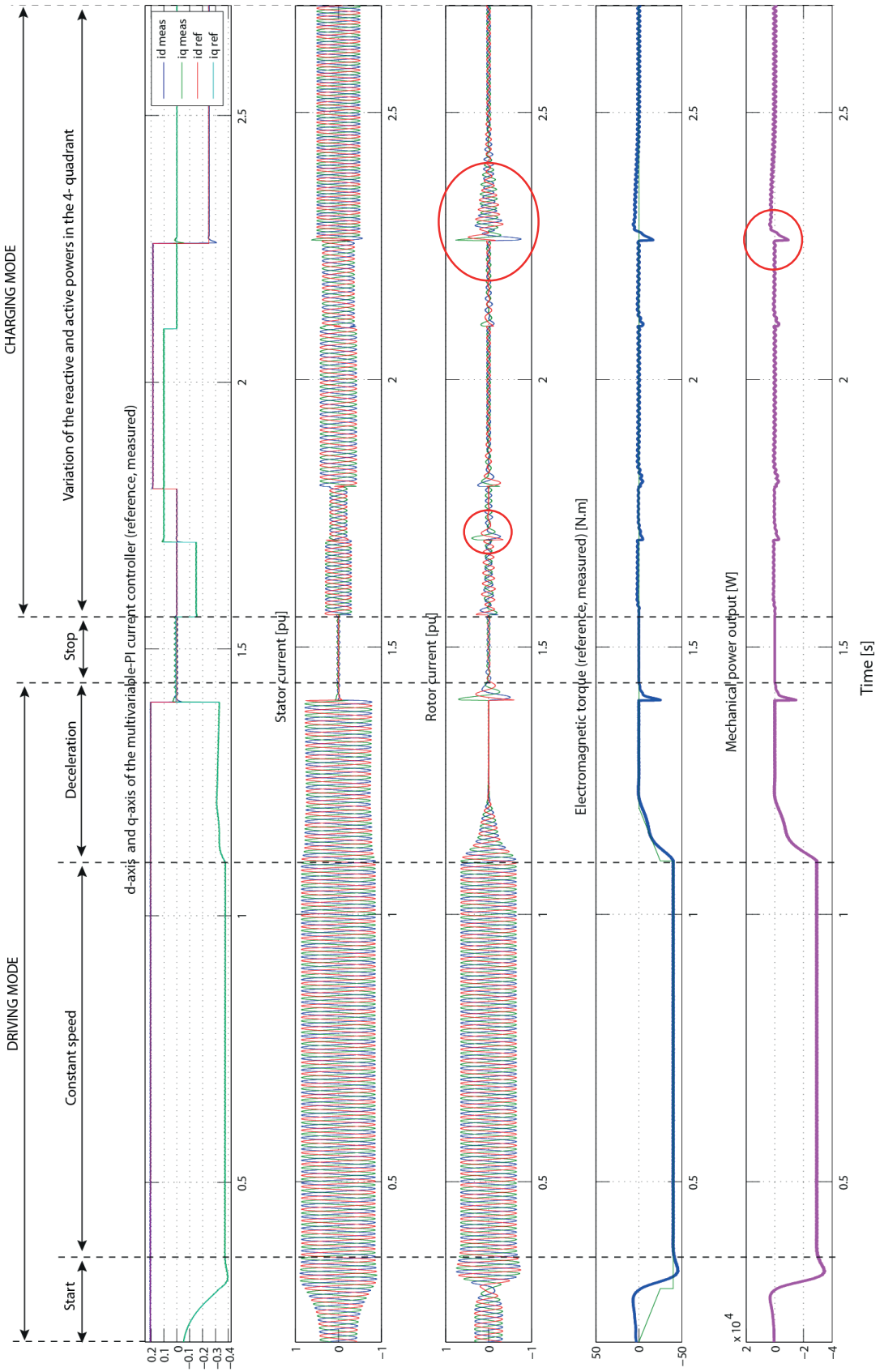

Figure 3.31: Performance evaluation of the multivariable-PI controller

3.5.3.1 Driving mode:

The simulation starts with a magnetization of the motor by imposing a current through the d-axis of the multivariable-PI controller. Then the speed is increased slowly by increasing the q-axis current vector of the multivariable-PI controller. It should be noted that the system starts with full load of 48 N.m, which corresponds to the nominal load. Therefore, it is expected to respond rapidly with an acceptable overshoot. It is shown in Figure 3.31 that the system responds perfectly and after 250 ms the nominal speed/torque is reached. This speed is kept until the simulation time of 1'200 ms while the deceleration is starting. Then, the system is stopped.

3.5.3.2 Charging mode:

At the simulation time of 1 600 ms the charging mode is performed; the d-axis and q-axis currents references are altered in somehow to operate the Flex-EV in the 4 quadrants of the PQt power plane. It is shown that the system responds perfectly however the decoupling between the d-axis and the q-axis shows a poor figure. It should be noted that the six arm currents are controlled by one PI multivariable controller which has been designed for three phase system. This is really an issue in terms of standard MMC control design.

3.5.4 Drawback of this first approach

The performance of the system has been evaluated by simulation and it is shown that the concept has the following characteristics:

- configurable in driving and in charging through the input of the multivariable-PI controller.
- capable to track the d-axis and q-axis current reference signals
- fast dynamic response with an acceptable tolerance overshoot
- decoupled vector control

Although, the control structure is relatively simple; it has been shown that the overall control has poor decoupling. For instance in driving mode, the figure illustrates a poor control of the reactive power due to the non-linearity of the induction machine. It is important to have a voltage control which is able to control the common mode voltage of the circuit.

In addition the frequency is almost constant because the induction machine is non-linear; for instance, for p=2 in induction machine, n_s is the synchronism speed (for instance, $n_s = \frac{f}{p} = 1500\ rpm$). In steady-state, the speed depends on the slip f_r which is between $0\ to\ 0.047$ when stator flux is equal to the nominal flux of the machine. This is roughly around 4% of margin to control the speed. This is the reason why the flexibility of the control is reduced.

Furthermore, one the main drawback of this approach is that the line-to-line stator voltages are not directly measurable; it must be estimated from the arm voltages. Therefore the control becomes complex. More details can be seen during the modeling of the system in chapter 4.

As a conclusion, multivariable PI control are considered as the most conventional approach, however, due to the their well-known drawbacks, such as a non-zero steady-state error, other approach such as the double current controllers based on state space variable has been investigated. In addition, in charging mode the state variable (stator current) become six variables instead of

three, this cannot anymore controlled with one PI multivariable controller since the balancing power between the upper and lower arm is not guaranteed.

3.5.5 Control configuration based on double state space current controllers

3.5.5.1 Description:

First of all, as seen in the standard control, during the charging mode, the current state variable became six current variables (three for the upper arm and three for the lower arm), therefore the PI multivariable controller which is basically designed for three phase system cannot control this system anymore. Moreover, the Flex-EV is designed without data communication with the charging station; It has to adapt with different charging infrastructures. Therefore since the grid voltage and current are not directly measured, the CMMC has to manage the connection with the charging station internally. This is there reason why I came up with new approach of control based on double state space current controller. Indeed, the CMMC can be considered as a controlled system which consists of a two motor drives in series where each half motor is controlled like a standard AC motor, as depicted in the following Figure 3.32.

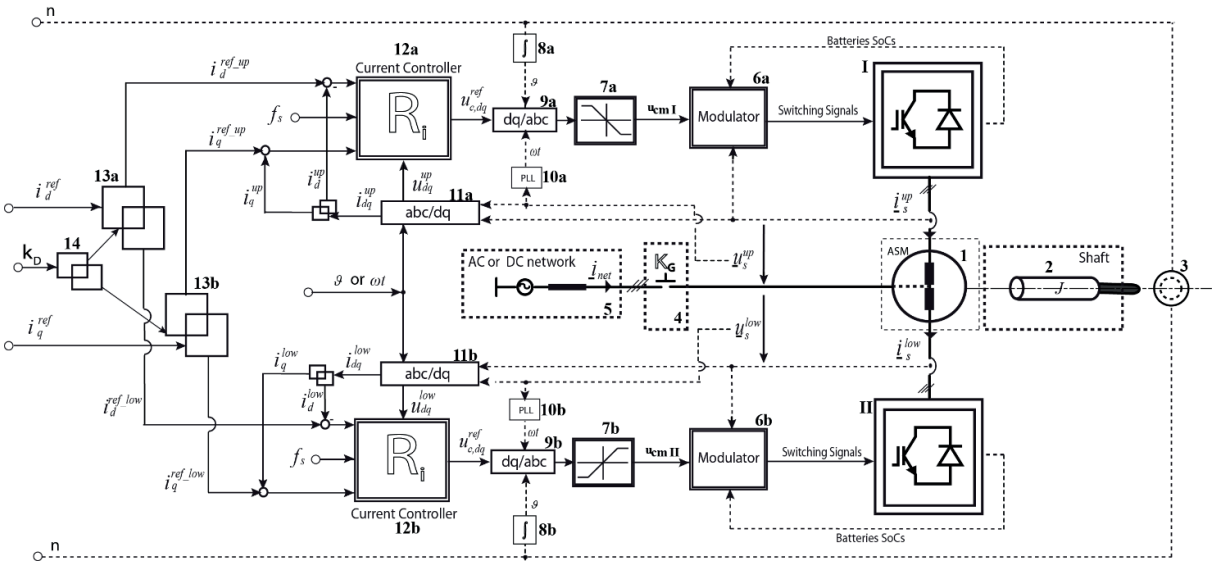

Figure 3.32: Structural diagram of the CMMC control with double multivariable state-space controller

This figure can be seen from right to left. Here the current controller is based on multivariable state-space control and the dimensioning is done in pseudo-continuous, more details regarding this approach are seen in the in [52]. Therefore this paragraph focuses on the operating principle of the control strategy. In fact, the system can be seen as a double three phase system where:

- In driving mode the speed/torque is the controller objective, this is done through imposition of the state variable which can be resumed below for each three phase arms:

For rotor model:

Input: $u = [\underline{u}_s, \underline{0}]^T$

State: $x = [\underline{\psi}_r, \underline{i}_s]^T$

Ouput = $x_2 = \underline{i}_s$

For flux model:

Input: $u = [\underline{u}_s, \underline{0}]^T$

State: $x = [\underline{\psi}_s \ \underline{\psi}_r]^T$

Ouput: = $[\underline{i}_s \ \underline{i}_r]^T$

It should be noted that the choice of the model depends on the control strategy.

- In charging mode, the rotor circuit disappears, therefore the control is done with the stator model in rotating reference frame:

  Input: $u = [\underline{u_s}, \underline{0}]^T$

  State: $x = [\underline{\psi_s}, \underline{i_s}]^T$

  Ouput: $y = x_2 = \underline{i_s}$

However, for the upper and the lower arm, the stator fluxes are expected to be cancelled out each other, only the stator currents play role as state variables for each arm. The notation in Figure 3.32 can be seen in the flowing table:

Notation	Description	Roles
I	The upper arm of the CMMC	Acts as voltage source converter
II	The lower arm of the CMMC	Acts as voltage source converter
1	Open end squirrel cage asynchronous machine (ASM)	The existing stator windings are used as filter inductance during charging mode
2	Shaft	Transmits the mechanical power
3	Speed sensor	Measures the mechanical speed
4	Universal plug for EV charging	Allows to connect to a large range of charging infrastructure
5	EV charging station	For power supply or load according to the power flow.
6a and 6b	Modulator with sorting and selecting algorithm	Converts the continuous signal references to a switching signal for the modules dc/dc converter
7a and 7b	Limitation circuit	For keeping the system in working range.
8a and 8b	Integrator	Converts the speed in angle
9a and 9b	Conversion blocs	Form the phasor element to the space abc dimension
10a and 10b	Phase locked loop (PLL)	For synchronizing with the given phase
11a and 11b	Conversion	For converting the space element to the rotating frame element
12a and 12b	Current multivariable controller	For decoupling the control of the real part and the imaginary part of the system (in rotating frame dq)
13a and 13b	conversion blocs for sharing the current reference between the upper and the lower arms according to the circulating current and the state of the power	$\begin{cases} i_d^{ref} = k_D^d \cdot i_d^{up\_ref} \\ i_d^{ref} = \left(1-k_D^d\right) \cdot i_d^{low\_ref} \end{cases} where, 0 \le k_D^d \le 1 \quad (i)$ $\begin{cases} i_q^{ref} = k_D^q \cdot i_d^{up\_ref} \\ i_q^{ref} = \left(1-k_D^q\right) \cdot i_d^{low\_ref} \end{cases} where, 0 \le k_D^q \le 1 \quad (ii)$
14	Conversion bloc for balancing the upper arm power and the lower arm power.	$\begin{cases} i_d^{ref} = k_D k_D^d \\ i_q^{ref} = \left(1-k_D\right) \cdot k_D^q \end{cases} where, 0 \le k_D \le 1 \quad (iii)$

Table 3.2: Component description of Figure 3.32

3.5.5.2 *Structure diagram of the double current controllers*

Very good results concerning steady state and dynamic behaviour are obtained by a *multivariable state-space controller* in the rotating reference frame as well. While the control takes place in the rotating reference frame, the studies should be made in the same coordinate system. As a result, it leads to a simplification of the structure of the multivariable state-space controller while keeping the same properties, especially regarding the decoupling between the d- and q-axes. This permits establishing a block diagram of the control circuit, adapted to a pseudo-continuous approach. Then, the basic relations of a multivariable state-space controller are expressed with the help of the space vectors. Thus, an equation of operation will be found permitting to deduct the hints for the controller coefficient dimensioning by the imposition of the roots. Then, the structure of the multivariable state space controller can be shown and the decoupling at the closed-loop control level, can be verified.

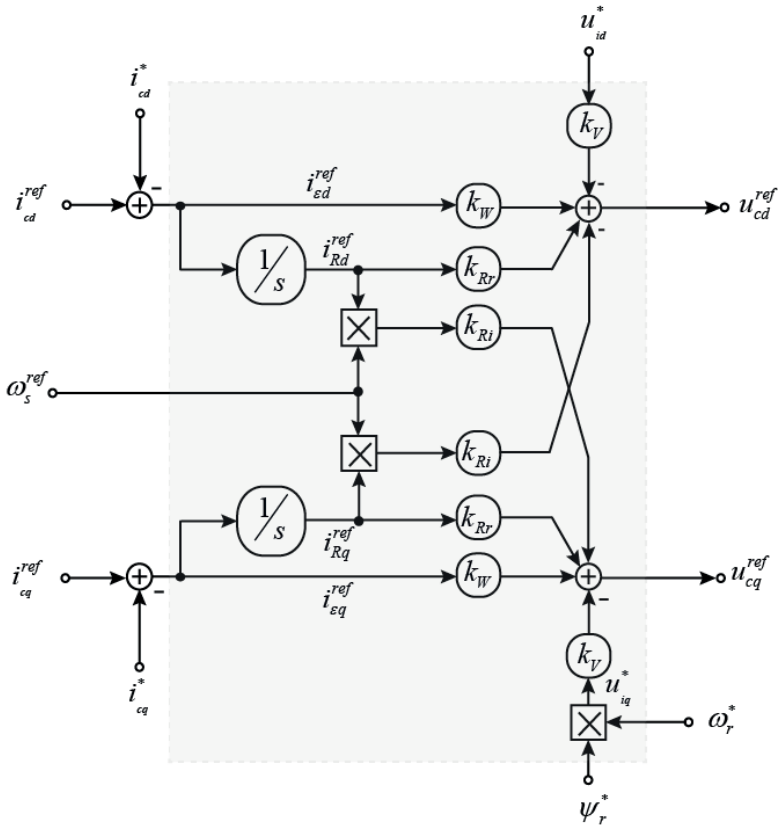

Figure 3.33: Structure diagram of the multivariable state-space controller

Figure 3.33 illustrates the multivariable state-space controller structure which has two inputs and two outputs in concordance with a bivariable state-space controller. As in the current case $k_w = k_{Ri}$, it is possible to form the two control errors $i_{\varepsilon d}$ and $i_{\varepsilon q}$, on the one side for the proportional component in the direct branches and on the other side, for the integral component both in the direct and crossed branches. The last ones decouple the d- and q-axes. The adjustment takes place according to the operating point given by the stator frequency f_s. The direct intervention of the disturbance value is different on the two axes. On the axis there is an adjustment according to the

operating point, given this time by the rotational speed ω_r The signals $\omega_s = \omega_e - \omega_r$ and ω_r can be obtained from the rotor flux imposition strategy by the stator current components according to Figure 3.36. A certain simplification of the structure is obtained whilst abandoning the direct disturbance intervention by ψ_r. The structure of the multivariable state-space controller is then equivalent to that of the multivariable PI controller.

3.5.5.3 Dynamic performance evaluation of the double current controllers

First, the performance evaluation of the two multivariable current controllers (12a and 12b) is demonstrated. It is in rotating frame therefore the simulation results in Figure 3.34 are largely sufficient to assess the performance of the controller in term of time response and the overshoot tolerance.

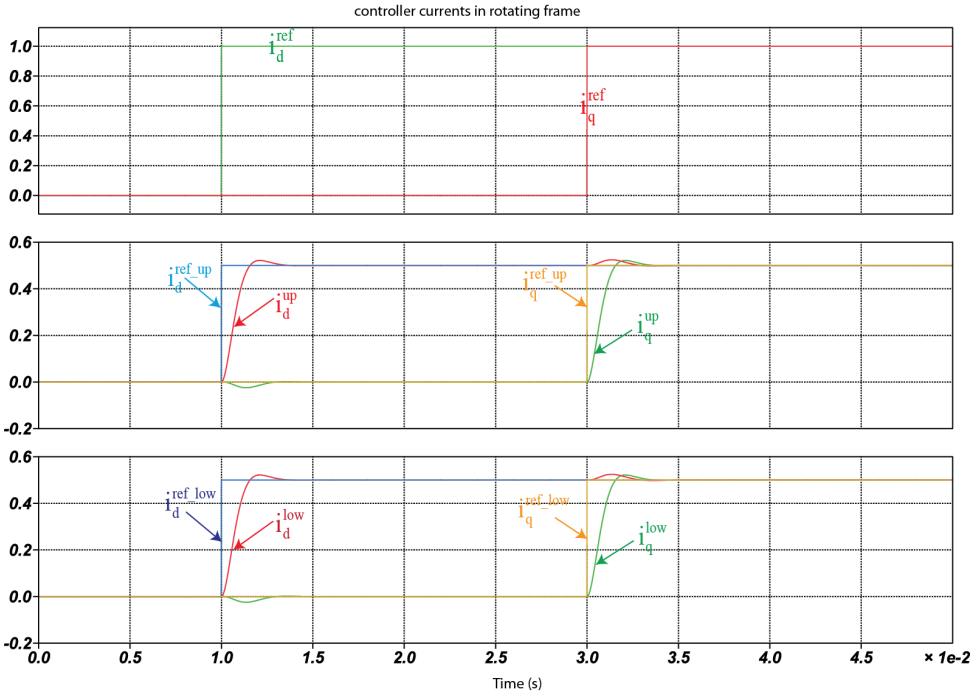

Figure 3.34: Performance evaluation of the controllers during AC charge configuration

As result, Figure 3.34 shows that the current controllers track the current reference perfectly. So, it allows controlling the CMMC system using vector controller in order to decouple the real and the imaginary parts of the system. It seems that the CMMC state variable can be decoupled easily in order to reach a very high dynamic performance. However, it should be noted that the time constant should be well tuned.

In charging mode, the system can perfectly operate like a double star full bridge string converter, without DC link however the neutral point is assimilated to the internal circulating current of the

system. In rotating frame the power flow is controlled by the d-axis and the q-axis of the inner current controller.

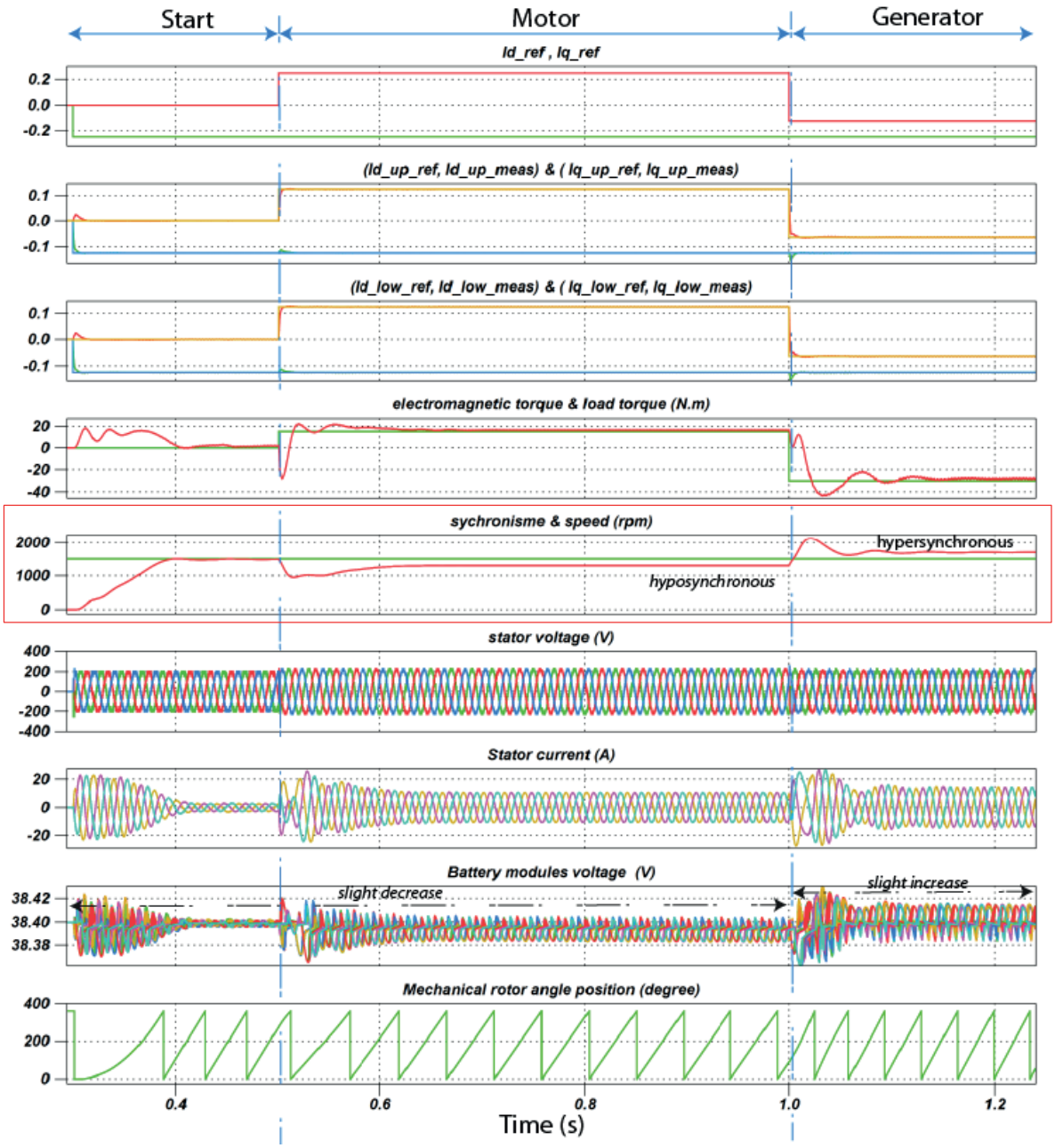

Figure 3.35: Performance evaluation of the double controllers during the driving mode

Figure 3.35 demonstrates the performance of the double current control in driving mode in terms of the fast dynamic response and the acceptable overshoot in comparison to the previous conventional multivariable-PI controller. With this method, the torque is also directly in proportion to the current q-axis which is directly proportional to the synchronism. In fact, for a positive slip ($s > 0$), the torque acts in direction of the rotating field. So the machine operates between standstill and synchronous speed as motor; above synchronous speed, the torque is opposed to the direction of

the rotation, hence the machine performs as generator (hypersynchonism). However the double current control increases the speed control flexibility because there is no need to control the DC voltage directly. Also, this simulation emphasizes the variation of the frequency as well as the rotor mechanical angle during the driving mode. However, it is important to have a better insight of the operation principle of the CMMC in order to define accurately the current references, which depend on the CMMC strategies. Therefore the following circle diagram is used to define the operating point of the induction machine for both the charging and the driving.

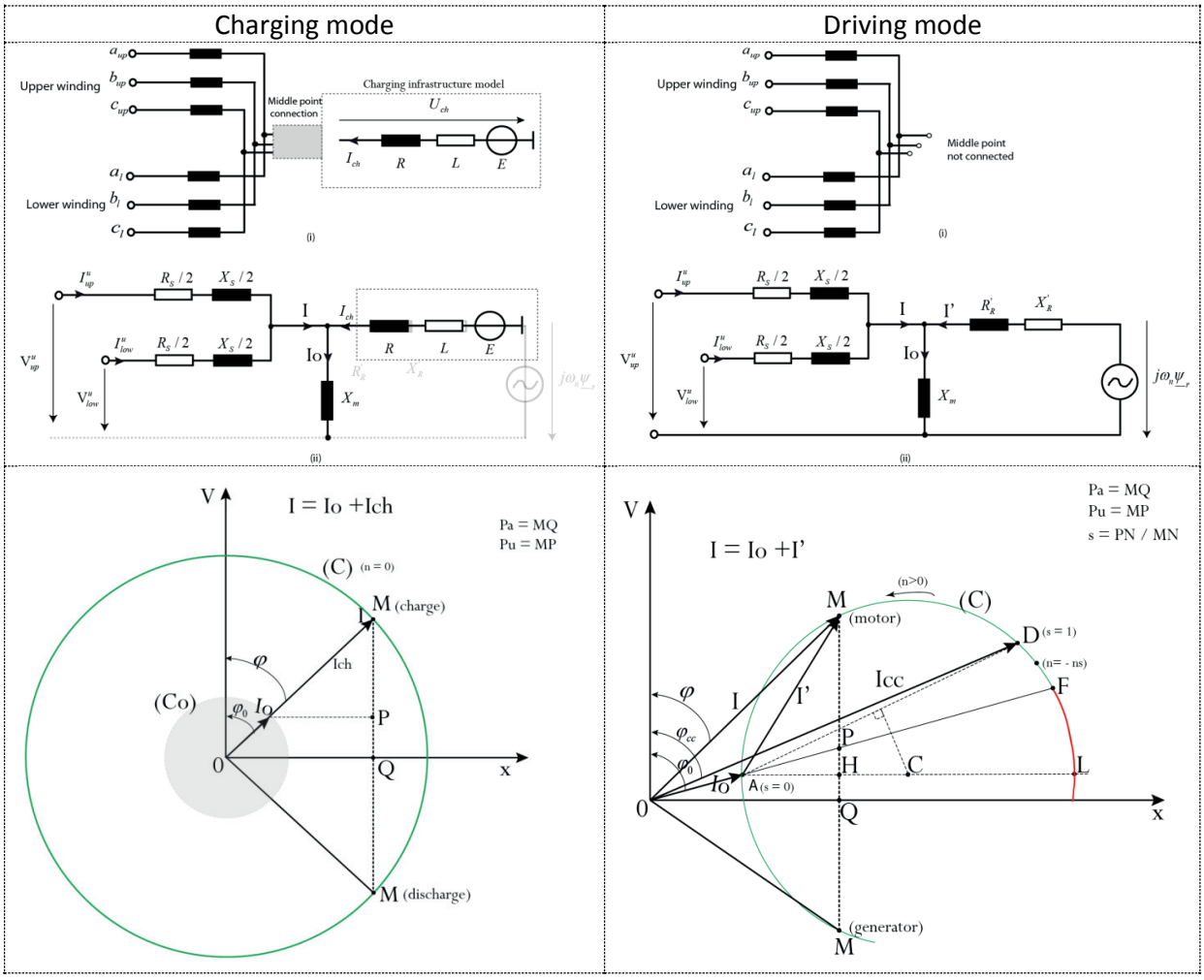

Figure 3.36: equivalent scheme configuration and the circle diagram of the IM

Figure 3.36 shows the circle diagram of the Induction Machine (IM) in charging mode and driving mode. Also, the equivalent schemes of the induction machine are represented in order to highlight the current flows. In this figure, the rotor circuit disappears during charging mode due to the charge compensation phenomena, and vice versa the grid circuit disappears during the driving mode.

In charging mode the battery charge and/or discharge current should be between the discharge and charge C-rate. This boundary condition is highlighted by the green circle in Figure 3.36. How-

ever, the power flow in the converter is controlled by two inner-loop multivariable current controllers in rotating frames. Further, outer-controllers are needed to control the circulating current and the power flow during charging mode.

During the driving mode, two of the important parameters are the slip and torque limits (s_k, C_k). The torque crosses the torque limit C_k when the speed n equal to s_k which corresponds to the point F in Figure 3.36, the roughly C_k is $1.7 * C_n$, where C_n stands for the nominal torque. It is depicted by the green curve. The induction machine is operated as generator when the operating point M is located in the negative part as depicted in Figure 3.36. However, a speed/torque up stream controller and a magnetizing current upstream controller is required to give appropriated references to the downstream current controllers during driving mode.

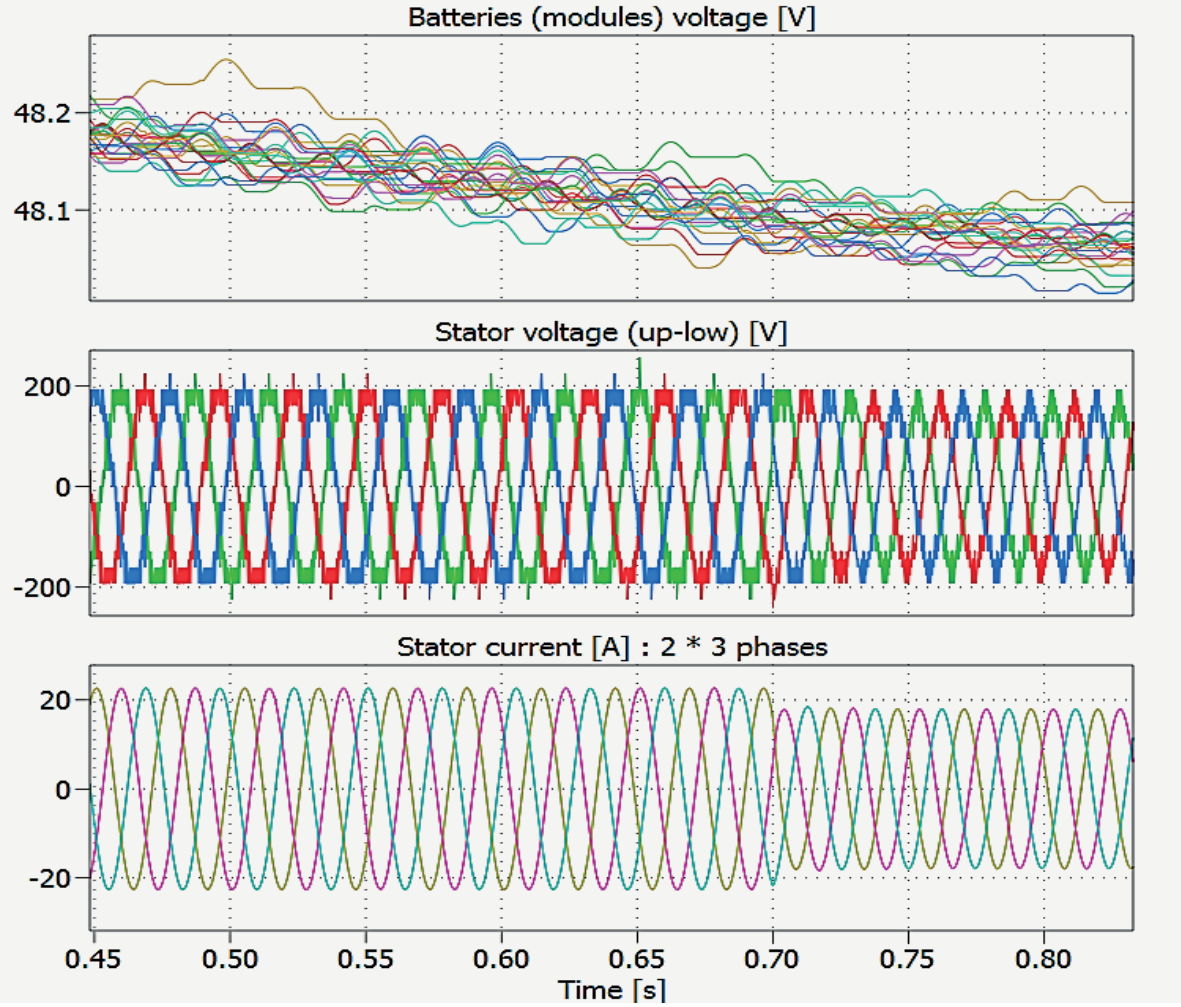

Figure 3.37: Typical batteries and stator voltages as well as stator currents during driving mode (N=5)

Figure 3.37 highlights the split integrated battery module voltages in the CMMC, in fact there are thirty voltages (5 levels*6 arms). It is demonstrated that they are well balanced because they converges in the same direction. The line-to-line stator voltages as well as the stator currents are also shown in this figure. They give the best expected waveform for CMMC in driving mode.

3.6 Conclusion

To summarize, the actual problem may be re-formulated by three distinctive EV-related terms of range, range flow-rate, charging compatibility:

1. Range is the average distance an EV is able to cover with the maximally recharged battery in given conditions (capacity, charging current, initial state of charge etc.). This depends also on the EV's aerodynamic shape, mass, as well as the EV's powertrain performance.

2. Range flow-rate is the driving distance augmentation per time unit of recharge, expressed in km/min or km/h. This depends on EV's battery power density and the overall efficiency of the EV's powertrain.

3. The charging compatibly is the flexibility of the EV to charge with a large range of charging infrastructures; from basic supply AC household to AC or DC ultra-fast charging station, meaning from level 1 to level 4 of charging infrastructure according to IEC 61.

In order to answer those EV requirements, the Flex-EV is proposed, it is based on is a three phase power electronics structure where each phase comprises a plurality of stages connected in cascade. In turn, each stage consists of a battery module and a 2- or 4-quadrant converter and the overall realizes a double star cascaded converter which feeds a three phase open-ended and tapped electrical machine. This structure is configurable in AC/DC, DC/AC and AC/AC conversions according to the configuration mode. This allows the electric vehicles to be compatible with a large range of charging infrastructures, from single phase AC low power to AC or DC high power. This is utterly attractive for EV applications; this is the reason why the CMMC converter for Flex EV has been proposed in this thesis for a universal and flexible charging system. With regards to modularity, flexibility, bidirectional power flow control, multi-port charging system, etc. the Flex-EV design based on the CMMC offers a re-think approach to integrate the battery subsystem, the motor subsystem as well as the power modules subsystem, into a Modular Multilevel Converter (MMC) with Split Integrated Storage (SIS) where the control unit is centralized. It offers a centralised active balancing strategy at the level of the modulation by splitting the conventional battery pack into multi modules; this can increase the energy saving in comparison to the standard passive balancing. Also, it reduces the use of row components such as copper because the current filter is reduced. It can also increase the fault-ride-through capabilities of the EV battery against thermal runaways, which could lead to the destruction of the battery pack. The concept allows a universal and flexible charging.

However, the design of the motor doesn't only take into account the driving condition but also the charging scenario in order to be able to receive or deliver the required power. In fact, the worst case occurs during charging mode (ancillary services) when the full reactive power circulates. This means that the stator winding must be chosen by considering the best compromise between the battery voltage, the modulation index, the switching ripple current as well as the transfer power capability.

Chapter 4 CMMC Modelling and Control

"The sciences do not try to explain, they hardly even try to interpret, they mainly make models. By a model is meant a mathematical construct which, with the addition of certain verbal interpretations, describes observed phenomena. The justification of such a mathematical construct is solely and precisely that it is expected to work."

Johannes von Neumann (1903-1957)

4.1 Introduction

It is generally agreed that, in an area as wide as MMC control theories, it is impossible to cover all topics in a single text, even briefly. In this thesis, it is therefore optimal to focus exclusively on deterministic systems, which are mathematically different but closely related in the area of robust control. This approach deals with the design of control laws that are guaranteed to perform even if the assumed model of the system to be controlled is not exactly correct, with the allowed deviations quantified in appropriate norms or under the possibility of imperfect controller design.

It should be noted that the approach is based on mathematical fundamentals and stresses physical the system modelling and practical control systems with realistic system specifications. The equation is relatively simple; therefore it is easy to have a better insight of the meaning. It is believed that the most important and productive approach to control a system is to follow a control engineering methodology that will fit to the controlled system. The flowchart of the method that is applied for the design of the CMMC control is presented below.

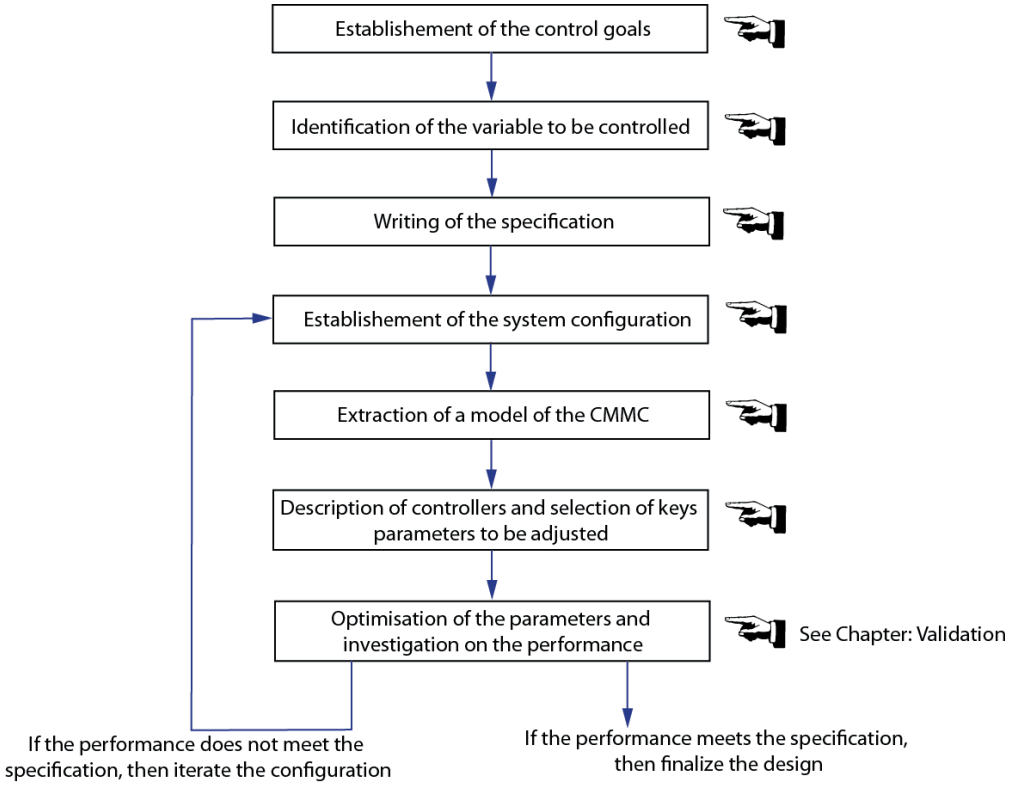

Figure 4.1: The control system design process

The CMMC for Flex-EV is definitely a mechatronics system; it consists of the synergistic integration of mechanical, electrical and computer systems of the electric vehicle. It is leading to a new breed

of intelligent technology. Therefore, along the design of the control system this approach is implicitly followed.

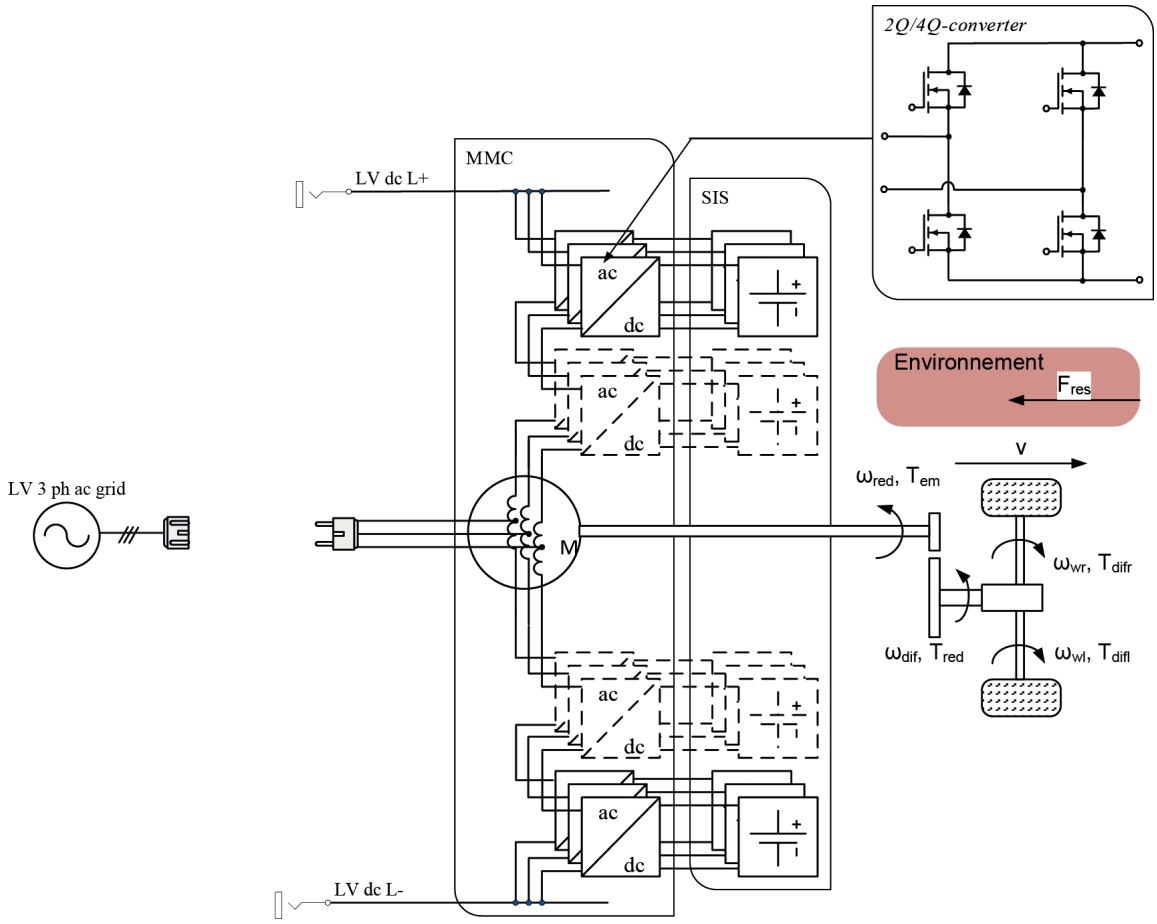

Figure 4.2: Flex-EV architecture

Figure 4.2 recalls the architecture of the Flex-EV which is based on the CMMC, the CMMC concept consists of six arms converters, which in turn consist of a series-connection of a number L of 2Q/4Q-converters.

The tap-dc bus can be turned-on and -off instantaneously in order to generate an AC multilevel voltage, the so-called arm voltage (U_{arm}). Therefore, this resulting multilevel voltage is nearly a perfect sinewave form because it is the result of a quantification step of the tap-dc bus U_{bat_k}.

$$u_{arm}(\omega t) = \sum_{k=1}^{N\,or\,P} S_k . U_{bat_k} \tag{4.1}$$

The line to line voltage output u_{arm} is the sum of the tap-dc bus voltages generated by the battery modules, which are turned on. The S_k is the quantification function which model the insertion or the bypass of the battery DC sources.

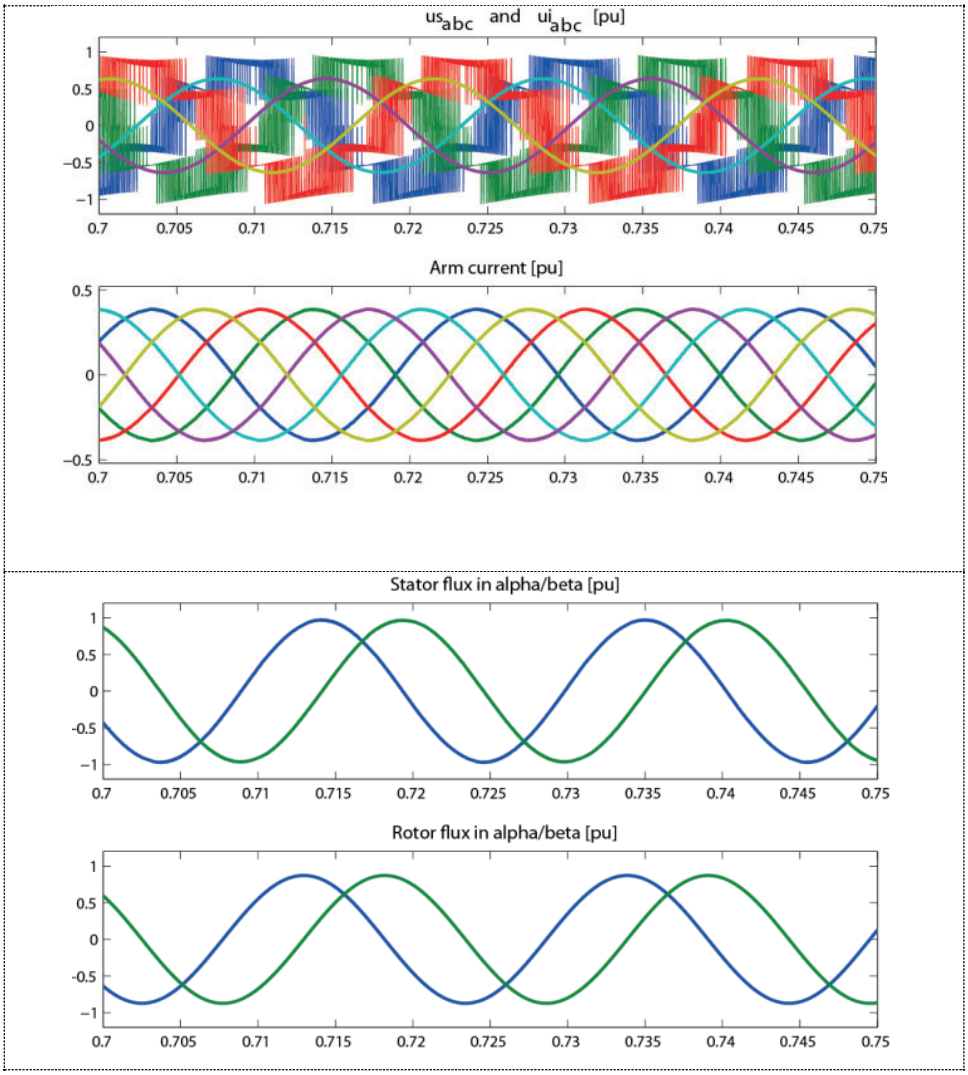

Figure 4.3: Typical generated waveform of the CMMC (N=3)

In Figure 4.3, on the top, the stator voltage and the induced back electromagnetic force (EMF) are shown on top-plot, whereas the six arm currents are presented in the lower plot. In fact, it is a double three-phase current because for each phase, the upper and lower arm currents are in the same direction during the driving mode.

On the bottom, the stator fluxes are shown in alpha-beta stationary reference frames on the top-plot, whereas the rotor fluxes are shown in alpha-beta stationary frames on the lower-plot. In fact, there are slightly shifted each other because it is an asynchronous machine. It should be noted that it is difficult to measure the stator and rotor fluxes as well as the EMF voltage in reality.

4.2 Standalone, grid connected applications and their characteristics

4.2.1 Generality

The Flex-EV is designed not only to draw current from the grid but also as power source, which can be used in standalone applications, in a micro-grid, in extended local grids or interconnected grids of large territory.

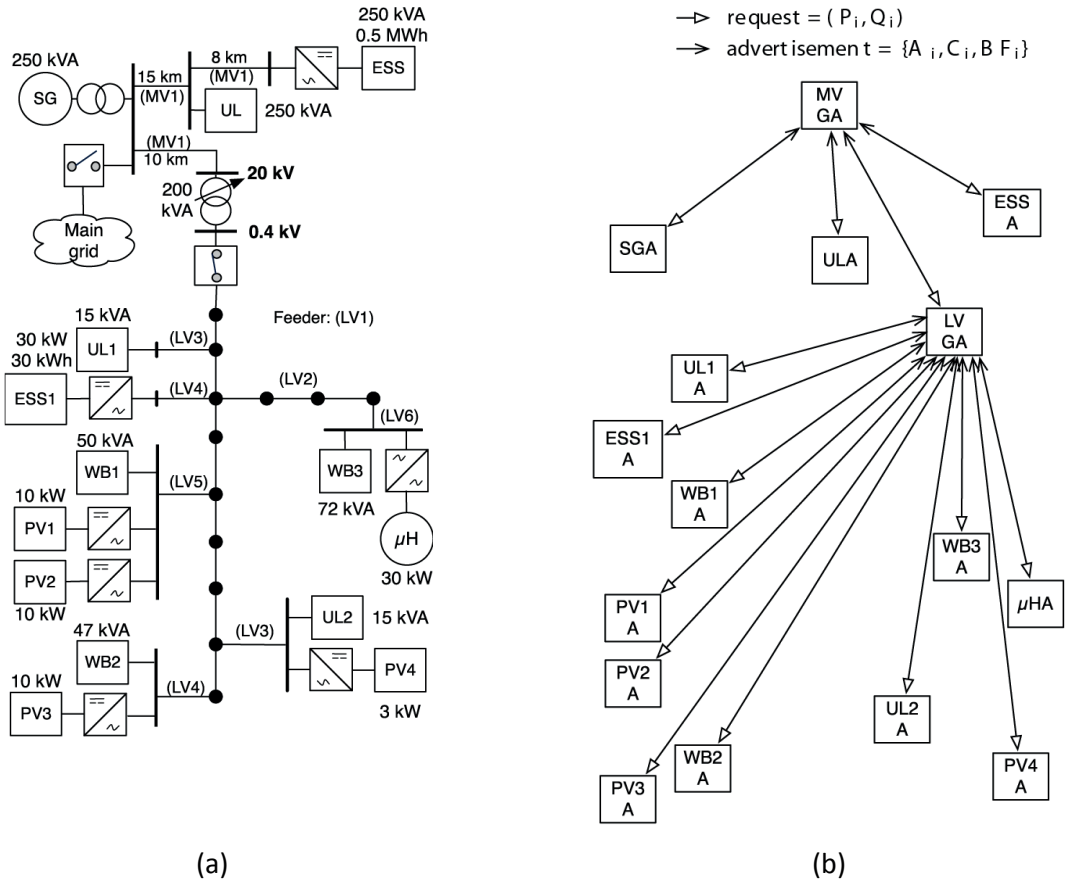

Figure 4.4. Typical example of an electrical network and agents: (a) Microgrid (b) Agents [48]

Figure 4.4 illustrates the architecture of a typical microgrid (on the left) and the corresponding agents (on the right), where each agent is characterised by its request and its advertisement. In paper [48], the authors show a better approach on how to supervise this grid interconnection, and particularly how a DC grid can be interconnected with an AC grid in distributed generation network.

However, it is generally agreed that standard loads are designed for AC, even for small power applications such as laptops, phone chargers, etc. DC/AC converters are used to connect to DC power supply systems. More often, they are unbalanced between the consumed power and the pro-

duced power. To control the power delivery of each grid connected power source, droop controls are traditionally used in power systems. In particular, The main point of the "**Flex**-"is to create an extendable power systems which is capable to use the distributed power sources efficiently both in the case of a public grid but also to electrify rural areas step by step.

Then, the Flex-EV can play an important role in reactive power injection. In fact, it is more convenient to disconnect the tapped batteries during the ancillary services operation (only the tap-capacitors are connected) in the submodules in order to avoid operating the battery during the injection of reactive power. Nevertheless, it is possible to provide active power from the battery, but this will discharge the EV battery and this could lead to a reduction of the battery life cycle.

4.2.2 The Flexible charging

The basic idea is to reproduce the characteristic of the synchronous generators connected to a steam/water turbine regulated through a speed governor, which are controlled in such a way that the frequency decreases as the fed reactive power increases. The principle can be explained by looking at the power transfer between the EV and the charging station in a Distributed Generation (DG). This can be derived using a π-line model and complex phasors.

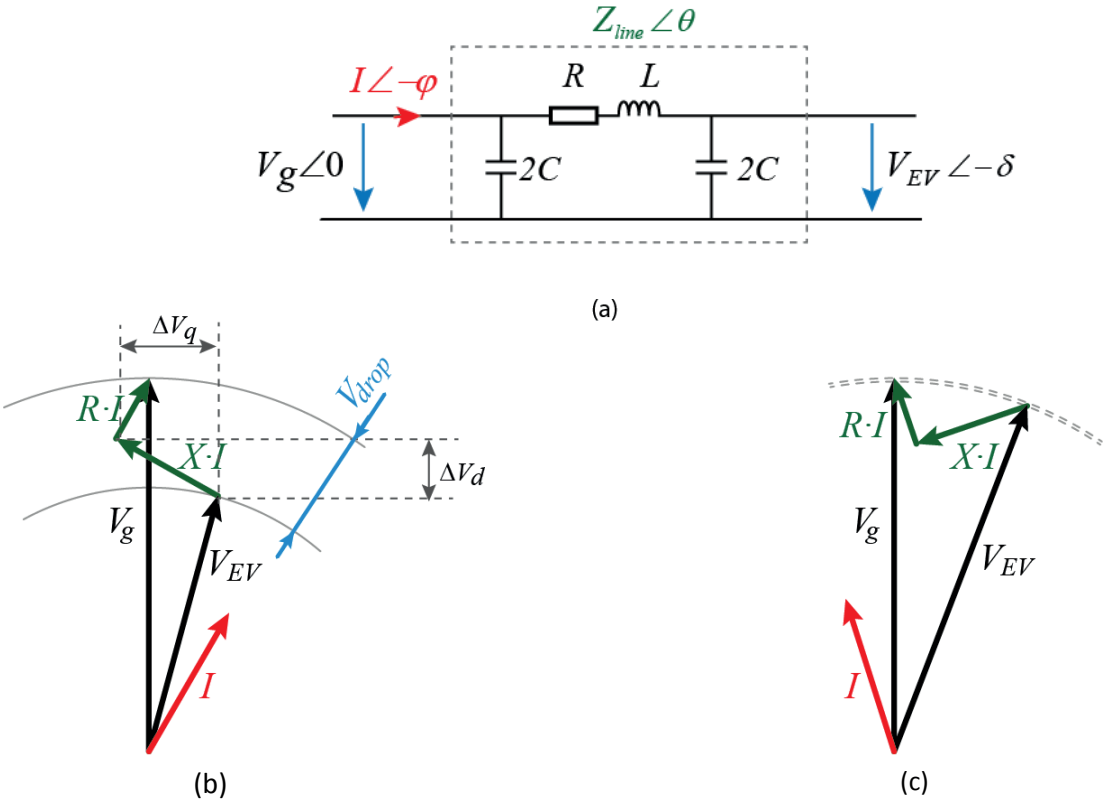

Figure 4.5: (a) Power flow through a line charging cable, (b) typical phasor diagram in charging mode and (c) typical phasor diagram in discharging mode

Figure 4.5 illustrates the power management through phasor diagrams, in (a) the line cable is represented in a simplified π model. In most cases, it consists of a well shielded coaxial cable; the phasor voltage as well as the line impedance is highlighted. In (b) the voltage drop between the electric vehicle and the grid voltage is emphasised in order to highlight the required reactive power which has to be injected for maintaining the grid power factor. In (c) the voltage drop compensation is illustrated where a pure reactive power is injected. According to Figure 4.5 active and reactive power flow can be expressed as:

$$\begin{cases} P_g = \dfrac{V_{EV}}{Z}\cos\theta - \dfrac{V_{EV}\cdot V_g}{Z}\cos(\theta+\delta) \\ Q_g = \dfrac{V_{EV}^2}{Z}\sin\theta - \dfrac{V_{EV}\cdot V_g}{Z}\sin(\theta+\delta) \end{cases} \tag{4.2}$$

where δ is the power angle and θ is the power factor angle at the section of the EV side. This represents basically the phasor diagram in charging mode. Then, by assuming that well-shielded coaxial cables are used as the charging cable, the line capacitance can be neglected. As result, it is possible to express the resistance and the reactance as function of the power factor angle:

$$\begin{cases} R = Z\cos\theta \\ X = Z\sin\theta \end{cases} \tag{4.3}$$

By combining the equations (4.2) and (4.3), the active and the reactive power can be defined as:

$$\begin{cases} P_g = \dfrac{V_{EV}}{R^2+X^2}\left[R\left(V_{EV} - V_g\cos\delta\right) + X\cdot V_g\sin\delta\right] \\ Q_g = \dfrac{V_{EV}}{R^2+X^2}\left[-RV_g\sin\delta + X\left(V_{EV} - V_g\cos\delta\right)\right] \end{cases} \tag{4.4}$$

Therefore, the voltage variation in the direct and quadrature axis can be expressed as:

$$\begin{cases} \Delta V_d = V_{EV} - V_g\cos\delta = \dfrac{R\cdot P_{EV} + X\cdot Q_{EV}}{V_{EV}} \\ \Delta V_q = V_g\sin\delta = \dfrac{X\cdot P_{EV} - R\cdot Q_{EV}}{V_{EV}} \end{cases} \tag{4.5}$$

When the Flex-EV is connected to the grid through a mainly inductive line transmission where the three-phase distribution line is $X >> R$, R may be neglected. If in addition the power angle δ is small, then $\sin\delta \cong \delta$ and $\cos\delta \cong 1$. Therefore:

$$\begin{cases} \delta \cong \dfrac{X\cdot P_{EV}}{V_{EV}\cdot V_g} \\ V_{EV} - V_g \cong \dfrac{X\cdot Q_{EV}}{V_{EV}} \end{cases} \tag{4.6}$$

In micro grid applications (Figure 4.4), it is not possible to have DG sources which lead to uncontrollable active/reactive power flows. Therefore depending on the small differences of the amplitudes, the active power can be adjusted by regulating the angle δ of the frequency f, whereas the reactive power can be controlled by regulating the Flex-EVs injected voltage V_{EV} in such way to inject reactive power Q. This can be interpreted in mathematical way as:

$$\begin{cases} f - f_0 = -K_P(P - P_0) \\ V - V_0 = -K_Q(Q - Q_0) \end{cases} \tag{4.7}$$

f_0 and V_0 are respectively the rated frequency and voltage and P_0 and Q_0 are respectively the set-points for active and reactive power. It should be noted that the set point should be included in the PQt profile, which represent the capability of the Flex-EV. The Flex-EV will find a working point characterized by a V, f working point that will force the DG units to feed P, Q depending on the adopted coefficients K_P and K_Q.

4.2.3 Power levelling in a large scale charging station

In the near future, a large scale charging station is expected to play an important role in energy trading by contributing to the energy management.

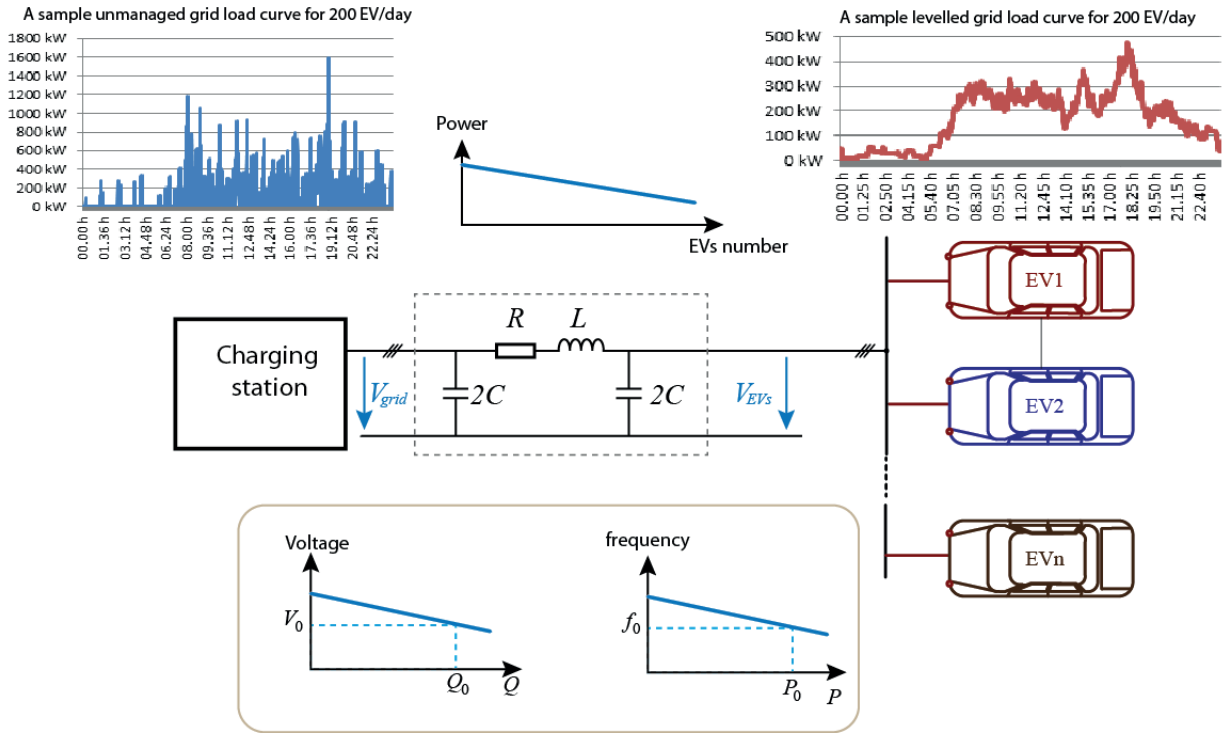

Figure 4.6: Power levelling and grid control in a large scale EV charging station

Figure 4.6 illustrates the equivalent droop control in a large charging station, where the EVs can contribute to the power levelling during the peak hours. For instance, the required power at the charging station is up to 460 kW at 18:25 in the evening. This power can be provided by a number of electric vehicles which are able to inject active power at the charging station. However, this operation will discharge usually the EVs battery; it will also decrease the battery life cycle. Only the reactive power injection is sustainable for the EV owner because the tap batteries can be disconnected from the submodules circuit and only the reactive components (tap-dc bus capacitors and stator windings) will contribute to the ancillary services.

In summary, if a choice is made to control the power at the charging station, as a function respectively of the produced active and reactive power, the overall system will find an equilibrium point that will guarantee proper power sharing as a function of the control characteristic.

In the frame work of the charging cable, a simplified π-line model has been taken in order to take into consideration *the insulation*; it is generally that the high power cable is a full science on itself, it has the structure elements of one or more conductors, insulation and protective jacket. High power cables differ from lower-power cables in that they have additional internal layers in the insulation jacket to control the electric field around the conductor.

4.2.4 The boundary condition in terms of power

The CMMC principle of operation is similar to the principle of operation of a synchronous generator of a transmission line (neglecting the capacitive coupling). Basically the CMMC controls the active and reactive power transfers acting on the amplitude and phase of the produced voltage, as shown in following figure.

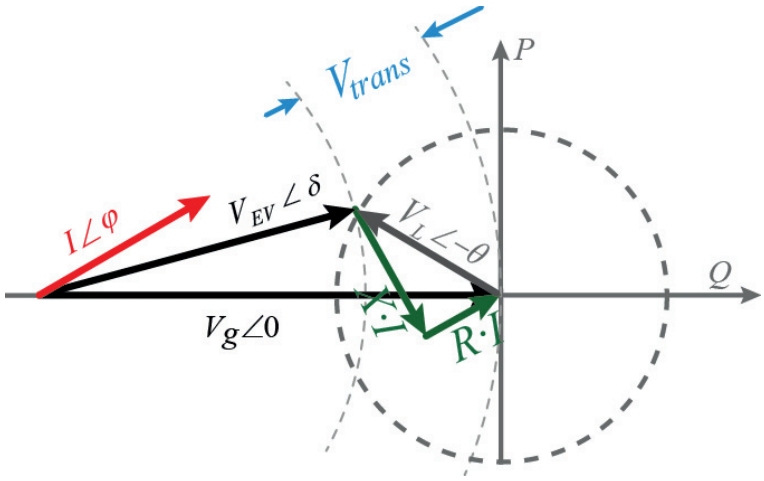

Figure 4.7: The phasor diagram for the active/reactive power at the Point of Common Coupling (PCC)

The capability of the exchanging reactive power is limited by the power handling capability, which depends on the capability of the Flex-EV to absorb or to deliver power. This operating time is also limited depending on the capacity of the Flex-EV in terms of energy.

4.3 Controlled system modelling

4.3.1 Generality

In a three-phase system, R_c and L_c represent respectively the short-circuited equivalent resistance and inductance of the CMMC on the AC side. In order to simplify the control of the active and reactive power of the three-phase system, it is optimal to implement the controller in a dq reference frame. The active and the reactive power command signals are therefore translated into d and q components of the reference current, using the following matrix:

$$\begin{pmatrix} i_{sd}^* \\ i_{sq}^* \end{pmatrix} = \frac{1}{v_{gd}^2 + v_{gq}^2} \begin{pmatrix} v_{gd} & -v_{gq} \\ v_{gq} & v_{gd} \end{pmatrix} \begin{pmatrix} P_c^* \\ Q_c^* \end{pmatrix} \tag{4.8}$$

v_g is the measured grid voltage. The voltage oriented control is based on the use of a dq frame rotating at ω_e speed and it is oriented in such a way that the d axis is aligned on:

- The grid voltage for the grid and converter control during the charging mode
- The rotor speed or rotor flux for the driving mode

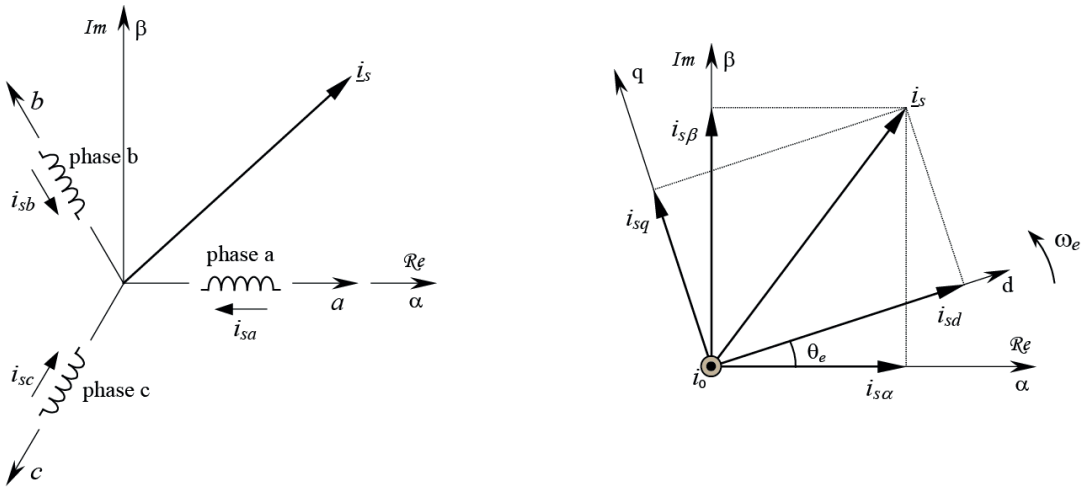

Figure 4.8: Reference frame: arbitrary on the left and stator and rotor frame on the right

Figure 4.8 illustrates the geometrical transformation between the arbitrary reference frame, the stationary frame and the rotating frame. The left figure represents an idealized three-phase asynchronous motor, showing identical armature coils a, b and c. On the right, the direct axis heads the quadrature axis by 90° in the anticlockwise direction of the rotation. Generally, the selection of the study reference frame is mostly based on the complexity of the implementation and the dynamic performance of the required control. Of course, in the automotive industry the robustness of the

control has to be validated, therefore the approach has to be well defined. This can be done in both open loop and closed loop. Recently, in MMCs literature, several papers argue about the necessity of the optimisation of the dynamics of the reactive/active power control to be decided as a consequence of a variation of a grid voltage change. More often the power controllers are done in the alpha-beta reference frame because the Proportional Resonant (PR) controller seems to give the best performance [53] for the circulating current control. However, the modelling design is based on the stored energy controlled where the arm capacitance is assumed to be fixed. This is problematic because in reality the arm capacitance is varying, therefore the model seems limited in terms of the controllability.

In the frame work of the Flex-EV control design, the controlled system model has been carefully studied with different approaches; the outcome is that the controlled system consists of a multivariable system with a coupling state. Therefore, it is straightforward to implement multivariable controllers in state space. The stability and robustness of the designed control can be studied. The dimensioning of the time constant can be done as pseudo-continuous approach; it is also possible to implement an advanced and modern control since the state matrix of the system is known.

In term of strategy, the active and the reactive power can be controlled independently in the appropriated reference frame; however, in order to get a better understanding of this approach, the next paragraph is dedicated to highlighting the concept.

4.3.2 Modelling of the motor in the arbitrary reference frame

A simplified equivalent circuit for the tapped and open ended stator winding motor is developed, which is shown in an arbitrary reference frame in Figure 4.9.

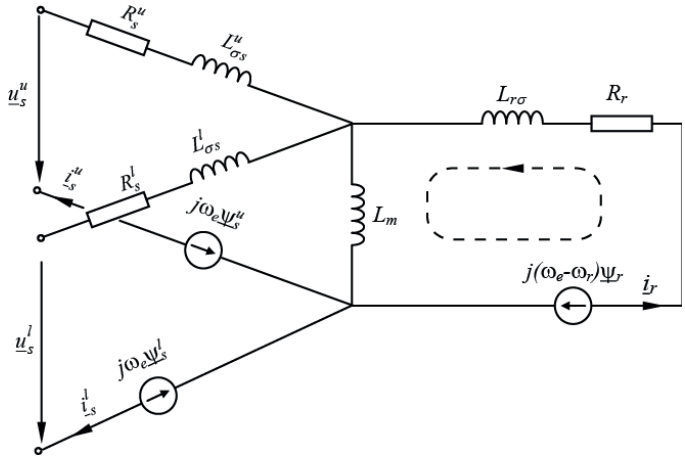

Figure 4.9: Motor equivalent scheme in the arbitrary reference frame

It should be noted that the basics of electrical machine are not explained in this thesis. The reference current d component i_{sd}^* is controlled to manage the active power exchange and typically to perform the DC regulation while the reference current q component i_{sq}^* is controlled to manage the

reactive power exchange and typically to obtain a unity power factor. For instance, in order to obtain a grid current vector in phase with the grid voltage, the vector i_{sq}^{*}should be zero. The active and reactive powers can be expressed as:

$$\begin{cases} P_c = \frac{3}{2}\left(V_{sd} i_{sd} + V_{sq} i_{sq}\right) \\ Q_c = \frac{3}{2}\left(V_{sq} i_{sd} - V_{sq} i_{sq}\right) \end{cases} \tag{4.9}$$

Then, by orienting the d axis with the stationary voltage, for instance when $\omega_e = 0$, the system can be represented in a stationary reference frame, which is shown in the next paragraph.

4.3.3 Modelling of the motor in the stator reference frame $\omega_e = 0$

This reference frame offers a simplification in terms of the modelling of the electrical machine with electrical circuits because the stator fluxes are cancelled and the rotor flux can be easily estimated.

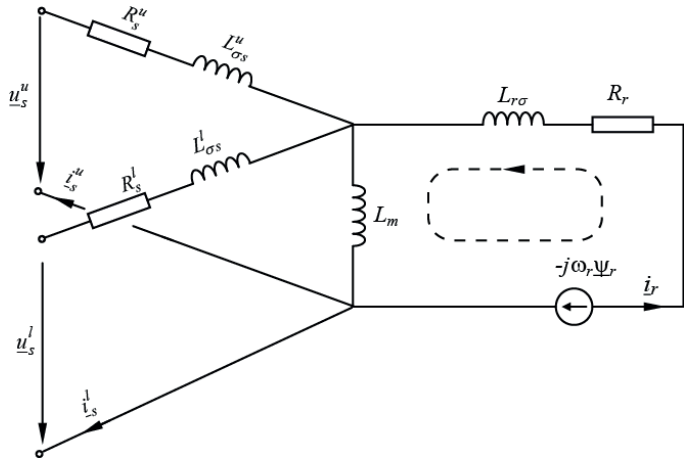

Figure 4.10: Motor equivalent scheme in the stationary reference frame

For instance, this model has been adopted during the simulation, however in the stationary αβ frame, the relation between active and reactive power as well as the vector currents components are more complex. The active and the reactive power produced by the grid converter can be expressed as:

$$\begin{cases} P_c = \frac{3}{2}\left(V_{s\alpha} i_{s\alpha} + V_{s\beta} i_{s\beta}\right) \\ Q_c = \frac{3}{2}\left(V_{s\beta} i_{s\alpha} - V_{s\alpha} i_{s\beta}\right) \end{cases} \tag{4.10}$$

The control of the DC voltage acts directly on the amplitude value; the PLL is indispensable for providing the grid voltage reference phase with the capacity to calculate the phase displacement of the current in view of the desired reactive power injection. In fact the active and reactive power are calculated using the measurements at the PCC and theirs values are compared with their set point. In this context, the d axis is oriented with the synchronism voltage, $\omega_e = \omega_r$.

4.3.4 Modelling of the motor in the rotor reference frame $\omega_e = \omega_r$

It is generally agreed that there are several strategies which can be implemented in rotating frame such as the direct power control, flux oriented control, voltage oriented control (VCO), etc. Basically, the main point consists of aligning:

- the grid voltage along the d-axis, in case of charging mode
- the rotor flux or the rotor speed along the d-axis in case of the driving mode.

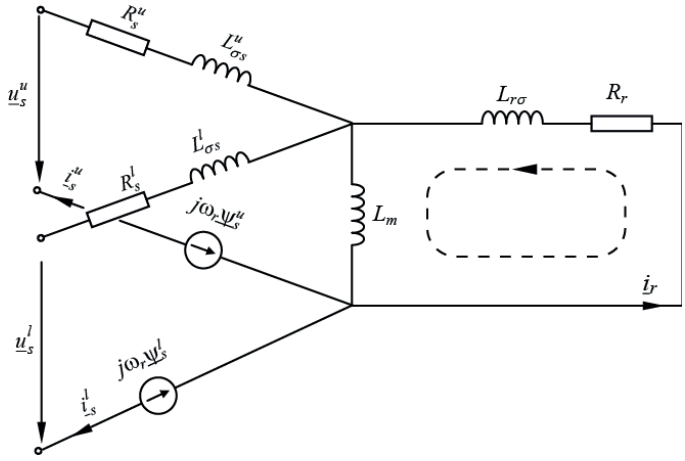

Figure 4.11: Motor equivalent scheme in the rotating reference frame

This allows eliminating the rotor flux in the equivalent circuit during the driving mode control and therefore the rotor circuit can be easily computed. The active and reactive power can be expressed as:

$$\begin{cases} P_c = \frac{3}{2} \cdot \left(V_{sd} i_{sd} \right) \\ Q_c = -\frac{3}{2} \cdot \left(V_{sd} i_{sq} \right) \end{cases} \tag{4.11}$$

In particular, during driving mode, the magnetization of the machine is directly driven by the d-axis whereas the torque and the speed as well as the slip have a strong relationship with the q-axis. It should be noted that the design of the power control as well as the speed/torque control depends on the required performance dynamic of the system.

4.4 Modulation

4.4.1 Submodule working principle

This section is devoted to study the submodule commutation. Generally speaking, the purpose of the commutation submodule is to “chop” the battery voltage into a square wave, because by controlling the turn on and off times (the duty cycle), the output voltage can be regulated. In addition, the submodule is configurable as half-bridge (2Q- converter) or full-bridge (4Q-converter), however, the use of the full-bridge is necessary for the direct AC/AC conversion. As mentioned in paragraph 3.3.6, each stage should include a battery unit and switch means adapted to bypass the battery or to interconnect the battery with other batteries across a load in a programmed fashion. The basic schematic of the commutation is shown in Figure 4.12.

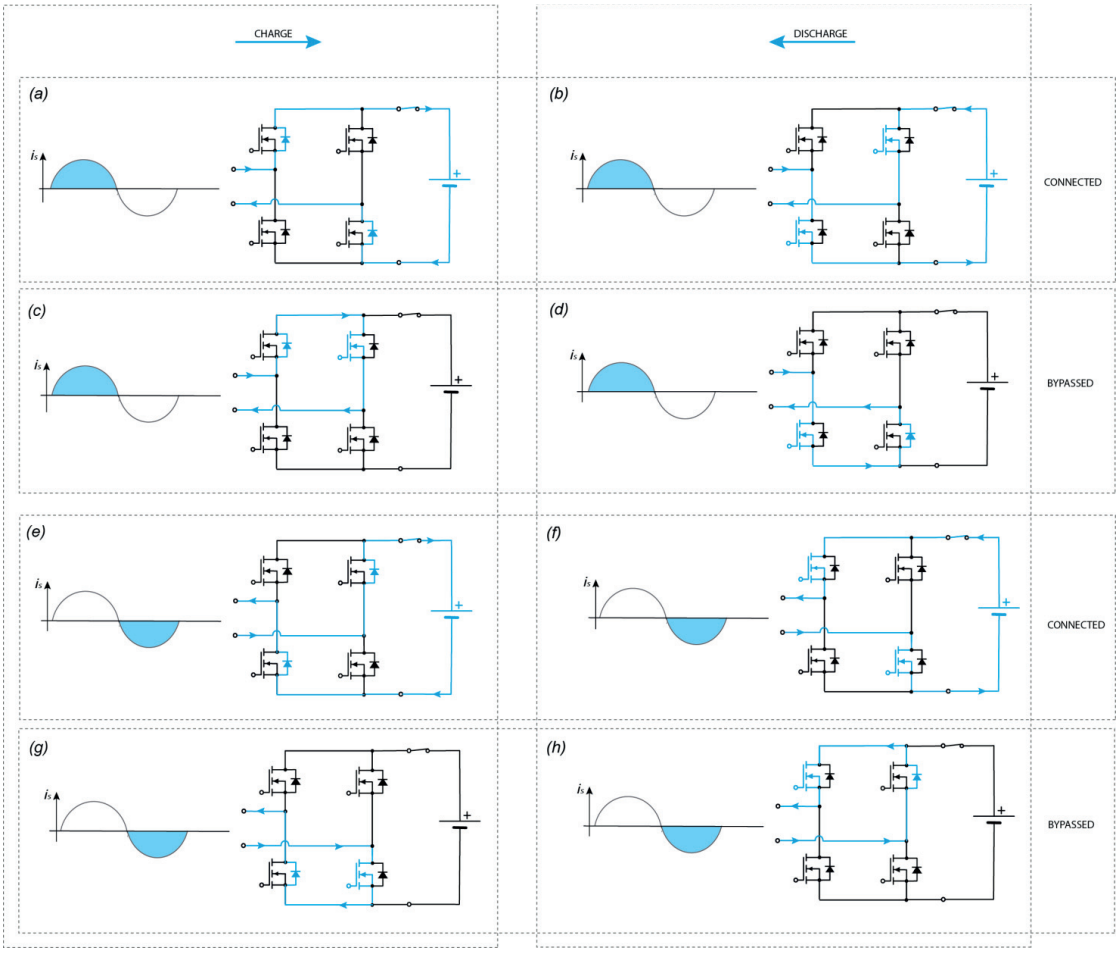

Figure 4.12: The current flow in the CMMC submodules according to the operating mode.

Depending on the sign of the arm current and the submodule batteries SoCs in an arm, the submodule batteries can be connected or bypassed. The Figure 4.12 shows also the possible path of the current flow according to the arm current. The numbers of the connected submodules depends on the modulation index references. In fact when operating as a DC power source (such as

capacitors or batteries) and in the Pulse Width Modulation (PWM) control, a zero voltage condition can be obtained by turning on only one of the switches, with the current freewheeling through the switch and a diode. Therefore, a positive current will charge the battery module and a negative load current will discharge the battery submodule. In addition, it could be also possible to operate the 4-Q converters in 2 levels or 3 levels according to the modulation strategies. However, in this application it is optimal to use 2 levels modulations in each stage in order to reduce the voltage drop and to increase the redundancy.

4.4.2 Possible modulation strategy

4.4.2.1 Literature background

The industrial electronics laboratory (LEI-EPF Lausanne) has addressed a lot of questions issues in this field [54] [55]. Basically there are mainly four algorithms for modulation in asymmetrical multilevel converter [56], [57] such as:

- Sort-and-select-based modulation and balancing: it is directly incorporated on the level of the modulation; the main drawback of this technique is the fact that there is no possibility to generate commutation without contribution of the output voltage waveforms [58].
- Multiple-carriers-based modulation and balancing: this is based on the classical multilevel modulation (horizontal or vertical shifted carriers); however the voltage references have to be generated by a closed loop control which ensures the balancing independently from the modulation [20].
- Rotating commutation patterns in each period: the main purpose of this approach is to share the conduction times of each 4Q-converter. This modulation takes into account the distribution of commutation losses [59].
- Modulation with current and voltage balancing: this technique requires additional controllers for each stage converter for current and voltage control. However, its implementation is much more complex and there is no possibility to have a direct balancing of the split integrated batteries [60].

It is obvious that, there are many methods to modulate a classical modular multilevel converter, however it should be noted that the CMMC is also designed for flexible charging. The modulation should also work even if the referential function is not perfectly sinusoidal. This is an important fact in ancillary services operation where an active harmonic filter has to be implemented, while the AC voltages aren't perfectly sinusoidal. The better modulation method would be, a method which is able to fulfill the following requirements:

- Easy implementation as processor algorithm or as digital state machine
- Very short delay time from the general reference function to the switching signals
- Symmetrical distribution of the losses on all the switches and split batteries
- Symmetrical distribution of the battery DoDs
- Reduction of the switching losses to a minimum

- Very low harmonic content in the generated voltage
- High redundancy

4.4.2.2 The CMMC submodules pass/bypass method

Assuming the length of the pass of a given submodule is γ_k, and then the arm voltage can be decomposed with the sum of the individual submodules output voltages.

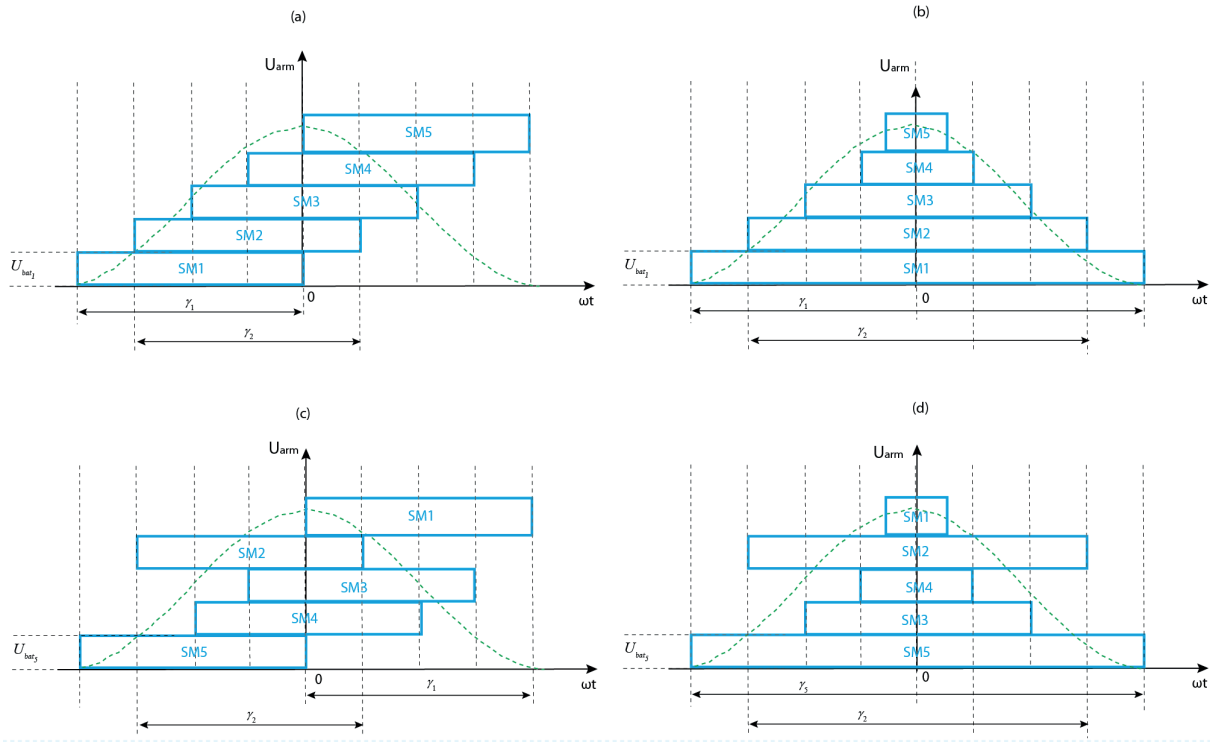

Figure 4.13: (a): fix γ_k, (b): variable γ_k, (c): fix γ_k with rotating step, (d): variable γ_k with rotating step

According to this Figure 4.13, there are four manners to modulate the arm voltage. By assuming a period of π, the submodule output voltage can be expressed as:

$$\begin{cases} u_{SM}(\omega t) = 0 & for \quad bypass \\ u_{SM}(\omega t) = U_{bat} & for \quad -\frac{\gamma}{2} < \omega t < \frac{\gamma}{2} \end{cases} \tag{4.12}$$

Then, the average voltage which is generated by the submodule, can be expressed as:

$$< U_{SM} >= \frac{1}{\pi} \int_{-\frac{\gamma}{2}}^{\frac{\gamma}{2}} u_{SM}(\omega t) \cdot d\omega t = \frac{U_{bat}}{\pi} \cdot \gamma \tag{4.13}$$

- *Pass/bypass with fix (γ_k).*

This method corresponds to part (a) and the (c) in Figure 4.13 the pass method depends on the firing angle α_k of the submodules. The main advantage of this method is the fact that it contributes to the distribution of the losses in the overall submodules stages. In fact, for rotating commutation patterns each period needs to be implemented in order to share the conduction times over all submodules. The main drawback of this approach is the fact that it requires a multiple-carriers-based modulation for the voltage balancing, which is based on classical multilevel modulation (horizontal or vertical shifted carriers).

Furthermore, the voltage references have to be generated by a closed loop control which ensures the balancing independently of the modulation [20]. In this context, it is important to find out the number of steps which have to be activated, according to the modulation degree and the number of the available steps. In general, the modulation aims to generate a multilevel voltage which follows as accurately as possible a reference. The threshold values are always in pairs with positive and negative arms. Therefore there are L threshold values. The number of the active steps is given by the value l_{step} and it is defined in the following equation:

$$l_{steps} = round\left(m_i, L\right) \tag{4.14}$$

The firing angles are calculated after knowing how many steps are active. The multiple-carriers-based modulation with horizontal or vertical shifted carriers is one of the easiest modulation strategies.

- *Pass/bypass method with variable (γ_k)*

The next approach corresponds to the part (b) and (d) of Figure 4.13, it has a higher flexibility regarding the battery submodules balancing in terms of the thermal management. This approach allows a free operation of the switches of the 4Q-converters. In fact, the introduction of the modulation strategy with a sorting and selecting algorithm becomes interesting. This can be done actively on the level of the modulation.

As seen before, the choice of balancing solutions is based on cost, size, control complexity and implementation. This provides guidance for selecting the optimal solution for a given application. The key parameter for varying the battery power is the parameter γ_k. The next section is dedicated to the study of the arm balancing.

4.5 Analysis of the MMC with split integrated battery energy storage

Since the introduction of the modular multilevel converters, many investigations have been conducted to develop and to compare MMC topologies [37]. Some approaches have been proposed in terms of MMC topologies and others approaches have been proposed in terms of MMC control strategies where several publications deal with control strategies for reactive power compensation. According to the published articles, it is seen that the MMC control performance have been optimized in order to improve the reactive power flow and/or to eliminate harmonic currents in the AC grid. However, the CMMC requires:

- High active power transmission for fast battery charging, and drive
- High reactive power handling for ancillary service
- Low harmonic content of the output voltage, instead of low harmonics currents
- Small range of the amplitude modulations index
- Very small range of the output frequency
- Fast response time at load changes
- Very high reliability and efficiency of the total power conversion

This coincides to the needs of the Flex-EV for answering the EV requirements. In order to get a better insight of the system related study, it is important to remember some basic physics laws.

4.5.1 Definition: charge, capacity, energy

The electric current that flows through a defined cross section of energy storage such as capacitors or batteries, is defined by the sum of the electric charges variation, and can be defined as:

$$i = \frac{dq}{dt} \tag{4.15}$$

From physics law, every charge is a multiple of the elementary charge $e = \pm 1.602 \cdot 10^{-19}\ coulomb$. The electric current i is the charge dq passing through a conductor cross-section area during an interval time dt. The direction of the positive current is the direction of the positive charges. It is generally agreed that a charging current will flow, if a voltage is applied to a capacitor or battery in order to charge it. Therefore, the energy that is supplied to the electrochemical energy storage is stored in the electric field and not, as with a resistance, transformed into heat. This energy can be described by:

$$W = \int_0^{t_1} v(t) \cdot \underbrace{i(t)dt}_{dQ} = \int_0^{Q_1} v(t) \underbrace{dQ}_{Cdv} = C \cdot \int_0^{V_1} v dv = \frac{1}{2} C \cdot V_1^2 \tag{4.16}$$

In general, this stored energy can be expressed as:

$$W = \frac{1}{2} C \cdot V^2 = \frac{1}{2} Q \cdot V = \frac{1}{2} \frac{Q^2}{C} \tag{4.17}$$

However, the time scale is not highlighted in this above equation, so it is important to define the state of the electrochemical energy storage for a defined time. A capacitor charging system, where the capacitor is charged by a given current I between a defined time t_1 and t_2, is depicted in the figure below.

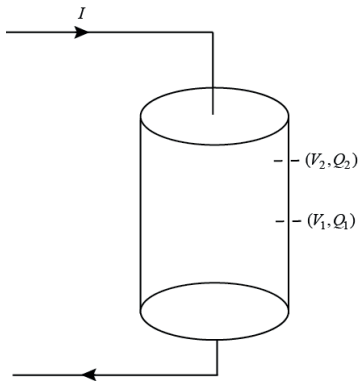

Figure 4.14: Illustration of a capacitor state variation

This illustrates the variation of the stored energy in a capacitor during the charging process. By neglecting the energy losses during this process, the energy conservation can be stated as:

$$\Delta W = W_{final} - W_{initial} \Leftrightarrow \frac{1}{2} Q_2 V_2 - \frac{1}{2} Q_1 V_1 = \Delta W \tag{4.18}$$

This means that there is an integral duality between the stored charge ΔQ and the variation of voltage across the battery. However the charge balance is zero if and only if the charge input is all given back during a discharge. In addition, the ratio between the charge Q and the voltage is called *capacitance*.

$$C = \frac{Q}{V}, \quad \frac{[A \cdot s]}{V} = [F] \tag{4.19}$$

4.5.2 The controversy theory of the equivalent arm capacitance of MMC

It should be noted that in literature, most articles about the MMC control assume that the arms capacitance can be expressed as the tap dc-bus submodule capacitance divided by the number of submodules [61][62]. But, this would only be true if and only if all capacitors in the arm are connected. However, in order to generate an alternating voltage, some capacitors must be disconnected; therefore the arm capacitance is varying.

$$C_{branch} = C_{arm} = \frac{Q_{arm}}{\sum u_{SM_k}} = C_{SM_1} + C_{SM_1} + \cdots + C_{SM_k} = \frac{C_{SM}}{k} \qquad k = 1, 2, \cdots, n_{\max} \tag{4.20}$$

So, even though the tap dc-bus submodules have the same capacitance, the arms or branches capacitances vary in function of the connected submodules level number k . This can be expressed as function of the control signal u_{cm}:

$$C_{branch} = C_{arm} = \frac{C_{SM}}{N} u_{cm}(\omega t) \tag{4.21}$$

This control signal reference remains the same as for the standard MMC in charging mode, for instance for the phase U, in charging mode with direct modulation control:

$$u_{cm}(\omega t) = \begin{cases} u_{cm}^{up} = U_{dc} \cdot (\frac{1 + \hat{m} \cdot \cos(\omega t)}{2}) \\ u_{arm}^{low} = U_{dc} \cdot (\frac{1 - \hat{m} \cdot \cos(\omega t)}{2}) \end{cases} \text{ for Charging mode} \tag{4.22}$$

However in driving mode, the control signal corresponds to the internal generated voltage by two adjacent MMC branches. Therefore, it can be expressed as:

$$u_{cm}(\omega t) = \begin{cases} u_{cm}^{up} = U_{dc} \cdot (\frac{1 + \hat{m} \cdot \cos(\omega t)}{4}) \\ u_{arm}^{low} = U_{dc} \cdot (\frac{1 + \hat{m} \cdot \cos(\omega t)}{4}) \end{cases} \text{ for driving mode} \tag{4.23}$$

The denominator is 4 instead of 2

It can be seen that the denominator is 4 instead of 2. This is very important, because during the driving mode operation, if the same amplitude reference as the standard direct modulation in MMC is applied to the motor, the motor will see the double of the nominal voltage which will damage the isolation of the stator windings and break the motor.

Back to the expression of the equivalent arm capacitance, the arm equivalent capacitance can be therefore expressed as:

$$C_{arm} = \begin{cases} C_{arm}^{up} = \dfrac{C_{SM}}{N}\left(\dfrac{1+\hat{m}\cdot\cos(\omega t)}{2}\right) \\ C_{arm}^{low} = \dfrac{C_{SM}}{N}\left(\dfrac{1-\hat{m}\cdot\cos(\omega t)}{2}\right) \end{cases} \quad \text{for charging mode} \tag{4.24}$$

where $\hat{m}$ is the relative amplitude of the modulation index. This equation demonstrates that the MMC arm capacitance is varying according to the AC side generated voltage. Therefore, the energy balanced equation based on a constant equivalent capacitance model is very limited and the charge balance equation has been introduced; it gives a better understanding of the equilibrium charge of the MMC.

4.5.3 The submodule controlled variable

The Flex-EV model trend is toward greater complexity, due mainly to the requirements of complex tasks and good accuracy. In fact, by definition the state space model is defined by two differential equations:

$$sx = Ax + Bu \tag{4.25}$$

$$y = Cx$$

u is the input vector, x is the state vector, y is the output vector and s is the Laplace derivative operator., A is the state matrix, B is the input matrix, and C is the output matrix. Of course, this can be extended depending on the environment where the system is operated and depending on the system behaviour.

The state variables of the CMMC submodule can be defined as:

Input: u = $[i_s , 0]^T$

State: x = $[q_k, \vartheta_k]^T$

Output: y = $x_2 = u_{SM_k}$

where:

i_s the upper or lower arm current vector,

q_k the battery charge state vector for the N° =k submodule

ϑ_k the battery temperature state vector for the N° =k submodule

u_{SM_k} the submodule feeding voltage vector for the N° =k submodule

Before going through the analytical study of the CMMC, it is important to define the modulation strategy because this is one of the major problems of the actual MMC; the arm balancing and the balancing of the tapped dc-bus submodules is a big topic in literature (see next paragraph).

4.5.4 Arm charge analysis

4.5.4.1 Identification of the variable to be controlled

In the literature, the term "charge" is uncommon for MMCs, however in this thesis the term charge has been used because it simplifies the mathematical demonstration while keeping the physical propriety of the described system. However, as seen in the above paragraph (4.5.1), there are difference between charge and current, so it isn't right to amalgamate them.

Typically there are two main variables to be control:

- The first corresponds to the state variable of the arm subsystem, which can be defined as:

  Input: u = $[i_{sN/sP}, 0]^T$

  State: x = $[q_k, 0]^T$

  Output: y = $x_2 = u_{iL/iU}$

where:

i_{sN} and i_{sP} are respectively the upper and the lower arms current vector,

q_k is the connected battery charge state vector for the N° =k submodule

u_{iL} and u_{iU} are respectively the upper and the lower arm feeding voltage vector

- The second main control variable is the transferring power, which depends mainly on the behavior of the CMMC. However, one of the key discussions is the sizing of the submodule capacitors, which depends mainly on the pulsing power.

For instance, suppose that the fundamental of the generated AC voltage can be expressed as:

$$v_s^1(t) = \hat{v}_s^1 \cos(\omega t) \tag{4.26}$$

Since the AC side is an inductive load, the current is delayed by φ behind the voltage:

$$i_s(t) = \hat{i}_s \cos(\omega t + \varphi) \tag{4.27}$$

Basically, in a standard single phase system, the instantaneous input power balance is given by:

$$p = u_s \cdot i_s = \hat{u}_s \cos(\omega t) \cdot \hat{i}_s \cos(\omega t + \varphi) \tag{4.28}$$

After decomposition according to the frequency, this results in:

$$p = \frac{1}{2}\hat{u}_s \hat{i}_s \cos(\varphi) + \frac{1}{2}\hat{u}_s \hat{i}_s \cos(2\omega t + \varphi) \tag{4.29}$$

The first constant term refers to the average transferring power that is used to charge or discharge the battery. The second oscillating term, doesn't contribute to the transfer power. This issue has attracted a lot of interest, in particular, many investigations on the possibility of the mitigation of the pulsating power have been carried out in the thesis [20].

4.5.4.2 Equivalent switching model of the one phase CMMC

Because of the series connection of the submodules, one phase of the CMMC can be modelled as variable voltage source commutator, as depicted in Figure 4.15. It represents one branch of MMC, which consist of two arms. Each arm is connected to the terminal of the on phase of the opened and tapped stator winding of the motor. Therefore, the two arms can generate multilevel voltage at the terminals of the stator winding. However, the generated voltage is only positive for 2-Q submodule. Mainly, it consists of two arms, where each arm is composed of a chain of dc-bus submodules, which can be turned on or off according to the position of the two commutators in the both side of the inductance. This inductance represents the tapped stators windings

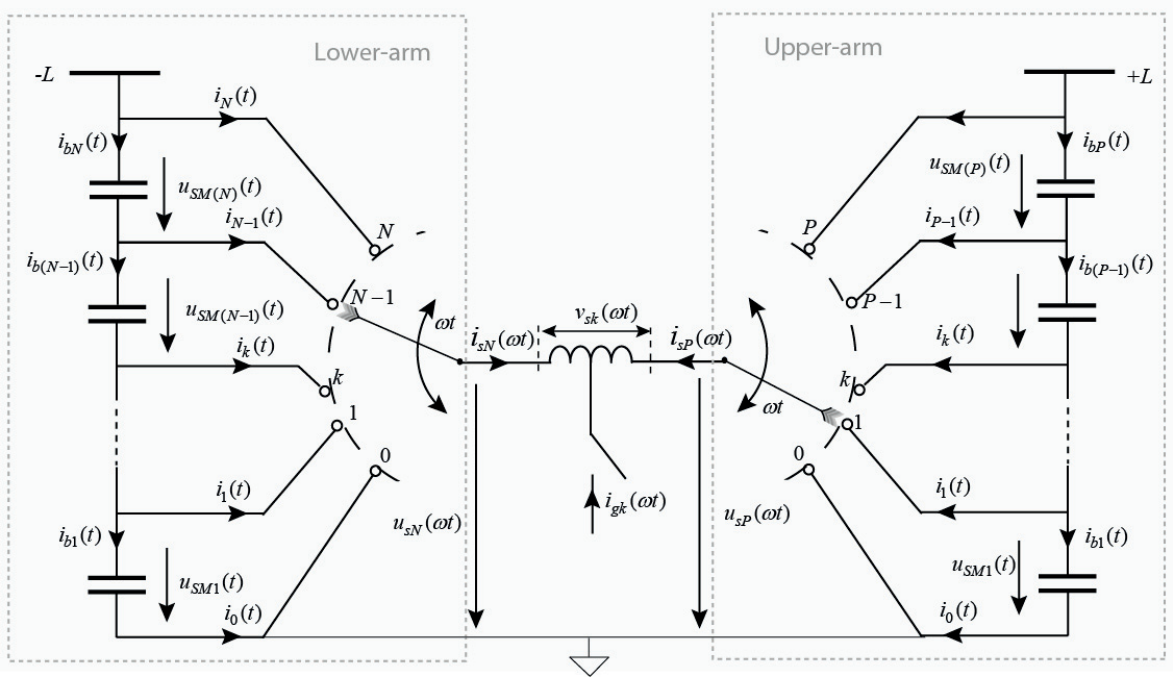

Figure 4.15: CMMC phase switching principle

In charging mode, the generated multilevel voltages from the upper and lower arm are in the opposite phase, it allows the cancellation of the solenation fluxes between the upper and the lower arm windings.

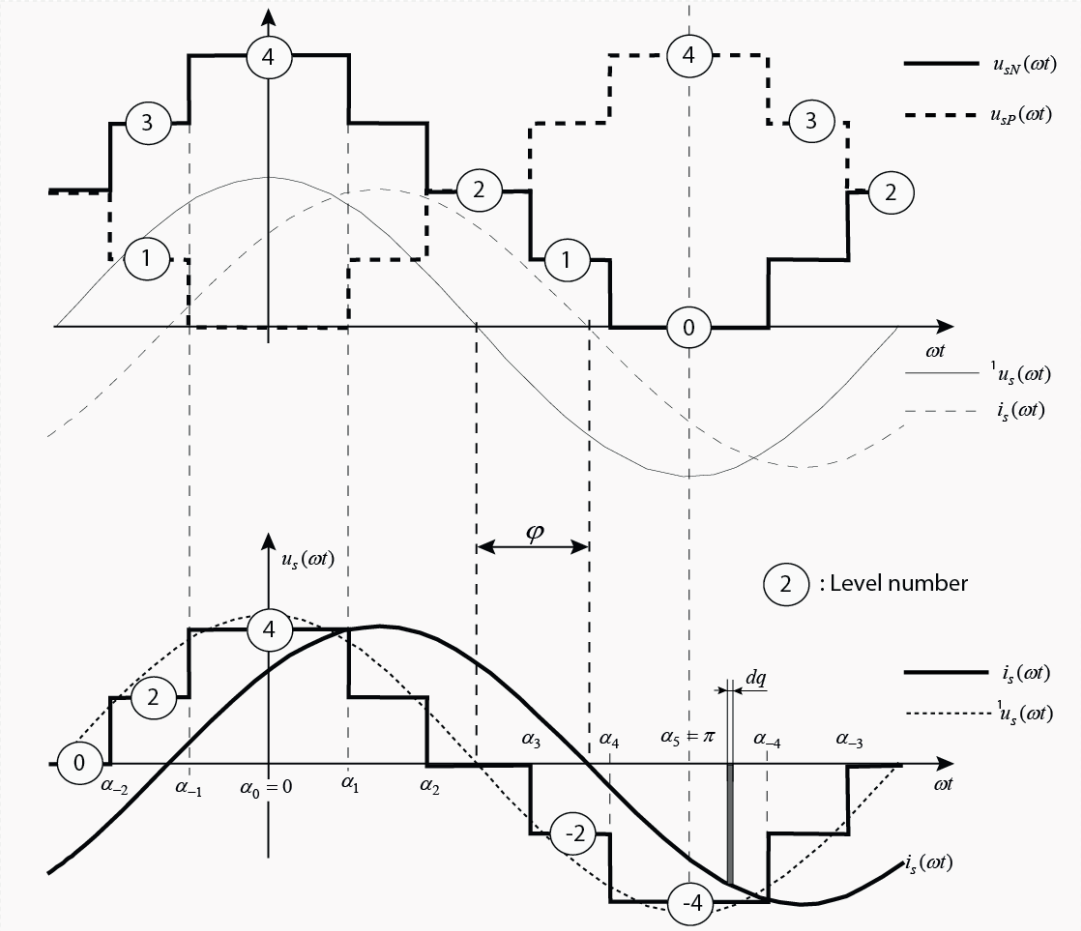

Figure 4.16: Output voltage and output current for a 4 level basic CMMC

For instance, a 4-level stage has been chosen in Figure 4.16 so that the generated waveform can be drawn. Figure 4.16 is used to illustrate the charge balance in one period. In fact, an elementary charge dq of the current arm overs a sample time dt can be evaluated by using the integral of the arm current $i_s(t)$ over an elementary angle $d\omega t$. Mathematically, this can be expressed as:

$$q_k = \int_{t_{k-1}}^{t_k} i_s(t)dt = \frac{1}{\omega}\int_{\alpha_{k-1}}^{\alpha_k} i_s(\omega t)d\omega t \tag{4.30}$$

The output voltage is a cosinus function, which is an even function; $v_s(t) = v_s(-t)$. As a result, the elementary charge q_k can be calculated with the following equation:

$$q_k = \frac{1}{\omega}\int_{\alpha_{k-1}}^{\alpha_k} \hat{I}\cos(\omega t+\varphi)d\omega t + \frac{1}{\omega}\int_{-\alpha_k}^{-\alpha_{k-1}} \hat{I}\cos(\omega t+\varphi)d\omega t \tag{4.31}$$

It should be noted at the starting time, the submodules capacitors must be charged before enabling the switching of the semiconductor devices. Generally speaking, this is due to the converter pre-charge condition. After some calculations this results in:

$$q_k = \frac{2\cdot\hat{I}}{\omega}\left(\sin\alpha_k - \sin\alpha_{k-1}\right)\cdot\cos\varphi \tag{4.32}$$

The MMC charge equilibrium can be only reached if and only if the amount of charge accumulated during the first haft period is given back in next haft period. Therefore, the system equilibrium [63] is reached if and only if this charge equation is zero, and since it is a product of two terms, one of the two terms must be zero.

$$\begin{aligned} q_k = 0 \quad &\Leftrightarrow \left(\sin\alpha_k - \sin\alpha_{k-1}\right) = 0 \quad or \quad (\cos\varphi = 0) \\ &\Leftrightarrow \quad \underbrace{\alpha_k = \pi - \alpha_{k-1}}_{1^{st}\ condition} \quad or \quad \underbrace{\varphi = 0}_{2^{nd}\ condition} \end{aligned} \tag{4.33}$$

The first condition is true only if there is a balance in the current sharing. Unfortunately this is impossible in the physics point of view due to an inhomogeneity of the Flex-EV operation. For instance a grid unbalance can induce an imbalance of the sharing of the AC current. However this can be compensated by a small adaptation of the switching pulses. Also, this could be an opportunity to implement more functionalities such as an injection of specific harmonics ranks through this common mode current for harmonic elimination. Furthermore, it is also common to inject a second order harmonics current for reducing the capacitors size by reducing the pulsating power.

The second condition is mainly used in the MMC for producing solely reactive power, for instance reactive power compensation, voltage support, STATCOM, etc. It also used for charging the split integrated battery in submodules for the Flex-EV. An injection of the second harmonic is also possible for increasing the transferring power by maximizing the modulation index.

4.6 Corollary of the 1st condition

4.6.1 The circulating current

Generally speaking, it states: "*the first condition is only true if and only if the levels are situated exactly in the middle of the DC voltage level of the arms*". For instance, according to Figure 4.16 , this first condition is true in $level\ number\ \ 2$ and in $level\ number\ -\ 2$, because the number of connected and disconnected submodules in the upper arm is equal to the ones in the lower arm. However, during one period this first condition is true if only the amount of charge accumulated during the first haft period, is totally given back during the next haft period. This proposition can be expressed as:

$$1^{st}\ condition\ is\ true\ \Leftrightarrow\ \forall k \in \left[0, l_{step}\right],\quad \int_{-\alpha_k}^{-\alpha_{k-1}} i_s(\omega t)d\omega t = \int_{\alpha_{k-1}}^{\alpha_k} i_s(\omega t)d\omega t \tag{4.34}$$

Otherwise, an imbalance occurs between the upper and the lower arm converter; the elementary residual charge dq_{circ} is the origin of the circulation current. This induces the common mode voltage.

$$i_{circ}(\omega t) = \omega \cdot dq_{circ} \tag{4.35}$$

In general, it is possible to write:

$$\begin{cases} \alpha_{-k} = \alpha_k \\ \beta_k = \pi - \alpha_k \end{cases} \tag{4.36}$$

Hence, the charge balance in the middle point of the stator winding can be calculated by:

$$q_M = \frac{1}{\omega}\int_0^{2\pi} \hat{I}\cos(\omega t + \varphi)d\omega t - \sum_k^{l_{step}}\left(\frac{1}{\omega}\int_{\alpha_k}^{\beta_k} \hat{I}\cos(\omega t + \varphi)d\omega t + \frac{1}{\omega}\int_{-\beta_k}^{-\alpha_k} \hat{I}\cos(\omega t + \varphi)d\omega t\right) \tag{4.37}$$

The first integral corresponds to the mean value of the current whereas the second expression in the brackets corresponds to the sum of the submodule output currents and defines the elementary charge dq_{circ} for one period. Therefore, in symmetrical condition, q_M is zero too.

4.6.2 Literature background: the common mode voltage injection

The degree of freedom to achieve this is the injection of a common-mode voltage [23]:

$$u_{cm} = \hat{u}_{cm}\cos(\varphi_{cm}) \tag{4.38}$$

where, its phase φ_{cm} and its amplitude $\hat{u}_{cm}$ are calculated for a three-phase balanced system. This balance can be written as:

$$\begin{cases} \varphi_{cm} = \varphi - \theta \\ \hat{u}_{cm} = \dfrac{2\Delta P_{ph}}{\hat{\imath}\cos\varphi} \end{cases} \tag{4.39}$$

$\hat{\imath}$ and φ are respectively the shifted phase and the amplitude of the measured stator current and ΔP_{ph} is the phase power variation. More details regarding this calculations can be found in the paper [23]. Several MMCs control approaches have been proposed by academics and industries to deal with the energy unbalanced. The thesis [58] gives a great state-of-the-art of the MMCs control, it is highlighted that there are mainly three broad lines of approach:

- The multivariable approach
- The open-loop approach
- The cascaded control

Basically, the MMC control is characterized by three levels control:

- The inner current and voltage control loop
- The control of the active and reactive power, which is enhanced in order to deal with unbalance and to provide a voltage sag ride through capability
- The supervisory control that decides the active and reactive power set points.

4.6.3 The limitation of the standard energy balancing

In general, the standard approaches have performed a great dynamic performance in terms of time response and overshoot tolerance. However, the decoupling of the system model is highly simplified, therefore some important components are missing, for instance the back EMF reference frame is not highlighted, the leakage fluxes are neglected and the system is assumed to be controllable. In the appendix the modelling of the controlled system demonstrates that there is a strong coupling between the state variables in the MMC, those facts are not negligible and it even becomes important in industrial drive applications.

In literature, the first assumption for computing the arm energy is the equivalent arm capacitance, however it has been demonstrated in the previous paragraph 4.5.2 The controversy theory of the equivalent arm capacitance of MMC that the MMC arm capacitance is varying according to the AC side generated voltage. Therefore the arm energy equation based on a constant equivalent capacitance model is very limited. This is the reason why, the charge balance equation has been introduced; it gives a better understanding of the equilibrium charge of the MMC. Moreover, this wrong assumption induces another variable to be control:

- The vertical balancing; this vertical balancing control is mostly implemented in the $\alpha\beta$ reference frame.
- The horizontal balancing which controlled in arbitrary reference frame abc

In the frame work of the CMMC, this is unthinkable because it is complicated to control an asynchronous motor imbalanced in space abc reference frame. This should be done in rotating frame. In order to simplify the dynamic matrix of the induction motor.

4.6.4 The charge balance approach in the CMMC

The main challenge of the CMMC control can be summarized in two points:

1-In standard MMC, the AC load which is the grid is known because it is a fix installation, the voltage and the current can be therefore measured. The applied voltage from the MMC can be adjusted in somehow to control the current flow through the AC load impedance. However, in case of the CMMC, the AC load which is the charging station is unknown, the Flex-EV isn't a fix installation, the Flex-EV has to adapt with various charging stations. In addition the voltage and the current are not directly accessible, because there is not communication between the EV and the charging station. Therefore, the control system is not anymore the charging line cable impedance which is the outer AC load, the branches inductances become the control system in case of the CMMC, which are an internal variable for the system basically.

2- During the driving mode the phase voltage is not sinusoidal, means that the line-to-ground branch voltage cannot perform a phasor. Therefore it is not possible to control the system in rotating synchronous frame base on the branch voltage like in standard MMC control (Figure 3.27). However, the upper and the lower arm voltage form a double space phasors.

$$\underline{u}_{cm}^{up} = \underline{u}_{cm}^{low} e^{i\phi}, \quad where \ \ \phi = \begin{cases} \pi & \text{in charging mode} \\ 0 & \text{in driving mode} \end{cases} \tag{4.40}$$

Therefore, they form a double three phase system. This is the reason why the control is based on double inner-current control in rotating frame.

4.6.4.1 Structural diagram of the CMMC control

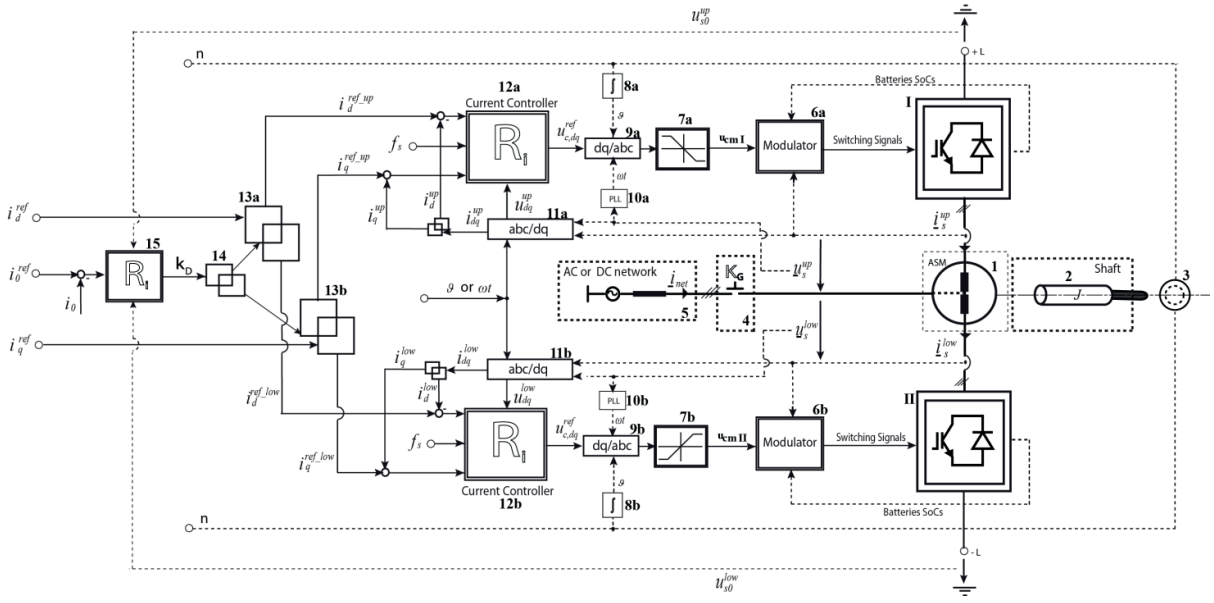

Figure 4.17: Possible control implementation of the CMMC control (without supervisory control)

In this context, the current controller for the CMMC is dedicated to controlling the inner arms current instead of the outer AC load (grid or motor) same as for the standard MMC. This is due to the

fact that the measured AC quantities are the inner-arms currents and voltages; the outer-arms AC quantities, which is the grid, disappears during the driving mode, whereas the rotor circuits disappears during charging mode. In addition, an outer voltage control is required in order to control the charge balance between the upper and the lower arms. This is represented by block 15 in the Figure 4.17 above. The current controllers 12a and 12b are based on the state space multivariable controller in the rotating reference frame with direct feedforward. In fact, the outer current control in standard MMC, is replaced by double inner current controllers. More details can be found in the previous paragraph (3.5).

4.6.4.2 Illustration of the 1st condition

This paragraph is dedicated to illustrate the sensitivity of the zero sequence current injection under unbalanced condition between the upper arms and the lower arms.

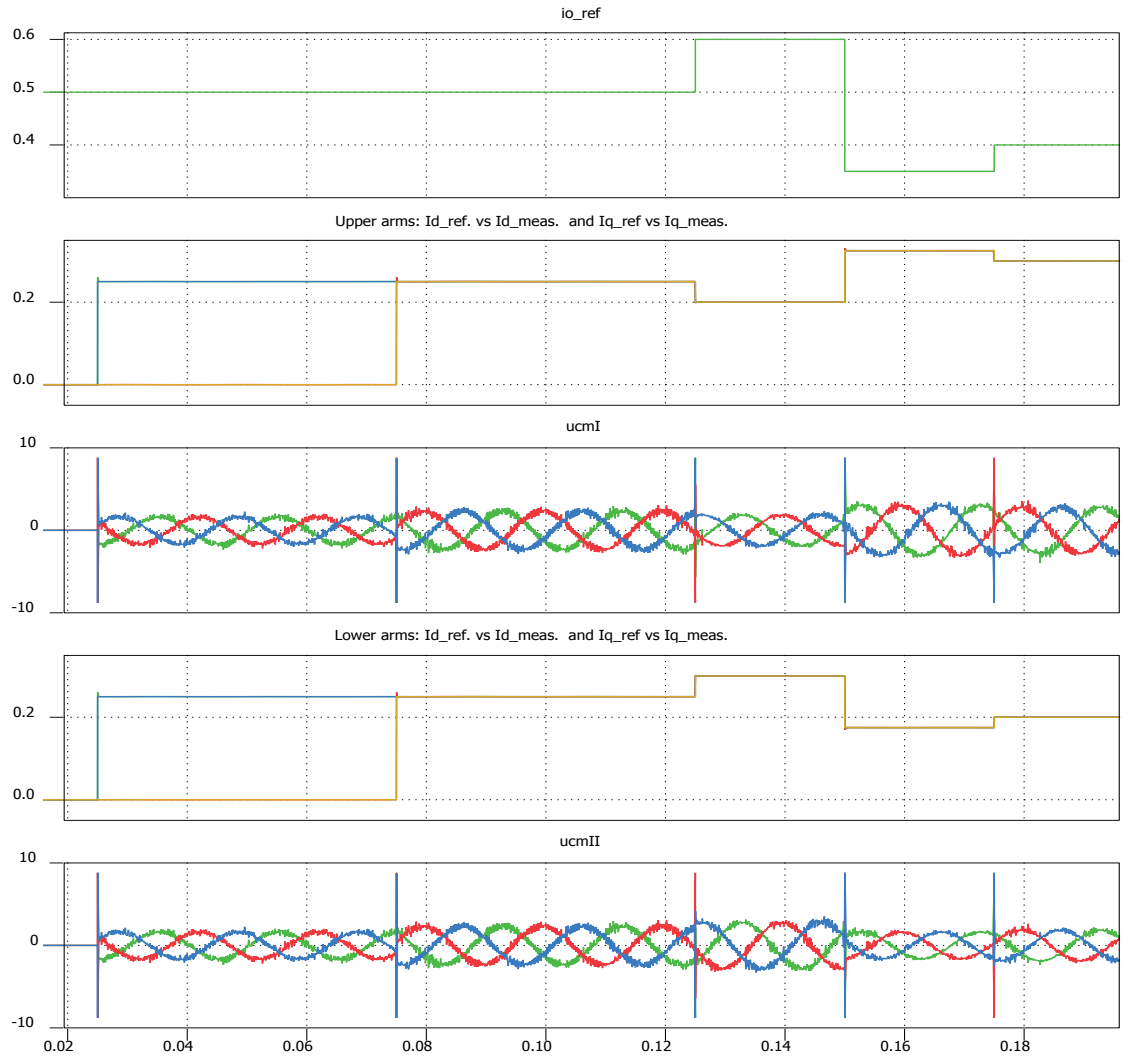

Figure 4.18: The sensitivity of the common mode current injection for the 1st condition

Figure 4.18 illustrates the sensitivity analysis of the zero sequence current injection against the reference signals u_{cmI} and u_{cmII} in order to balance the distribution of the shared power between the upper and lower arms. In fact, the simulation can be divided in two parts where the first 0.125 seconds corresponds to the fact that the 1st condition is verified. The second part of the simulation corresponds to the fact that there is imbalance due to the zero sequence current injection.

4.7 Corollary of the 2nd condition

4.7.1 The transferred power flow

The key parameter is $\cos(\varphi)$. It offers the possibility to control the active and reactive power flow across the point of common coupling (PCC) during the so called flexible charging mode. In charging mode, it allows also controlling the motor during driving mode.

4.7.1.1 Test profile and simulation parameters

The main goal is to highlight that the CMMC is able to track the given set-points in the 4 quadrant area of the PQt profile.

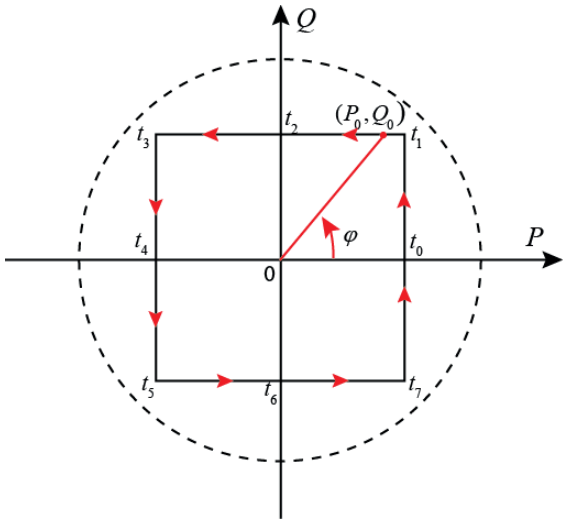

Figure 4.19: Dynamic set-points for the PQt profile

In fact, the reference starts at t_0 where the active power is positive, and no reactive power is requested. Then, the set-point follows the red arrows shown in Figure 4.19 above.

Induction machine	Configurable Modular Multilevel Converter
S_N= 2.78 [kVA]	***Submodule: configurable in half- or full-bridge***
P_N= 2.2 [kW]	S_N= 1 [kVA]
FP=0.79	I_N= 12 [A]
U_{NS}= 220 [V]	U_N= 85 [V]
I_{NS}= 8.8 [A]	
F_{NS}= 50 [Hz]	***Arms: 6***
p= 2 [-]	N=P=4; four levels
N_S= 1500 [rpm]	Modulation with selecting and sorting algorithm
R_S= 1.1 [Ω]	
R_R= 1.2 [Ω]	***Branches: 3***
L_h= 0.143 [mH]	Three phase structure: double star
$L_{\sigma S}$= 4.50 [mH]	Multiport inputs/outputs
$L_{\sigma R}$= 4.50 [mH]	Power conversion configurable (DC/AC, AC/AC, AC/DC)

Table 4.1: Real rated values of the induction machine and the CMMC

Table 4.1 gives the real rated values of the induction machine as well as the CMMC parameters. In fact there are the rated values of the implemented demonstrator. The same parameters are used in simulation validation and in the experimental validation.

4.7.1.2 Simulations results

The simulation is performed with 8 states and the state-flow is depicted in Figure 4.19:

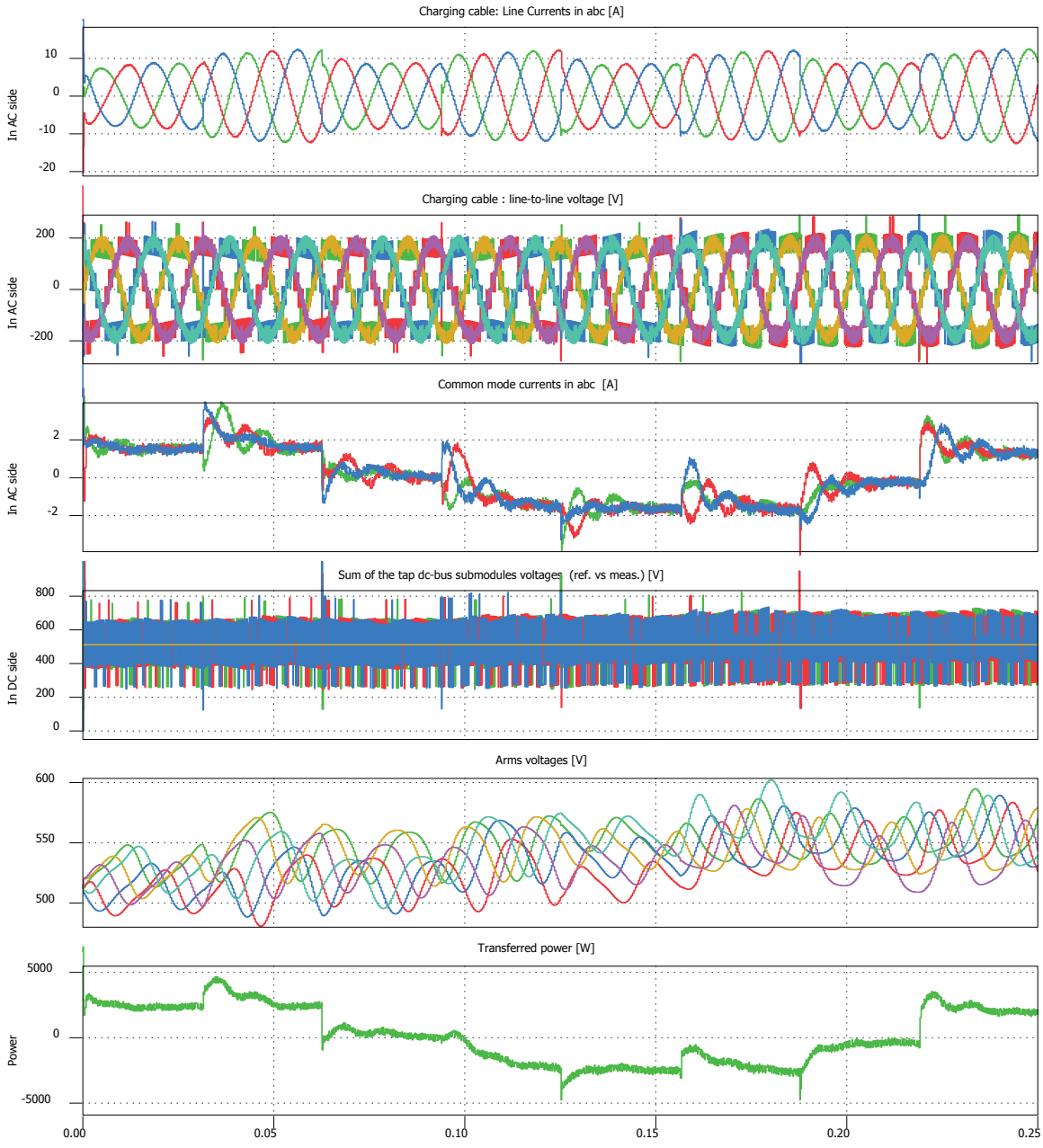

Figure 4.20: Flex-charging: state variables versus *PQt* profile (N=4)

4.7.1.3 Comment

Figure 4.20 shows the simulation results during 250 ms, this simulation time is divided into eight states according to the position of the set-points in PQt plane. It is highlighted that the controller is able to adjust the phase as well as the current amplitudes according to the required power. In addition, the arms voltages converge. This means that the balancing strategy works well.

- 0.0 < t < Ts/8

This phase (t_0) corresponds to the state where the active power is positive and there are no requests for reactive power. The required active power is about 2.2 kW and the CMMC is following this reference well. This corresponds to the vehicle-to-grid (V2G) operation where pure active power is given to the network facility.

- Ts/8 < t < Ts/4

This phase (t_1) corresponds to the state where both active and reactive power are required, therefore, it can be seen that the transferred power is increasing. An overshoot is seen during the transient, however, it remains acceptable. An unbalance is seen in the common mode current, however the CMMC balancing strategy is able to recover the charge balance in a very short time.

- Ts/4 < t < 3*Ts/8

This third phase (t_2) is characterised by the lack of active power requirement. Therefore, the transferred power is reduced; also the line current amplitude is reduced.

- 3*Ts/4 < t < Ts/2

In this state (t_3), an active power is required, the current amplitude is increasing. However the transferred power becomes negative because the required active power is negative.

- Ts/2 < t < 5*Ts/8

This phase (t_4) is characterized by the pure negative active power requirement; this corresponds to the charging of the submodule battery where active power is drawn from the grid.

- 5*Ts/2 < t < 3*Ts/4

In this phase (t_5), both the required active and reactive power are negative. It is seen that the peak power is around 4.4 kW, this corresponds to twice the nominal power. The stator current is around 1.4 times of the nominal current. This might induce damages of the stator windings.

- 3*Ts/2 < t < 7*Ts/8

Here (t_6), the required reactive power is negative and no requests for active power.

- 7*Ts/8 < t < Ts

Here (t_7), the active power becomes positive that why the transferred power is increasing.

4.7.2 Active filter for ancillary service

4.7.2.1 Description

Nowadays, negative impacts on power quality, caused by standard large charging system, welding lines or computers' power supply units for example, can have serious consequences: if a sensitive device, such as an electronic control unit, is damaged by harmonics, total production failure may result. Even the supply grid itself can experience impermissible interference or dangerous overloading due to reactive power, load imbalance, fluctuation in voltage (flicker), and high harmonic currents.

Therefore, the Flex-EV is design to filter reliably and accurately compensate for this interference. The CMMC can measure current and voltage of a grid at the charging station and supply precisely the amount of current required for the desired effect. To reduce voltage fluctuations (flicker), active filters make use of the fact that inductive reactive power reduces the line voltage and capacitive reactive power increases it. Active filters therefore reliably take the strain off grids, extend the service life of devices and increase the safety of industrial systems in charging point.

4.7.2.2 Approach

According to the model of CMMC branch, which is modelled by a switch commutator with N output states (Figure 4.15), the median output current can be expressed as:

$$\bar{I}_k = \frac{1}{\pi}\left(\sin\alpha_k - \sin\alpha_{k-1}\right)\cdot\hat{I}\cos\varphi = K_k\cdot\hat{I}\cos\varphi \tag{4.41}$$

where the factor K_k corresponds to the ponderation current sharing factor, this factor can be tuned in such a way that specific harmonics of the output voltage are minimized or eliminated. Therefore, the firing time should be computed in such a way to achieve a complete symmetrical switching:

$$t_{\beta_k} = \frac{T}{2} - t_{\alpha_k} \tag{4.42}$$

In fact, the switching times for the second half-period have to be delayed by $\frac{T}{2}$. The amplitudes of the fundamental sinus wave and the harmonics can be determined by a Fourier-analysis:

$$u_s(t) = \frac{a_0}{2}\sum_{n=1}^{\infty}\left[a_n\cdot\cos\left(n\cdot\omega t\right) + b_n\cdot\sin\left(n\cdot\omega t\right)\right] \tag{4.43}$$

In fact, because of the symmetry of the output signal, no b_n coefficient exists and all even harmonics ($a_{2k},\ k\in N^*$) disappear. Therefore, the fundamental amplitude can be defined as:

$$a_k(t) = \frac{2}{\pi}\sum_{\alpha_k}^{\beta_k} u_s(\omega t)\cos(\omega t)\,d\,\omega t \tag{4.44}$$

Therefore, when harmonics arise, currents are actively generated, opposing the interference in the grid, so that the harmonics are wiped out.

4.8 Conclusion

It is well-known that control engineering is an exciting and challenging field. By its very nature, control engineering is a multidisciplinary subject, and it has taken its place as a core interest at Industrial Electronics Laboratory (LEI), for decades. However, it is reasonable to expect different approaches to mastering and practicing it from a strictly theoretical point of view, emphasizing theorems and proofs. On the other hand, since the ultimate objective is to implement controllers in real systems, some might take an ad hoc approach relying only on intuition and hands-on experience when designing a feed-back control system. Roughly speaking, there have been two main lines of work in MMC control theory, which sometimes seemed to proceed in very different directions but which are in fact complementary.

One of these is based on the idea that a good MMC model to be controlled is available and that one wants to somehow optimize its behavior. For instance, physical principles and engineering specifications can be and are used in order to calculate the arms energy profile and the appropriate capacitors voltages, to control the circulating current of the MMC.

The second takes into account the rational use of the energy and the protection of the MMC. In fact, the techniques here are closely related to the classical calculus of variations and to other areas of optimization theory; the end result is typically a pre-programmed real-time active distribution network. The other main line of work is based on the constraints imposed by uncertainty about the model or about the environment in which the object operates. The central tool here is the use of feedback in order to correct deviations from the desired behavior.

The main challenge of the CMMC control can be summarized in two points:

1. In the standard MMC, the AC load, which is the grid, is known because it is a fixed installation. Therefore the voltage and the current can be measured. The applied voltage from the MMC can be adjusted to control the current flow through the AC load impedance. However, in this thesis, the AC load which is the charging station is unknown, it isn't a fixed installation, so the Flex-EV has to adapt to various charging stations. In addition the voltage and the current are not directly accessible, because there is no communication between the EV and the charging station.

2. In half bridge submodule configuration and during the driving mode, the phase voltage is not sinusoidal; this means that the line to ground branch voltage is not a phasor. Therefore it is not possible to control the system in the rotating synchronous frame based on the branch voltages. However, the upper and the lower arm voltages form space phasors; therefore, they form a double three phase system. In addition the branch inductance which are the stators winding are bigger than the charging cable inductance. This is the reason why the control is based on double inner-current control in rotating frame.

Chapter 5 Demonstrator

«I am among those who think that science has great beauty. A scientist in his laboratory is not only a technician: he is also a child placed before natural phenomena which impress him like a fairy tale»

Marie Curie (1867-1934)

5.1 Introduction

In 2013, in EPE Lille France, it was the first time that, the configurable modular multilevel converter (CMMC) for a universal and flexible charging system in EV application, was published,. In 2014, the CMMC papers won the Best Paper Award at PCIM Europe in Nuremberg. Since then, the CMMC have attracted many researchers from industries and academics. The concept has been explained in the previous chapters whereas this chapter is dedicated to the experimental validation of the concept. In fact, a self-built laboratory prototype has been realized. The main point is to validate experimentally:

1- The self-compensation of the rotating electromagnetic field inside of the air-gap of the induction machine during the charging mode
2- The feasibility of the CMMC
3- The configurability of the CMMC in driving mode and in flexible charging mode
4- The control performance of the CMMC for Flex-EV

The self-built demonstrator does not only serve to demonstrate the feasibility of the CMMC for a flexible electric vehicle (Flex-EV), also it is expected to give a better understanding of the functionality of the CMMC. However the laboratory demonstrator does not represent a real sized CMMC for Flex-EV. Figure 5.1 shows the CMMC laboratory demonstrator. The overall system has been embedded in a 19-inch rack, which is a standardized frame or enclosure for mounting multiple equipment modules. In fact, each module has a front panel that is 19 inches (482.6 mm) wide, including edges or ears that protrude on each side, which allows the module to be fastened to the rack frame with screws. This figure also highlights particularly the systematic approach that has been undertaken during the development of the demonstrator. Starting from the submodule development, the first CMMC branch has been built. Next, the +NE1 unit has been developed; this consists of the measurements unit and the configuration unit, which is composed of relays. Particular attention has been paid to the configurability of the connection with the charging sources, in order to allow the system to connect at least with the three different power sources (1~AC, 3~AC, DC). After that, the three-branch power module has been built.

At the same time the CMMC Control Unit (CMMC-A1) has been developed because it is the main control unit of the CMMC demonstrator. After testing the first branch and the CMMC Control Unit, the three-phase CMMC branches (CMMC-A, CMMC-B, CMMC-C) have been developed. In fact, a standard MMC has been completed. Next, an asynchronous machine with squirrel cage rotor has been redesigned in order to have an asynchronous motor with tapped and open ended stator windings; this can be seen in Figure 5.1-6. The induction machine has been retested in order to gather its equivalent scheme parameters for the control. So, the standard MMC has been operated with the tapped windings motor in charging and in driving mode. In order to emulate the split energy storage based on batteries, twenty-four isolated dc power sources have been implemented instead of batteries, for simplifying the validation since the main focus is the validation of the CMMC. Therefore twenty-four dc power sources have been designed based on twelve double out-

puts toroidal transformers, each of them is connected directly to a diode rectifier in order to get an average output voltage of 32 Volt, 8.8 Amps. They are protected by fuses against over-current; in addition those fuses are also used to test the capability of the CMMC to ride through a battery failure. It should be noted that such prototyping requires many measurement equipment such oscilloscopes, current and voltage probes, speed measurement, torque measurement, etc.

Figure 5.1: Configurable Modular Multilevel Converter (CMMC), laboratory demonstrator in the Industrial Electronics Laboratory (LEI), *design by Martel Tsirinomeny*

5.2 The CMMC demonstrator description

The main control unit (CS) of the demonstrator consist of:

+NE1: the grid connection switchboard, comprising the main switch, current transformers for stator windings values'measurements (LEM-LV, LEM-LA), +/- 15 V, + 5 V, 24 V dc auxiliaries supply units, fuses, circuit breakers for protecting the auxiliaries and the main contactors. As the demonstrator is to be connected to the charging sources by a configurable-plug[17], the inputs are considered to be protected by an upstream circuit breaker and a residual current circuit breaker. Therefore, it is characterised by a simultaneous connection with three different power sources (1~AC, 3~AC, DC), which represents the four modes of the charging standard.

+A1: the control assembly comprises a DSP motherboard, which embeds a TI TMS320C28346 controller card. It hosts the DSP and its related memory as well as the power supplies. The motherboard also handles the communication with two types of Field-Programmable Gate Array (FPGA) cards: the measurement & GPO and the slave control cards (+CMMC-A, +CMM-B and +CMMC-C). The latter are dedicated to provide the desired gating signals for the three phases CMMC arms, it includes the modulation strategy with sorting and selecting algorithm for balancing the submodule voltages on the level of the arms. It also retrieves internal measurements such as the arm currents and submodule voltages via sequential serial peripheral interface (SPI).

The measurement FPGA in turn retrieves the external measurements via General Purpose inputs (GPI); it is a completed data acquisition system. It combines also a General Purpose Interface which allows to configure the operating mode via relay outputs (GPO), which are located in the +NE1. In fact, one control FPGA handles an entire phase with 8 modules and the appropriated measurements.

It should be noted that, in the framework of the Flex-EV, the upstream part of the AC grid is not accessible because it is not a fixed installation and there is no communication between the EV and the charging station. Therefore the Flex-EV has to measure internally the downstream voltage of the charging voltage after checking the compatibility of the power connection. This allows the CMMC to synchronize with the grid even with the lack of communication between the EV and the charging points.

[17] A configurable plug is a plug which allows the connection to different type of the charging sources (1~AC, 3~AC, DC). Then the internal +NE1 manages the configurability of the connection according to the operating mode.

5.2.1 The data flow architecture

The control system (CS) was designed to coordinate the data transfer and control actions between the subassemblies of the CMMC demonstrator. Figure 5.2 illustrates the data flows in the CMMC control Unit. This control unit includes a graphical user interface (GUI) for man-machine interaction (MMI) based on the code composer studio (CCS) from Texas Instrument which run with Windows XP as the operational system. The runtime and programming environment are supplied by the same manufacturer. In the same rack +A1, there are the local slave modules and backplane card for connecting the signal wires.

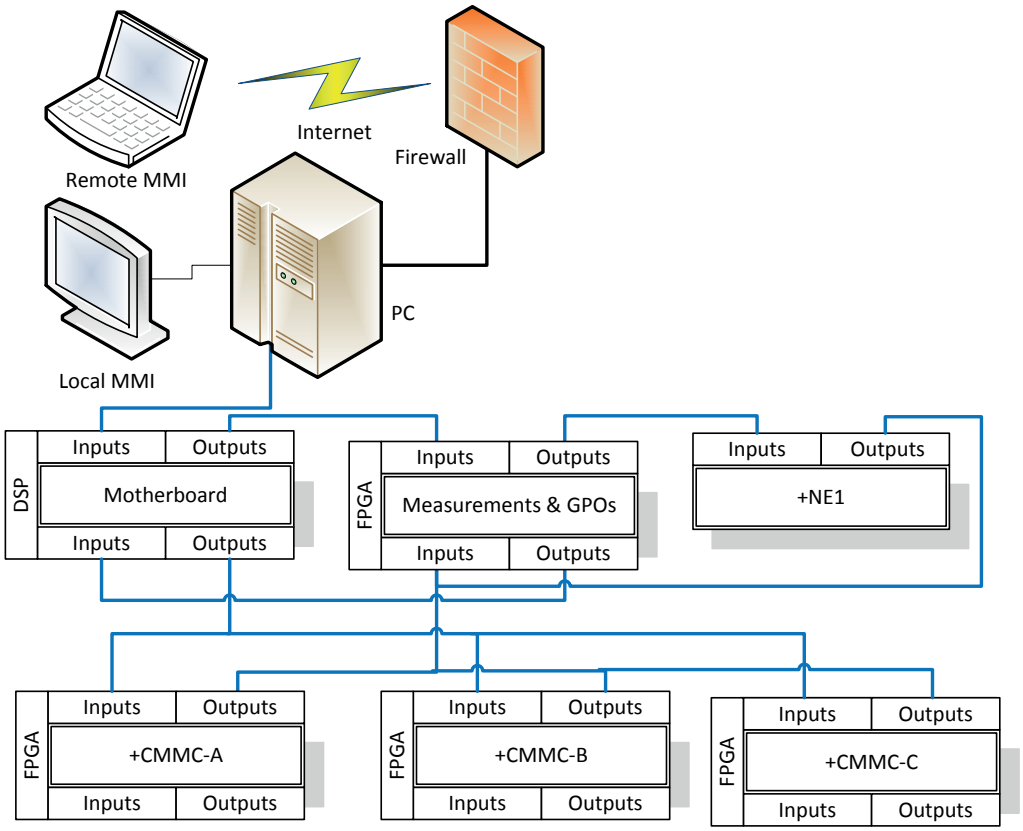

Figure 5.2 : Data flow architecture in +A1 unit

5.2.2 The protection unit

Particular attention has been paid to the protection unit; the programmed protections operate redundantly to the inbuilt low-level ones. The events to react to are:

1) over- and undervoltage
2) overcurrent

The protections are implemented on two reaction levels. The first level signals a non-critical deviation from the allowed parameter and the implemented code sends a warning; this is represented by the yellow alarm in the following Figure 5.3, whereas the second level triggers tripping: the

converters are stopped and all contactor coils, and capacitors are de-energised, thus insulating the sub-assemblies; the red signal light is activated as well. For alarm and trip levels, lower and upper values are defined.

Figure 5.3: Alarm and trip levels.

For instance, if the sum of the tap-dc submodule voltages is higher than 300 Volt, the demonstrator is tripped and the capacitors and coils are de-energized instantaneously. The CMMC is isolated from the external power sources. This is followed by the red alarm which is located in front of the demonstrator (see Figure 5.1). However, after the fault has been cleared, the protections must be reset by a user input from the MMI. The voltage and current limits are also configurable by the user by the means of an industrial keyboard.

5.2.3 The variable name syntax

The standard IEC 61131-3 permits using several variable types; in addition to BOOLEAN, REAL, INT and FLOAT, user-defined ones can be applied. For example, a relay state can be defined as an ENUM variable, which is basically a list of possible values. In the relay case, these values are ON, OFF and FAULT – the latter for the situation when the position does not correspond to the coils/capacitors energise command and which is useful to detect broken circuits or welded contacts. The variables can be grouped into structures, e.g. the configurable modular multilevel three-phase structure can contain variables for the voltage, current, which yields the variables more transparent for processing. For instance, the structured variable can be explained by the following Figure 5.4 for the lower split current set-point of the converter. The structure and variable names are separated by a dot.

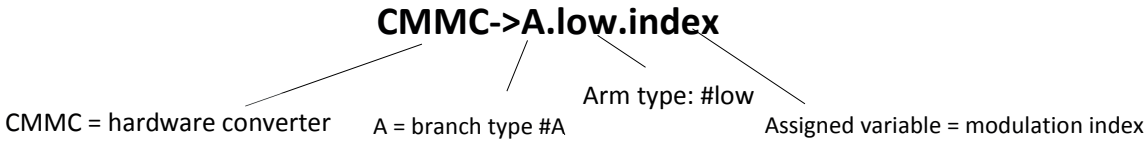

Figure 5.4: Variable name syntax

5.3 The Direct modulation

- Typical modulation instructions:

```
// Compute the modulation indexes:
switch(modstyle){
    case FULLOPENLOOP:    // typically for V2G operating mode, in ancillary services operation
        CMMC->A.low.index   = 0.5*(1+moddepth*sin(OMEGA_3PH*realtime+0));
        CMMC->A.up.index    = 0.5*(1-moddepth*sin(OMEGA_3PH*realtime+0));
        CMMC->B.low.index   = 0.5*(1+moddepth*sin(OMEGA_3PH*realtime-TWO_PI_OVER_THREE));
        CMMC->B.up.index    = 0.5*(1-moddepth*sin(OMEGA_3PH*realtime-TWO_PI_OVER_THREE));
        CMMC->C.low.index   = 0.5*(1+moddepth*sin(OMEGA_3PH*realtime+TWO_PI_OVER_THREE));
        CMMC->C.up.index    = 0.5*(1-moddepth*sin(OMEGA_3PH*realtime+TWO_PI_OVER_THREE));
        break;
    case FULLOPENLOOPDRIVE:    //typically for EV drive, where the upper and lower arms voltage are in phase
        CMMC->A.low.index   = 0.25*(1+moddepth*f_ctrl*sin(OMEGA_1PH*f_ctrl*realtime+0));
        CMMC->A.up.index    = 0.25*(1+moddepth*f_ctrl*sin(OMEGA_1PH*f_ctrl*realtime+0));
        CMMC->B.low.index   = 0.25*(1+moddepth*f_ctrl*sin(OMEGA_1PH*f_ctrl*realtime-TWO_PI_OVER_THREE));
        CMMC->B.up.index    = 0.25*(1+moddepth*f_ctrl*sin(OMEGA_1PH*f_ctrl*realtime-TWO_PI_OVER_THREE));
        CMMC->C.low.index   = 0.25*(1+moddepth*f_ctrl*sin(OMEGA_1PH*f_ctrl*realtime+TWO_PI_OVER_THREE));
        CMMC->C.up.index    = 0.25*(1+moddepth*f_ctrl*sin(OMEGA_1PH*f_ctrl*realtime+TWO_PI_OVER_THREE));
            break;
```

Figure 5.5: An extract of the direct modulation reference instruction in IDE Code Composer

- Experimental results:

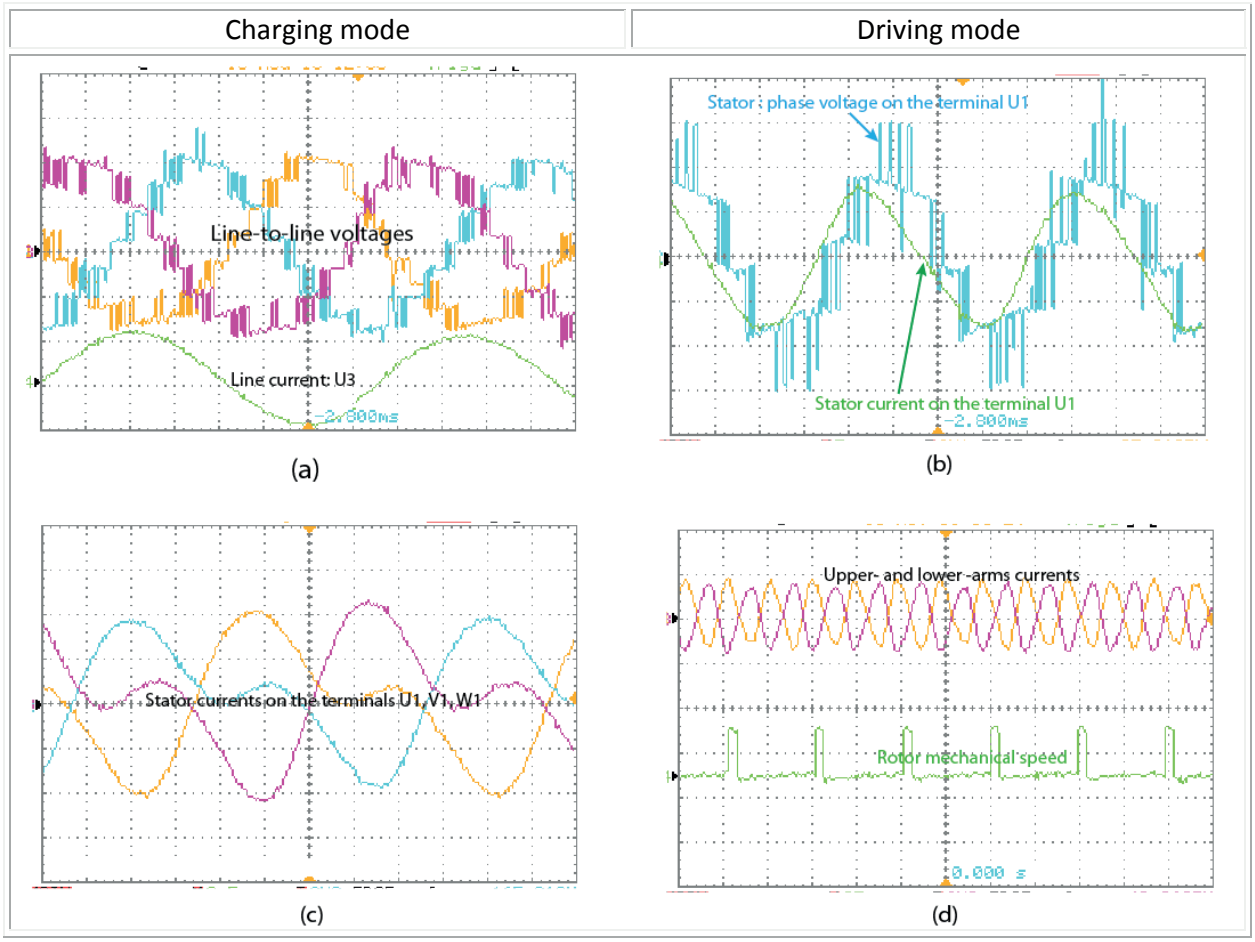

Figure 5.6: Experimental results: direct modulation full open loop

(In driving mode, the upper and lower arm are shown in opposite phase in order to highlight that there is no circulating current but in reality they are in same phase)

- Comments:

Figure 5.5 shows an extract of the implemented instruction, which corresponds to the direct modulation reference function where the configurability of the system is highlighted. In fact, in charging mode the instruction is well-known, however in driving mode, the instruction is especially uncommon; it is shown that the arm reference is ¼ of the sum of the tap-dc bus (battery pack voltage). This can be explained by the fact that the line-to-line stator voltage is performed by two adjacent CMMC-branches; for instance the stator voltage U is performed by the CMMC branch A and B. In contrast in standard MMC, the AC line voltage is performed by an independent branch (i.e: the phase voltage A is performed by the MMC branch A). This validates the formula (3.19), about the CMMC design requirement.

Furthermore, the parameter f_ctrl has been introduced because the stator voltage and the stator frequency have a proportional linearity; the amplitude must to be increased with the frequency otherwise the motor works in bad operating conditions, which leads to the destruction of the motor. This is a basic of the asynchronous machine drive principle. In addition, this equation demonstrates the manner for generating an alternating voltage inside a branch of MMC.

Figure 5.6 (a) shows the line-to-line voltages during charging mode, the submodules is commutated at 2 kHz. This is relatively low; however the multilevel structure allows a generation of nearly perfect sinusoidal currents without additional current filters, which are based on bulky inductances.

Figure 5.6 (b) shows the measured stator voltage waveform in blue and its corresponding current in green. The voltage is measured on the terminal side of the motor phase winding; meaning that the stator winding is supplied by twice this voltage on each six terminals during driving mode.

Figure 5.6 (c) is the measured stator current at the terminals (U1, V1, W1) of the motor, in the charging mode. These current waveforms are characterised by the second harmonics currents pulsation. As mentioned before, this can be damped by injection of second harmonics in the modulation references; however, this might reduce the dynamics of the CMMC.

Figure 5.6 (d) shows on top the upper and lower arm current in driving mode. It should be noted that the two ampere meter has been placed in opposite direction in order to demonstrate that the stator winding is traversed by the same current during the driving mode; there is no circulation current because there is a nearly perfect power balancing between the upper and lower arm in the same phase. The applied stator voltage leads to induced rotor current which allows a generating of rotating magnetic field in the airgap, which leads to an electromagnetic torque. The rotor mechanical speed is represented in green. For instance, the motor has 4 poles; therefore the green pulse which represents the rotor angle appears every two periods of the electric angle.

5.5 The Flexible charging

5.5.1 Vehicle to Grid (V2G) operation

This experiment is dedicated to demonstrate the vehicle-to-grid operation. In this context, active power is injected into the grid for ancillary service operation.

Experimental results:

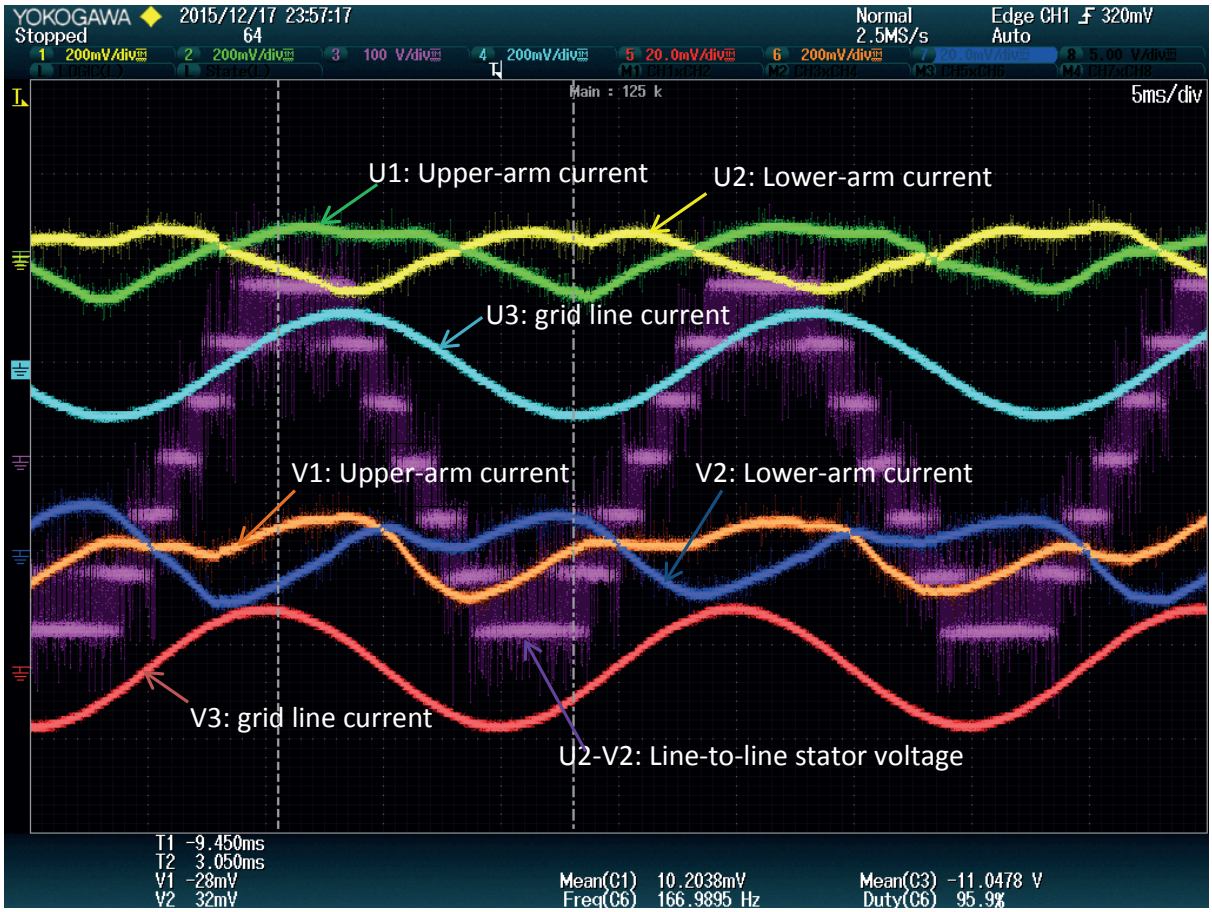

Figure 5.7: V2G operation

- Comments:

It has been stated that according to the equations (3.11) and (3.12), the motor-current components contained in the upper arm current i_{P_u} and in the lower arm current i_{N_u} are in opposite phase with respect to each other, meaning the shifted angle is $\emptyset = \pi$ during charging mode. This allows the compensation of electromagnetic field in the airgap. This is experimentally verified by Figure 5.7. Also, it is shown that the induced phase currents are purely sinusoidal. However the arm currents contain second order harmonics components. The theory meets exactly the experimental results.

5.5.2 MMC operation: DC charging

This experiment is dedicated to demonstrate the DC charging and the DC/AC operation of the CMMC. Firstly, the DC charging has been performed with the same algorithm that the standard MMC. In this case, the tap DC sources which emulate the batteries are disconnected because these sources are unidirectional. However, the tap dc bus submodule capacitors are still connected. The charging and the discharging can be adjusted through the required power set-point. The arm balancing strategies can be verified.

- Experimental results:

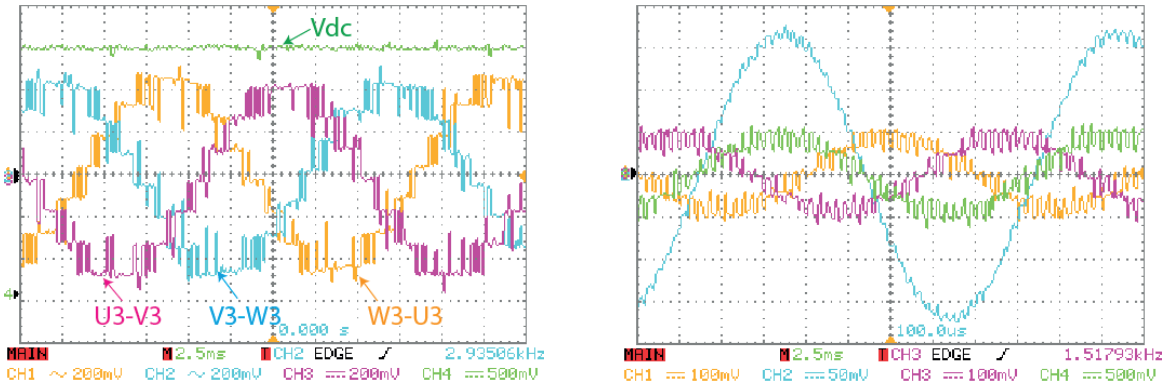

(a) The line to line stator voltages versus V_{DC}

(b) Resistive load: load voltages versus load current

Figure 5.8: DC/AC operation

- Comments:

On the right side, Figure 5.8 (a) shows the stator line-to-line voltage during the DC charging. In fact, a DC voltage power supply is connected between +L and –L, which is shown with the green curve in the left figure. The AC load is not connected; however, a similar modulation strategy as in Figure 5.5 is still validated.

On the left side, an AC resistive load has been connected; this experiment is dedicated to validate the DC/AC power conversion as for the standard MMC. The Figure 5.8 (b) shows the phase voltage of the AC resistive load. The blue curve is the phase current for one phase of the resistive load.

It should be noted that both experiments have been undertaken with direct modulation so the validation of the direct modulation is justified experimentally.

During this experiment, the DC/AC conversion for DC charging has been validated. The sorting and selecting algorithm for balancing the tap dc bus capacitors on the arm level has been also validated in direct modulation. In addition, the passive load discharge has been also validated.

5.5.3 The grid connected operation

The radical shift to green energy leads to a high penetration of distributed power generation in the electrical network which has introduced new issues in the stability and transient operation of the grid. By means, it is possible to enhance their performance and also to support the grid operation, as the new grid codes demand. The connection of FACTS based on Flex-EV, such as CMMC, are also contributing to the integration of renewable energies improving their behavior under contingencies. However, in both cases it is needed to have a grid voltage synchronization system, able to work under unbalanced and distorted conditions. This can be illustrated in diagram (Figure 5.9). This experiment is devoted to demonstrate the capability of the CMMC to synchronize with the grid facility; this allows generating the angle and the amplitude of the grid through a PLL.

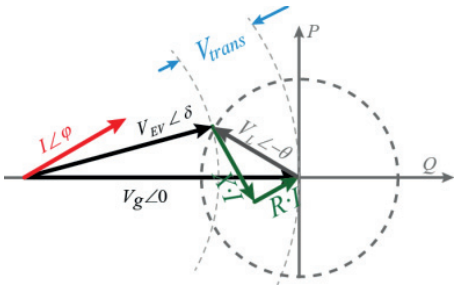

Figure 5.9: The phasor diagram for the active/reactive power at the Point of Common Coupling (PCC)

- Experimental results:

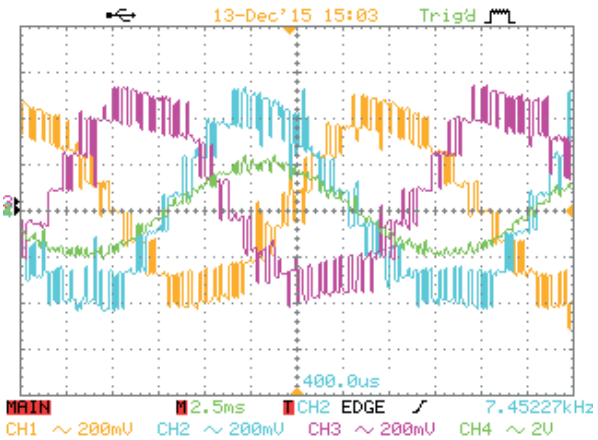

(a) Voltage synchronisation

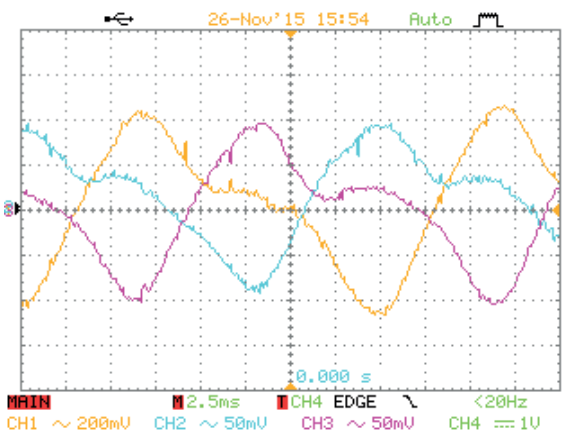

(b) Typical arm current

Figure 5.10: The grid connected operation for ancillary services

- Comments:

:It is shown in the Figure 5.10-(a) that the CMMC line-to-line AC voltages (U3: magenta, V3: cyan and W3: yellow) are synchronited with grid line-to-line voltage (V: green). The induction machine stator is connected directly and continuously to the grid. The CMMC can exchange active and reactive power with the grid according to the set point (PQt profile). Also, Figure 5.10 (b) shows the typical arm currents in during this grid connected operation.

5.6 The driving mode operation

5.6.1 The basic driving mode

- Description

This experiment is dedicated to demonstrate the driving mode operation of the CMMC. The induction machine has been operated at nominal speed around 1420 rpm. In particular, this experiment has been carried with full bridge submodules configuration.

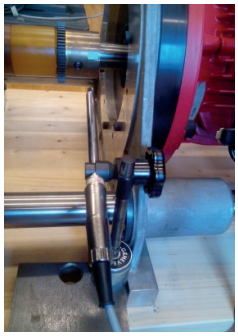

(a) Infrared sensor

(b) Speed displays

Figure 5.11: Speedometer

Figure 5.11 shows the speedometer or speed meter, which is the gauge that measures and displays the mechanical speed of the rotor. It is based on IR sensor as depicted on the left side of the Figure 5.11, whereas the revolution speed in rpm is displayed on the right side. For instance, the speed of 1500 rpm corresponds to the synchronism.

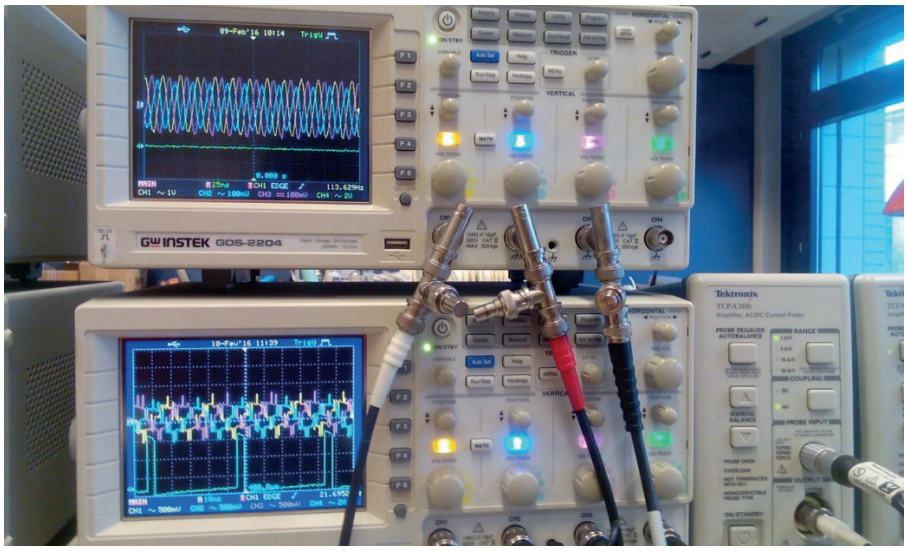

Figure 5.12: Three-phase current on top, line-to-line upper arm voltage versus speed on bottom

Figure 5.12 shows the stator three phase currents at 50 Hz on the top oscilloscope, whereas the bottom oscilloscope shows the upper arm line-to-line voltages versus the speed. It is highlighted that 2 periods of the voltage correspond to 1 speed revolution, it is verified that the motor has 2 pair poles.

- Experimental results:

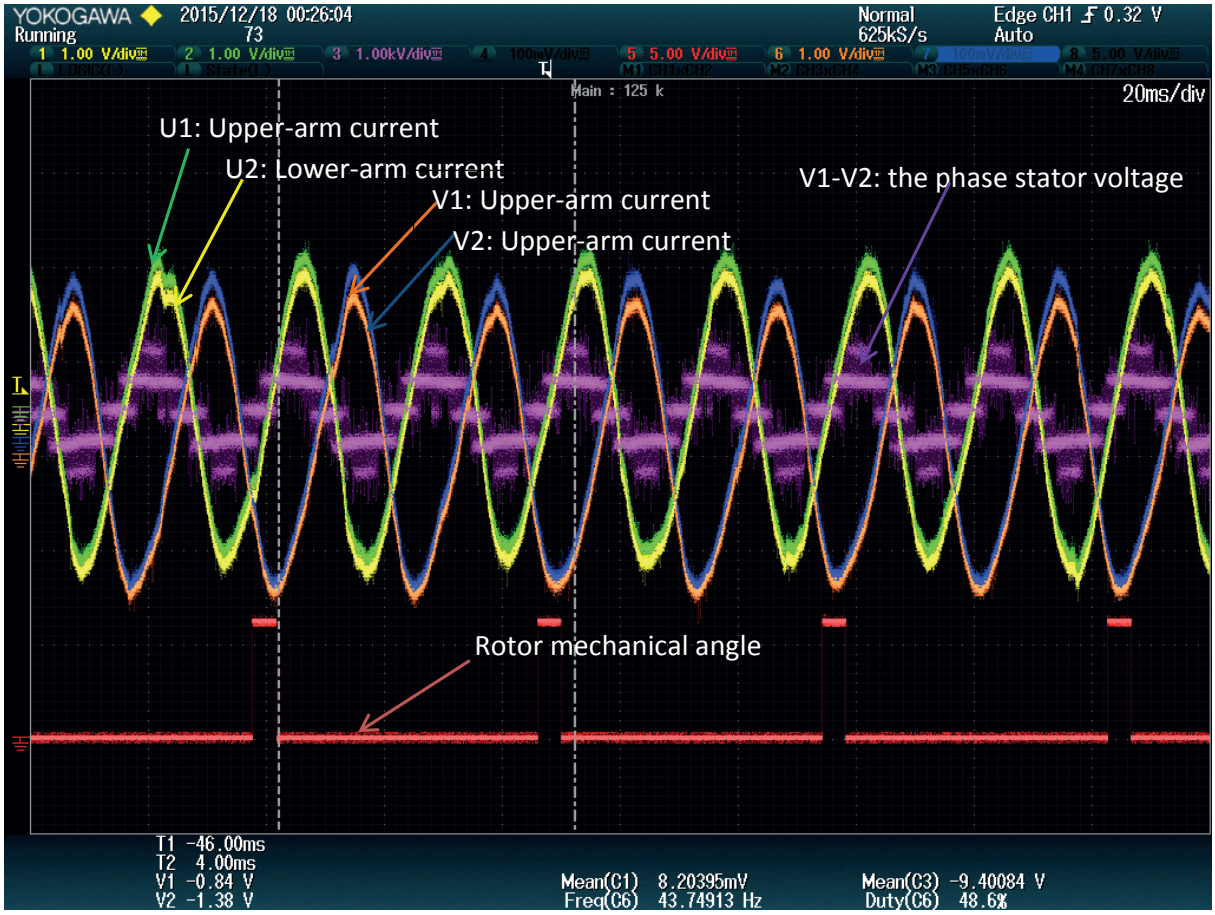

Figure 5.13: Driving mode operation

- Comments:

It is shown that the upper and the lower arm currents are equal; also they are purely sinusoidal without second order harmonic components. It is also shown that the rotor mechanical angle corresponds perfectly to the angle of the stator current which is a factor of 2. This corresponds to the number of the pair poles of the induction machine. The phase voltage U (magneta color) is sinusoidal because the CMMC is operated with full bridge submodule configuration. It should be noted that in this figure the reference has been shifted vertically in order to show the upper and the lower arm currents, because for each phase, the same stator current passes through by the upper and the lower arms.

5.6.2 Driving mode operation in permanent regime

- Experimental results:

The experimental results correspond to the permanent regime in driving mode at nominal speed with full load. The submodule is operated with full-bridge, therefore it becomes possible to generate an AC stator arm voltage.

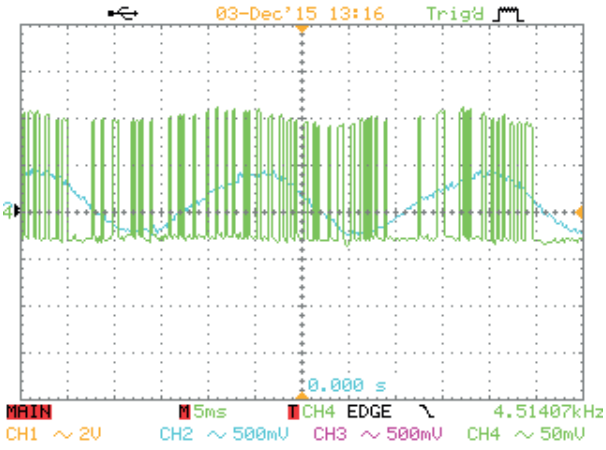

(a) Submodule output voltage (green), arm current (blue)

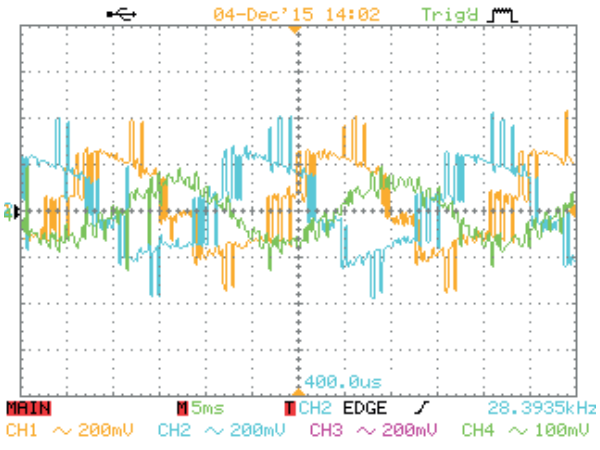

(b) Stator: line to line voltage: U1-V1 (blue), V1-W1 (yellow), stator phase V voltage (green)

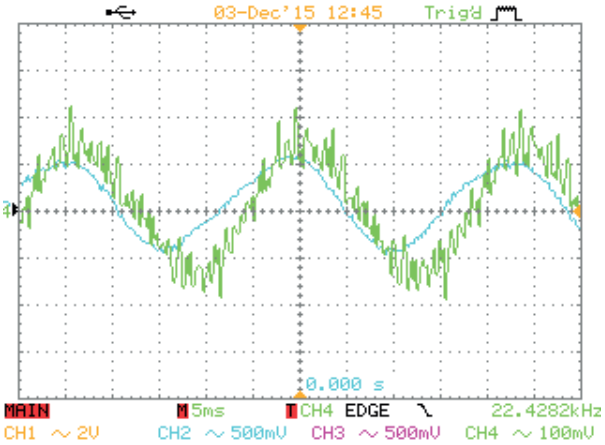

(c) Stator phase: voltage (green) and current (blue)

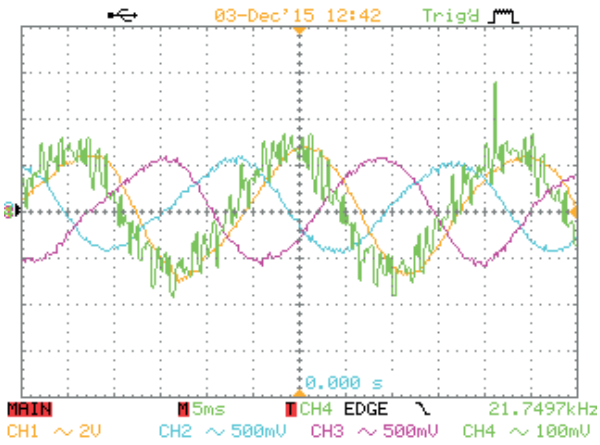

(d) Stator: phase voltage (green), 3 phase currents

Figure 5.14: Experimental results: driving mode in permanent regime (full bridge configuration)

- Comments:

Figure 5.14-(a) displays the submodule feeding voltage, which is the output of the CMMC submodule. It is in green color, whereas as the arm current is plotted with the blue curve. Next, Figure 5.14-(b) shows the line-to-line arm voltages (U1-V1 in blue, V1-W1 in yellow) versus the stator winding phase voltage (green). It should be noted that this line-to-line voltages are viewed from

one side of the open ended stator winding. After, Figure 5.14-(c) shows the stator winding phase voltages versus its corresponding current. Figure 5.14-(d) shows a typical stator phase voltage (in green curve) versus the three phase current of the stator windings. It should be noted that the motor is operated at full load with nominal voltage. These results have been taken after 30 minutes of running of the demonstrator, therefore they represent perfectly the permanent regime of the demonstrator.

5.6.3 Low speed consideration in driving mode

- Experimental results:

Speed: 1238 rpm

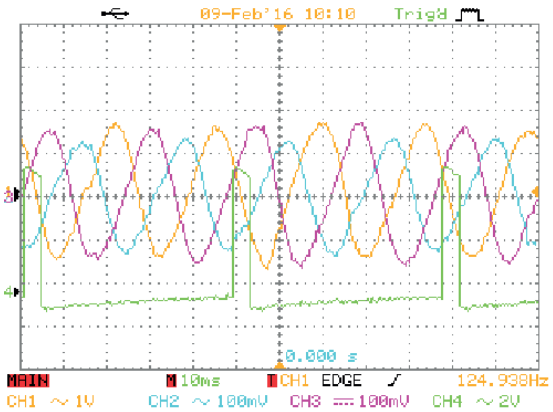

(a.1) Stator currents versus rotor speed

Speed: 300 rpm

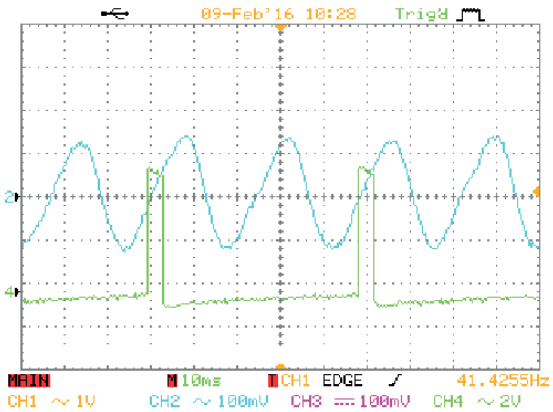

(a.2) Stator current versus rotor speed

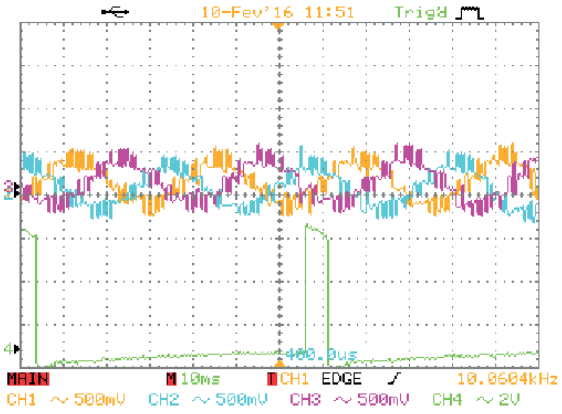

(b.1) Stator voltages versus rotor speed

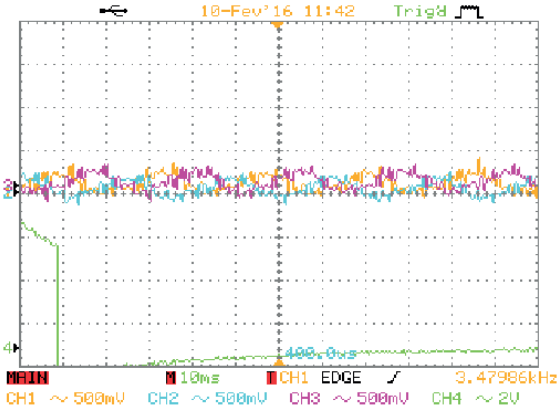

(b.2) Stator voltages versus rotor speed

Figure 5.15: Assessment of the speed variation in driving mode

Figure 5.15 displays the experimental results of the comparison between the line-to-line arm voltage and stator currents versus rotor speed at speed of 1238 rpm and at speed of 300 rpm. In fact

this shows the impact of the slip on the stator voltage frequency. It should be noted that the scale has not been changed, expect for the time scale of the Figure 5.15 (a.2). The test has been done with the same condition. On the left side, the slip is around 0.12 which is closed to 0 because the motor is operated at nominal operation with the nominal torque. It is seen that the arm voltage frequency is roughly around 2 times the frequency of the rotor. On the right side, the slip is around 0.78 which is closed to 1 because the motor is operated at low speed, the arm voltage frequency is then higher than the rotor speed, as depicted in Figure 5.15-(b.2). It should be noted that the rotor speed is not covered in this figure because the motor is operated at very low speed (300 rpm). No special issues have been contacted so far, the system has a very high dynamic performance in comparison to standard commercial convert.

5.7 Discussion

The experimental results show that the self-build laboratory demonstrator has verified the functionality of the concept. In addition, some critical aspects have been taken into consideration such as the low speed operation in driving mode and the grid synchronisation in charging mode for ancillary services operation.

In driving mode:

The CMMC control allows changing the rotation speed of the AC drive; this is achieved by changing the voltage/ frequency of the stator side. During the change of the frequency, we could observe that the voltage has also changed. The ratio of the stator voltage and frequency has to be constant value in order to avoid saturation of the iron core. The linear dependency is measured in several points and a sample of example is shown in Figure 5.15. The CMMC control is designed to maintain a rotation speed which is set by the user, however by changing the load torque, the CMMC will impact on the electromagnetic torque in order to keep a constant rotation speed.

In charging mode:

In driving mode, the motor is cooled based on a forced air, fans cooling system which is driven by the rotor shaft, however, in charging mode, the rotor is at standstill. I realized during the experiments that even at full power, the motor doesn't heat up, this can be explained by the fact that there is no active power transferred, only the reactive part of the motor contribute to the charging mode; since the stator winding are made out of copper, therefore the stator resistance is very low. Moreover, one of the important questions was about the influence of the magnetizing inductance during the charging mode. I realized that in charging mode, there is no vibration in the rotor shaft, can be explained that there are no circulating current tin AC side, this is one of the main advantage of controlling the upper and lower arm separately as a double three-phase system, otherwise the circulating current in standard MMC makes this charging mode impossible without external mechanical locking of the rotor. This can be illustrated in the Figure 3.29. Therefore, there are no induced current in the rotor part, and the magnetizing current through the magnetizing inductance is zero. So the magnetizing inductance does not contribute into the model of the induction machine in charging mode.

Moreover, it is generally agreed that those samples of experimental results cannot reply to the all of the questions of the reader of this thesis. For instance the arm voltage balancing is not included in the experiment results because this can only view in the GUI of the demonstrator. In addition, we have realised that the noise of the electrical machine has been largely reduced by using the CMMC in comparison to standard with 2 level converters. A lot has been written what CMMC can do, it has been descripted why we end up with a such a complex topologies, it has been explained how we can model and control this CMMC in simple and better way. The proposed formula of the working principle of the concept has been validated by experimental results. Finally, the next chapter is dedicated to give a general conclusion of the thesis.

Chapter 6 Conclusion

«The only way to be truly satisfied is to do what you believe is great work. And the only way to do great work is to love what you do. If you haven't found it yet, keep looking. Don't settle»

Steve Jobs (1955-2011)

6.1 How to reduce fossil oil dependency?

It is believed than on day when our strong dependency on fossil oil will be damped, our world will be much better. As state by Elon Musk "*I think there are more politicians in favour of electric cars than against. There are still some that are against, and I think the reasoning for that varies depending on the person, but in some cases, they just don't believe in climate change - they think oil will last forever*". It is believed that on day when the range flow rate[18] of the electric vehicle will be higher than the range flow rate the conventional car, the electric vehicle will be much more competitive. This can be only done by improving the technology of the energy storage system, the distribution grids and the power conversion system.

6.1.1 Charging our car faster than tanking of gasoline car without disturbing the grid network

As seen from the vehicle side, the actual problem may be re-formulated by two distinctive EV-related terms of range, range flow-rate:

1. Range is the average distance an EV is able to cover with the maximally recharged battery in given conditions (capacity, charging current, initial state of charge etc.). This depends also to the EV's aerodynamic shape, mass, as well as the EV's powertrain performance.
2. Range flow-rate is the driving distance augmentation per time unit of recharge, expressed in km/min or km/h. This depends on EV's battery power density and the overall efficiency of the EV's powertrain.

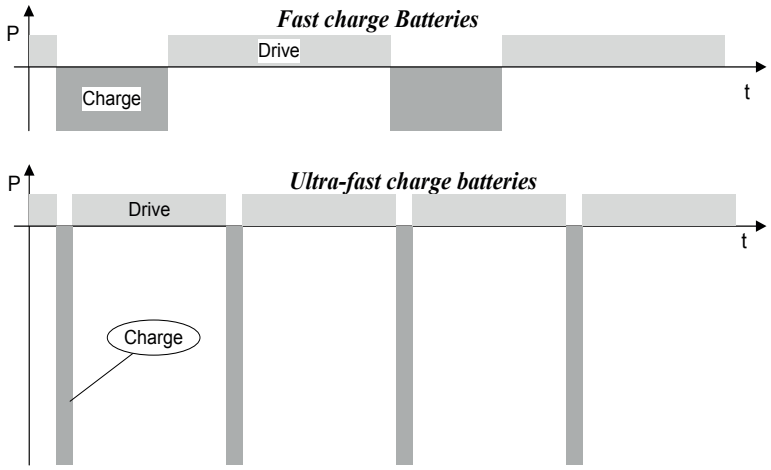

Figure 6.1: Range flow rate comparison between fast charge and ultra-fast charge batteries

[18] Range flow rate: driving range resulting with a minute charging/fuelling time [13]

Figure 6.1 illustrates the comparison between comparison between fast charge and ultra-fast charge batteries. It is highlighted that the best comprise between the energy and power density must be found during the specification of the EV battery.

To increase the appeal of electric vehicles, the trends are to shorten the charging time and to lengthen the autonomy. The proposed ultra-fast compatible battery on nano-lithium-titanate gives the best compromise between the charging time and the distance covered. The state-of-the art of the fast charged electric vehicles has been demonstrated and an evaluation tool for determining the possibility of shorted charging times (objective mean 5min) from the battery traction view has been proposed. The lithium titanate battery offers shorter charging time (in the scale of 5 min) than currently applied lithium-manganese oxide and lithium-iron phosphate, etc. batteries, however there exists a trade-off between shortening the charging time and maintaining the autonomy, even though the average speed is improved. In addition, with better acceptance, nLTO battery batteries have an advantage in urban driving thanks to a better re-use of braking energy (~30 % more autonomy with the same capacity).

As seen from the distribution grid, the actual problem may be re-formulated by two distinctive grid-related terms of capacity, flexibility:

3. In the framework of Ultrafast Charging of Electric Vehicles (UFCEV), a direct connection to the medium voltage grid facility would be an appropriate solution in order to alleviate the power demand. However, this leads to a demand of a huge change in the existing public infrastructure such as installations of medium voltage transformer and change in distribution line cables, which will cost a lot for governments. To decrease the Ultra-Fast Charging Station (UFCS) impacts on utility grid, the load must be at least partially decoupled from the mains grid source. This can be done by implementing energy storage elements, which acts as buffer between the EV and the grid. This can be illustrated by the following Figure 6.2.

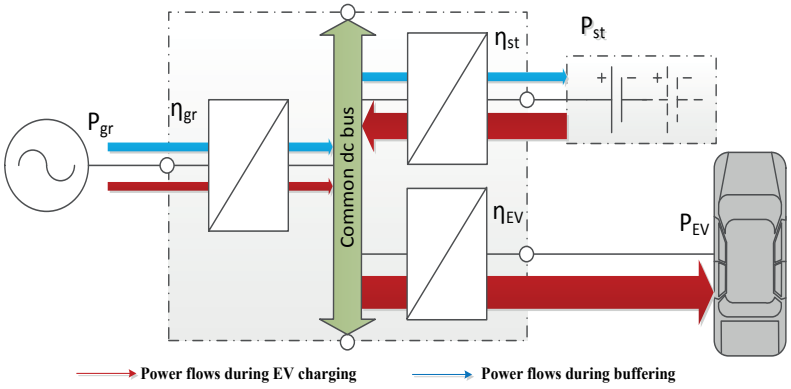

Figure 6.2: UFCS general concept architecture

4. However, The IEC 60851 standard, applicable for conductive charging systems, defines four charging modes. Nevertheless, a discrepancy between the above mentioned standard and the market situation exists. Usually the EV manufacturers prefer to sell their products in set with a Mode 1 one-phase on-board charger; as standard household 16 A sockets are used, which are de-rated to 10 A … 12 A at constant load, the charging power is even more limited, to 2.3 kW … 3.6 kW. The Mode 4, using off-board chargers, has been implemented by the CHAdeMO consortium and Tesla Company. But for today, its charging current is limited up to 120 A by the used connector, which enables to recharge a commercial EV within 20 min … 30 min depending on the battery capacity. As for Mode 3, the manufacturers have not yet reached an agreement on the standard connector, but the increased charging rate is achieved by reversing the power flow in the traction inverter and using motor windings as smoothing reactors, thus the charging power can be nearly equal to the rated driveline power.

A baseline calculation of the ultra-fast charge battery is given in chapter 2 where:

- With buffering, the EV can be charged from a 400 V, 32 A low voltage outlets, allowing a charging interval of one EV in less than an hour.
- The partial use of buffer capacity gives a possibility to exploit the battery more effectively at smaller charging and discharging rates. However in this variant, the converters and battery must be designed to operate in wider voltage range.
- With cost, mass and volume restrictions, the EV battery is optimally based on lithium iron titanate cells. Electrochemical storage, however, is related to additional losses thanks to poorer roundtrip efficiency than i.e. ultracapacitors.

6.1.2 New EV architecture for universal and flexible charging system

The electric vehicle owners are faced to the limited compatibility of the electric vehicle with the available charging stations. The “Configurable Modular Multilevel Converter”, with the given acronym CMMC is a three phase power electronics structure, it has been designed to answer to EV’s requirement in terms of compatibility with the upgradeable charging stations infrastructure.

6.1.2.1 Motivation

The charging compatibly is the flexibility of the EV to charge with a large range of charging infrastructures; from basic supply AC household to AC or DC ultra-fast charging station, meaning from level 1 to level 4 of charging infrastructures according IEC IEC 60851. In fact, electrical energy is distributed with alternating current (AC), whereas, batteries are a direct current (DC) sources. Therefore, power electronics are required to convert the alternating current into direct current for charging batteries. In the framework of electric vehicle applications, this could be off-board or on-board chargers. EVs require a high power as well as compact charger. High power chargers are often implemented off-board because of size, whereas low power chargers are regularly embarked into the cars. A combination of off-board and on-board charger are often implemented in order to achieve the appropriated compatibility regarding the voltage and the current ratings between the AC grid and the EVs batteries. Therefore it has been found out that a universal and flex-

ible on-board charging system based on embedded system gives the best trade-off between the charging compatibility and the power density of the electric vehicle.

6.1.2.2 Description

The Configurable Modular Multilevel Converter (CMMC) offers a large flexibility in order to handle the different voltage levels and current intensities in electric vehicle's battery charging and discharging. It is a smart method to achieve a high power density and a compact power conversion for electric vehicles. It allows interfacing EVs to worldwide charging infrastructures, meaning from the standard household single phase socket to direct-current (DC) ultra-fast charging stations.

During the ultra-fast charging, the transferred power can be kept constant while forcing the charging current to the value, where the product of high power charger's input voltage and current corresponds the set-point under the voltage limits of the buffer and EV batteries as well as current limits of the current-carrying components.

Additional limitations can be given by the temperature. All these adjustments can be carried out by the upstream supervisory controller, which changes the current set-point value incrementally to match the preset conditions. A soft start must be foreseen for the EV charger in order not to apply the full charging current in the scale of 600 A abruptly. The main reason for that is to avoid tripping of system protections.

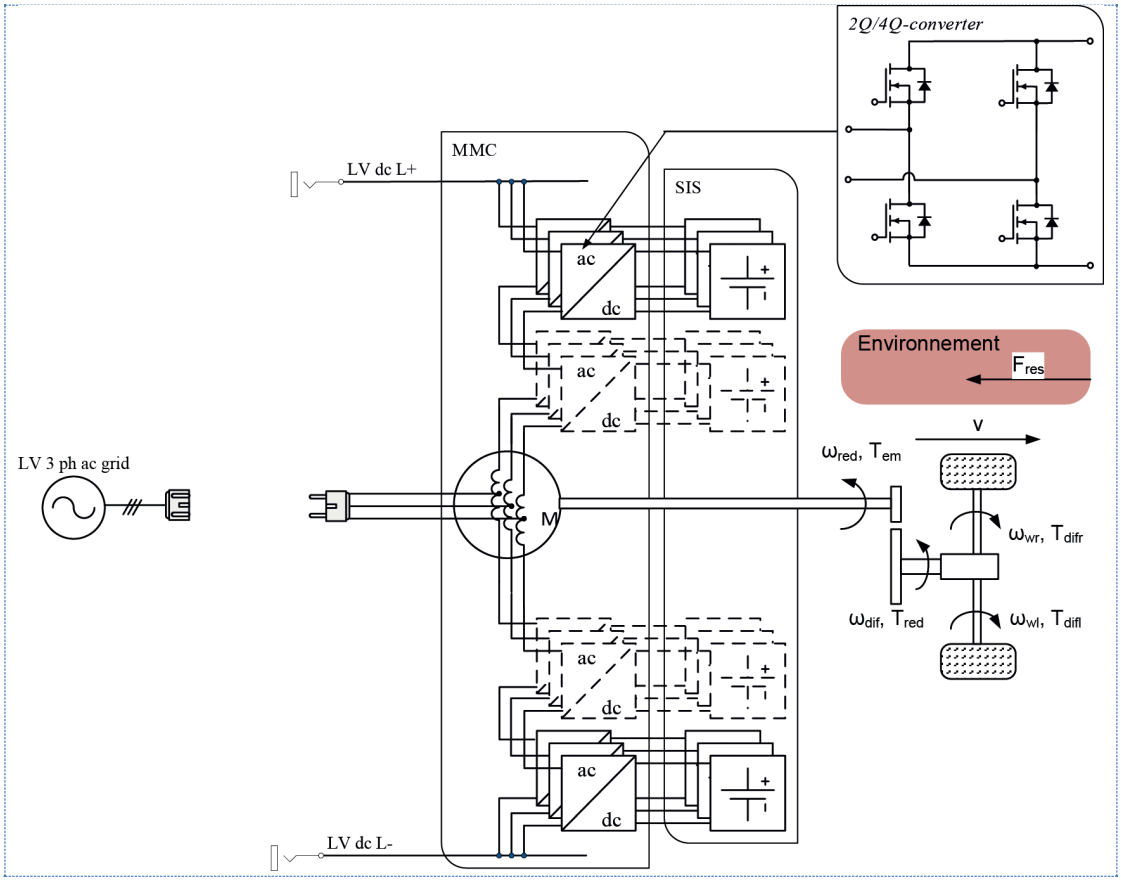

Figure 6.3: Flex-EV architecture

Figure 6.3 shows the Flex-EV architecture base on the configurable modular multilevel converter (CMMC). This topology is not only designed for electric vehicle traction system but also it is designed for enhancing bidirectional and flexible charging system which cannot be done with standard converter sufficiently. This allows the EV to participle sufficiently into the future smart grid system. In fact, this concept is based on integration of the motor subsystem and the battery management subsystem as well as the universal and flexible charging subsystem. The power conversion is based on Modular Multilevel Converter (MMC) with split integrated storage (SIS) based on battery modules.

6.1.3 The radical shift to green energy requires contributions from bidirectional and flexible EV charging system

The main challenge of the CMMC control can be summarized in two points:

1-In standard MMC, the AC load which is the grid is known because it is a fix installation, the voltage and the current can be therefore measured. The applied voltage from the MMC can be adjusted in somehow to control the current flow through the AC load impedance. However, in case of the CMMC, the AC load which is the charging station is unknown, the Flex-EV isn't a fix installation, the Flex-EV has to adapt with various charging stations. In addition the voltage and the current are not directly accessible, because there is not communication between the EV and the charging station. Therefore, the control system is not anymore the charging line cable impedance which is the outer AC load, the stator windings as arm inductances become the control system in case of the CMMC, which are an internal variable for the system basically.

2- During the driving mode, basically since the submodule is based on half-bridge, the phase voltage is not sinusoidal, means that the three phase line-to-ground branch voltage cannot perform a phasor because they are not sinusoidal. Therefore it is not possible to control the system in rotating synchronous frame base on the branch voltage. However, the upper and the lower arm voltages form a space phasors; it can be seen as double three phase system. This is the reason why the control is based on double inner-current control in rotating frame.

Even though the concept of CMMC is based on MMC topology, it has been shown that news approaches have been introduced in driving mode and in charge balance as well as in control.

The CMMC concept has been validated in charging mode and in driving mode; however the ancillary services operation such as active filtering is not included in this experimental validation. In addition, the single phase AC charging is not included in the experimental validation.

Of course, it is not possible to answer to all questions which may interest the reader in this thesis, because this top is very large and it is multi-disciplinary research, however, the key point has been highlighted and the basic has not been included in this thesis. For instance the basic of electric drive is not included.

6.2 The potentiality impacts of the Flex-EV on the EV market

The advantages of the Flex-EV in comparison to the standard EV architecture include:

- Universal and flexible EV charger: the EV owners benefits a large degree of freedom in term of compatibility with the available charging stations; the Flex-EV is compatible with a large range of charging stations, from standard household socket which is based on single phase AC to high power charging based on DC power supply
- Multifunctional converter: the CMMC it allows difference type of power conversion as depicted in the following table

Mode 4	Mode 1	Mode 2 , 3	Charging system
DC	1~AC	3~AC	Power conversion
0	0	0	DC/AC
0	0	1	DC/AC
0	1	0	AC/AC
0	1	1	AC/AC
1	0	0	DC/AC
1	0	1	DC/AC

Table 6.1: Merging charging converter from basic single phase AC to high power AC or DC ultra-fast charging, with the traction converter DC/AC for motor mode and AC/DC for generator mode

In this context a mechanical input is possible, meaning, it is possible to imagine in the future, to charge the EV battery through mechanical torque input. In fact the rotor can be turned by external motor which acts as charger, then the EV motor can acts as generator, thereby the EV traction converter can acts as charger in order to charge the embarked EV battery. The CMMC basic concept is still compatible with such application in the future.

- It uses the existing passive components of the electric vehicle: the stator windings are used as current filter in charging mode and the charger converter is used as traction converter in driving mode
- It splits the traditional battery packs into multilevel battery module: this allows dynamic balancing of the state of charge of the battery modules in the level of the modulation
- High redundancy: it becomes possible to operate the system under fault condition, in fact it is possible to bypass the faulted submodules and continue to operate the CMMC with the available healthy submodules
- Multilevel stator voltage: the generated output AC voltages are nearly sinusoidal waveform thanks to the multistage submodules

- Bidirectional and flexible charging: it is generally agreed that a lot have been written in literature about standard converter can do with bidirectional charging, however they are limited in terms of the flexibility of the converter. Therefore, the CMMC has shown a great potentiality to handle the bidirectional and flexible charging.
- Compact system: this Flex-EV concept is attended to compact the whole EV power module in mechatronics approach, by merging the multi-charger converters with the traction inverter and the battery management system
- Simple control system: the control is simple because it is based on standard three phase drive control
- Modular and scalability in terms of the design: it is possible to design and redesign a CMMC without requiring a lot change on the layout of PCB according to a specified power rating.

However, this EV architecture requires multi-disciplinary knowledge; this concept requires a large view of the whole system because there are strong relationships between the Flex-EV subsystems. For instance the design of the motor is not only depends on the required driving power but it has to take also account the current handling in charging mode.

Finally, this thesis which entitles “Contribution to the Ultra-Fast charging of Electric Vehicles- the Configurable Modular Multilevel Converter (CMMC)” gives a better insight of the electric vehicles environment. However, it is generally agreed that it is difficult to write a thesis which corresponds exactly to the expectation of the readers, since this CMMC convers a large topic. Even though, substantial progress is expected in the area of electric vehicles.

Chapter 7 Future work

«The difference between genius and stupidity is; genius has its limits»

Albert Einstein (1879-1955)

7.1 Prototyping of the Flex-EV

This chapter is dedicated to argue about the perspective of this research project. In this thesis, it has been shown that the even the CMMC requires an integration of many semiconductors, its potentiality regarding to the future EV market is extremely high. It is a convenient approach in order to answer to the technical needs of electric vehicles. However, it has been shown that even the CMMC functionality has been verified experimentally, its implementation remains an important concern for car manufacturers. Therefore, a new perspective is foreseen for improving the Flex-EV potentiality for EV market, this can be done by operating the CMMC motor at high frequency; this will reduce the electric motor energy consumption while producing the same torque output. However, this will require advanced power semiconductors devices.

7.1.1 Design of a high frequency traction motor

The integration of the electric vehicle in the mobility should respect the human behaviour. It is generally agreed that people like powerful and high speed car. This will require an increase of the fundamental frequency of the electric motor. This requires a new design of electric motor. However, this allows also designing an ultra-light weight, small volume, low losses, fault tolerance and an excellent dynamic motor behaviour. Today, in the most cases, the EV motor is design at 50, 60 or 400 Hz, which required bulky stator windings. Therefore, here the point is that, it is possible to design a motor at slightly high frequency like 0.5…1 kHz, at low input currents, thereby reducing the energy consumption of the motor, but at the same output torque in driving mode. This will reduce the energy consumption of the electric vehicle during the driving mode. However, the motor should be designed also for ultra-fast charging, which require high current capability handling. It should be noted that as frequency increases, the induced emf and hence current and torque in the rotor coil increase.

7.1.2 Flex-EV semiconductor devices

The design of the submodule becomes a great challenge where advanced semiconductors are necessary. In fact, it is well-know that low unipolar devices such Wide Band Gap (WBG) devices have extremely low switching and low conduction losses. This enables to realise an ultra-low loss CMMC submodule. Therefore the cooling equipment and the passive filters such as submodule capacitor will be reduced drastically, reducing weight. However; the main challenge is the Electromagnetic Interferences (EMI). Figure 7.1 illustrates architecture of the Flex-EV based on FET semiconductor devices instead of the MOSFET with antiparallel diode.

7.2 Modular High Frequency Submodules for Flex-EV

It is generally agreed that multilayer boards are well suitable for extremely low inductance design. In order to ensure good scalability, eliminate bulky bus bars and external tapped dc capacitors, it is very desirable to have a design, which is based on small configurable half/full bridge submodule with small tap dc-capacitor. The CMMC is therefore designed to be able to operate with very small capacitors (low pulsating energy in the split integrated battery). In this case, small ceramic chip capacitors (of high temperature operating capability) can be located close to the semiconductor chips. Apart from necessary high switching frequencies (fp >> 100kHz) this concept makes sense, solely, if parasitic oscillations between the switching submodules can be avoided and good current sharing can be achieved. Regarding the power chips themselves, new SMD packages without external leads or internal bond wires are very helpful for the new concept. [64].

7.2.1 Design of a high frequency submodule

It is a truly acknowledged that light weight is one of the main EV requirements; the passive components (tap-dc bus-capacitors, chokes, EMI-filters) have to be reduced drastically. In addition, the industrial scalability, safe fault behaviour and EMI limits are also important points. It is trivial that these requirements cannot be reached suitably with standard semiconductors devices.

Independent of the material, lower voltage semiconductors have the following, general advantages:
- The achievable, maximum operating temperatures are higher than those of high voltage devices.
- Converter losses are smaller than those associated with higher voltage FETs.
- Using low voltage FETs, it becomes feasible to discard the diodes, by turning on the gate controlled channels.
- For a given switching frequency and given switching losses, the stray inductance is lower, leading to reduce EMI. [64]–[66]
- Monolithic integration of power chips (together with gate drive, control electronics, measurement electronics) becomes feasible, because low voltage technologies fit together in semiconductor processing.

Therefore, it is possible to design CMMC with advanced semiconductor devices such as GaN HEMT based on low voltage FET. This allows designing a CMMC at high frequency with extremely low weight, low power loss and excellent dynamic control behaviour can be achieved. Moreover, low voltage FET-structures based on silicon or GaN has high potential for further improvements. Initially intended for low voltage devices up to 200V and multilevel converters, new SMD packages are extending the useful range of this concept to 600V devices, in future.

7.2.2 Flex-EV architecture based on High Frequency (HF) CMMC

In order to meet the EV requirements, a combination of new converter topologies such as Flex-EV and advanced semiconductors is necessary. In fact, low voltage wind band gap devices has extremely low switching and low conduction losses, it becomes possible to design an ultra-low loss CMMC. Cooling equipment and passive filters will be reduced drastically, reducing the weight. According to these trends a CMMC based on high frequency open-ended and tapped stator windings could be designed, while a configurable half/full bridge submodule could be designed with focus on low stray inductance, fast gate drive and good scalability is suitable for Flex-EV. This is depicted in the following Figure 7.1.

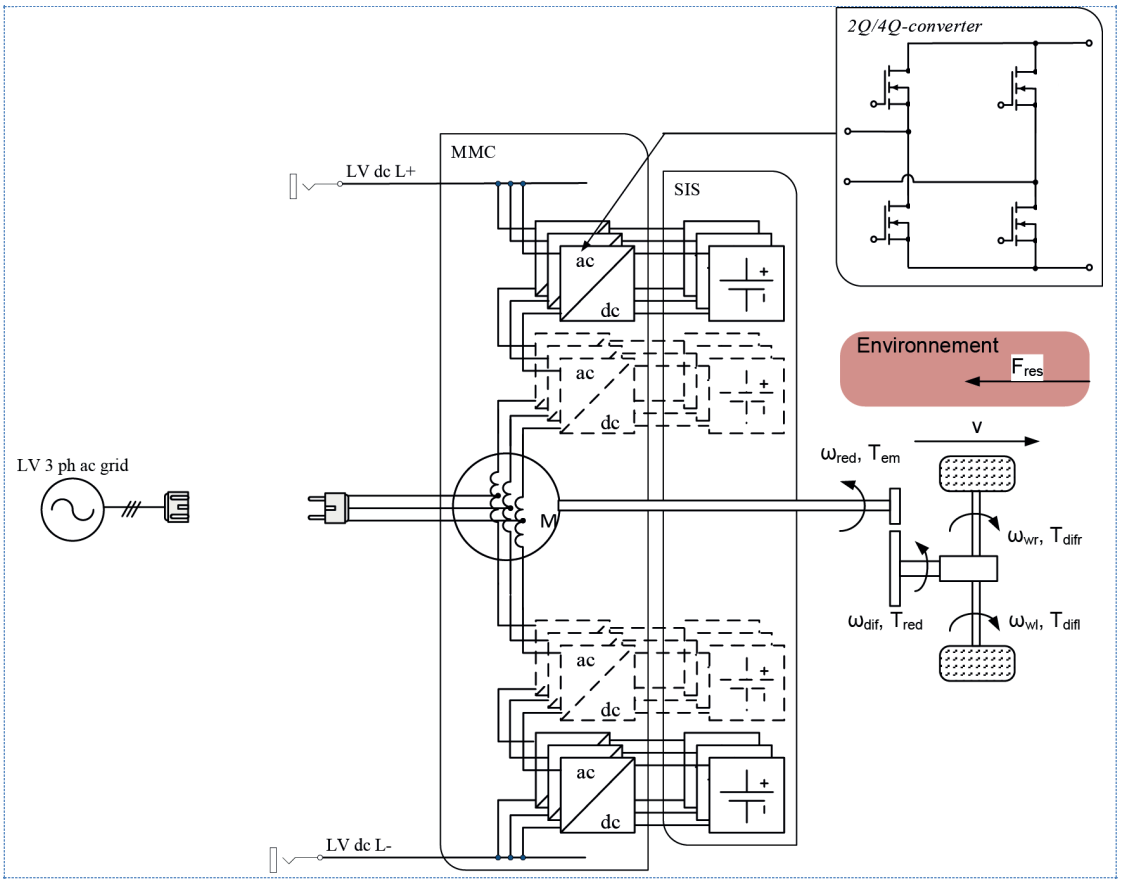

Figure 7.1: Flex-EV based on High Frequency (HF) CMMC

Figure 7.1 illustrates the architecture of the Flex-EV based on high frequency configurable modular multilevel converter. In fact, it uses high frequency submodules based on zero current switches (ZCS); the power semiconductors are always turned on actively and turned off passively (for load current zero). Accepting the low of one control possibility compared to hard switch (HS), active switch may be performed with far lower power losses thanks to sufficient series inductance. This makes it possible to achieve higher frequency than for hard switching. This allows increasing the efficiency of the CMMC submodules.

Appendix

A. UFCEV demonstrator

1. Technical specification of the system assembly for the ultrafast EV charging demonstrator

The UFCEV project is committed to the problems arising from the ultrafast (in the range of 5 min) charging of an electric vehicle (EV). In this context, the ultrafast charging station (UFCS) demonstrator consist of a high power output with minimal influence on the electricity transmission system, which can only be achieved by the application of energy storage acting as an additional buffer between the vehicle and the grid. Besides storage, interfaces between a fast charging station and the outside environment (vehicle, utility grid) are designed to fulfil a set of requirements (Figure 0.4).

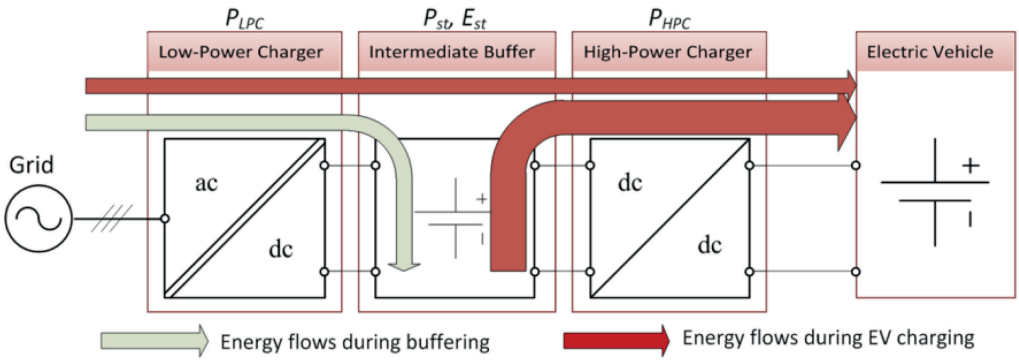

Figure 0.1: Decoupling an EV charging station from the grid by intermediate buffer

One of the main goals of the project consists in designing and building a transportable full scale demonstrator adapted for personal vehicles with a typical battery of 20-30 kWh. It aims to charge passenger cars of 16 kWh of battery in time frame of ten minutes and from a standard plug, while ensuring no discretion of the suppling power system.

The charging station is design for 200 electric vehicles per day according to the data traffic in Switzerland. The demonstrator has been realized; it serves to demonstrate the ultrafast recharging possibilities of an electric vehicle (EV) under limited grid connection conditions. A charging station concept with an intermediate DC-bus connected to a buffer battery has thus been thoroughly investigated and thereafter realized.

2. General description

This challenging task is done by complex assembling system. First of all, the AC grid is coupled to the trailer through EMPA installation. The grid plug is considered to be protected by an upstream

circuit breaker and a residual current circuit breaker. Then it goes to the interface board at +NE1, which was design by LEI-EPFL.

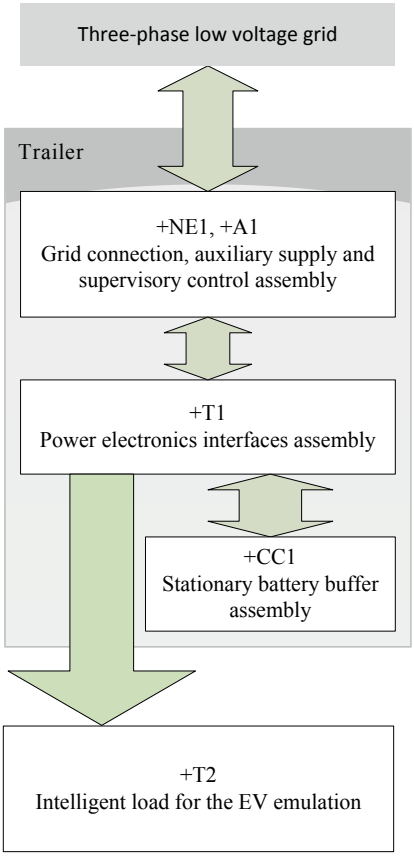

Figure 0.2: General architecture of the UFCEV demonstrator

Figure 0.2 gives a great picture of the architecture of the UFCEV demonstrator, in fact the system consist of:

+NE1: it is located in the rear side of the supervisory control (SPC) rack. It is composed of a switch-board, comprising main switch, current transformers for grid values measurement, a 24 V dc auxiliary supply unit buffered a 7.2 Ah lead-acide battery, circuit breakers for protecting the auxiliaries and the main contactor.
+A1: the supervisory control assembly comprises an industrial PC, the local input/output module and a touchscreen for man machine interface (MMI). It is also located in the same 19-inch rack with +NE1.
+T1: the power electronics interfaces assembly comprises the input ac/dc converter, the isolated low power dc/dc converter and the high power dc/dc charger converter. The dc contactors serve to isolate and connect the stationary buffer and the intelligent load emulating an electric vehicle, whereas the current and voltage transducers monitor the power flow.

+CC1: the stationary buffer, based on the lithium iron phosphate (LFP) batteries helps to decouple the high power load-the vehicle-from the limited source. The buffer is equipped with a battery management system (BMS) and separate charging/discharging contactors.

3. Schematic

The system assembly has been design by LEI-EPFL team with my contribution between 2011 to 2015. The following Figure 0.3 shows furthermore details about the cabling interconnection between the system subsystems.

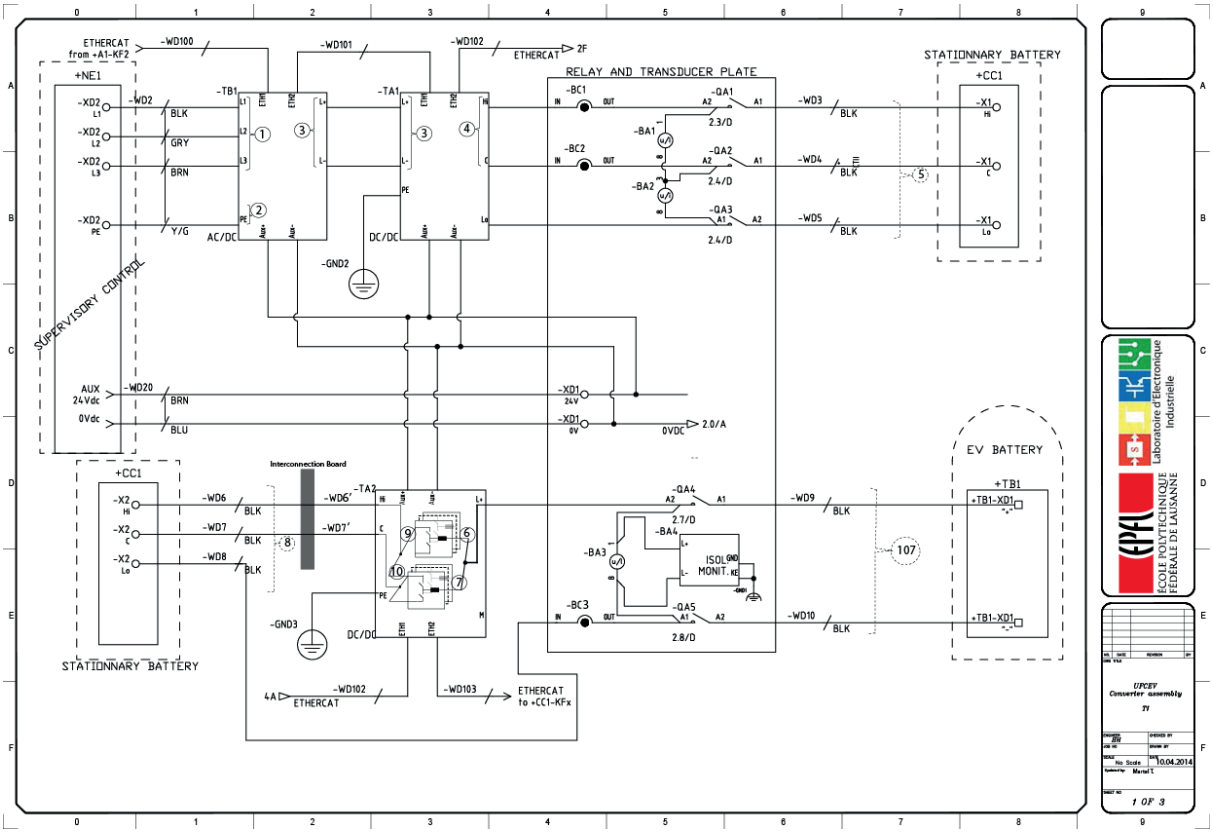

Figure 0.3: Cabling assembly of the UFCEV demonstrator

The Figure 0.3 shows the cabling interconnection for UFCEV demonstrator. This schematic can be read from left to right and it should be noted that the two stationary battery blocks represent the same intermediate battery connection. First, the -TB1 converter represents the ac/dc converter, which convert the low power ac (230V, 32A) to low power dc (800 V, 27.5 A). Then, the –TA1 converter represents the isolated dc/dc converter, controlling the power flows between the grid and the intermediate stationary buffer +CC1. This stationary battery with its inbuilt lower-level super-

vision system translating the CANopen-based status messages into a readable format for the upstream main converter. The +TA2 represents the high power dc/dc converter which control the power flows between the stationary battery +CC1 and the EV emulator. However, it should be noted that this isolated dc/dc converter is composed by two antiparallel cascaded dc/dc converter in order to interleaved the output high dc current, as depicted in Figure 0.3 .

Figure 0.4: Global view of the UFCEV demonstrator [*Source: UFCEV internal report*]

Figure 0.4 shows the global view of the UFCEV demonstrator, which now located at EMPA-Dübendorf, Switzerland. Upon common agreement of the members of the UFCEV consortium, the demonstrator becomes propriety of EMPA within the Future Mobility Fuel-Hub that is being built in Dübendorf, in close collaboration with PSI, (see http://nest.empa.ch/en/innovation/mobility-demonstrator/).

On the left side, the intermediate battery is shown, whereas on the right side, from top to bottom: the interconnection board system is seen, the picture is also shown on the next Figure 0.7. Then the AC/DC converter is seen, next the DC/DC isolated converter for charging the intermediate battery, and then, the high power charger is located on bottom. It is demonstrated that the power converters have very high specific power and very high power density.

The converter has been designed by the team of Prof. Biela in Laboratory for High Power Electronic Systems, ETH Zurich [67], [68], [69]. Furthermore, the cabling can be also classified according the type of connection:

- Low power connections
- High power connections
- Ctrl. Connection

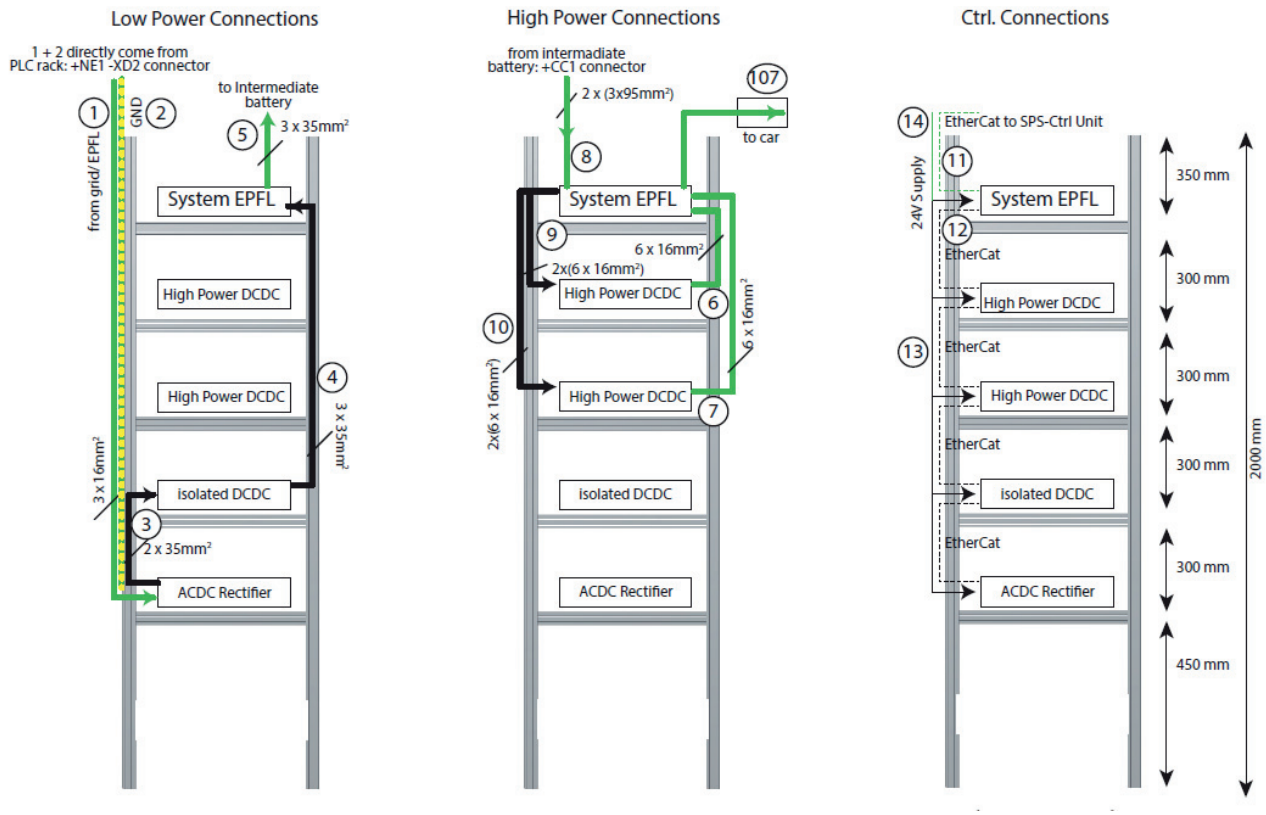

Figure 0.5: Converters rack

However, my contributions in this UFCEV demonstrator are mainly on the supervisory control and interconnection board between the system subsystems, it can be seen in:

Interconnection board

The measured values are captured by external transducers in the interconnection board, depicted on Figure 0.6.

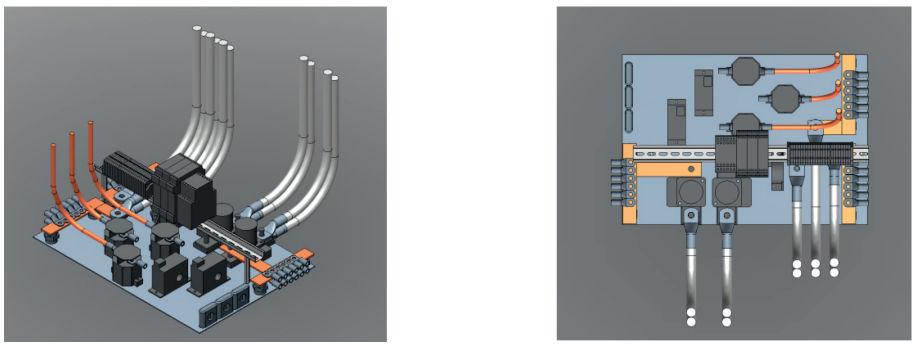

Figure 0.6: Perspective view (left) and top view (right) of the interconnection board drawing

In order to ensure better resistance to interferences, the standardised current signal from 4 mA to 20 mA is selected for transmission; this also eliminates the need for shielded cables.

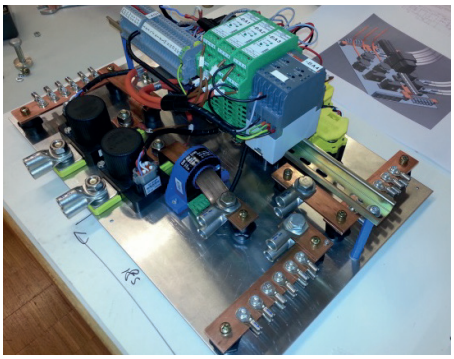

Figure 0.7: UFCEV demonstrator interconnection, design by Martel Tsirinomeny

Supervisory control system

From the man-machine interface (MMI) side the user inputs are either analogue (e.g. setpoints) or digital (binary commands on/off, system start/stop and reset after fault). The outputs from the SCADA to user can as well be digital (pilot lights and visual symbols indicating system state) or analogue (gauges). The control algorithms run in an industrial PC with stock operating system.

Figure 0.8: The supervisory control for the UFCEV demonstrator

Figure 0.8 shows the supervisory control for the UFCEV demonstrator with is based on Beckhoff automation system. All SCADA components are fed by a 24 V DC auxiliary supply. Besides control-

ling the charging parameters, the SCADA can easily be adjusted in software to perform other actions, like container ventilation and driving cooling fans in the stationary battery assembly. The PLC programming is based on the IEC 61131-3 standard.

The SCADA hardware used in the demonstrator has the following main characteristics:

1. Industrial PC type C6915-0000 with 1.6 GHz CPU Intel Atom, 2 GB RAM, 4 GB Compact Flash memory, operating system Microsoft Windows Embedded Standard 2009.
2. Three-phase grid values measurement module EL3403-0010, current measurements over x/5 A transformers.
3. Three 8-channel digital input modules EL1018.
4. Two 8-channel analog input modules EL3058 for current signals from 4 mA to 20 mA.
5. Two 8-channel digital output modules EL2008.
6. Two EtherCAT Bridge Terminal EL6692
7. CAN master terminal.
8. 12-inch touchscreen CP6901-0001-0000 for man-machine interaction.

The input/output modules are connected to the industrial PC coupling units using EtherCAT protocol in a daisy chain topology. Additional inputs and outputs can be connected remotely over the EtherCAT data bus as slaves.

B. CMMC coupling demonstration

This paragraph is dedicated to highlight the intrinsic coupling in the CMMC. This can be done by modelling the CMMC in the frequency domain because it is simpler in comparison to the time domain modelling, and since the main goal is just to emphasis the coupling parameter in the system.

It is well-known that modelling is a mathematical description of a studied system. However, modelling a complete mechatronic system is always complex, therefore since the phenomena is the same among the three phases of the CMMC, only one phase is considered among the three phases. An equivalent electric circuit model is chosen over the existing MMC approach in literature because it gives the best trade-off between a functional and a structural model [58]. It allows to easily assessing the energy balance of the whole powertrain / power charge. Moreover, the connected grid network is considered as part of the system instead of considering it as a disturbance, which allows to increase the dynamic performance of the designed controller. Furthermore, the charging cable is included in the system model because in high power charging, the electromagnetic compatibility (EMC) problem becomes significant. Similarly, the motor air-gap is also included in the system model because the motor is not coupled and the upper- and lower arms voltage are dependent voltage sources. In fact, Figure 0.9 is an electrical circuit model of the controlled system in the Laplace domain.

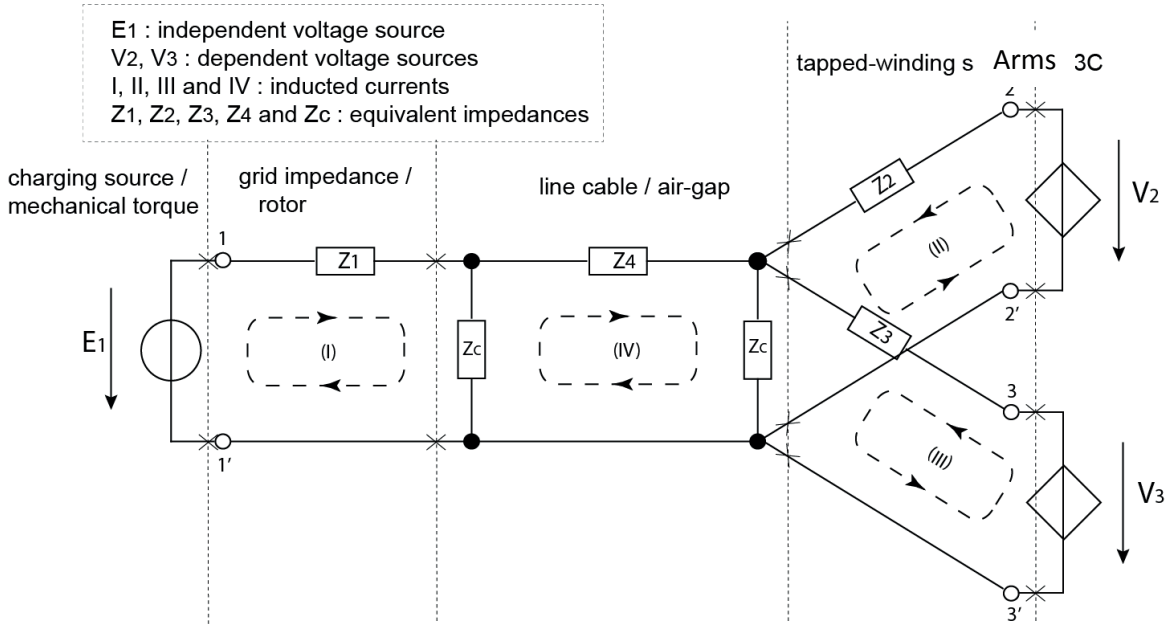

Figure 0.9: Model of the controlled system in Laplace domain

From right to left, the dependent voltage sources $V_2$and V_3 represent respectively the upper- and lower-arm of the CMMC which are the two controllable voltage source of the system, previously called upper- and lower- arm voltage. The stator impedance is represented by the impedance Z_2 and Z_3. Particular attention is paid to the charging cable because the common mode current and differential mode voltage become non negligible in high power charging. This conducts an additional internal current; meaning a zero common mode voltage is not guaranteed. Thereafter, by considering a well-shielded coaxial cable, a π transmission line model is implemented, therefore, the impedance could be reduced to $Z_C = 2C$ which is the floating capacitance of the coaxial cable. Similarly, during traction mode, the π transmission line model is kept in order to model the motor air-gap. After, the charging infrastructure impedance and the squirrel cage rotor model are modelled by impedance Z_1, which can be defined by a short circuit test of the motor. Finally, the charging source and the electromagnetic torque are modelled by an independent voltage source. Load torque and charging current imperfections are considered as disturbance. Therefore the studied system model can be represented as multipoles network which has four nodes and four meshes. Therefore by resolving the Kirchhoff's law, it is deducted:

$$\begin{pmatrix} \overline{E_{10}} \\ \overline{V_{11}} \\ \overline{V_{12}} \\ 0 \end{pmatrix} = \begin{pmatrix} \overline{Z_{10}} + \overline{Z_{C1}} & 0 & 0 & -\overline{Z_{C1}} \\ 0 & \overline{Z_{11}} + \overline{Z_{C1}} & \overline{Z_{C1}} & \overline{Z_{C1}} \\ 0 & \overline{Z_{C1}} & \overline{Z_{12}} + \overline{Z_{C1}} & \overline{Z_{C1}} \\ -\overline{Z_{C1}} & \overline{Z_{C1}} & \overline{Z_{C1}} & \overline{Z_{01}} + \overline{Z_{C1}}/2 \end{pmatrix} \begin{pmatrix} \overline{I_{10}} \\ \overline{I_{11}} \\ \overline{I_{12}} \\ \overline{I_{01}} \end{pmatrix} \quad (0.1)$$

In fact, the independence of the internal currents $\mathrm{I}_1, \mathrm{I}_2, \mathrm{I}_3,$ and I_4 are the necessary condition for the existence of the impedance matrix $\mathrm{Z(s)}$. In literature, there are divergent notations between common mode and differential mode current. Therefore in this paper the current I_4 represents the current which flows through the neutral, however, the system is partitioned in way to cancel out this neutral current. This is the reason why the impedance matrix is a symmetrical matrix ($\mathrm{Z^T} = \mathrm{Z}$). In blocs, the system can be written as:

$$\begin{pmatrix} \overline{E_A} \\ 0 \end{pmatrix} = \begin{pmatrix} \overline{Z_{AA}} & \overline{Z_{AB}} \\ \overline{Z_{BA}} & \overline{Z_{BB}} \end{pmatrix} \begin{pmatrix} \overline{I_A} \\ \overline{I_B} \end{pmatrix} \quad (0.2)$$

where $\mathrm{E_A}$ and $\mathrm{I_A}$ are respectively the controllable voltage and current vectors. Therefore, the admittance matrix $\mathrm{Y(s)}$ of the system can be deduced by the following equation:

$$\begin{pmatrix} \overline{I_A} \\ 0 \end{pmatrix} = \begin{pmatrix} \overline{Y_{AA}} & \overline{Y_{AB}} \\ \overline{Y_{BA}} & \overline{Y_{BB}} \end{pmatrix} \begin{pmatrix} \overline{E_A} \\ \overline{E_B} \end{pmatrix} \tag{0.3}$$

where E_B is the common mode voltage of the system. The admittances Y_{AA},Y_{AB}, Y_{BA} and Y_{BB} are respectively the inverse of: Z_{AA}, Z_{AB}, Z_{BA} and Z_{BB}. Thereafter, this impedance matrix represents also the transfer function of the system. The transfer function can be written as:

$$\begin{aligned} \overline{I_A} &= \overline{Y_{AA}} \cdot \overline{E_A} + \overline{Y_{AB}} \cdot \overline{E_B} \\ 0 &= \overline{Y_{BA}} \cdot \overline{E_A} + \overline{Y_{BB}} \cdot \overline{E_B} \end{aligned} \tag{0.4}$$

It should be note that 0 corresponds to the neutral vector

Then the relation between the input voltages and the generated arm current is clearly portrayed by the block diagram in Figure 0.10. This diagram is utterly important to illustrate the cause-and-effect relationship by facility to represent the relationship of the variables by diagrammatic means.

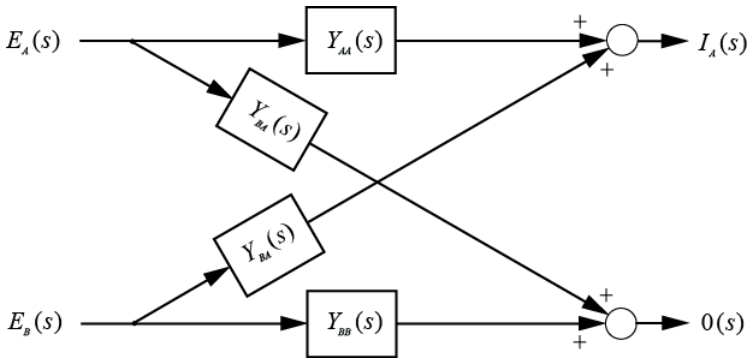

Figure 0.10: Block diagram of the controlled system

In conclusion, the CMMC cannot be reduced to like a three phase system because the circulating current or the common mode voltage is intrinsic of the system but it is not a perturbation; therefore it is optimum to include this variable in the model of the system. This makes the difference in comparison to the most approaches in the literature. Therefore, the CMMC is considered as double star three phase system with virtual neutral current which is the circulating current.

C. Parameter identification

Basically, the controlled system is the induction machine, therefore its parameters has to be defined properly. Standard test has been carried out in order to gather the parameters of an equivalent scheme of the induction machine.

Test at no load:

R_s = 2.1 Ohms // stator resistance

U_0 = 220 V // line to line stator voltage

I_0 = 4.80 A // stator line current

P_0 = 310 W // active power

S_0 = 1.83 KVA // apparent power

Q_0=1.8 KVar // reactive power

$\cos\varphi_0$ = 0.17 // power factor

Short circuit test:

$I_{sc}=I_n$= 8.8 A // nominal stator line current

U_{sc} = 53.8 V // short circuit voltage

P_{sc}=530 W // short circuit active power

S_{sc}= 840 VA // short circuit apparent power

Q_{sc}= 650 Var // short circuit reactive power

$\cos\varphi_{sc}$ =0.63 // short circuit power factor

$$P_{sc} = 3.R_{sc}.I_{sc}^2 = 3(Rs + R_r').I_{sc}^2$$

Therefore, $R_{sc} = \frac{P_{sc}}{3.I_{sc}^2} = \frac{530}{3.(8.8)^2} = 2.28\ Ohms$

R_{sc} = 2.28 Ohms // short circuit power factor

Hence $R_r'= R_{sc} - R_s$= 2.28-2.1 = 1.18 Ohms // the rotor resistance, viewed from the stator side

Afterward, the other parameters of the induction can be computed easily.

Bibliography

[1] "Automobile: Emissions de CO2 supérieures de 40% aux chiffres officiels - Économie - 24heures.ch." [Online]. Available: http://www.24heures.ch/economie/Emissions-de-CO2-superieures-de-40-aux-chiffres-officiels/story/27831665. [Accessed: 26-Feb-2016].

[2] J. Bartos and E. P. Division, "Emergency response – IEA raison d ' être," no. April, 2014.

[3] "Volkswagen Schweiz." [Online]. Available: http://www.volkswagen.ch/de.html. [Accessed: 17-Feb-2015].

[4] "Renault ZOE – Mode d'emploi." [Online]. Available: http://zoe.renault.fr/mode_demploi. [Accessed: 17-Feb-2015].

[5] "A propos | www.observatoire-vehicule-entreprise.info." [Online]. Available: http://www.observatoire-vehicule-entreprise.com/. [Accessed: 16-Feb-2015].

[6] M. Kamachi, H. Miyamoto, and Y. Sano, "Development of power management system for electric vehicle 'i-MiEV,'" *2010 Int. Power Electron. Conf. - ECCE ASIA -*, pp. 2949–2955, 2010.

[7] G. Dinger, Andreas; Martin, Ripley; Mosquet, Xavier; Rabl, Maximilian; Rizoulis, Dimitrios; Russo, Massimo, Sticher, "Focus Batteries for Electric Cars," p. 18, 2010.

[8] "Altairnano." [Online]. Available: http://www.altairnano.com/. [Accessed: 16-Feb-2015].

[9] M. Tsirinomeny, H. Hõimoja, A. Rufer, G. Dziechciaruk, A. Vezzini, M. Tsirinomeny, A. Vezzini, H. Himoja, and A. Rufer, "Optimizing EV driving-recharge time ratio a under limited grid connection," *7th IET Int. Conf. Power Electron. Mach. Drives (PEMD 2014)*, pp. 1–6, 2014.

[10] "Statistique Suisse, Domaine 11 - Mobilité et transports, Comptage suisse automatique de la circulation routière." [Online]. Available: http://www.portal-stat.admin.ch/sasvz/files/fr/00.xml. [Accessed: 17-Feb-2015].

[11] S. Bai, Y. Du, and S. Lukic, "Optimum design of an EV/PHEV charging station with DC bus and storage system," *2010 IEEE Energy Convers. Congr. Expo. ECCE 2010 - Proc.*, pp. 1178–1184, 2010.

[12] K. Yunus, H. Z. D. La Parra, and M. Reza, "Distribution grid impact of Plug-In Electric Vehicles charging at fast charging stations using stochastic charging model," *Proc. 2011 14th Eur. Conf. Power Electron. Appl.*, pp. 1–11, 2011.

[13] H. Hõimoja, M. Vasiladiotis, S. Grioni, M. Capezzali, A. Rufer, and H. B. Püttgen, "Toward Ultrafast Charging of Electric Vehicles," in *2012 CIGRE Session, Paris, France, August 26-31, 2012*.

[14] "Buy IEC 61851-1 ed2.0 - Electric vehicle conductive charging system - Part 1: General requirements | IEC Webstore | Publication Abstract, Preview, Scope." [Online]. Available: http://webstore.iec.ch/webstore/webstore.nsf/artnum/044636!opendocument. [Accessed: 19-Feb-2015].

[15] H. Hõimoja and A. Rufer, "Infrastructure Issues Regarding the Ultrafast Charging of Electric

Vehicles," in *IAMF 2012 : International Advanced Mobility Forum, Geneva,* 2012.

[16] "CHAdeMO Association." [Online]. Available: http://www.chademo.com/. [Accessed: 19-Feb-2015].

[17] H. Hõimoja, M. Vasiladiotis, and A. Rufer, "Power interfaces and storage selection for an ultrafast EV charging station," in *Power Electronics, Machines and Drives, University of Bristol, UK, 27 - 29 March 2012*, 2012.

[18] R. M. D. Tsirinomeny, H. Hõimoja, and A. Rufer, "Ultrafast Charging Compatibility of Electric Vehicles," *IAMF 2012 Int. Adv. Mobil. Forum, Geneva, Switzerland, March 7-8, 2012*, 2012.

[19] S. Delalay, "Étude systémique pour l'alimentation hybride – application aux systèmes intermittents," Thesis EPFL N° 5768, 2013.

[20] M. Vasiladiotis, "Modular Multilevel Converters with Integrated Split Battery Energy Storage," Thesis EPFL, 2014.

[21] A. Rufer, S. Lemofouet, M. Habisreutinger, M. Heidari, and A. Leuba, "Driving and Filling Personal Vehicles – The Questions of Energy - and Power - Density (A Fast Filling Station for the Compressed Air Car)."

[22] M. Vasiladiotis and A. Rufer, "Balancing control actions for cascaded H-bridge converters with integrated battery energy storage," *2013 15th Eur. Conf. Power Electron. Appl. EPE 2013*, pp. 1–10, 2013.

[23] M. Vasiladiotis, S. Member, and A. Rufer, "Transformer With Integrated Split Battery Energy Storage for Versatile Ultrafast EV Charging Stations," vol. 62, no. 5, pp. 3213–3222, 2015.

[24] M. Multilevel, C. Converter, and H. Akagi, "Classification, Terminology, and Application of the Modular Multilevel Cascade Converter (MMCC)," *IEEE Trans. Power Electron.*, vol. 26, no. 11, pp. 3119–3130, Nov. 2011.

[25] A. Lesnicar and R. Marquardt, "A new modular voltage source inverter topology Universität der Bundeswehr München Keywords Concept of the new Modular Multi Level Converter M 2 LC Principle of M 2 LC," pp. 1–10, 2003.

[26] R. Marquardt, "Modular Multilevel Converter: An universal concept for HVDC-Networks and extended DC-Bus-applications," *IPEC 2010 - Sapporo*, 2010.

[27] R. Marquardt and A. Lesnicar, "New Concept for High Voltage – Modular Multilevel Converter," *PESC 2004 - Aachen*, 2004.

[28] M. Hagiwara, R. Maeda, and H. Akagi, "Negative-Sequence Reactive-Power Control by the Modular Multilevel Cascade Converter Based on Double-Star Chopper-Cells (MMCC-DSCC)," *IPEC 2010 - Sapporo*, 2010.

[29] H. Akagi and R. Kitada, "Control and Design of a Modular Multilevel Cascade BTB System Using Bidirectional Isolated DC/DC Converters," *IEEE Trans. Power Electron.*, vol. 26, no. 9, pp. 2457–2464, Sep. 2011.

[30] A. S. L. olivier. auge@ch. abb. co. Global Product Manager, "Keynotes | epe2015 : TOSA concept: a full electric large capacity urban bus system." 2015.

[31] M. Anderman, “xEV Battery Technology and Market Presentation Outline Energy-Storage Solutions for xEV Battery Market,” in *Advanced Automotive Battery Conference*, 2014.

[32] L. Lorenz, “Key Technology Driver for Power Device Development: High Power Density System Design & Devices High Efficient Power Converters „ High Rug,” in *ECPE Workshop Power Electronics for charging Electric Vehicles Power Semiconductors for charging Electric Vehicles, ECPE Workshop Power Electronics for charging Electric Vehicles Power Semiconductors for charging Electric Vehicles*.

[33] P. Van Den Bossche, “Connector Standards for the Connection to the Car: Overview on International Standards,” in *ECPE Workshop, Valencia*, 2011, pp. 1–37.

[34] N. Butcher, “ABB Power Electronics moves to deliver DC Fast Charge Station,” *Electric Vehicle Infrastructure: ABB Power Electronics moves to deliver advanced offboard vehicle charging solution. High power for rapid recharging, enabling long distance travel and eliminating range anxiety*, 2011.

[35] H. Hoimoja, A. Rufer, G. Dziechciaruk, and A. Vezzini, “An ultrafast EV charging station demonstrator,” in *International Symposium on Power Electronics Power Electronics, Electrical Drives, Automation and Motion*, 2012, pp. 1390–1395.

[36] T. Christen and M. W. Carlen, “Theory of ragone plots,” *J. Power Sources*, vol. 91, no. 2, pp. 210–216, 2000.

[37] Akagi, “Classification, Terminology, and Application of the Modular Multilevel Cascade Converter (MMCC),” *IPEC 2010 - Sapporo*, 2010.

[38] A. Tsirinomeny, Rosa Martel Danoary; Hõimoja, Hardi; Rufer, “ULTRAFAST CHARGING COMPATIBILITY OF ELECTRIC VEHICLES,” in *IAMF 2012 : International Advanced Mobility Forum, Geneva, Switzerland, March 7-8, 2012*, 2012.

[39] A. Bouscayrol, P. Delarue, W. Lhomme, and B. Lemaire-semail, “Teaching drive control using Energetic Macroscopic Representation – From maximal to practical control schemes Keywords 2 . EMR of the studied traction system,” in *14th European Conference on Power Electronics and Applications (EPE 2011),* pp. 1 – 6.

[40] C. Saber, D. Labrousse, B. Revol, and A. Gascher, “Achieving Unity Power Factor with a Unidirectional Single- Phase Four Reverse Blocking IGBTs Buck Type Rectifier,” *PCIM Europe 2015; International Exhibition and Conference for Power Electronics, Intelligent Motion, Renewable Energy and Energy Management; Proceedings of*. pp. 1–8, 2015.

[41] C. Saber, D. Labrousse, B. Revol, and A. Gascher, “Challenges Facing PFC of a Single-phase On-board Charger for Electric Vehicles based on a Current Source Active Rectifier Input Stage,” *IEEE Trans. Power Electron.*, vol. PP, no. 99, pp. 1–1, 2015.

[42] M. Hartmann, T. Friedli, and J. Kolar, “Three-phase unity power factor mains interfaces of high power EV battery charging systems,” in *ECPE – Workshop Power Electronics for Charging Electric Vehicles 21 – 22 March 2011 Valencia, Spain*, 2011, pp. 1–66.

[43] S. Zeltner, “Actual and Advanced Converter Technologies for On-Board Chargers,” in *ECPE –*

Workshop Power Electronics for Charging Electric Vehicles 21 – 22 March 2011 Valencia, Spain, 2011, no. March, pp. 1–26.

[44] N. Sakr, D. Sadarnac, and A. Gascher, "A review of on-board integrated chargers for electric vehicles," *Power Electron. Appl. (EPE'14-ECCE Eur. 2014 16th Eur. Conf. Date Conf. Page(s)1 - 10*, pp. 1–10.

[45] W. Lhomme, P. Delarue, X. Kestelyn, P. Sandulescu, and a. Bruyere, "Control of a combined multiphase electric drive and battery charger for electric vehicle," *2013 15th Eur. Conf. Power Electron. Appl. EPE 2013*, pp. 1–10, 2013.

[46] T. Martel and A. Rufer, "Electric vehicle driving and fast charging system based on configurable modular multilevel converter (CMMC)," in *2013 15th European Conference on Power Electronics and Applications (EPE)*, Sep-2013, pp. 1–10.

[47] M. Daowd, N. Omar, P. Van Den Bossche, and J. Van Mierlo, "Passive and active battery balancing comparison based on MATLAB simulation," in *2011 IEEE Vehicle Power and Propulsion Conference*, 2011, pp. 1–7.

[48] L. Reyes-Chamorro, A. Bernstein, J.-Y. Le Boudec, and M. Paolone, "A composable method for real-time control of active distribution networks with explicit power setpoints. Part II: Implementation and validation," *Electr. Power Syst. Res.*, vol. 125, pp. 265–280, 2015.

[49] R. M. Baker, "Electrical Apparatus," no. 3909685. 1975.

[50] R. Marquardt, A. Lesnicar, and J. Hildinger, "Modulares Stromrichterkonzept fuer Netzkupplungsanwendungen bei hohen Spannungen," *ETG-Conference*, 2002.

[51] M. Tsirinomeny and A. Rufer, "Configurable Modular Multilevel Converter (CMMC) for a universal and flexible integrated charging system," in *PCIM Europe 2015; International Exhibition and Conference for Power Electronics, Intelligent Motion, Renewable Energy and Energy Management; Proceedings of*, 2014, pp. 1–8.

[52] B. Bahrani, S. Kenzelmann, and A. Rufer, "Multivariable-PI-Based dq Current Control of Voltage Source Converters With Superior Axis," *Ieee Trans. Ind. Electron.*, vol. 58, no. 7, pp. 3016–3026, 2011.

[53] M. Zhang, L. Huang, W. Yao, Z. Lu, and S. Member, "Circulating Harmonic Current Elimination of a CPS-PWM-Based Modular Multilevel Converter With a Plug-In Repetitive Controller," *IEEE Trans. Power Electron.*, vol. 29, no. 4, pp. 2083–2097, Apr. 2014.

[54] N. Schibli, "Symmetrical multilevel converters with two quadrant DC-DC feeding," Thesis EPFL, 2000.

[55] J. Song Manguelle, "Convertisseurs multiniveaux asymétriques alimentés par transformateurs multi-secondaires basse-fréquence," 2004.

[56] D. Siemaszko, A. Antonopoulos, K. Ilves, M. Vasiladiotis, L. Angquist, and H.-P. Nee, "Evaluation of Control and Modulation Methods for Modular Multilevel Converters," *IPEC 2010 - Sapporo*, 2010.

[57] S. Kenzelmann, "Modular DC / DC Converter for DC Distribution and Collection Networks," EPFL Thesis, N°5430, 2012.

[58] N. Cherix, “Functional Description and Control Design of Modular Multilevel Converters - Towards Energy Storage Applications for Traction Networks,” EPFL Thesis N°6479, 2015.

[59] J. Song Manguelle, “Convertisseurs Multiniveaux Asymétriques Alimentés Par Transformateurs Multi-Secondaires Réactions Au Réseau D ’ Alimentation,” EPFL Thesis N°3033, 2004.

[60] C. Fahrni, “Principe d ’ alimentation par convertisseurs multiniveaux à stockage intégré - Application aux accélérateurs de particules,” EPFL Thesis N°4034, 2008.

[61] L. Angquist, A. Antonopoulos, D. Siemaszko, K. Ilves, M. Vasiladiotis, and H.-P. Nee, “Inner Control of Modular Multilevel Converters - An Approach using Open-loop Estimation of Stored Energy,” *IPEC 2010 - Sapporo*, 2010.

[62] M. Vasiladiotis, N. Cherix, and A. Rufer, “Accurate Capacitor Voltage Ripple Estimation and Current Control Considerations for Grid-Connected Modular Multilevel Converters,” *IEEE Trans. Power Electron.*, vol. PP, no. 99, pp. 1–1, 2013.

[63] J. von Bloh and R. W. De Doncker, “Design rules for diode-clamped multilevel inverters used in medium-voltage applications,” *Power Electron. Congr. 2002. Tech. Proceedings. CIEP 2002. VIII IEEE Int.*, pp. 165–170, 2002.

[64] M. Schulz, L. Lambertz, and R. Marquardt, “Dimensioning of Modular High Frequency converter for drives,” *2013 IEEE ECCE Asia Downunder - 5th IEEE Annu. Int. Energy Convers. Congr. Exhib. IEEE ECCE Asia 2013*, pp. 675–680, 2013.

[65] M. Schulz, “Scalable high frequency converters for motor drives based on switching cells,” *Integr. Power Syst. (…*, vol. 1, pp. 25–27, 2014.

[66] L. Lambertz, R. Marquardt, and A. Mayer, “Modular converter systems for vehicle applications,” *2010 Emobility - Electr. Power Train, EEPT 2010*, 2010.

[67] D. Christen, S. Tschannen, and J. Biela, “Highly efficient and compact DC-DC converter for ultra-fast charging of electric vehicles,” *15th Int. Power Electron. Motion Control Conf. Expo. EPE-PEMC 2012 ECCE Eur.*, pp. 1–8, 2012.

[68] F. Jauch and J. Biela, “Single-phase single-stage bidirectional isolated ZVS AC-DC converter with PFC,” *15th Int. Power Electron. Motion Control Conf. Expo. EPE-PEMC 2012 ECCE Eur.*, pp. 1–8, 2012.

[69] F. Jauch and J. Biela, “Generalized Modeling and Optimization of a Bidirectional Dual Active Bridge DC-DC Converter including Frequency Variation,” pp. 1788–1795, 2014.

Curriculum Vitae

CONTACT INFORMATION

○ Name	Tsirinomeny
○ First name	Martel Danoary
○ Nationality	Malagasy (Madagascar)
○ Date of birth	20th December 1984
○ Address	Rue de l'Ale 1, 1003 Lausanne, Switzerland
E-mail	martel.tsirinomeny@epfl.ch
Web	http://personnes.epfl.ch/martel.tsirinomeny
	http://ufcev.epfl.ch/partners

PhD research

"Contribution to the Ultra-Fast Charging of Electric Vehicles -The configurable Modular Multilevel Converter (CMMC)", École Polytechnique Fédérale de Lausanne (EPFL).

Group research

"Ultra-Fast Charging of Electric Vehicle (UFCEV)", (The Partner : EPF-Lausanne, ETH-Zürich, BFH-TI, EMPA-Dübendorf, Peugeot-Citroën PSA, Leclanché S.A., ESORO A.G.).

University education

Feb. 2005 – May 2010: School of Engineering at École Supérieure Polytechnique d'Antsiranana (ESPA) Madagascar for Diploma (eq. to Master).
Sept 2009 – May. 2010: Diploma thesis at ESPA on "Model Based System Design (MBSD) of Hybrid Electric Vehicle (HEV)".
Jan 2011: Short time Internship at Industrial Electronics laboratory (LEI). EPFL Lausanne, Switzerland.

- Simulation of an ultrafast charging station for EV.
- Presentation of Model Based System Design approach for HEV.

Contribution into the Ultra-Fast Charging of Electric Vehicle (UFCEV) project:

May 2011 – Jun. 2015: researcher assistant for the UFCEV project, from EPFL group.

- Study of the impact of a UFCEV system on local distribution systems: update of an existing system and green-field design, with specific attention to high short duration power peaks.
- Detailed assessment of various energy storage technologies, both intermediate buffer and embarked in EVs, including their applicability and interface issues.
- Modelling and optimization of power electronics converter architectures with the aim of achieving outstanding high efficiency of the converter systems for the fast charging station.
- Design of the system assembly of the ultra-fast charging station for validating the concept.
- Commissioning of the automation control unit (PLC control Beckhoff\ TwinCAT 2 and 3)
- Design and implementation of the interconnection board between the UFCEV subassemblies.
- Mechanical and electrical drawing of the UFCEV system assembly (tools: AutoCAD-Electrical, Autodesk-Inventor, SOLIDWORKS, etc.).
- Study analysis of a high-cycle efficient and high-discharge rate energy storage system for the load-levelling at the ultra-fast charging station, (lithium battery technology, flywheel, supercapacitors, compressing air).
- May. 2014 – Jun. 2015: Part time engineer visitor at EMPA Dübendorf, for the commissioning of the UFCEV demonstrator; validating the ultra-fast charging capability (Battery charging current up to 600 A) and the grid integration.

PhD works: "Configurable Modular Multilevel Converter (CMMC)":

May 2012. – Nov. 2015: PhD research project at LEI-EPF-Lausanne.

- On-board and off-board EV converters characterization.
- Analyses and measurements of advanced cells batteries for EVs.
- Investigation on suitable semiconductors for the CMMC.
- Modelling and specification of a down-scale laboratory prototype dedicated to the CMMC (Tools: Simulink, Gecko, PLECS).
- Refurbish study analysis of a six phases induction machine for CMMC.
- Construction of power modules for the CMMC (tools: Altium designer, Autodesk inventor).
- Construction of control platform for the CMMC prototype.
- Construction of measurement board for the CMMC.
- Update MMC software for the CMMC (TI\code composer).
- Assessment of various strategies for controlling the CMMC.
- Validation of the CMMC concept.
- Ancillary services application for the CMMC.

SKILLS:

- Automation technology: industrial schematic design, PLC control (Beckhoff TwinCat)
- System design: stationary buffer converter system such as a fast charging station for EVs
- Embedded software: modelling and implementation (TI\Code Composer, IBM\Rhapsody)
- Power electronics: design and prototyping of a configurable modular multilevel converter
- Electrical machine: design, characterization and control
- Energy storage: lithium battery, flywheel
- Mechanic: Design, drawing and assembling
- Control: advanced control in power conversion for electrical energy generation

MAIN PUBLICATIONS:

[1] R. M. D. Tsirinomeny and A. Rufer. *Configurable Modular Multilevel Converter (CMMC)*. EPE 2015: 18th European Conference on Power Electronics and Applications, Geneva, Switzerland, 2015.

[2] Minghao Xu, Martel Tsirinomeny, Alfred Rufer, *A flexible and robust power management mechanism based on single-phase Modular Multilevel Converter with integrated energy storage elements*. IECON 2015, Yokohama, JAPAN.

[3] R. M. D. Tsirinomeny and A. Rufer. *Influence of High Frequency Charge-Discharge Cycling Induced by a Configurable Modular Multilevel Converter*. PCIM ASIA 2015: International Exhibition and Conference for Power Electronics, Intelligent Motion, Renewable Energy and Energy Management, Shanghai, China, 2015.

[4] R. M. D. Tsirinomeny and A. Rufer. *Configurable Electric Vehicle (CEV) demonstrator*. PCIM 2015: International Exhibition and Conference for Power Electronics, Intelligent Motion, Renewable Energy and Energy Management, Nuremberg, Germany, 2015.

[5] R. M. D. Tsirinomeny and A. Rufer. *Configurable Modular Multilevel Converter (CMMC) for a universal and flexible integrated charging system*. PCIM 2014: International Exhibition and Conference for Power Electronics, Intelligent Motion, Renewable Energy and Energy Management, Nuremberg, Germany, 2014.

[6] M. Tsirinomeny, H. Hõimoja, A. Rufer, G. Dziechciaruk and A. Vezzini. *Optimizing EV driving-recharge time ratio a under limited grid connection*. PEMD, the 7th IET International Conference on Power Electronics, Machines and Drives, Manchester, UK, 2014.

[7] R. M. D. Tsirinomeny. *Modular multilevel battery packaging for a universal and flexible EVs charging system*. AABC 2014: The 14th International Advanced Automotive Battery Conference, Atlanta, Georgia, USA, 2014.

[8] R. M. D. Tsirinomeny and A. Rufer. *Electric Vehicle Driving and Fast Charging System based on Configurable Modular Multilevel Converter (CMMC)*. EPE 2013: 15th European Conference on Power Electronics and Applications, Lille, France, 2013.

[9] R. M. D. Tsirinomeny, H. Hõimoja and A. Rufer. *Ultrafast Charging Compatibility of Electric Vehicles*. IAMF 2012: International Advanced Mobility Forum, Geneva, Switzerland, 2012.

INVITES SPEAKER AS AN EXPERT IN MMC:

R. M. D. Tsirinomeny. *Advanced Automotive System based on Modular Multilevel Converter*. ECPE 2014: Workshop on Advanced Multicell / Multilevel Power Converters, Toulouse, France, 2014.

LANGUAGES:

English fluency

French fluency

German basic skills

Malagasy fluency

AWARDS: FORUM DE LA RECHERCHE MADAGASCAR 2008 - BEST PROTOTYPE AWARD

PCIM EUROPE 2014, NUREMBERG - BEST PAPER AWARD